BCS TO BEC EVOLUTION AND QUANTUM PHASE TRANSITIONS IN SUPERFLUID FERMI GASES

A Thesis
Presented to
The Academic Faculty

by

Menderes Iskin

In Partial Fulfillment
of the Requirements for the Degree
Doctor of Philosophy in Physics in the
School of Physics

Georgia Institute of Technology
August 2007

BCS TO BEC EVOLUTION AND QUANTUM PHASE TRANSITIONS IN SUPERFLUID FERMI GASES

Approved by:

Prof. Carlos A. R. Sá de Melo,
Committee Chair
School of Physics
Georgia Institute of Technology

Prof. Andrew Zangwill
School of Physics
Georgia Institute of Technology

Prof. T. A. Brian Kennedy
School of Physics
Georgia Institute of Technology

Prof. David S. Citrin
School of Electrical and Computer Engineering
Georgia Institute of Technology

Prof. Michael Chapman
School of Physics
Georgia Institute of Technology

Date Approved: June 26^{th}, 2007

To my family Salih and Murside,

and Sermet and Ibrahim

for their constant support and encouragement.

ACKNOWLEDGEMENTS

There are definitely many people without whose support, inspiration and encouragement this thesis would not have been completed. In this limited space, I will only mention the ones who have had direct influence on my research and/or on my life over the last years.

First of all, I am most grateful to my advisor Prof. Carlos A. R. Sá de Melo for all of his constant support and encouragement during the formation of this thesis work. Working with him has been very enlightening and stimulating experience, and the independence I was given helped to stimulate a variety of research topics which could not have been completed without his expertise in physics. I wish to thank him for everything he has taught me, and for the friendly relationship we have had over the years.

I wish to thank some of the faculty members in the School of Physics at Georgia Tech for keeping high standards of excellence in their teachings and for being great lecturers, including Professors Ian R. Gatland, Jean Bellissard, Predrag Cvitanovic, Phillip First, M. Raymond Flannery, Roman Grigoriev, T. A. Brian Kennedy, Uzi Landman, Carlos A. R. Sá de Melo, Alexei Marchenkov, Michael Pustilnik, Chandra Raman, John L. Wood and also Dr. Martin Jarrio, who taught most of what I know today in a variety of courses. Special thanks to Dr. Eric Murray for his help regarding the teaching assistant assignments, and to the graduate coordinator Prof. Andrew Zangwill for his help over the years.

I have had so many friends and room mates within the graduate students of School of Physics including Selcuk Akturk, Sergio S. Botelho, Wei Zhang and Serdar Ozdemir as well as of other departments including Erhan Ozalevli, Faik Baskaya, Gungor Ozer, Can Uslay and Juan Larrahando, and I wish to thank all of them for making Georgia Tech such an enjoyable place. I also wish to thank to Doctors Sergio S. Botelho and Wei Zhang for their help, colloboration and most importantly for their friendship as well as for all of the conversations we have had during their stay.

In addition, I am very grateful to my thesis advisor Prof. Carlos A. R. Sá de Melo,

and to Professors Igor O. Kulik and T. A. Brian Kennedy for supporting me with their invaluable recommendation letters, and for helping me to survive in the highly competitive research community of physics.

I would like to thank National Science Foundation (Grant No. DMR-0304380), Aspen Center for Physics, Gilbert F. Amelio Fellowship, and to thank Student Government, College of Sciences and especially to School of Physics for the financial support that I have given over the years, making it possible to present my research at various conferences and workshops.

I would also like to thank the members of my thesis committee: Professors Carlos A. R. Sá de Melo, T. A. Brian Kennedy, Michael Chapman and Andrew Zangwill from School of Physics, and David S. Citrin from School of Electrical and Computer Engineering for their careful reading of this thesis and valuable feedback as well as for their time spent during the thesis defense.

Finally, I would like to thank my parents Salih and Murside and to my brothers Sermet and Ibrahim for their constant support and encouragement, and to them I dedicate this thesis.

PREFACE

In this thesis, I focus on the analysis of the evolution from the Bardeen-Cooper-Schrieffer (BCS) limit of loosely bound and largely overlapping Cooper pairs to the Bose-Einstein condensation (BEC) limit of tightly bound small bosonic molecules. This evolution occurs when the strength of the attractive interparticle interaction increases from weak to strong values, and has been recently observed in ultracold superfluid Fermi gases. This thesis is an overview of some of my contribution (in colloboration with C. A. R. Sá de Melo) to the field of ultracold superfluid Fermi gases, and it consists of four main chapters and two appendices.

In Chapter I, I initially discuss quantum statistics of Bose and Fermi particles, and their condensation as two separate phenomena: BEC and BCS, respectively. Then, I introduced the pioneering idea that combines these two fundamentally very different phenomena into one: BCS to BEC crossover. After discussing the early ideas that lead to this theory and its development in condensed matter community, I present a brief introduction on how this phenomenon is currently being studied in atomic physics experiments by using ultracold gases of fermionic alkali atoms.

In Chapter II, I analyze zero and nonzero orbital angular momentum pairing effects, and show that a quantum phase transition occurs for nonzero angular momentum pairing, unlike the $\ell = 0$ s-wave case where the BCS to BEC evolution is just a crossover. This quantum phase transition is topological in its nature, characterized by a gapless superfluid on the BCS side and a fully gapped superfluid on the BEC side. This chapter is a detailed overview of the following publications and preprints:

- "*Evolution from BCS to BEC superfluidity in p-wave Fermi gases*", Phys. Rev. Lett. **96**, 040402 (2006); cond-mat/0510300.
- "*Nonzero orbital angular momentum pairing in superfluid Fermi gases*", Phys. Rev. A **74**, 013608 (2006); cond-mat/0602157. [long paper]

In Chapter III, I analyze two-species fermion mixtures with mass and population imbalance in continuum, trap and lattice models. In contrast with the crossover physics found in the mass and population balanced mixtures, I demonstrate the existence of phase transitions between normal and superfluid phases, as well as phase separation between superfluid (paired) and normal (excess) fermions in imbalanced mixtures as a function of scattering parameter, and mass or population imbalance. This chapter is a detailed overview of the following publications and preprints:

- "*Two-species fermion mixtures with population imbalance*", Phys. Rev. Lett. **97**, 100404 (2006); cond-mat/0604184.
- "*Asymmetric two-component Fermi gas with unequal masses*", cond-mat/0606624. [unpublished]
- "*Superfluid and insulating phases of fermion mixtures in optical lattices*", cond-mat/0612496. [in review]
- "*Mixtures of ultracold fermions with unequal masses*", to be published in Phys. Rev. A (2007); cond-mat/0703258. [long paper]

Finally, in Chapter IV, I present a brief summary of current results, and a short outlook for possible future extentions of the problems discussed in Chapters II and III.

In addition to these, I have contributed to other publications and preprints during my Ph.D. thesis research, but they are not discussed as a part of this thesis due to space and time constraints, including

- "*BCS-BEC crossover of collective excitations in two-band superfluids*", Phys. Rev. B **72**, 024512 (2005); cond-mat/0408586.
- "*Exotic p-wave superfluidity of single hyperfine state Fermi gases in optical lattices*", cond-mat/0502148. [unpublished]
- "*Superfluidity of p-wave and s-wave atomic Fermi gases in optical lattices*", Phys. Rev. B **72**, 224513 (2005); cond-mat/0508134. [long paper]

- "*Two-band superfluidity from the BCS to the BEC limit*", Phys. Rev. B **74**, 144517 (2006); cond-mat/0603601.
- "*Ultracold heteronuclear molecules and ferroelectric superfluids*", cond-mat/0610380. [in review]

In my opinion, these papers are as important as the ones overviewed in Chapters II and III, but with a small overlap in between.

TABLE OF CONTENTS

LIST OF TABLES

LIST OF FIGURES

SUMMARY

This thesis focuses on the analysis of Bardeen-Cooper-Schrieffer (BCS) to Bose-Einstein condensation (BEC) evolution in ultracold superfluid Fermi gases when the interaction between atoms is varied. The tuning of attractive interactions permits the ground state of the system to evolve from a weak fermion attraction BCS limit of loosely bound and largely overlapping Cooper pairs to a strong fermion attraction limit of tightly bound small bosonic molecules which undergo BEC. This evolution is accompanied by anomalous behavior of many superfluid properties, and reveals several quantum phase transitions. This thesis has two parts: In the first part, I analyze zero and nonzero orbital angular momentum pairing effects, and show that a quantum phase transition occurs for nonzero angular momentum pairing, unlike the s-wave case where the BCS to BEC evolution is just a crossover. In the second part, I analyze two-species fermion mixtures with mass and population imbalance in continuum, trap and lattice models. In contrast with the crossover physics found in the mass and population balanced mixtures, I demonstrate the existence of phase transitions between normal and superfluid phases, as well as phase separation between superfluid (paired) and normal (excess) fermions in imbalanced mixtures as a function of scattering parameter and mass and population imbalance.

CHAPTER I

INTRODUCTION

The theoretical framework of quantum mechanics was established during the first half of the twentieth century by Planck, de Broglie, Bohr, Heisenberg, Schrödinger, Dirac, Pauli and others [1]. The word 'quantum' in quantum mechanics refers to a discrete unit that quantum theory assigns to some of the physical quantities such as the energy of particles. This discrete spectrum of quantum theory lead physicists to a fundamentally different understanding of nature than ever before.

For instance in classical mechanics, it is always, in principle, possible to determine the position and momenta of any particle at any given time since, intuitively, each particle can be distinguished from the others. On the contrary, in quantum mechanics, it is not possible to determine the position and momenta of particles more accurately in phase space than the fundamental volume, which is a consequence of the Heisenberg's uncertainity principle [2]. Accordingly, one cannot know which particular particle is in this volume, but instead can only determine the probability of finding it.

One of the consequences of indistinguishability of identical particles is the classification of particles in nature with respect to their exchange symmetry [3]. When the particles are indistinguishable, the probability of finding one particular particle in one particular state and another particular particle in another particular state must be equal to the case when the particles are exchanged. This leads to two possibilities for the probability amplitudes under exhange symmetry, hence classification of all particles into two fundamental groups: (i) bosons are described by symmetric wavefunctions, and (ii) fermions are described by anti-symmetric wavefunctions. The symmetry character of the wavefunction has important consequences for the thermodynamic and statistical properties of a system. Therefore, in order to study a given quantum system, one first needs to determine the symmetry of the constituents of that system. The answer to the question of which particles are fermions

and which are bosons was given by Belinfante and Pauli in 1940 in their spin-statistics theorem [4, 5], and it is discussed next.

1.1 Bose-Einstein and Fermi-Dirac Statistics

According to the spin-statistics theorem, the symmetry character of the wavefunctions can be related to the intrinsic spin of the particles. This leads to the division of all known particles of nature into two groups with respect to their integer or half-integer intrinsic spin angular momentums (spin is in units of $\hbar$), such that even the elementary particles in the whole universe are characterized as either bosons or fermions named after physicists S. N. Bose and E. Fermi, respectively.

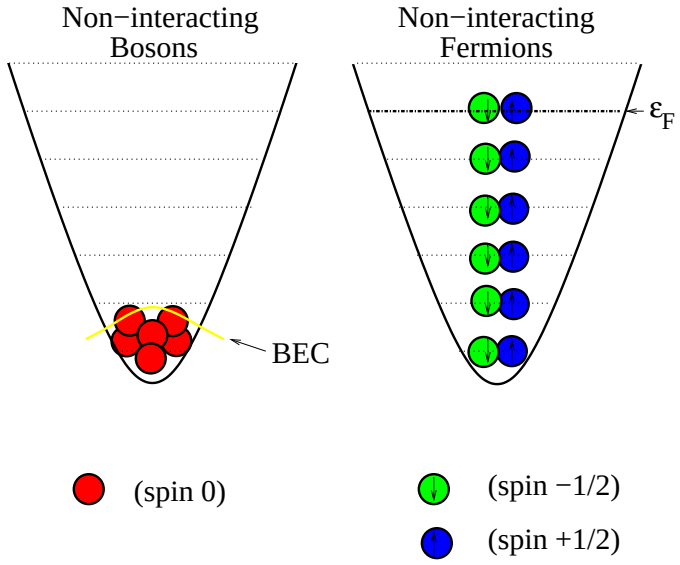

Figure 1.1: Illustration of quantum statistics for identical non-interacting (or ideal indistinguishable) bosons and fermions at zero temperature. (a) Identical spin-0 bosons undergo a BEC in which all of the particles macroscopically occupy a single quantum state. (b) Due to the Pauli exclusion principle, identical spin-1/2 fermions form a Fermi sea that is pairs of fermions occupy only the quantum states which are below the Fermi energy, and leaving other states unoccupied.

Bosons such as quanta of light (photons), sound (phonons), spin wave (magnons), etc. have integer intrinsic spins, and obey Bose-Einstein statistics. A consequence of Bose-Einstein statistics is the Bose-Einstein condensation (BEC) of non-interacting bosons at sufficiently low temperatures. This manifests itself in many different areas of physics ranging from condensed matter, nuclear to atomic, molecular and optical physics. Due to their

quantum statistics, this phenomenon relies on the fact that nothing prevents infinitely many identical bosons to share the same quantum state. In contrast, fermions such as electrons, protons, neutrons, etc. have half-integer intrinsic spins, and obey Fermi-Dirac statistics. A consequence of Fermi-Dirac statistics is the formation of Fermi sea and Fermi pressure for non-interacting fermions at sufficiently low temperatures. Due to their quantum statistics, this phenomena relies on the fact that the Pauli exclusion principle prevents multiple occupancy of identical fermions to share the same quantum state. Therefore, while identical bosons like to stick together, identical fermions avoid each other in space at a given time. An illustration of the zero temperature occupation of available quantum states by non-interacting (ideal) spin-0 bosons and spin-1/2 fermions is shown in Fig. 1.1 for a harmonic potential.

In addition to the elementary bosons and fermions discussed above, there are also composite particles which are made up of elementary particles. Composite particles such as mesons, baryons, atoms, etc. are also classified as fermions or bosons with respect to their integer or half-integer total intrinsic spin angular momentums. Accordingly, depending only on the number of fermions they contain, a composite particle containing an even number of fermions is a boson and a composite particle containing an odd number of fermions is a fermion, such that the number of bosons within a composite particle has no effect on whether it is a boson or a fermion. For instance, neutral atoms fall into one of these two categories depending on the total number of neutrons, since there are equal number of protons and electrons. Therefore, if the number of neutrons is even, the neutral atom is a boson; if it is odd, the neutral atom is a fermion which makes ^{4}He, ^{7}Li, ^{85}Rb, ^{23}Na, etc. bosons and ^{3}He, ^{6}Li, ^{40}K, ^{171}Yt, etc. fermions.

This distinction between identical (or indistinguishable) bosons and fermions, and their quantum mechanical Bose-Einstein and Fermi-Dirac statistics are important only when the quantum effects are not negligible, i.e. for sufficiently dense gases at low temperatures. On the other hand, when the de Broglie wavelength, which is proportional to the inverse square root of mass of the particles and the temperature of the gas, becomes much smaller than the average interparticle distance for sufficiently low densitites and high temperatures, the

distinction is lost. When this is the case, all particles become distinguishable, and their statistics is well-described by classical Maxwell-Boltzmann statistics [3]. For Bose gases, the quantum limit is separated from this classical limit by a BEC transition occurring at finite temperatures in three dimensions, while there is no phase transition for Fermi gases which separates the low and high temperature phases.

Having discussed the low temperature behavior of non-interacting Bose and Fermi gases, next I discuss the low temperature behavior of weakly interacting Bose and Fermi gases with attractive and repulsive interactions.

1.1.1 Weakly Interacting Bose Gases

In the previous section, I argued that non-interacting indistinguishable Bose gases undergo a phase transition towards BEC at low temperatures with a diverging compressibility, i.e. vanishing pressure. Therefore, it should not be surprising that even the very weak interactions between particles may effect dramatically the low temperature properties of very dilute gases. So the remaining question is what happens if the Bose gas is interacting? Is there a difference between a repulsive and an attractive interaction? For the weakly interacting Bose gas, this problem was solved by Bogoliubov in 1947 [6], and his method is the basis of modern approaches for studying BEC, details of which can be found in almost all textbooks on modern techniques [7, 8].

By using the Bogoliubov method, it can be shown that a uniform Bose gas with attractive interactions is unstable at zero temperature because the system can lower its energy by increasing density of particles. In the absence of a strong enough short range repulsive interaction to oppose this increasing density, the attractive Bose gas is susceptible to collapse, since Bose-Einstein statistics does not prevent overlap of multiple particles. Therefore, even arbitrarilly weak interactions between bosons change dramatically the ideal gas behavior in the case of attractive interactions as mentioned above.

More technically, the condition of thermodynamic stability requires that the compressibility of the gas to be positive. It can be shown that the compressibility of a weakly interacting Bose gas is inversely proportional to the density of bosons and the strength of

interparticle interactions, which suggests that the compressibility diverges as the interparticle interaction vanishes, recovering the non-interacting Bose gas result [8]. I arrive at a very important conclusion that the weakly interacting Bose gas with attractive interactions collapses mechanically since the compressibility of the gas becomes negative. Collapse dynamics of such an attractive Bose gas has been the subject of previous studies in various contexts [9, 10, 11, 12], and it will not be further discussed in this thesis.

Therefore, a uniform weakly interacting dilute gas may undergo a BEC transition only if the interparticle interactions are repulsive, which is discussed next.

1.1.2 Bose-Einstein Condensation (BEC)

The possibility of the BEC transition of identical non-interacting bosons is a consequence of Bose-Einstein statistics, and was predicted long ago by Bose in 1924 [13] and by Einstein in 1925 [14]. They claimed that a finite fraction of bosons (at zero temperature all of the bosons) should occupy a single quantum state below a critical transition temperature, which is determined by mass and density of the bosons. This exotic phenomenon was initially seen only as a mathematical artifact until London reinterpreted it to explain the superfluidity (frictionless flow) of ^{4}He soon after its discovery in 1938 by Kapitza [15], and independently by Allen and Misener [16]. He proposed that the superfluidity of ^{4}He was a consequence of BEC of bosonic ^{4}He atoms which are made up of an even number of electrons, protons and neutrons [17]. However, it was the subsequent works by Bogoliubov [6] and Landau [18] that established theoretically the connection between superfluidity and BEC.

After years of struggle, atomic physicists have successfully cooled down bosonic gases to quantum degeneracy (to nano Kelvin temperatures), and this quantum phenomena was observed in weakly interacting dilute atomic gases at ultracold temperatures for the first time in 1995 in a series of remarkable experiments [19, 20], and has been the subject of intense theoretical and experimental research worldwide [21, 22]. A good summary of the history of atomic BECs is provided by the 2001 Nobel Prize lectures of Cornell and Wieman [23] and, of Ketterle [24].

It is important to emphasize that ultracold gases of bosonic atoms such as ^{85}Rb and

^{23}Na were used in atomic physics experiments to produce atomic BECs. These bosonic atoms, in fact, are small tightly bound composite particles made up of an even number of fermions. In addition, it is possible and easy to manipulate the strength of interparticle interactions, as well as to change the nature of these interactions from repulsive to attractive and vice versa, which makes atomic Bose systems an ideal toolbox for studying fundamental many-body physics.

This success in Bose systems naturally lead to the question of whether one can also trap and cool fermionic atoms to ultracold temperatures, and control and manipulate the interparticle interactions. The possibility of studying small composite bosonic molecules which may be formed from tightly bound fermionic atoms, and their condensation (molecular BECs) is the main focus of this thesis, and it is discussed next.

1.1.3 Weakly Interacting Fermi Gases

I argued that the ground state of a non-interacting Fermi gas at zero temperature corresponds to the Fermi sea with complete filling of the single particle states up to the Fermi energy, and the complete absence of particles in other states. It is well-known from quantum statistics of non-interacting particles that the low temperature phases of fermionic gases and liquids differ dramatically from that of bosons. At finite temperatures, excitations of such Fermi systems correspond to transfer of particles from occupied to unoccupied states [25].

After the realization of atomic BECs, the natural complement to the bosonic research is to study weakly as well as strongly interacting fermionic atoms at ultracold temperatures. Using similar techniques developed for bosonic atoms, in their pioneering work, DeMarco and Jin successfully produced for the first time a quantum degenerate Fermi gas of ^{40}K atoms, and studied the effects of Fermi statistics in 1999 [26]. Due to this exciting possibility of studying quantum degenerate Fermi gases in atomic systems, many other experimental groups have achieved quantum degeneracy in either ^{40}K, ^{6}Li or ^{171,173}Yb [27]. Like their Bose counterparts, Fermi systems also offer great control of experimental parameters including the particle density, strength of interactions, spin populations and temperature. Thus, studies of superfuidity in atomic Fermi gases can provide a better understanding of

the pairing mechanisms in many other systems ranging from metals and neutron stars to nuclear matter.

The ground state of interacting Fermi systems also depends crucially on the nature of the interparticle interactions. For instance, if a Fermi gas consisting of half-integer intrinsic spin angular momentum fermions has repulsive interparticle interactions, then the energy spectrum is different from the boson counterparts. However, if the interparticle interactions are attractive, and tend to associate particles into pairs, then the constituents of the resulting gas consists of integer intrinsic spin angular momentum molecules, leading to a bosonic energy spectrum, which is discussed next.

1.1.4 Bardeen-Cooper-Schrieffer (BCS) Superconductivity

The macroscopic phenomenon for fermions that is analogous to BEC for bosons is the superfluidity of Cooper pairs described by the Bardeen-Cooper-Schrieffer (BCS) theory, and the possibility of observing BCS transition is an important motivation for studying ultracold fermionic gases [28, 29].

Long after the discovery of metallic superconductivity of mercury in 1911 [30] (charged superfluidity in which electrical current flows without resistance), the microscopic theory of superconductivity was formulated in 1957 by Bardeen, Cooper, and Schrieffer [31], and it is known today as the BCS theory of conventional superconductors. The authors of the BCS theory were awarded the Nobel prize in Physics in 1972, and their work was based on a model calculation performed by Cooper in 1956 [32], which relies on the existence of attractive interparticle interactions.

The basic idea of Cooper was that a weak attraction can bind pairs of fermions into bound pairs in the presence of the Fermi sea, and that the Fermi sea is unstable against formation of at least one bound pair regardless of how weak the attractive interparticle interaction was [32]. This crucial result is a consequence of Fermi-Dirac statistics and existence of the Fermi surface. If it was not for the Pauli exclusion principle and the presence of the Fermi surface, a bound state between two fermions does not occur until the strength of the interparticle interaction reaches a finite threshold value in three dimensions [33].

Furthermore, Cooper showed that these bound pairs have largest binding energy when they are at rest with respect to the Fermi sea such that their center of mass momentum is zero.

The BCS theory consisted then of a non-trivial many-body extention of Cooper's problem in which the ground state was constructed from pairs of fermions including the necessary anti-symmetrization of the full wave function, and the attractive interaction was assumed to arise due to electron-phonon interactions. Most important of all, below a finite critical temperature, this theory predicted a finite energy gap in the excitation energy of the superconducting state, and this gap was just necessary to understand the basic properties of known superconductors [31]. In their theory, BCS assumed that the Cooper pairs consist of spin singlet fermion pairs which have zero net spin, and the center of mass of every pair is at rest with respect to the Fermi sea.

The BCS transition in atomic Fermi gases is expected to be very similar to the transition from normal conductor to super conductor in ordinary metals or normal fluid to super fluid transion in liquid ^{3}He. Thus, the possibility of studying such a transition in atomic systems has attracted intense theoretical and experimental interest worldwide [28, 29] as discussed next.

1.2 BCS to BEC Crossover

So far, I discussed two fundamentally very different descriptions for understanding the low temperature behavior of superfluidity in Bose and Fermi systems. To summarize, the BEC of bosons occur at a much higher critical temperature that is of the order of their degeneracy temperature. In most cases, these bosons are tightly bound small composite particles which are made up of an even number of fermions. These composite particles form at some very high temperature scale which is of the order of their binding energy, and they condense only at much smaller temperatures. On the other hand, in the BCS theory of superconductivity, the normal state is a degenerate Fermi gas which undergoes a pairing instability below a critical temperature that is much less than the Fermi energy. In contrast to BEC of composite particles, the formation of Cooper pairs and their condensation occur simultaneously at the same transition temperature.

The possibility of studying the formation and condensation of small composite bosonic molecules starting from fermionic atoms opens up the exciting possibility of exploring the connection between Bose-Einstein and Fermi-Dirac statistics in the same physical system. This also raises the question of whether or not it is possible to observe bosonic statistics emerge from the underlying fermionic statistics. This problem is known today as the BCS-BEC crossover, and is an important topic of current research for condensed matter, nuclear, atomic and molecular physics communities. A brief history of this problem is discussed next.

1.2.1 History of Composite Bosons

The idea that the small electron pairs undergo BEC is older than the BCS theory itself. In their theory of quasichemical equilibrium, as early as 1954, Blatt, Schafroth, and Butler originally proposed to explain metallic superconductivity in terms of BEC of pairs of electrons into localized bound states [34]. Unfortunately, this theory could not compete with the striking success of the BCS theory due to some mathematical difficulties which did not allow the authors to obtain the famous BCS results [31] which agreed with the experiments. Then the triumph of the BCS theory replaced the far more obvious concept of small tightly bound local pairs and their BEC by the loosely bound and largely overlapping Cooper pairs, and their instability to momentum space pairing which takes place in the necessary presence of a Fermi surface. It should be also emphasized that Blatt later showed in 1962 that their theory could be extended to give the BCS results [35].

Several years later, in 1969, the first discussion on the possibility of BCSBEC crossover appeared, where pairing above the superconductivity transition temperature for a low density of carriers was carried out by Eagles in the context of a condensed matter system, a ceramic superconductor of Zr-doped $SrTiO_3$ [36]. He noted that, when the carrier density is low, the system is in a regime where the Cooper pair size is small, and the critical transition temperature of BCS theory does not correspond to a phase transition but corresponds to the formation of preformed pairs. He also argued that the superconducting transition would take place at a much lower temperature in this low density regime, corresponding to the BEC of preformed pairs. Then, he proposed to study the crossover problem by varying the

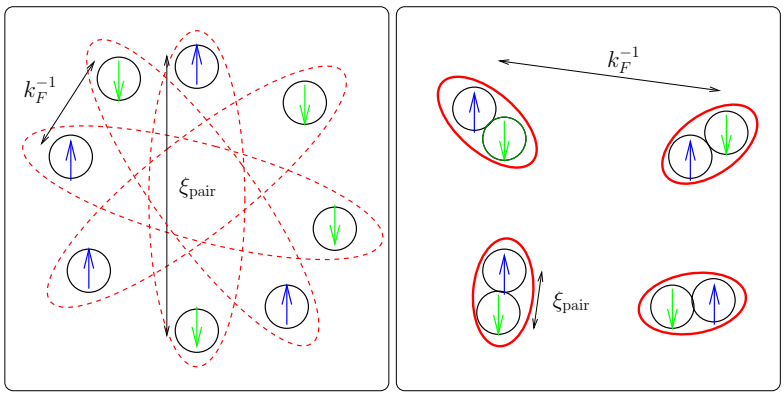

Figure 1.2: Illustration of the loosely bound and largely overlapping Cooper pairs and the small tightly bound local pairs in the BCS and BEC regimes, respectively, where $\xi_{\rm pair}$ is the size of the pair and k_F^{-1} is the Fermi momentum and it is of the order of interparticle distance. While the size of the Cooper pairs is much larger than the interparticle spacing in the BCS regime, it decreases with inreasing interaction strength and becomes much smaller than the interparticle spacing in the BEC regime.

carrier density.

An illustration of the loosely bound and largely overlapping Cooper pairs and the tightly bound small pairs are shown in Fig.1.2 in the BCS and BEC regimes, respectively, where $\xi_{\rm pair}$ is the size of the pair, and k_F^{-1} is the Fermi momentum which is of the order of interparticle spacing. While the size of the Cooper pairs is much larger than the interparticle spacing in the BCS regime, it decreases with increasing interaction strength and becomes much smaller than the interparticle spacing in the BEC regime. However, it was Leggett in 1980 [37, 38], who independently from Eagles, analyzed the crossover problem of dilute Fermi gases as a function of the s-wave scattering length at zero temperature. His work lead to insight into the wavefunction of the ground state throughout the BCS-BEC crossover as discussed next.

1.2.2 Leggett's Ground State

Motivated by early ideas of the quasi-chemical equilibrium theory [34], in his pioneering work [37, 38], Leggett proposed that the extended BCS wavefunction is more widely applicable then just to the weakly interacting limit [31]. In the context of superfluid ^{3}He, at zero temperature, he studied a dilute Fermi gas with attractive interactions, and showed within a variational approach that there is a smooth crossover from a BCS ground state with large Cooper pairs (giant diatomic molecules) overlapping in space to a BEC of small tightly

bound diatomic molecules. The main difference between the BCS-BEC crossover problem and the simple BCS theory is that the Cooper pairing is not allowed only for fermions with energies close to the Fermi energy but is also allowed for all other fermions. To take this into account, Leggett noted that the chemical potential of fermions is not necessarily fixed at the Fermi energy but must be determined self-consistently together with the BCS order parameter.

Self-consistent solutions of Leggett's ground state recovers, by construction, the well-known BCS results in the weak interparticle interaction limit. However, in the opposite limit, when the attractive interparticle interaction strength is large, the chemical potential of fermions becomes large and negative and its magnitude is given by just half the binding energy of the two-body bound state. In addition, the BCS order parameter equation reduces to nothing but the Schrödinger equation of independent diatomic molecules, where twice the chemical potential of fermions plays the role of the energy eigenvalue as expected for a weakly interacting composite boson gas. Thus in this limit, Leggett arrived simply a BEC of weakly interacting diatomic molecules. It is also remarkable that self-consistent calculations admits a unique solution for all interaction strengths even in the intermediate region.

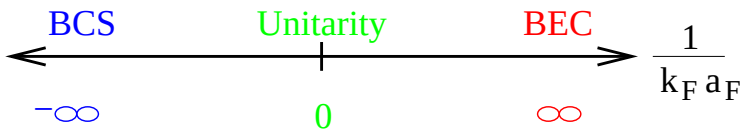

Figure 1.3: There are three important limits in Leggett's BCS-BEC crossover problem. (i) In the BCS limit, the scattering length is small and negative, and the interparticle fermion-fermion interaction is small and attractive. (ii) In the BEC limit, the scattering length is small but positive, and although the interparticle fermion-fermion interaction is large and attractive, the interparticle composite boson-boson interaction is small and repulsive which suggests that the composite boson gas is stable. (iii) At unitarity limit, the scattering length diverges, and the interparticle fermion-fermion interaction is very large and attractive. In this latter limit, for dilute systems, the superfluid properties does not depend on the actual value of the diverging scattering length, and the Fermi momentum k_F is the only relevant length scale left in the problem, an important cosequence of which is the universality of the superfluid properties. Here, k_F is the Fermi momentum and it is related to the density of fermions by $n = k_F^3/(3\pi^2)$.

Leggett considered a dilute Fermi gas at zero temperature where the range of the interatomic potential is much smaller than the interparticle distance such that the scattering particles never explore the fine details of the short-range scattering potential, and only the s-wave scattering is important. Under these assumptions, superfluid properties are governed by a single parameter, which is the s-wave scattering length a_F. He argued that while a two-body bound state exists beyond a critical interaction strength corresponding to $a_F > 0$, the pairing is purely a many-body effect for $a_F < 0$. Then, he analyzed three important limits in the BCS-BEC crossover problem, and they are illustrated in Fig. 1.3.

This simple mean-field approach by Leggett describes equally well the weak and strong attraction limits, where the constituents of the gas are weakly interacting. (i) In the BCS limit, the scattering length is small and negative, and the interparticle fermion-fermion interaction is small. (ii) In the BEC limit, the scattering length is small but positive, and the interparticle composite boson-boson interaction is small but repulsive. Notice that the repulsive composite boson-boson interaction is in fact necessary for the stability of the boson gas resulting in the BEC limit. While in between, around what is called the (iii) unitarity limit, the scattering length and the interparticle fermion-fermion interaction are very large, leading to a strongly interacting system. When the scattering length diverges, the superfluid properties should no longer depend on the actual value of the diverging scattering length, and the Fermi momentum k_F is the only relevant length scale left in the problem, an important cosequence of which is the universality of the superfluid properties including the critical temperature, average energy, thermodynamic quantities, etc [39, 40]. This means that results obtained with dilute ultracold Fermi gases at unitarity is directly related to other systems including nuclear matter and neutron stars. For instance, the critical temperature at unitarity is simply a universal constant times the Fermi energy.

It is very important to note here that although the attractive interparticle fermion-fermion interaction is strongest in the BEC limit, the gas is weakly interacting since the interparticle composite boson-boson interaction is weak and proportional to the scattering length of fermions. Therefore, the most strongly interacting gas occurs in the unitarity limit where many-body calculations are the most difficult. Furthermore, in this generalized BCS

theory, while only the fermionic (bosonic) nature of particles dominates the low temperature behavior of the system with decreasing (increasing) attractive interaction, the fermionic and bosonic degrees of freedom play equally important roles in the intermediate region. However, in contrast to the BCS and BEC limits, an exact solution of the many-body problem is not available for the unitarity limit, and as a first approximation Leggett argued that the self-consistent solutions may be qualitatively valid as an interpolation scheme for arbitrary interactions, which has been the focus of intense theoretical and experimental research.

Motivated by the possibility of exciton condensation in semiconductors, Nozieres and Schmitt-Rink used a diagrammatic approach, and extended the analysis of Leggett to a lattice model and more importantly to finite temperatures [41]. They showed that the evolution from weak to strong interaction limit is smooth such that the critical transition temperature saturates in the BEC limit going continuously from an exponentially small values in the BCS limit (where it is controlled by pair breaking) to an ideal Bose gas limit (where it is contolled by the center-of-mass motion of bound pairs).

A schematic phase diagram of crossover from the BCS transition of Cooper pairs to the BEC of preformed pairs is shown in Fig. 1.4. When the interparticle interaction is weak, the ground state is a BCS condensate of loosely bound and largely overlapping Cooper pairs where the pair formation and condensation occur simultaneously at the same temperature. For intermediate interparticle interactions, the pair formation and the condensation temperature scales are different that is the latter occurs at a much lower temperature. When the interparticle interaction is large, the ground state is a BEC of tightly bound and small local pairs, and the critical condensation temperature saturates at the BEC temperature of preformed pairs. Therefore, the critical superfluid transition temperature is of the order of the Fermi energy, $T_c \sim 0.2\epsilon_F$, in the BEC limit, and it is much higher than the exponentially small values characterizing the BCS limit.

In addition to these developments, with the discovery of high temperature copper-oxide superconductors by Bednorz and Müller in 1986 [42], it became clear that, besides their very high critical temperatures and low carrier densities, the size of the Cooper pairs is of the same order with the average interparticle distance (or lattice spacing). This is in

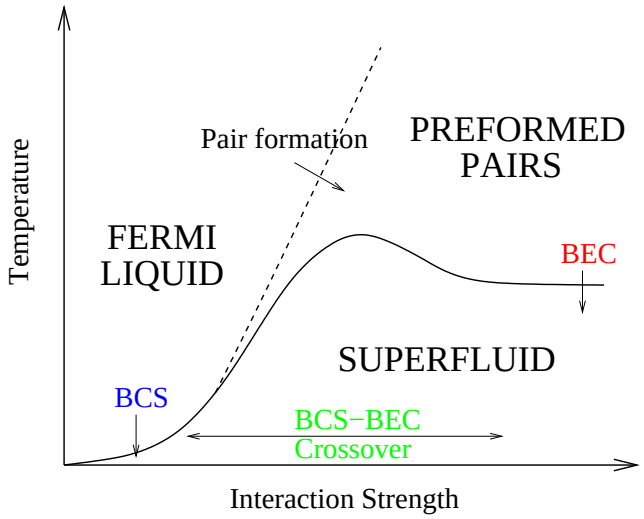

Figure 1.4: Schematic phase diagram of crossover from the BCS to the BEC of preformed pairs. The dashed line is the simple BCS result characterizing the pair formation, and the solid line is the true critical normal to superfluid transition temperature due to Nozieres and Schmitt-Rink [41]. When the interparticle interaction is weak, the ground state is a BCS condensate of loosely bound and largely overlapping Cooper pairs where the pair formation and condensation occur simultaneously at the same temperature. For intermediate interparticle interactions, the pair formation and the condensation temperature scales are different that is the latter occurs at a much lower temperature. When the interparticle interaction is large, the ground state is a BEC of tightly bound and small local pairs, and the critical condensation temperature saturates at the BEC temperature of preformed pairs. In the BEC limit, the critical transition temperature is of the order of the Fermi energy, and it is much higher than the exponentially small values characterizing the BCS limit.

sharp contrast with the conventional low temperature superconductors that is the size of the Cooper pairs is much larger than the lattice spacing. Although the BCS-BEC crossover problem is of great fundamental interest, it was the experimental discovery of copper-oxide superconductors that made this problem directly relevant to a particular system.

While the critical transition temperature T_c (in units of Fermi energy) was about 10^{-5} to 10^{-4} for conventional low temperature superconductors and about 10^{-3} for ^{3}He, it was about 10^{-2} for high critical temperature superconductors. Motivated by these results, it was suggested that these high temperature superconductors were in the intermediate regime between the limit of large and overlapping Cooper pairs found in the BCS theory and the opposite limit of BEC of small composite bosons consisting of tightly bound fermions. Therefore, a good understanding of the BCS-BEC crossover may be one of the key ingredients to solve the long standing mystery of high temperature superconductivity [43, 44].

The seminal works of Leggett [37, 38] and of Nozieres and Schmitt-Rink [41] had a major influence on many of the recent works in the field of high temperature superconductivity in the condensed matter community, and more recently in the field of quantum degenerate ultracold Fermi gases in the atomic physics community [44, 45, 46]. In the latter context, their theoretical formalism is extended to include the trapping potential [47, 48] as well as the effects of multiple scattering channels [49, 50] which are both present in atomic systems as discussed below.

With new advances developed in atomic physics experiments, it has become possible to study the intermediate interparticle interaction or strongly interacting regime as well as the theoretically predicted crossover from the BCS to the BEC limit, which is discussed next.

1.3 Ultracold Atomic Fermi Gases

With the ultimate success of the techniques for trapping and cooling bosonic atoms developed and improved gradually since the 1980s, ultracold atomic Bose gases have emerged as a unique testing ground for many theories of exotic matter in nature, allowing for the creation of complex, but yet very accessible and well controlled many-body quantum systems. A good summary of the history of cooling, trapping and manipulating neutral atoms can be found in the 1997 Nobel Prize lectures by Chu [51], Cohen-Tannoudji [52], and Phillips [53].

The successfull BEC of dilute gases of bosonic atoms [19, 20] (atomic BECs) led to the possibility of also cooling and trapping fermionic atoms to quantum degeneracy [54]. In contrast to Bose gases with strong interactions (large scattering lengths) where rapid three-body decay prevents experiments to reach the strongly interacting regime [55, 56], research in ultracold atomic Fermi gases is mostly motivated by the idea of creating a clean strongly interacting system with the controllability which is absent in condensed matter systems. In principle, the particle density and interparticle interactions as well as the temperature can be fully controlled, and the physical properties can be studied as a function of particle density, interaction strength and temperature.

One of the main objectives of such experiments is the condensation of composite bosons which are made up of two fermionic atoms that behave statistically like bosons, namely the

creation of molecular BECs. For this purpose, one needs to create an effectively attractive interparticle interaction between fermionic atoms, and to be able to change the strength of this interaction from weak to strong values such that the system evolves from the BCS limit of large Cooper pairs to the BEC limit of tightly bound molecules.

In the conventional theory of superconductors, s-wave Cooper pairing occurs between spin-up and spin-down electrons with opposite momenta, and a similar pairing could also be realized with the creation of a two-pseudo-spin component atomic Fermi gas as follows [57]. Alkali atoms have only one electron ($S = 1/2$) out of closed shells. This electron is in a zero orbital angular momentum ($L = 0$) channel, and its total angular momentum $\mathbf{J} = \mathbf{L}+\mathbf{S}$ gives $J = 1/2$. The nuclear angular momentum I and electron angular momentum J are combined in a hyperfine state with total angular momentum $\mathbf{F} = \mathbf{I} + \mathbf{J}$ which gives $F = I \pm 1/2$ for alkalis. Furthermore, the electron and nuclear spins are coupled by the hyperfine interaction that splits the atomic levels in the absense of magnetic field $H_{\rm hf} \propto \mathbf{I} \cdot \mathbf{J}$. A weak magnetic field causes Zeeman splitting of the hyperfine levels $|F, m_F >$ with different m_F, and atoms trapped in these hyperfine states can be made to correspond to pseudo-spin labels [22]. For instance, the energies of different hyperfine states is shown as a function of magnetic field in Fig. 1.5 for ^{6}Li atoms. Therefore, it is, in principle, possible to study pairing problem in ultracold atomic experiments, which have attracted an intense theoretical and experimental attention in recent years.

Short after the creation of the first quantum degenerate Fermi gas [26], it was in 2002 when the first strongly interacting resonant Fermi gas was created by Thomas and coworkers, where they observed the hydrodynamic behavior in the free expansion of a ^{6}Li gas [58]. In 2003 and 2004, within the span of a few months, several groups reported the creation of diatomic molecules from ultracold Fermi gases of ^{40}K [59] and ^{6}Li atoms [60, 61, 62]. It turned out that these diatomic molecules made up of strongly interacting fermionic atoms were remarkably stable against inelastic decay, and they were surprisingly long-lived, allowing for the formation of stable molecular quantum gases. The remarkable stability of strongly interacting Fermi gases was due to the fermionic nature of the atoms: inelastic three-body scatterings were strongly suppressed due to Pauli exclusion principle, since

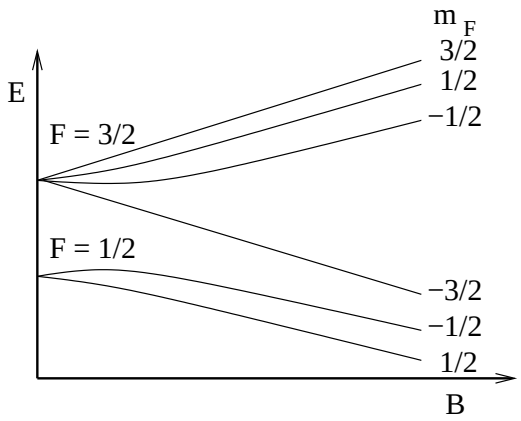

Figure 1.5: The energies of different hyperfine states as a function of magnetic field is shown for ^{6}Li. The *s*-wave Cooper pairing can occur between atoms trapped in any two of these pseudo-spin components corresponding to spin-up and spin-down electrons of the usual BCS theory.

this process would involve at least two identical fermions with the same spin state to be very close [63]. This was the key ingredient that enabled all of the subsequent studies on superfluid Fermi gases.

Later that year, four groups achieved the creation of molecular BEC with ^{6}Li [64, 65, 66] and ^{40}K atoms [67], which were followed by the condensation of atomic pairs in strongly interacting Fermi gases with resonant interactions [68, 69]. These experiments demonstrated a new macroscopic quantum state of ultracold matter beyond the well-established BEC physics, and due to its universal behavior [39, 40], they have stimulated an intense theoretical as well as experimental interest in different fields of physics ranging from condensed matter, nuclear, astro to atomic, molecular and optical physics.

Then, it became possible to investigate some properties of BCS-BEC evolution, and the theoretically predicted smooth crossover [37, 38, 44] was experimentally realized in an adiabatic and reversible way [70]. It should be emphasized that, since two-body bound states do not exist in the BCS limit, the observed pairing was necessarily a many-body effect. Following experiments also provided clear evidence for pairing throughout the crossover region including measurements of collective excitations, radio-frequency spectroscopy, molecular probe technique, and measurements of the heat capacity [71, 72, 73, 74]. However, the observation of vortices reported by Ketterle and coworkers in 2005 was the final and most

convincing evidence of superfluidity in strongly interacting Fermi gases [75]. Most recently, population imbalanced two-component Fermi mixtures have been created and several phase transitions have been reported leading to an immense activity in this field [76, 77]. The mass and/or population imbalanced fermion mixtures is the subject of Chapter III of this thesis.

In most of these experiments, the control over the strength of interparticle interactions is very crucial, and this is accomplished via Feshbach resonances by varying the strength of the externally applied magnetic field as discussed next.

1.3.1 Feshbach Resonances: Tuning the Interactions

Feshbach resonances proposed by H. Feshbach in 1958 [78] (see also [79]) is one of the most powerful techniques used in dilute atomic gases to control the strength of interparticle interactions in both Bose and Fermi systems. In practice, the tuning of interparticle interactions is accomplished by varying a magnetic field, providing experiments on dilute atomic gases a knob to control the interactions. This precision control has made atomic gases an ideal toolbox to study many-body phenomena.

In atomic systems, the attractive potential is provided by the interatomic van der Waals interactions which are due to mutually induced dipole moments of atoms, and these potentials are deep enough to support a large number of bound vibrational states. A Feshbach resonance occurs when the energy of one of these bound states coincides with the kinetic energy of the colliding pair of atoms in a different scattering channel as shown in Fig. 1.6. Such a degeneracy can occur only when the bound state exists in a potential that has a higher threshold energy than that of the colliding atom pair, which is satisfied in ultracold atomic systems due to the presence of atomic hyperfine structure [80]. These resonances were first observed in 1998 in a ^{23}Na Bose-Einstein condensate [81] and in a laser cooled ^{85}Rb [82] cloud.

The main effect of a Feshbach resonance is that the elastic scattering in one channel can be altered dramatically if there is a low energy bound state in a second channel. The

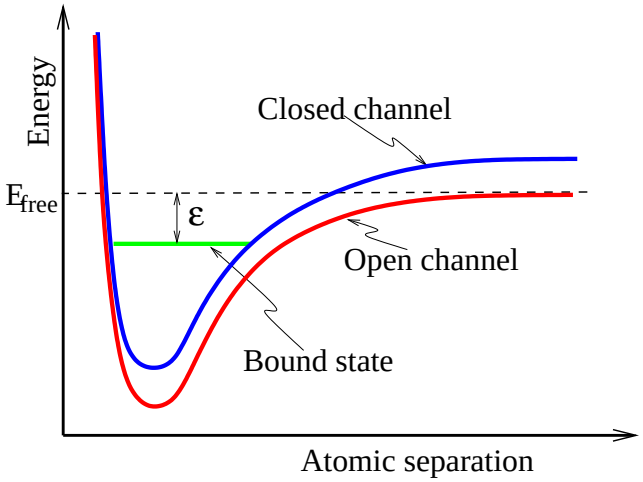

Figure 1.6: A simplified illustration of the interatomic potentials involved in a Feshbach resonance. The solid lines represent the potential energy versus internuclear separation for the colliding atoms. The dashed lines show the threshold energy of the open scattering channel. A Feshbach resonance occurs when energy of one of the closed channel bound states, shown by the short horizontal line, coincides with the threshold energy of the open channel potential. The atoms are initially prepared in the open channel, and the relative splitting of the internal states of the atoms ε called detuning is varied through the Zeeman effect using an external magnetic field to create a resonance.

interatomic potential of the two free atoms is often referred to as the open or triplet scattering channel, while the potential containing the bound state is referred to as the closed or singlet scattering channel. The threshold of the singlet potential generally appears above the threshold of the triplet potential, and it is unfavored for atoms to scatter out of the singlet potential. These singlet and triplet spin states may couple to one another through hyperfine interactions with the spin of the nucleus. When the singlet and triplet channels describe atoms in different magnetic sublevels, the relative separation of the internal states of the atoms may be varied through the Zeeman effect using an external magnetic field. Typically the effect of the coupling between the singlet and triplet channels is small, but at a Feshbach resonance, the effect of the coupling can be significantly enhanced which changes the effective interatomic potential leading to a change in the scattering length which is known as the resonance scattering [28].

The presence of the bound state near zero energy dramatically affects the scattering properties of colliding atoms, since these atoms can make transition to the bound state and stay there before moving apart after the collision. To first order in coupling between singlet

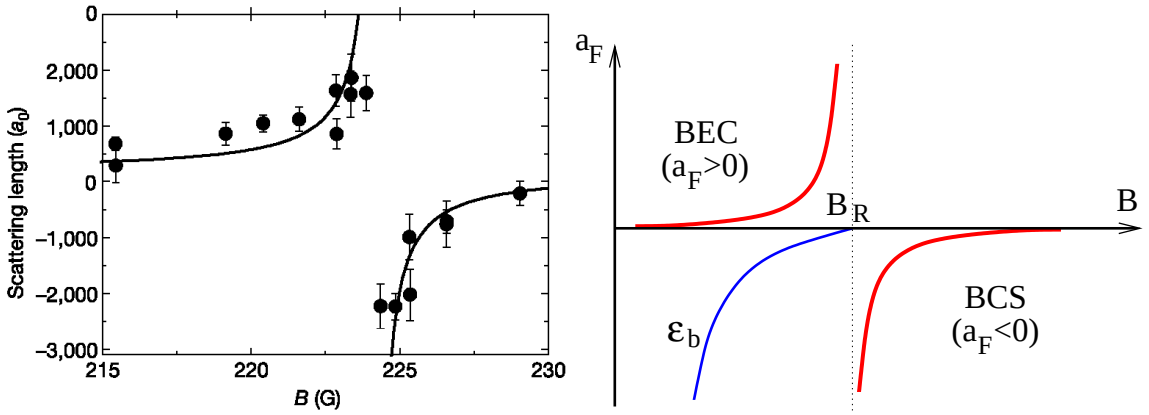

Figure 1.7: (a) Behavior of the s-wave scattering length a_F between the $|F = 9/2, m_F = -9/2 >$ and $|F = 9/2, m_F = -7/2 >$ states at a Feshbach resonance in a ^{40}K gas. (Adapted from [83].) (b) Illustration of the scattering length as a function of the externally applied magnetic field. The BCS limit is in the higher magnetic field side where the scattering length is small and negative, while the BEC limit is in the lower magnetic field side where the scattering length is small but positive. Unitarity limit is at the resonance field where the scattering length diverges. Notice that the scattering length has a sign change at the resonance magnetic field, and two-body bound states exist only for the magnetic field strengths that lead to positive scattering length.

and triplet channels, the scattering is unaltered. However, two triplet channel particles may scatter into an intermediate state in the singlet channel, and decay back into triplet channel. Using perturbation theory, such second order processes suggest huge contributions when the energies are nearly degenerate. Even though the bound state exists in a different interatomic potential from that of the colliding atoms, the variable bound state energy can still dramatically change the scattering length which characterizes the strength of the interparticle interaction. This technique has been extensively used in experiments with Bose and Fermi atoms, and it has become one of the most important ingredients to the production of molecular BECs.

For instance, Jin and coworkers observed in 2003 the suggested behavior of the scattering length at a Feshbach resonance in a ^{40}K Fermi gas [83], as shown in Fig. 1.7. There are three important regions in this figure: (i) higher magnetic field region where the scattering length is small and negative corresponding to BCS regime, (ii) lower magnetic field region where the scattering length is small but positive corresponding to BEC regime, and (iii) around resonance region where the absolute value of the scattering length is large corresponding

to unitarity regime. Notice that the scattering length has a sign change at the resonance magnetic field, since a new bound state emerges at the onset of two-body bound state formation, leading to divergence of the scattering length.

So far, I argued that the Feshbach resonances have proved to be very convenient to study BCS to BEC crossover in trapped geometries. These resonances have been recently observed in optical lattices [84, 85, 86], and the superfluid properties of strongly interacting Fermi gases in optical lattices are just beginning to be studied [87], as discussed next.

1.3.2 Optical Lattices

The interaction between induced dipole moments of atoms and the electric field of laser beams is used to trap Fermi atoms in optical lattices [88, 89, 90]. Initially, tunable optical lattices have been extensively used to study phase transitions in atomic Bose gases, since they allow the controlled manipulation of the particle density and of the ratio between the particle transfer energy, and the interparticle interaction strength. This kind of control is not fully present in standard fermionic condensed matter systems, and has hindered the development of experiments that could probe systematically the effects of strong correlations. Because of the greater tunability of experimental parameters, novel superfluid phases may be more easily accessible in the experiments involving ultracold atomic gases. For instance, recent studies of Bose atoms in optical lattices have revealed the existence of superfluid and Bose-Mott insulator (BMI) phases [91, 92].

The research explosion that followed this discovery, guarantees *a priori* another research explosion following the very recent experimental observation of superfluid and insulating phases of Fermi atoms in optical lattices [87]. Thus, it is only natural to propose that optical lattices could be used to study the normal state and superfluid properties of ultracold fermionic systems as a function of particle density, atom transfer energy, interaction strength, filling fraction, and lattice symmetry and dimensionality. These systems are also of broad interest not only for the atomic physics community but also for the nuclear, condensed matter and more generally for the many-body physics communities, where models for superfluidity have been investigated in various contexts.

Eventhough great success was achieved in cooling and studying Bose atoms in optical lattices, it was not until very recently that Fermi atoms (mixtures of two-hyperfine states) [87] or mixtures of Bose and Fermi atoms begun to be experimentally studied [93]. In addition, several groups around the world are attempting to create fermion mixtures made of two types of Fermi atoms, similar to experiments with boson mixtures consisting of two types of Bose atoms [94]. Ultracold fermions in optical lattices are ideal systems to study novel atomic and/or condensed matter phases in particular because attractive fermions can lead to Bose behavior (Bose molecules made of two-fermions), as well as to combined Bose-Fermi behavior where there are bound Bose molecules and unbound excess fermions. Thus, the resulting quantum phases of fermion mixtures are much richer than those of Bose atoms or Bose-Fermi mixtures in optical lattices.

The lattice and continuum models describe essentially the same physics in the BCS limit, and the fact that fermions are confined to a lattice geometry makes no difference, since the size of the Cooper pairs is much larger than the lattice spacing. In the opposite BEC limit, significant differences arise once the pair size becomes comparable to the lattice spacing. In this limit, there can only be a single composite boson on any lattice site forming local hard-core bosons on a given site with a high binding energy, and other fermions are blocked by the Pauli exclusion principle. These particles can move only via pair breaking, and therefore, their nearest neighbor tranfer energy decreases with increasing interaction, that is they become heavier with increasing interaction and the critical BEC transition temperature decreases to zero. This is in sharp contrast with the continuum case where the composite boson mass (equals to the total mass of fermion pairs) and critical BEC temperatures are finite constants [41, 95].

However, lattice and continuum models have one common feature. In order to obtain the collective mode of the superfluid ground state, it is necessary to include correlations between bound pairs with finite center of mass momentum. While the critical transition temperature results from thermal excitation of collective modes in the BEC limit, it results from thermal excitation of individual particles in the BCS limit. Therefore, the physics is quite different in two limits: pair breaking in one case, and motion of bound pairs in the

other [95].

Having discussed the history and experimental background of the BCS-BEC crossover problem, I briefly discuss next the functional integral formalism, which is the theoretical framework of this thesis.

1.4 Functional Integral Formalism

Under some circumstances, several many-body systems can be well-described by some effective actions such that the original actions involving fundamental particle fields such as electrons, atoms, etc. are replaced by the ones containing auxiliary quantum fields characterizing the order parameter of those systems such as in superconductors, superfluids, ferromagnets, ferroelectrics, etc. Functional integrals provide a powerful tool for studying such many-body systems, in which the partition function is written as an integral over the field configurations, providing both a physically intuitive description of the system and a useful starting point for approximations.

This formalism uses Feynman path integrals, in which the transformation to auxiliary fields amounts to mere changes of integration variables in functional integrals. The essence of the path integral approach was introduced by Dirac in 1933 [96], and later developed extensively by Feynman in 1948 [97], and the details of this formalism can be found in most of the modern textbooks [98, 99, 100].

In addition to quantum field theory [101], functional integral methods have also been widely used in statistical physics to deal with collective excitations such as Goldstone phonons and quantum vortices in superfluids and superconductors [7, 102]. One of the advantages of this formalism is that it is, in principle, easier to do and calculate perturbative expansions to any order. In particular to the BCS-BEC crossover problem, in addition to recovering the stationary BCS results originally obtained from a variational approach, this formalism can be used to determine the collective modes of the system by including fluctuations about the stationary solutions [43, 44, 103]. In fact, this will prove to be extremely important at finite temperatures as will be discussed in this thesis.

1.5 Outline

In this thesis, I focus on the analysis of Bardeen-Cooper-Schrieffer (BCS) to Bose-Einstein condensation (BEC) evolution in ultracold superfluid Fermi gases as a function of interparticle interaction strength. The tuning of attractive interactions permits the ground state of the system to evolve from the weak fermion attraction (BCS) limit of largely overlapping Cooper pairs to the strong fermion attraction limit of tightly bound bosonic molecules which undergo BEC. This evolution is accompanied by anomalous behavior of many superfluid properties, and reveals several quantum phase transitions, as briefly introduced next.

1.5.1 Nonzero Angular Momentum Pairing

For paired identical fermions, the Pauli exclusion principle requires the total pair wave function to be anti-symmetric. The total orbital angular momentum should be odd for pseudo-spin symmetric pairs and even for pseudo-spin anti-symmetric ones. Therefore in the case of trapping two-hyperfine-states (THS), s-wave scattering of atoms between fermions from different hyperfine states is dominant. One also expects that the superfluid ground state of such two-component Fermi gases with equal populations to be s-wave and pseudo-spin singlet for which the theoretically proposed BCS to BEC crossover has been experimentally realized in recent experiments [71, 72, 73, 75].

However, the properties of single-hyperfine-state (SHS) ultracold fermions and their possible superfluid behavior are beginning to be investigated [104, 105, 106, 107, 108, 109]. These systems are probably the next frontier for experiments with ultracold atoms. When identical fermionic atoms are trapped in a single-hyperfine-state, the interparticle interaction is strongly influenced by the Pauli exclusion principle, which prohibits s-wave scattering of atoms in identical pseudo-spin states. As a result, in SHS degenerate Fermi gases, two fermions can interact with each other at best via p-wave scattering. Thus, one expects that the superfluid ground state of such SHS Fermi gases to be p-wave and pseudo-spin triplet.

Motivated by these recent experiments [71, 72, 73, 75], in Chapter II, I analyze zero and nonzero orbital angular momentum pairing effects, and show that a quantum phase transition occurs for nonzero angular momentum pairing, unlike the s-wave case where the

BCS to BEC evolution is just a crossover. This quantum phase transition is topological in its nature, characterized by a gapless superfluid on the BCS side, and by a fully gapped superfluid on the BEC side.

Similar topological quantum phase transitions with much richer phase diagram also occur in mass and population imbalanced THS mixtures, as as briefly introduced next.

1.5.2 Imbalanced Fermion Mixtures

The lack of precise control over standard condensed matter systems hindered the development of experiments that could probe systematically the effects of strong correlations, and makes atomic systems a powerful tool for studying novel superfluid phases. For instance, a new frontier with population imbalanced fermion mixtures has been recently reported. Since the population of each component as well as the interaction strength between two components are experimentally tunable, these knobs enabled the study of the BCS to BEC evolution in population imbalanced two-component fermion superfluids [76, 77]. In contrast with the crossover physics found in the population balanced case [37, 38, 41, 44, 110], these experiments have demonstrated the existence of phase transitions between normal and superfluid phases, as well as phase separation between superfluid (paired) and normal (excess) fermions as a function of population imbalance [111, 112].

Motivated by these very recent experiments, in Chapter III, I analyze two-species fermion mixtures with mass and population imbalance in continuum, trap and lattice models. In contrast with the crossover physics found in the mass and population balanced mixtures, I demonstrate the existence of phase transitions between normal and superfluid phases, as well as phase separation between superfluid (paired) and normal (excess) fermions in imbalanced mixtures as a function of scattering parameter, and mass and population imbalance. In optical lattices, in addition to the standard superfluid, phase separated or coexisting superfluid/excess fermion phases, I find several insulating phases including a molecular Bose-Mott insulator (BMI), a Fermi-Pauli (band) insulator (FPI), a phase separated BMI/FPI mixture, and a Bose-Fermi checkerboard phase depending on fermion filling fractions.

CHAPTER II

NONZERO ORBITAL ANGULAR MOMENTUM SUPERFLUIDITY IN ULTRACOLD FERMI GASES

In single hyperfine state Fermi gases, s-wave scattering of identical atoms is prohibited by the Pauli exclusion principle, and two fermions can interact with each other at best via p-wave scattering. When this is the case, the superfluid ground state corresponds to a p-wave and pseudo-spin triplet pairing. The evolution of p-wave superfluidity from the BCS to the BEC limit is very different from the usual s-wave case as discussed next in this chapter.

2.1 Introduction

Experimental advances involving atomic Fermi gases enabled the control of interactions between atoms in different hyperfine states by using Feshbach resonances [58, 59, 60, 61, 62, 65, 66]. These resonances can be tuned via an external magnetic field and allow the study of dilute many-body systems with fixed density, but varying interaction strength characterized by the scattering parameter a_ℓ. This technique allows for the study of new phases of strongly interacting fermions. For instance, the recent experiments from the MIT group [75] marked the first observation of vortices in atomic Fermi gases corresponding to a strong signature of superfluidity in the s-wave ($\ell = 0$) channel. These studies combined [68, 71, 72, 73, 74, 75] correspond to the experimental realization of the theoretically proposed Bardeen-Cooper-Schrieffer (BCS) to Bose-Einstein condensation (BEC) crossover [36, 37, 41, 44, 110] in three dimensional (3D) s-wave superfluids. Recent extensions of these ideas include trapped fermions [47, 48] and fermion-boson models [49, 50].

One of the next frontiers of exploration in ultracold Fermi systems is the search for superfluidity in higher angular momentum states ($\ell \neq 0$). Substantial experimental progress has been made recently [104, 105, 106, 107, 108, 109] in connection to p-wave ($\ell = 1$) cold Fermi gases, making them ideal candidates for the observation of novel triplet superfluid phases. These phases may be present not only in atomic, but also in nuclear (pairing

in nuclei), astrophysics (neutron stars), and condensed matter (organic superconductors) systems.

The tuning of p-wave interactions in ultracold Fermi gases was initially explored via p-wave Feshbach resonances in trap geometries for ^{40}K atoms in Ref. [104, 105] and ^{6}Li atoms in Ref. [106, 107]. Finding and sweeping through these resonances is difficult since they are much narrower than the s-wave case, because atoms interacting via higher angular momentum channels have to tunnel through a centrifugal barrier to couple to the bound state [105]. While losses due to two-body dipolar [106, 113] or three-body [104, 105] processes challenged earlier p-wave experiments, these losses were still present but were less dramatic in the very recent optical lattice experiment involving ^{40}K atoms and p-wave Feshbach resonances [108].

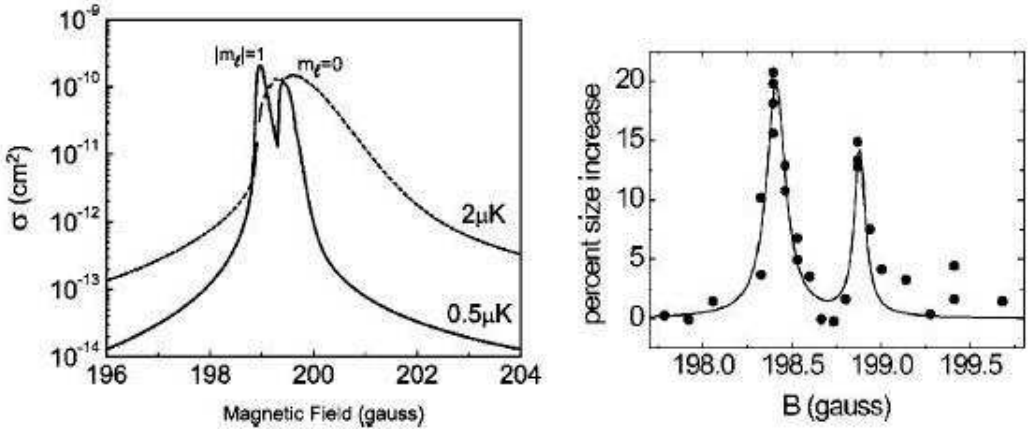

Figure 2.1: (a) Theoretical calculation of the thermally averaged elastic cross section for the p-wave FR, including all partial-wave projections $m_\ell = -1, 0, 1$. At low temperatures, the doublet splitting emerges clearly, but it is washed out a higher temperatures due to thermal broadening. The lower field resonance has $m_\ell = \pm 1$ and the higher field resonance has $m_\ell = 0$. (b) Experimental observation of the p-wave FR through heating of the gas, clearly showing the doublet feature of the p-wave resonance. The cloud started at $T = 0.34$mK and then was held at a constant magnetic field. Inelastic processes at the FR, three-body dominated, heat the cloud resulting in an increase in the measured size of the trapped cloud. (Adapted from [105].)

Furthermore, due to the magnetic dipole-dipole interaction between valence electrons of alkali atoms, the nonzero angular momentum Feshbach resonances corresponding to projections of angular momentum ℓ $[m_\ell = \pm\ell, \pm(\ell-1), ..., 0]$ are nondegenerate (separated from each other) with total number of $\ell+1$ resonances. In Fig.2.1, the lifting of degeneracy

is shown for a ^{40}K p-wave resonance [105]. Therefore, in principle, these resonances can be tuned and studied independently if the separation between them is larger than the experimental resolution. Since the ground state is highly dependent on the separation and detuning of these resonances, it is possible that p-wave superfluid phases can be studied from the BCS to the BEC regime. For sufficiently large splittings, it has been proposed [114, 115] that pairing occurs only in $m_\ell = 0$ and does not occur in the $m_\ell = \pm 1$ states. However, for small splittings, pairing occurs via a linear combination of the $m_\ell = 0$ and $m_\ell = \pm 1$ states. Thus, the $m_\ell = 0$ or $m_\ell = \pm 1$ resonances may be tuned and studied independently if the splitting is large enough in comparison to the experimental resolution.

The BCS to BEC evolution of d-wave ($\ell = 2$) superfluidity was discussed previously in the literature using continuum [116, 117, 118] and lattice [119, 120] descriptions in connection to high-T_c superconductivity. More recently, p-wave superfluidity was analyzed at $T = 0$ for single hyperfine state (SHS) systems in two dimensions (2D) [121, 122, 123], and for two hyperfine state (THS) systems in 3D [127] using fermion-only models. Furthermore, fermion-boson models were proposed to describe p-wave superfluidity at zero [114, 115] and finite temperature [128] in 3D.

In this chapter, I present a generalization of the zero and finite temperature analysis of both THS pseudo-spin singlet and SHS pseudo-spin triplet [122, 129] superfluidity in 3D within a fermion-only description. My main results are as follows.

Through an analysis of the low energy scattering amplitude within a T-matrix approach, I find that bound states occur only when the scattering parameter $a_\ell > 0$ for any ℓ. The energy of the bound states $E_{b,\ell}$ involves only the scattering length a_0 for $\ell = 0$. However, another parameter r_ℓ related to the interaction range $1/k_0$ is necessary to characterize $E_{b,\ell}$ for $\ell \neq 0$. Therefore, all superfluid properties for $\ell \neq 0$ depend strongly on k_0 and a_ℓ, while for $\ell = 0$ they depend strongly only on a_0 but weakly on k_0.

At zero temperature ($T = 0$), I study the possibility of a topological quantum phase transition in $\ell \neq 0$ atomic Fermi gases during the evolution from BCS to BEC regime [116, 117, 121, 122, 123, 114, 115, 129, 135]. I show that there is a fundamental difference between the $\ell = 0$ and $\ell \neq 0$ cases. In the s-wave ($\ell = 0$) case, there is no phase transition

as the magnetic field is tuned through the Feshbach resonance from the BCS to the BEC limit. That is, the zero temperature thermodynamic properties are analytic functions of the scattering length a_0 when the Feshbach resonance is crossed. In this case, the superfluid ground state does not change in any fundamental way as a_0 is varied. This has been noted in the condensed matter literature long ago [37, 41, 44, 110] and it is referred to as the BCS-BEC crossover problem. However, for $\ell \neq 0$, I show that there is a phase transition as the magnetic field is swept through the $\ell \neq 0$ Feshbach resonance. The phase transition does not occur when two-body bound states are first formed, but occurs when the many-body chemical potential crosses a critical value.

To show that such a zero temperature (quantum) phase transition occurs in $\ell \neq 0$, I calculate the order parameter, chemical potential, quasiparticle excitation spectrum, momentum distribution, atomic compressibility, low energy collective excitations and average Cooper pair size as a function of a_ℓ, and show that they are non-analytic at $T = 0$ when the chemical potential μ_ℓ crosses a critical value. The symmetry of the order parameter remains unchanged through the transition, as the ground state wavefunction experiences a major rearrangement of its analytic structure. In addition, the elementary excitations of the superfluid also change from gapless in the BCS side to fully gapped in the BEC side leading to qualitatively different thermodynamic properties in both sides. Thus, I conclude that there is a potentially observable BCS-BEC phase transition in $\ell \neq 0$ atomic Fermi gases in contrast to the BCS-BEC crossover already found in s-wave ($\ell = 0$) gases.

At finite temperatures, I develop a gaussian fluctuation theory near the critical temperature ($T \approx T_{c,\ell}$) to analyze the number of unbound, scattering and bound fermions as well as the chemical potential. I show that while the saddle point number equation is sufficient in weak coupling where all fermions are unbound, the fluctuation contributions have to be taken into account in order to recover the BEC physics in strong coupling where all fermions are bound.

I also derive the time-dependent Ginzburg-Landau (TDGL) functional near $T_{c,\ell}$ and extract the Ginzburg-Landau (GL) coherence length and time. I recover the usual TDGL equation for BCS superfluids in weak coupling, whereas in strong coupling I recover the

Gross-Pitaevskii (GP) equation for a weakly interacting dilute Bose gas. The TDGL equation exhibits anisotropic coherence lengths for $\ell \neq 0$ which become isotropic only in the BEC limit, in sharp contrast to the $\ell = 0$ case, where the coherence length is isotropic for all couplings. Furthermore, for any ℓ, the GL time is a complex number with a larger imaginary component for $\mu_\ell > 0$ reflecting the decay of Cooper pairs into the two-particle continuum with short lifetimes. However, the imaginary component vanishes for $\mu_\ell \leq 0$ and Cooper pairs become stable with long lifetimes above $T_{c,\ell}$.

The rest of the chapter is organized as follows. In Section 2.2, I analyze the interaction potential in both real and momentum space for nonzero orbital momentum channels. I introduce the imaginary-time functional integration formalism in Section 2.3, and obtain the self-consistency (order parameter and number) equations. There I also discuss the low energy scattering amplitude of a finite range interaction for all possible angular momentum channels, and relate the self-consistency equations to scattering parameters. In Section 2.4, I discuss the evolution from BCS to BEC superfluidity at zero temperature. There I analyze the order parameter, chemical potential, quasiparticle excitation spectrum, momentum distribution, atomic compressibility and ground state energy as a function of scattering parameters. I also discuss gaussian fluctuations and low energy collective excitations at zero temperature in Section 2.5. In Sec 2.6, I present the evolution of superfluidity from the BCS to the BEC regimes near the critical temperature. There I discuss the importance of gaussian fluctuations, and analyze the number of unbound, scattering and bound fermions, critical temperature and chemical potential as a function of scattering parameters. In Section 2.7, I derive TDGL equation and extract the GL coherence length and time. There, I recover the GL equation in the BCS and the GP equation in the BEC limit. A short summary of my conclusions is given in Section 2.8. Finally, I present in Appendices A.1 and A.2 the coefficients for the low frequency and long wavelength expansion of the action at zero and finite temperatures, respectively.

2.2 Generalized Hamiltonian

To describe a dilute Fermi gas in three dimensions, I start from the Hamiltonian ($\hbar = 1$)

$$H = \sum_{\mathbf{k},s_1} \xi(\mathbf{k}) a^\dagger_{\mathbf{k},s_1} a_{\mathbf{k},s_1} + \frac{1}{2\mathcal{V}} \sum_{\mathbf{k},\mathbf{k}',\mathbf{q}} \sum_{s_1,s_2,s_3,s_4} V^{s_3,s_4}_{s_1,s_2}(\mathbf{k},\mathbf{k}') b^\dagger_{s_1,s_2}(\mathbf{k},\mathbf{q}) b_{s_3,s_4}(\mathbf{k}',\mathbf{q}), \tag{2.1}$$

where s_n labels the pseudo-spins corresponding to trapped hyperfine states and $\mathcal{V}$ is the volume. These states are represented by the creation operator $a^\dagger_{\mathbf{k},s_1}$, and $b^\dagger_{s_1,s_2}(\mathbf{k},\mathbf{q}) = a^\dagger_{\mathbf{k}+\mathbf{q}/2,s_1} a^\dagger_{-\mathbf{k}+\mathbf{q}/2,s_2}$. Here, $\xi(\mathbf{k}) = \epsilon(\mathbf{k}) - \mu$ where $\epsilon(\mathbf{k}) = k^2/(2M)$ is the energy with M being the mass, and μ is the chemical potential of fermions.

The interaction term can be written in a separable form $V^{s_3,s_4}_{s_1,s_2}(\mathbf{k},\mathbf{k}') = \Gamma^{s_3,s_4}_{s_1,s_2} V(\mathbf{k},\mathbf{k}')$, where $\Gamma^{s_3,s_4}_{s_1,s_2}$ is the spin and $V(\mathbf{k},\mathbf{k}')$ is the spatial part, respectively. In the case of THS case, where $s_n \equiv (\uparrow,\downarrow)$, both pseudo-spin singlet and pseudo-spin triplet pairings are allowed. However, I concentrate on the pseudo-spin singlet THS state with

$$\Gamma^{s_3,s_4}_{s_1,s_2} = \Gamma^{s_3,s_4}_{s_1,s_2} \delta_{s_1,-s_2} \delta_{s_2,s_3} \delta_{s_3,-s_4} \delta_{s_4,s_1}. \tag{2.2}$$

In addition, I discuss the SHS case ($s_n \equiv \uparrow$), where only pseudo-spin triplet pairing is allowed, and the interaction is given by

$$\Gamma^{s_3,s_4}_{s_1,s_2} = \Gamma^{s_3,s_4}_{s_1,s_2} \delta_{s_1,s_2} \delta_{s_2,s_3} \delta_{s_3,s_4} \delta_{s_4,\uparrow}. \tag{2.3}$$

In this chapter, I analyze THS singlet and SHS triplet cases for all allowable angular momentum channels. THS triplet pairing is more involved due to the more complex nature of the vector order parameters, and is not discussed here.

The two fermion interaction can be expanded as

$$V(\mathbf{k},\mathbf{k}') = \int d^3\mathbf{r} V(r) e^{i(\mathbf{k}-\mathbf{k}')\cdot\mathbf{r}}, \tag{2.4}$$

and should have the necessary symmetry under the Parity operation, where the transformation $\mathbf{k} \to -\mathbf{k}$ or $\mathbf{k}' \to -\mathbf{k}'$ leads to $V(\mathbf{k},\mathbf{k}')$ for singlet, and $-V(\mathbf{k},\mathbf{k}')$ for triplet pairing. Furthermore, $V(\mathbf{k},\mathbf{k}')$ is invariant under the transformation $(\mathbf{k},\mathbf{k}') \to (-\mathbf{k},-\mathbf{k}')$, and $V(\mathbf{k},\mathbf{k}')$ reflects the Pauli exclusion principle.

In order to obtain an approximate expression for the atomic interaction potential, I use the Fourier expansion of a plane wave in 3D

$$e^{i\mathbf{k}\cdot\mathbf{r}} = 4\pi \sum_{\ell,m_\ell} i^\ell j_\ell(kr) Y^*_{\ell,m_\ell}(\widehat{\mathbf{r}}) Y_{\ell,m_\ell}(\widehat{\mathbf{k}}), \tag{2.5}$$

where $j_\ell(kr)$ is the spherical Bessel function of order ℓ and $Y_{\ell,m_\ell}(\widehat{\mathbf{k}})$ is the spherical harmonic of order (ℓ, m_ℓ), in Eq. 2.4 to evaluate the matrix elements of the interaction potential in $\mathbf{k}$-space

$$V(\mathbf{k},\mathbf{k}') = 4\pi \sum_{\ell,m_\ell} V_\ell(k,k') Y_{\ell,m_\ell}(\widehat{\mathbf{k}}) Y^*_{\ell,m_\ell}(\widehat{\mathbf{k}'}). \tag{2.6}$$

Here, $\sum_{\ell,m_\ell} = \sum_{\ell=0}^{\infty} \sum_{m_\ell=-\ell}^{\ell}$, and $\widehat{\mathbf{k}}$ denotes the angular dependence $(\theta_{\mathbf{k}}, \phi_{\mathbf{k}})$. The (k,k') dependent coefficients $V_\ell(k,k')$ are related to the real space potential $V(r)$ through the relation

$$V_\ell(k,k') = 4\pi \int_0^\infty dr r^2 j_\ell(kr) j_\ell(k'r) V(r). \tag{2.7}$$

The index ℓ labels angular momentum states in 3D, with $\ell = 0, 1, 2, ...$ corresponding to $s, p, d, ...$ channels, respectively.

In the long wavelength limit ($k \to 0$), one can show that the k dependence of this potential becomes exactly separable. In fact, for $kr \ll 1$ and $k'r \ll 1$, the asymptotic expression of the spherical Bessel function for small arguments can be used, giving $V_\ell(k,k') = C_\ell k^\ell k'^\ell$, with the coefficient C_ℓ dependent on the particular choice of the real space potential. In the opposite limit, where $kr \gg 1$ and $k'r \gg 1$, the potential is not separable. In this case, $V_\ell(k,k')$ mixes different k and k', and shows an oscillatory behavior (which is dependent on the exact form of $V(r)$) with a decaying envelope that is proportional to $1/(kk')$.

Under these circumstances, I choose to study a model potential that contains most of the features described above. One possibility is to retain only one of the ℓ terms in Eq. (2.6), by assuming that the dominant contribution to the scattering process between fermionic atoms occurs in the ℓth angular momentum channel. This assumption may be experimentally relevant since atom-atom dipole interactions split different angular momentum channels such that they may be tuned independently. Using the properties discussed above, I write

$$V_\ell(k,k') = -\lambda_\ell \Gamma_\ell(k) \Gamma_\ell(k'), \tag{2.8}$$

where $\lambda_\ell > 0$ is the interaction strength, and the function

$$\Gamma_\ell(k) = \frac{(k/k_0)^\ell}{(1 + k^2/k_0^2)^{\frac{\ell+1}{2}}} \tag{2.9}$$

describes the momentum dependence. Here, $k_0 \sim R_0^{-1}$ plays the role of the interaction range in real space and sets the scale at small and large momenta. In addition, the diluteness condition ($n_\ell R_0^3 \ll 1$) requires $(k_0/k_\mathrm{F})^3 \gg 1$, where n_ℓ is the density of atoms and k_F is the Fermi momentum. This function reduces to $\Gamma_\ell(k) \sim k^\ell$ for small k, and behaves as $\Gamma_\ell(k) \sim 1/k$ for large k, which guarantees the correct qualitative behavior expected for $V_\ell(k, k')$ according to the analysis above.

2.3 Functional Integral Formalism

In this section, I describe in detail the THS singlet case for even angular momentum states. A similar approach for the SHS triplet case for odd angular momentum states can be found in Ref. [122, 129], and therefore, I do not repeat the same analysis here. However, I point out the main differences between the two cases whenever it is necessary.

2.3.1 THS Singlet Effective Action

I would like to warn the reader that this section is rather technical, and it may be skipped entirely until Section 2.3.2 if desired.

In the imaginary-time functional integration formalism ($\hbar = k_\mathrm{B} = 1$, and $\beta = 1/T$), the partition function for the THS singlet case can be written as

$$Z_\ell = \int D(a^\dagger, a) e^{-S_\ell} \tag{2.10}$$

where S_ℓ is the action, and it is given by

$$S_\ell = \int_0^\beta d\tau \left[\sum_{\mathbf{k},s} a^\dagger_{\mathbf{k},s}(\tau)(\partial_\tau) a_{\mathbf{k},s}(\tau) + H_\ell(\tau) \right] \tag{2.11}$$

Here, τ is the imaginary time and $a^\dagger_{\mathbf{k},\sigma}(\tau)$ and $a_{\mathbf{k},\sigma}(\tau)$ are Grassmann variables [100, 124]. The Hamiltonian for the ℓ^th angular momentum channel is

$$H_\ell(\tau) = \sum_{\mathbf{k},s} \xi_\ell(\mathbf{k}) a^\dagger_{\mathbf{k},s}(\tau) a_{\mathbf{k},s}(\tau) - \frac{4\pi\lambda_\ell}{\mathcal{V}} \sum_{\mathbf{q},m_\ell} b^\dagger_{\ell,m_\ell}(\mathbf{q},\tau) b_{\ell,m_\ell}(\mathbf{q},\tau), \tag{2.12}$$

where $b_{\ell,m_\ell}(\mathbf{q},\tau) = \sum_{\mathbf{k}} \Gamma_\ell(k) Y_{\ell,m_\ell}(\widehat{\mathbf{k}}) a_{\mathbf{k}+\mathbf{q}/2,\uparrow} a_{\mathbf{k}-\mathbf{q}/2,\downarrow}$ and $\xi_\ell(\mathbf{k}) = \epsilon(\mathbf{k}) - \mu_\ell$. I first introduce the Nambu spinor $\psi^\dagger(p) = (a^\dagger_{p,\uparrow}, a_{-p,\downarrow})$, where $p = (\mathbf{k}, iw_j)$ denotes both momentum and fermionic Matsubara frequency $w_j = (2j+1)\pi/\beta$, and use a Hubbard-Stratonovich transformation [125, 126]

$$e^{-\sum_q \lambda |b(q)|^2} = \int D[\Phi^\dagger, \Phi] e^{\sum_q \left[\frac{|\Phi(q)|^2}{\lambda} + b^\dagger(q)\Phi(q) + \Phi^\dagger(q) b(q) \right]} \tag{2.13}$$

to decouple fermionic and bosonic degrees of freedom. The resulting integration have Gaussian form in fermionic fields , and it can be easily performed. Integration over the fermionic part $[D(\psi^\dagger, \psi)]$ leads to the action

$$S^{\text{eff}}_\ell = \beta \sum_{q,m_\ell} \frac{|\Phi_{\ell,m_\ell}(q)|^2}{4\pi \mathcal{V}^{-1} \lambda_\ell} + \sum_{p,q} \left[\beta \xi_\ell(\mathbf{k}) \delta_{q,0} - \text{Tr} \ln \left(\mathbf{G}_\ell / \beta \right)^{-1} \right], \tag{2.14}$$

where $q = (\mathbf{q}, iv_j)$, with bosonic Matsubara frequency $v_j = 2\pi j/\beta$. Here,

$$\mathbf{G}^{-1}_\ell = \Phi^*_\ell(q) \Gamma_\ell(p) \sigma_- + \Phi_\ell(-q) \Gamma_\ell(p) \sigma_+ + \left[i w_j \sigma_0 - \xi_\ell(\mathbf{k}) \sigma_3 \right] \delta_{q,0} \tag{2.15}$$

is the inverse Nambu propagator, $\Phi_\ell(q) = \sum_{m_\ell} \Phi_{\ell,m_\ell}(q) Y_{\ell,m_\ell}(\widehat{\mathbf{k}})$ is the bosonic field, and $\sigma_\pm = (\sigma_1 \pm \sigma_2)/2$ and σ_i is the Pauli spin matrix. The bosonic field

$$\Phi_{\ell,m_\ell}(q) = \Delta_{\ell,m_\ell} \delta_{q,0} + \Lambda_{\ell,m_\ell}(q) \tag{2.16}$$

has τ-independent Δ_{ℓ,m_ℓ} and τ-dependent $\Lambda_{\ell,m_\ell}(q)$ parts.

Performing an expansion in S^{eff}_ℓ to quadratic order in $\Lambda_{\ell,m_\ell}(q)$ leads to

$$S^{\text{gauss}}_\ell = S^{\text{sp}}_\ell + \frac{\beta}{2} \sum_{q,m_\ell,m'_\ell} \widetilde{\Lambda}^\dagger_{\ell,m_\ell}(q) \mathbf{F}^{-1}_{\ell,m_\ell,m'_\ell}(q) \widetilde{\Lambda}_{\ell,m'_\ell}(q), \tag{2.17}$$

where the vector $\widetilde{\Lambda}^\dagger_{\ell,m_\ell}(q)$ is such that $\widetilde{\Lambda}^\dagger_{\ell,m_\ell}(q) = [\Lambda^\dagger_{\ell,m_\ell}(q), \Lambda_{\ell,m_\ell}(-q)]$, and $\mathbf{F}^{-1}_{\ell,m_\ell,m'_\ell}(q)$ are the matrix elements of the inverse fluctuation propagator matrix $\mathbf{F}^{-1}_\ell(q)$. Furthermore, S^{sp}_ℓ is the saddle point action given by

$$S^{\text{sp}}_\ell = \beta \sum_{m_\ell} \frac{|\Delta_{\ell,m_\ell}|^2}{4\pi \mathcal{V}^{-1} \lambda_\ell} + \sum_{p} \left[\beta \xi_\ell(\mathbf{k}) - \text{Tr} \ln \left(\mathbf{G}^{\text{sp}}_\ell / \beta \right)^{-1} \right], \tag{2.18}$$

and the saddle point inverse Nambu propagator is

$$(\mathbf{G}^{\text{sp}}_\ell)^{-1} = i w_j \sigma_0 - \xi_\ell(\mathbf{k}) \sigma_3 + \Delta^*_\ell(\mathbf{k}) \sigma_- + \Delta_\ell(\mathbf{k}) \sigma_+, \tag{2.19}$$

with saddle point order parameter

$$\Delta_\ell(\mathbf{k}) = \Gamma_\ell(k) \sum_{m_\ell} \Delta_{\ell,m_\ell} Y_{\ell,m_\ell}(\widehat{\mathbf{k}}). \tag{2.20}$$

Notice that, $\Delta_\ell(\mathbf{k})$ may involve several different m_ℓ for a given angular momentum channel ℓ.

The matrix elements of the inverse fluctuation matrix $\mathbf{F}_\ell^{-1}(q)$ are given by

$$\begin{aligned}
(\mathbf{F}^{-1}_{\ell,m_\ell,m'_\ell})_{11} &= -\frac{1}{\beta}\sum_p (\mathbf{G}^{\rm sp}_\ell)_{11}(\frac{q}{2}+p)(\mathbf{G}^{\rm sp}_\ell)_{11}(\frac{q}{2}-p)\Gamma^2_\ell(p) Y_{\ell,m_\ell}(\widehat{\mathbf{k}}) Y^*_{\ell,m'_\ell}(\widehat{\mathbf{k}}) \\
&+ \frac{\delta_{m_\ell,m'_\ell}\mathcal{V}}{4\pi\lambda_\ell}, \qquad (2.21) \\
(\mathbf{F}^{-1}_{\ell,m_\ell,m'_\ell})_{12} &= \frac{1}{\beta}\sum_p (\mathbf{G}^{\rm sp}_\ell)_{12}(\frac{q}{2}+p)(\mathbf{G}^{\rm sp}_\ell)_{12}(\frac{q}{2}-p)\Gamma^2_\ell(p) Y_{\ell,m_\ell}(\widehat{\mathbf{k}}) Y^*_{\ell,m'_\ell}(\widehat{\mathbf{k}}). \qquad (2.22)
\end{aligned}$$

Notice that while $(\mathbf{F}^{-1}_{\ell,m_\ell,m'_\ell})_{12}(q) = (\mathbf{F}^{-1}_{\ell,m_\ell,m'_\ell})_{21}(q)$ are even under the transformations $\mathbf{q} \to -\mathbf{q}$ and $iv_j \to -iv_j$; $(\mathbf{F}^{-1}_{\ell,m_\ell,m'_\ell})_{11}(q) = (\mathbf{F}^{-1}_{\ell,m_\ell,m'_\ell})_{22}(-q)$ are even only under $\mathbf{q} \to -\mathbf{q}$, having no defined parity in iv_j.

The Gaussian action Eq. (2.17) leads to the thermodynamic potential $\Omega^{\rm gauss}_\ell = \Omega^{\rm sp}_\ell + \Omega^{\rm fluct}_\ell$, where

$$\begin{aligned}
\Omega^{\rm sp}_\ell &= \sum_{m_\ell} \frac{|\Delta_{\ell,m_\ell}|^2}{4\pi\mathcal{V}^{-1}\lambda_\ell} + \sum_{\mathbf{k}} \left\{ \xi_\ell(\mathbf{k}) - E_\ell(\mathbf{k}) - \frac{2}{\beta}\ln\left[1+\exp(-\beta E_\ell(\mathbf{k}))\right] \right\}, \qquad (2.23) \\
\Omega^{\rm fluct}_\ell &= \frac{1}{\beta}\sum_q \ln\det[\mathbf{F}^{-1}_\ell(q)/(2\beta)] \qquad (2.24)
\end{aligned}$$

are the saddle point and fluctuation contributions, respectively. Here,

$$E_\ell(\mathbf{k}) = \left[\xi^2_\ell(\mathbf{k}) + |\Delta_\ell(\mathbf{k})|^2\right]^{\frac{1}{2}}, \tag{2.25}$$

is the quasiparticle energy spectrum. Having completed the presentation of the functional integral formalism, I discuss next the self-consistency equations for the order parameter and the chemical potential.

2.3.2 Self-consistency Equations

The saddle point condition $\delta S^{\rm sp}_\ell / \delta \Delta^*_{\ell,m_\ell} = 0$ imposed on Eq. (2.18) leads to the order parameter equation

$$\frac{\Delta_{\ell,m_\ell}}{4\pi\lambda_\ell} = \frac{1}{\mathcal{V}}\sum_{\mathbf{k}} \frac{\Delta_\ell(\mathbf{k})\Gamma_\ell(k) Y^*_{\ell,m_\ell}(\widehat{\mathbf{k}})}{2E_\ell(\mathbf{k})} \tanh\frac{\beta E_\ell(\mathbf{k})}{2}, \tag{2.26}$$

which can be expressed in terms of experimentally relevant parameters via the T-matrix approach [127].

The low energy two-body scattering amplitude between a pair of fermions in the ℓ^{th} angular momentum channel is given by [130]

$$f_\ell(k) = -\frac{k^{2\ell}}{1/a_\ell - r_\ell k^2 + ik^{2\ell+1}}, \tag{2.27}$$

where $r_\ell < 0$ and a_ℓ are the effective range and scattering parameter, respectively. Here r_ℓ has dimensions of $L^{2\ell-1}$ and a_ℓ has dimensions of $L^{2\ell+1}$, where L is the length of the system. The energy of the two-body bound state is determined from the poles of $f_\ell(k \to i\kappa_\ell)$, and is given by $E_{\text{b},\ell} = -\kappa_\ell^2/(2M)$. Bound states occur when $a_0 > 0$ for $\ell = 0$, and $a_{\ell\neq 0} r_{\ell\neq 0} < 0$ for $\ell \neq 0$. Since $r_\ell < 0$, bound states occur only when $a_\ell > 0$ for all ℓ, in which case the binding energies are given by

$$E_{\text{b},0} = -\frac{1}{Ma_0^2}, \tag{2.28}$$

$$E_{\text{b},\ell\neq 0} = \frac{1}{Ma_\ell r_\ell}. \tag{2.29}$$

Notice that, only a single parameter (a_0) is sufficient to describe the low energy two-body problem for $\ell = 0$, while two parameters (a_ℓ, r_ℓ) are necessary to describe the same problem for $\ell \neq 0$. The point at which $1/(k_{\text{F}}^{2\ell+1} a_\ell) = 0$ corresponds to the threshold for the formation of a two-body bound state in vacuum. Beyond this threshold, a_0 for $\ell = 0$ and $|a_{\ell\neq 0} r_{\ell\neq 0}|$ for $\ell \neq 0$ are the size of the bound states.

For any ℓ, the two-body scattering amplitude is related to the T-matrix via

$$f_\ell(k) = -\frac{M}{4\pi} T_\ell[k, k; 2\epsilon(\mathbf{k}) + i0^+], \tag{2.30}$$

where the T-matrix is given by

$$T(\mathbf{k}, \mathbf{k}', E) = V(\mathbf{k}, \mathbf{k}') + \frac{1}{\mathcal{V}} \sum_{\mathbf{k}''} \frac{V(\mathbf{k}, \mathbf{k}'') T(\mathbf{k}'', \mathbf{k}', E)}{E - 2\epsilon(\mathbf{k}'') + i0^+}.$$

Using the spherical harmonics expansion for both $V(\mathbf{k}, \mathbf{k}')$ and $T(\mathbf{k}, \mathbf{k}', E)$ leads to two coupled equations,

$$\frac{1}{\lambda_\ell} = -\frac{M}{4\pi k_0^{2\ell} a_\ell} + \frac{1}{\mathcal{V}} \sum_{\mathbf{k}} \frac{\Gamma_\ell^2(k)}{2\epsilon(\mathbf{k})}, \tag{2.31}$$

$$r_{\ell\neq 0} = -\frac{\pi k_0^{2\ell}}{M^2 \mathcal{V}} \sum_{\mathbf{k}} \frac{\Gamma_\ell^2(k)}{\epsilon^2(\mathbf{k})} - \frac{\ell + 1}{k_0^2 a_\ell}, \tag{2.32}$$

relating λ_ℓ and k_0 to a_ℓ and r_ℓ. Except for notational differences, notice that these relations are related to recent results found in the literature [127]. After performing momentum integrations I obtain

$$k_0^{2\ell+1} a_\ell = \frac{M k_0 \lambda_\ell \sqrt{\pi}}{M k_0 \lambda_\ell \widetilde{\phi}_\ell - 4\pi\sqrt{\pi}}, \tag{2.33}$$

$$-\frac{1}{a_{\ell\neq 0} r_{\ell\neq 0}} = \frac{2k_0^2\sqrt{\pi}}{k_0^{2\ell+1} a_\ell \phi_\ell + 2(\ell+1)\sqrt{\pi}}, \tag{2.34}$$

where $\widetilde{\phi}_\ell = \Gamma(\ell+1/2)/\Gamma(\ell+1)$ and $\phi_\ell = \Gamma(\ell-1/2)/\Gamma(\ell+1)$. Here $\Gamma(x)$ is the Gamma function. Notice that, $k_0^{2\ell+1} a_\ell$ diverges and changes sign when $M k_0 \lambda_\ell \widetilde{\phi}_\ell = 4\pi\sqrt{\pi}$, which corresponds to the critical coupling for Feshbach resonances (the unitarity limit).

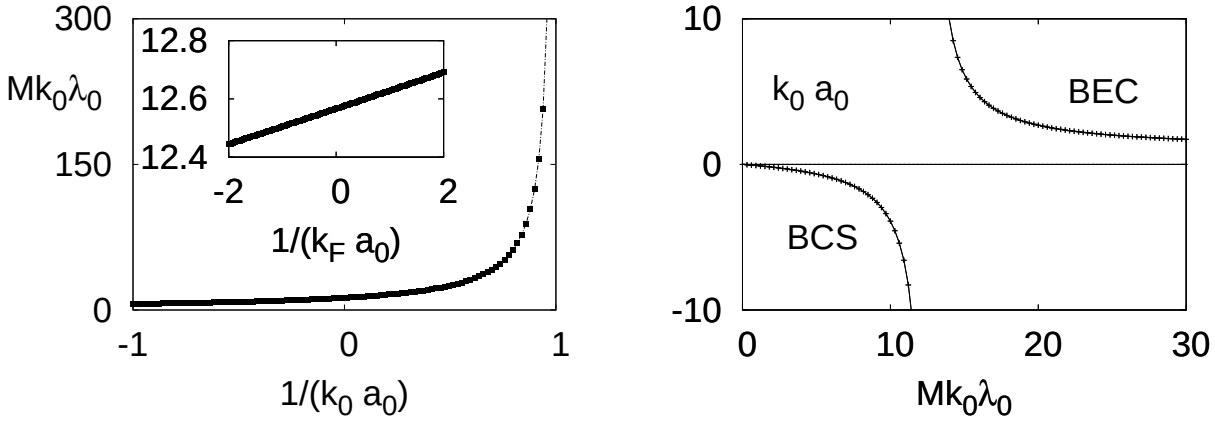

Figure 2.2: Plots of original interaction strength $Mk_0\lambda_0$ versus scattering parameter $1/(k_0 a_0)$. The inset shows $Mk_0\lambda_0$ versus $1/(k_{\rm F} a_0)$ for $k_0 \approx 200 k_{\rm F}$. Notice that the scattering length is small and negative (positive) in the weak (strong) interaction BCS (BEC) limit, and it diverges in the intermediate region where it also changes sign. Therefore, tuning the strength of the external magnetic field in atomic physics experiments (see Fig. 1.7) is equivalent to increasing the strength of the attractive interparticle interaction.

In addition, the scattering parameter has a maximum value in the zero ($\lambda_\ell \to 0$) and a minimum value in the infinite ($\lambda_\ell \to \infty$) coupling limits given respectively by

$$k_0^{2\ell+1} a_{\ell\neq 0}^{\rm max} = -\frac{2(\ell+1)\sqrt{\pi}}{\phi_\ell}, \ (a_\ell < 0), \tag{2.35}$$

$$k_0^{2\ell+1} a_\ell^{\rm min} = \frac{\sqrt{\pi}}{\widetilde{\phi}_\ell}, \ (a_\ell > 0). \tag{2.36}$$

The first condition Eq. (2.35) (when $\lambda_\ell \to 0$) follows from Eq. (2.34) where $r_{\ell\neq 0} < 0$ has to be satisfied for all possible $a_{\ell\neq 0}$. However, there is no condition on r_0 for $\ell = 0$, and

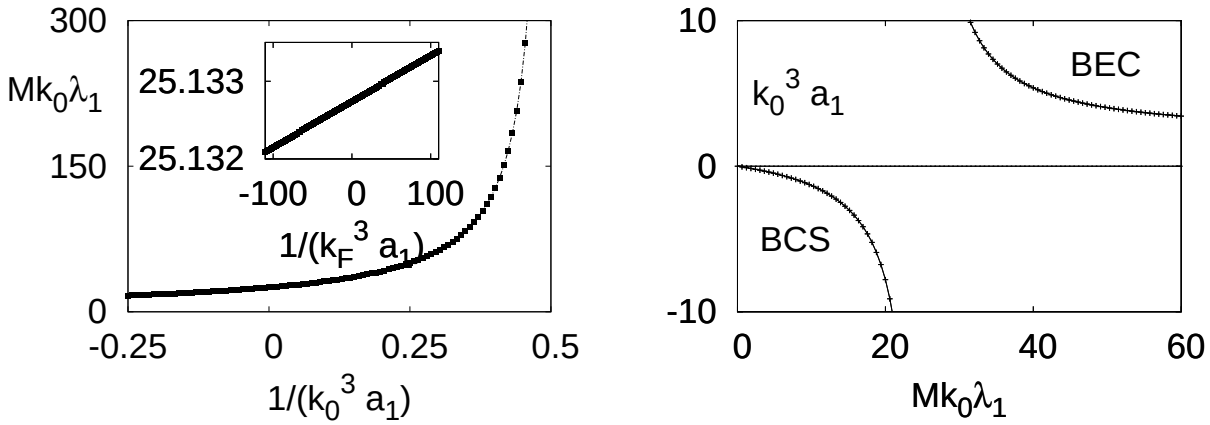

Figure 2.3: Plots of original interaction strength $Mk_0\lambda_1$ versus scattering parameter $1/(k_0^3 a_1)$. The inset shows $Mk_0\lambda_1$ versus $1/(k_{\rm F}^3 a_1)$ for $k_0 \approx 200 k_{\rm F}$. These figures are valid when $k_0^3|a_1| \geq 4$ in the BCS limit. Notice that the scattering parameter is small and negative (positive) in the weak (strong) interaction BCS (BEC) limit, and it diverges in the intermediate region where it also changes sign. Therefore, tuning the strength of the external magnetic field in atomic physics experiments (see Fig. 1.7) is equivalent to increasing the strength of the attractive interparticle interaction.

$k_0 a_0^{\rm max} = 0$ in the BCS limit. The second condition Eq. (2.36) (when $\lambda_\ell \to \infty$) follows from Eq. (2.33), which is valid for all possible ℓ. The minimum a_ℓ for a finite range interaction is associated with the Pauli principle, which prevents two identical fermions to occupy the same state. Thus, while the scattering parameter can not be arbitrarily small for a finite range potential, it may go to zero as $k_0 \to \infty$. Furthermore, the binding energy is given by

$$E_{{\rm b},\ell\neq 0} = -\frac{2\sqrt{\pi}}{M k_0^{2\ell-1} a_\ell \phi_\ell}, \tag{2.37}$$

when $k_0^{2\ell+1} a_\ell \phi_\ell \gg 2(\ell+1)\sqrt{\pi}$.

In Fig. 2.2, I plot the original interaction strength $Mk_0\lambda_0$ versus the scattering parameter $k_0 a_0$ for the s-wave ($\ell = 0$) channel. Notice that, $k_0|a_0| \to 0$ in the BCS and $k_0 a_0 \to 1$ in the BEC limit. A divergence in $k_0 a_0$ corresponds to an s-wave Feshbach resonance occurring at $Mk_0\lambda_0 = 4\pi$.

In Fig. 2.3, I plot the original interaction strength $Mk_0\lambda_1$ versus the scattering parameter $k_0^3 a_1$ for the p-wave ($\ell = 1$) channel. Notice that, $k_0^3|a_1| \to 4$ in the BCS and $k_0^3 a_1 \to 2$ in the BEC limit. A divergence in $k_0^3 a_1$ corresponds to a p-wave Feshbach resonance occurring at $Mk_0\lambda_1 = 8\pi$.

Thus, the order parameter equation in terms of the scattering parameter is rewritten as

$$\frac{M\mathcal{V}\Delta_{\ell,m_\ell}}{16\pi^2 k_0^{2\ell} a_\ell} = \sum_{\mathbf{k},m'_\ell} \left[\frac{1}{2\epsilon(\mathbf{k})} - \frac{\tanh[\beta E_\ell(\mathbf{k})/2]}{2E_\ell(\mathbf{k})}\right] \Delta_{\ell,m'_\ell} \Gamma_\ell^2(k) Y^*_{\ell,m_\ell}(\widehat{\mathbf{k}}) Y_{\ell,m'_\ell}(\widehat{\mathbf{k}}). \tag{2.38}$$

This equation is valid for both THS pseudo-spin singlet and SHS pseudo-spin triplet states. However, there is one important difference between pseudo-spin singlet and pseudo-spin triplet states. For pseudo-spin singlet states, the order parameter is a scalar function of $\mathbf{k}$, while it is a vector function for pseudo-spin triplet states discussed next.

In general, the triplet order parameter can be written in the standard form [131]

$$\mathbf{O}_\ell(\mathbf{k}) = \begin{pmatrix} -d_\ell^x(\mathbf{k}) + id_\ell^y(\mathbf{k}) & d_\ell^z(\mathbf{k}) \\ d_\ell^z(\mathbf{k}) & d_\ell^x(\mathbf{k}) + id_\ell^y(\mathbf{k}) \end{pmatrix}, \tag{2.39}$$

where the vector $d_\ell(\mathbf{k}) = [d_\ell^x(\mathbf{k}), d_\ell^y(\mathbf{k}), d_\ell^z(\mathbf{k})]$ is an odd function of $\mathbf{k}$. Therefore, all up-up, down-down and up-down components may exist for a THS pseudo-spin triplet interaction. However, in the SHS pseudo-spin triplet case only the up-up or down-down component may exist leading to $\Delta_\ell(\mathbf{k}) \propto (\mathbf{O}_\ell)_{s_1 s_1}(\mathbf{k})$. Thus, for the up-up case $d_\ell^z(\mathbf{k}) = 0$ and $d_\ell^x(\mathbf{k}) = -id_\ell^y(\mathbf{k})$, leading to $d_\ell(\mathbf{k}) = d_\ell^x(\mathbf{k})(1, i, 0)$, which breaks time reversal symmetry, as expected from a fully spin polarized state. The corresponding down-down state has $d_\ell(\mathbf{k}) = d_\ell^x(\mathbf{k})(1, -i, 0)$. Furthermore, the simplified form of the SHS triplet order parameter allows a treatment similar to that of THS singlet states. However, it is important to mention that the THS triplet case can be investigated using my approach, but the treatment is more complicated.

The order parameter equation has to be solved self-consistently with the number equation $N_\ell = -\partial\Omega_\ell/\partial\mu_\ell$ where Ω_ℓ is the full thermodynamic potential defined in Eqs. (2.23) and (2.24). In the approximations used,

$$N_\ell \approx N_\ell^{\text{gauss}} = N_\ell^{\text{sp}} + N_\ell^{\text{fluct}} \tag{2.40}$$

has two contributions. The saddle point contribution to the number equation is

$$N_\ell^{\text{sp}} = \sum_{\mathbf{k},s} n_\ell(\mathbf{k}), \tag{2.41}$$

where $n_\ell(\mathbf{k})$ is the momentum distribution given by

$$n_\ell(\mathbf{k}) = \frac{1}{2}\left[1 - \frac{\xi_\ell(\mathbf{k})}{E_\ell(\mathbf{k})}\tanh\frac{\beta E_\ell(\mathbf{k})}{2}\right]. \tag{2.42}$$

For the SHS triplet case, the summation over s is not present in $N_\ell^{\rm sp}$. The fluctuation contribution to the number equation is

$$N_\ell^{\rm fluct} = -\frac{1}{\beta}\sum_q \frac{\partial[\det \mathbf{F}_\ell^{-1}(q)]/\partial\mu_\ell}{\det \mathbf{F}_\ell^{-1}(q)}, \tag{2.43}$$

where $\mathbf{F}_\ell^{-1}(q)$ is the inverse fluctuation matrix defined in Eq. (2.21) and (2.22).

In the rest of the chapter, I analyze analytically the superfluid properties at zero temperature (ground state) and near the critical temperatures for THS singlet (only even ℓ) and SHS triplet (only odd ℓ) cases. In addition, I analyze numerically the s-wave ($\ell = 0$) channel of THS singlet and p-wave ($\ell = 1$) channel of SHS triplet cases, which are currently of intense theoretical and experimental interest in ultracold Fermi atoms.

2.4 BCS to BEC Evolution at $T = 0$

At low temperatures, the saddle point self-consistent (order parameter and number) equations are sufficient to describe ground state properties in the weak coupling BCS and strong coupling BEC limits [37]. However, fluctuation corrections to the number equation may be important in the intermediate regime [132].

Ground state properties ($T = 0$) are investigated by solving saddle point self-consistency (order parameter and number) equations to obtain Δ_{ℓ,m_ℓ} and μ_ℓ, which are discussed next.

2.4.1 Order Parameter and Chemical Potential

I discuss in this section Δ_{ℓ,m_ℓ} and μ_ℓ. In weak coupling, I first introduce a shell about the Fermi energy $|\xi_\ell(\mathbf{k})| \leq w_{\rm D}$ such that $\epsilon_{\rm F} \gg w_{\rm D} \gg \Delta_\ell(\mathbf{k}_{\rm F})$, inside of which one may ignore the 3D density of states factor ($\sqrt{\epsilon/\epsilon_{\rm F}}$) and outside of which one may ignore $\Delta_\ell(\mathbf{k})$. While in sufficiently strong coupling, I use $|\xi_\ell(\mathbf{k})| \gg |\Delta_\ell(\mathbf{k})|$ to derive the analytic results discussed below. It is important to notice that, in strictly weak and strong coupling, the self-consistency equations Eq. (2.41) and (2.38) are decoupled, and play reversed roles. In

weak (strong) coupling the order parameter equation determines Δ_{ℓ,m_ℓ} (μ_ℓ) and the number equation determines μ_ℓ (Δ_{ℓ,m_ℓ}).

In weak coupling, the number equation Eq. (2.41) leads to

$$\mu_\ell = \epsilon_{\rm F} \tag{2.44}$$

for any ℓ where $\epsilon_{\rm F} = k_{\rm F}^2/(2M)$ is the Fermi energy. In strong coupling, the order parameter equation Eq. (2.38) leads to

$$\mu_0 = -\frac{1}{2Ma_0^2}, \tag{2.45}$$

$$\mu_{\ell\neq 0} = -\frac{\sqrt{\pi}}{Mk_0^{2\ell-1}a_\ell\phi_\ell}, \tag{2.46}$$

where $\phi_\ell = \Gamma(\ell-1/2)/\Gamma(\ell+1)$ and $\Gamma(x)$ is the Gamma function. This calculation requires that $a_0k_0 > 1$ for $\ell = 0$ and that $k_0^{2\ell+1}a_\ell\phi_\ell > (\ell+1)\sqrt{\pi}$ for $\ell \neq 0$ for the order parameter equation to have a solution with $\mu_\ell < 0$ in the strong coupling limit. In the BEC limit $\mu_0 = -k_0^2/[2M(k_0a_0-1)^2]$ for $\ell = 0$. Notice that, $\mu_0 = -1/(2Ma_0^2)$ when $k_0a_0 \gg 1$ [or $|\mu_0| \ll \epsilon_0 = k_0^2/(2M)$], and thus, I recover the contact potential ($k_0 \to \infty$) result. In the same spirit, to obtain the expressions in Eq. (2.45) and (2.46), I assumed $|\mu_\ell| \ll \epsilon_0$. Notice that, $\mu_\ell = E_{{\rm b},\ell}/2$ in this limit for any ℓ.

On the other hand, the solution of the order parameter equation in the weak coupling limit is

$$|\Delta_{0,0}| = 16\sqrt{\pi}\epsilon_{\rm F}\exp\left[-2+\frac{\pi}{2}\frac{k_{\rm F}}{k_0}-\frac{\pi}{2k_{\rm F}|a_0|}\right], \tag{2.47}$$

$$|\Delta_{\ell\neq 0,m_\ell}| \sim \left(\frac{k_0}{k_{\rm F}}\right)^\ell \epsilon_{\rm F}\exp\left[t_\ell\left(\frac{k_0}{k_{\rm F}}\right)^{2\ell-1}-\frac{\pi}{2k_{\rm F}^{2\ell+1}|a_\ell|}\right], \tag{2.48}$$

where $t_1 = \pi/4$ and $t_{\ell>1} = \pi 2^{\ell+1}(2\ell-3)!!/\ell!$. These expressions are valid only when the exponential terms are small. Therefore, they suggest that the range of BCS to unitarity region in terms of $1/(2k_{\rm F}^{2\ell+1}|a_\ell|)$ is of order 1 for $\ell = 0$ and of order $(k_0/k_{\rm F})^{2\ell-1}$ for $\ell \neq 0$. The solution of the number equation in the strong coupling limit is

$$|\Delta_{0,0}| = 8\epsilon_{\rm F}\left(\frac{\mu_0}{9\epsilon_{\rm F}}\right)^{\frac{1}{4}}, \tag{2.49}$$

$$\sum_{m_\ell}|\Delta_{\ell\neq 0,m_\ell}|^2 = \frac{64\sqrt{\pi}}{3\phi_\ell}\epsilon_{\rm F}(\epsilon_{\rm F}\epsilon_0)^{\frac{1}{2}} \tag{2.50}$$

to order μ_ℓ/ϵ_0, where I assumed that $|\xi_\ell(\mathbf{k})| \gg |\Delta_\ell(\mathbf{k})|$ for sufficiently strong couplings with $|\mu_\ell| \ll \epsilon_0$.

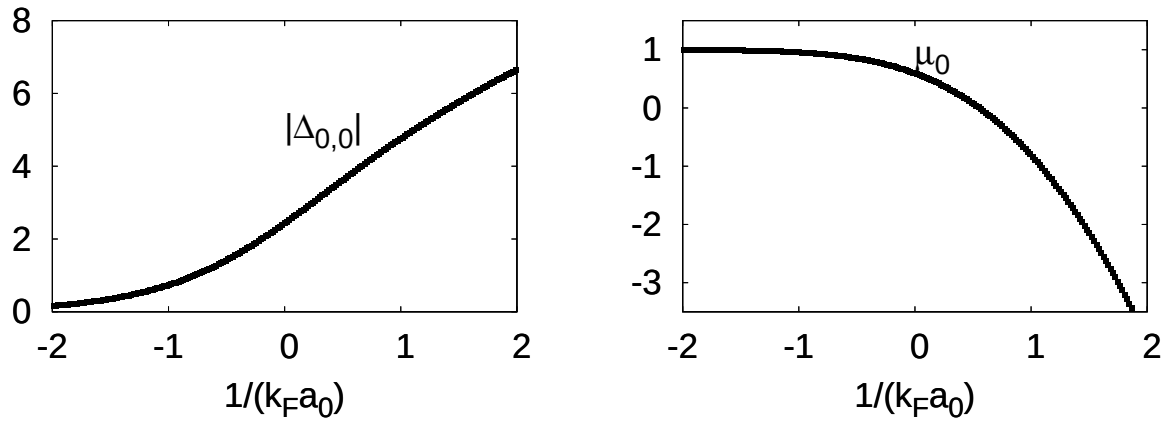

Figure 2.4: Plots of (a) order parameter $\Delta_{\rm r} = |\Delta_{0,0}|/\epsilon_{\rm F}$ and (b) chemical potential $\mu_{\rm r} = \mu_0/\epsilon_{\rm F}$ versus interaction strength $1/(k_{\rm F}a_0)$ for $k_0 \approx 200k_{\rm F}$. For $\ell = 0$ pairing, I show that the evolution of self-consistency parameters is analytic for all interactions.

Next, I present numerical results for two particular states. First, I analyze the THS s-wave ($\ell = 0, m_\ell = 0$) case, where

$$\Delta_0(\mathbf{k}) = \Delta_{0,0}\Gamma_0(k)Y_{0,0}(\widehat{\mathbf{k}}) \tag{2.51}$$

with $Y_{0,0}(\widehat{\mathbf{k}}) = 1/\sqrt{4\pi}$. Second, I discuss the SHS p-wave ($\ell = 1, m_\ell = 0$) case, where

$$\Delta_1(\mathbf{k}) = \Delta_{1,0}\Gamma_1(k)Y_{1,0}(\widehat{\mathbf{k}}) \tag{2.52}$$

with $Y_{1,0}(\widehat{\mathbf{k}}) = \sqrt{3/(4\pi)}\cos(\theta_{\mathbf{k}})$. In all numerical calculations, I choose $k_0 \approx 200k_{\rm F}$ to compare s-wave and p-wave cases.

In Fig. 2.4, I show $|\Delta_{0,0}|$ and μ_0 at $T = 0$ for the s-wave case. Notice that the BCS to BEC evolution range in $1/(k_{\rm F}a_0)$ is of order 1. Furthermore, $|\Delta_{0,0}|$ grows continuously without saturation with increasing coupling, while μ_0 changes from $\epsilon_{\rm F}$ to $E_{\rm b,0}/2$ continuously and decreases as $-1/(2Ma_0^2)$ for strong couplings. Thus, the evolution of $|\Delta_{0,0}|$ and μ_0 as a function of $1/(k_{\rm F}a_0)$ is smooth. For completeness, it is also possible to obtain analytical values of a_0 and $\Delta_{0,0}$ when the chemical potential vanishes. When $\mu_0 = 0$, I obtain for $|\Delta_{0,0}| = 8\epsilon_{\rm F}[\pi^2\sqrt{\pi}/\Gamma^4(1/4)]^{1/3} \approx 3.73\epsilon_{\rm F}$ at $1/(k_{\rm F}a_0) = (2\pi^3\sqrt{\pi}\epsilon_{\rm F}/|\Delta_{0,0}|)^{1/2}/[2\Gamma^2(3/4)] \approx 0.554$, which also agrees with the numerical results. Here $\Gamma(x)$ is the Gamma function.

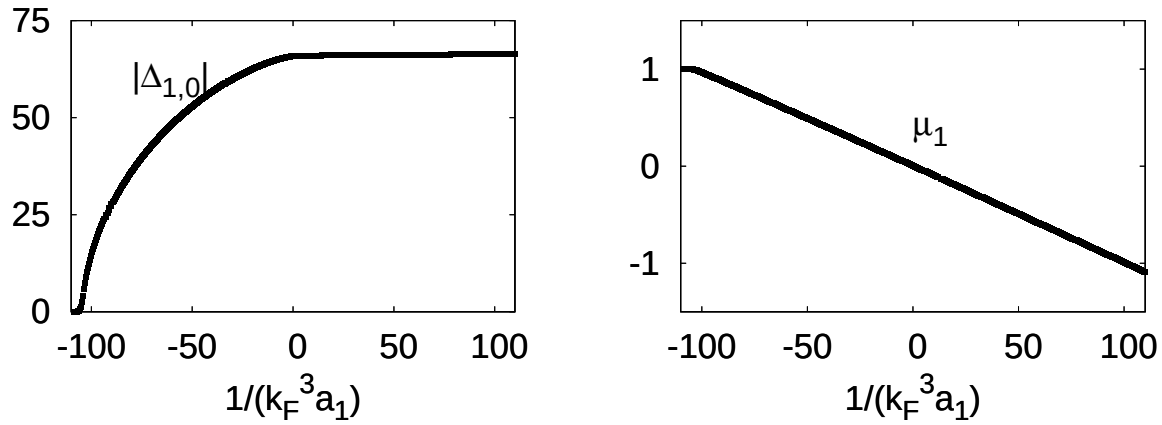

Figure 2.5: Plots of (a) order parameter $\Delta_{\rm r} = |\Delta_{1,0}|/\epsilon_{\rm F}$ and (b) chemical potential $\mu_{\rm r} = \mu_1/\epsilon_{\rm F}$ versus interaction strength $1/(k_{\rm F}^3 a_1)$ for $k_0 \approx 200 k_{\rm F}$. For $\ell = 1$ pairing, I show that the evolution of self-consistency parameters is non-analytic when μ_1 changes from positive values in the BCS side to negative values in the BEC side as a function of interaction strength.

In Fig. 2.5, I show $|\Delta_{1,0}|$ and μ_1 at $T = 0$ for the p-wave case. Notice that the BCS to BEC evolution range in $1/(k_{\rm F}^3 a_1)$ is of order $k_0/k_{\rm F}$. Furthermore, $|\Delta_{1,0}|$ grows with increasing coupling but saturates for large $1/(k_{\rm F}^3 a_1)$, while μ_1 changes from $\epsilon_{\rm F}$ to $E_{\rm b,1}/2$ continuously and decreases as $-1/(M k_0 a_1)$ for strong couplings. For completeness, I present the limiting expressions

$$|\Delta_{1,0}| = 24 \frac{k_0}{k_{\rm F}} \epsilon_{\rm F} \exp\left[-\frac{8}{3} + \frac{\pi k_0}{4 k_{\rm F}} - \frac{\pi}{2 k_{\rm F}^3 |a_1|}\right], \tag{2.53}$$

$$|\Delta_{1,0}| = 8\epsilon_{\rm F} \left(\frac{\epsilon_0}{9\epsilon_{\rm F}}\right)^{\frac{1}{4}}, \tag{2.54}$$

in the weak and strong coupling limits, respectively.

The evolution of $|\Delta_{1,0}|$ and μ_1 are qualitatively similar to recent $T = 0$ results for THS fermion [127] and SHS fermion-boson [115] models. Due to the angular dependence of $\Delta_1(\mathbf{k})$, the quasiparticle excitation spectrum $E_1(\mathbf{k})$ is gapless for $\mu_1 > 0$, and fully gapped for $\mu_1 < 0$. Furthermore, both $\Delta_{1,0}$ and μ_1 are nonanalytic exactly when μ_1 crosses the bottom of the fermion energy band $\mu_1 = 0$ at $1/(k_{\rm F}^3 a_1) \approx 0.48$. The nonanalyticity does not occur in the first derivative of $\Delta_{1,0}$ or μ_1 as it is the case in 2D [123], but occurs in the second and higher derivatives. Thus, in the p-wave case, the BCS to BEC evolution is not a crossover, but a quantum phase transition occurs, as can be seen in the quasiparticle

excitation spectrum to be discussed next.

2.4.2 Quasiparticle Excitations

The quasiparticle excitation spectrum

$$E_\ell(\mathbf{k}) = [\xi_\ell^2(\mathbf{k}) + |\Delta_\ell(\mathbf{k})|^2]^{1/2} \tag{2.55}$$

is gapless at $\mathbf{k}$-space regions where the conditions $\Delta_\ell(\mathbf{k}) = 0$ and $\epsilon(\mathbf{k}) = \mu_\ell$ are both satisfied. Notice that the second condition is only satisfied in the BCS side $\mu_\ell \geq 0$, and therefore, the excitation spectrum is always gapped in the BEC side ($\mu_\ell < 0$).

For $\ell = 0$, the order parameter is isotropic in $\mathbf{k}$-space without zeros (nodes) since it does not have any angular dependence. Therefore, the quasiparticle excitation spectrum is fully gapped in both BCS ($\mu_0 > 0$) and BEC ($\mu_0 < 0$) sides, since

$$\min\{E_0(\mathbf{k})\} = |\Delta_0(k_{\mu_0})|, \ (\mu_0 > 0), \tag{2.56}$$

$$\min\{E_0(\mathbf{k})\} = \sqrt{|\Delta_0(0)|^2 + \mu_0^2}, \ (\mu_0 < 0). \tag{2.57}$$

Here, $k_{\mu_\ell} = \sqrt{2M\mu_\ell}$. This implies that the evolution of the quasiparticle excitation spectrum from weak coupling BCS to strong coupling BEC regime is smooth when $\mu_0 = 0$ for $\ell = 0$ pairing.

In Fig. 2.6, I show $E_0(k_x = 0, k_y, k_z)$ for an s-wave ($\ell = 0, m_\ell = 0$) superfluid when (a) $\mu_0 > 0$ (BCS side) for $1/(k_{\rm F}a_0) = -1$, (b) $\mu_0 = 0$ (intermediate regime) for $1/(k_{\rm F}a_0) \approx 0.55$, and (c) $\mu_0 < 0$ (BEC side) for $1/(k_{\rm F}a_0) = 1$. Notice that the quasiparticle excitation spectrum is gapped for all three cases. However, the situation for $\ell \neq 0$ is very different as discussed next.

For $\ell \neq 0$, the order parameter is anisotropic in $\mathbf{k}$-space with zeros (nodes) since it has an angular dependence. Therefore, while the quasiparticle excitation spectrum is gapless in the BCS ($\mu_{\ell\neq 0} > 0$) side, it is fully gapped in the BEC ($\mu_{\ell\neq 0} < 0$) side, since

$$\min\{E_{\ell\neq 0}(\mathbf{k})\} = 0, \ (\mu_\ell > 0), \tag{2.58}$$

$$\min\{E_{\ell\neq 0}(\mathbf{k})\} = |\mu_\ell|, \ (\mu_\ell < 0). \tag{2.59}$$

This implies that the evolution of quasiparticle excitation spectrum from weak coupling BCS to strong coupling BEC regime is not smooth for $\ell \neq 0$ pairing having a nonanalytic

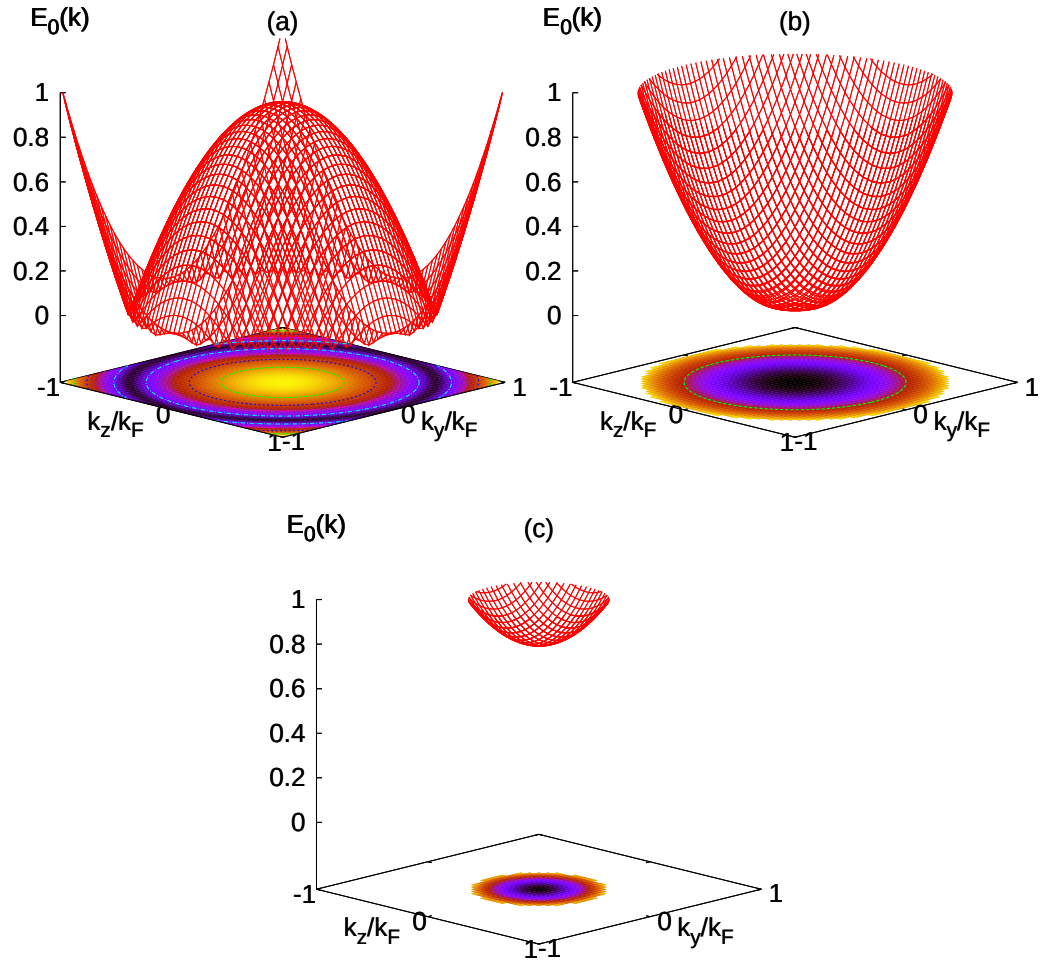

Figure 2.6: Plots of quasiparticle excitation spectrum $E_0(k_x = 0, k_y, k_z)$ when (a) $\mu_0 > 0$ (BCS side) for $1/(k_{\rm F}a_0) = -1$, (b) $\mu_0 = 0$ (intermediate regime) for $1/(k_{\rm F}a_0) \approx 0.55$, and (c) $\mu_0 < 0$ (BEC side) for $1/(k_{\rm F}a_0) = 1$ versus momentum $k_y/k_{\rm F}$ and $k_z/k_{\rm F}$. For $\ell = 0$ pairing, I show that the quasiparticle excitation spectrum is fully gapped for all interaction strengths.

behavior when $\mu_{\ell\neq 0} = 0$. This signals a quantum phase transition from a gapless to a fully gapped state exactly when $\mu_{\ell\neq 0}$ drops below the bottom of the energy band $\mu_{\ell\neq 0} = 0$.

In Fig. 2.7, I show $E_1(k_x = 0, k_y, k_z)$ for a p-wave ($\ell = 1, m_\ell = 0$) superfluid when (a) $\mu_1 > 0$ (BCS side) for $1/(k_{\rm F}^3 a_1) = -1$, (b) $\mu_1 = 0$ (intermediate regime) for $1/(k_{\rm F}^3 a_1) \approx 0.48$, and (c) $\mu_1 < 0$ (BEC side) for $1/(k_{\rm F}^3 a_1) = 1$. The quasiparticle excitation spectrum is gapless when $\Delta_1(\mathbf{k}) \propto k_z/k_{\rm F} = 0$ and $k_x^2 + k_y^2 + k_z^2 = 2M\mu_1$ are both satisfied in certain regions of $\mathbf{k}$-space. For $k_x = 0$, these conditions are met only when $k_z = 0$ and $k_y = \pm\sqrt{2M\mu_1}$ for a given μ_1. Notice that, these points come closer as the interaction (μ_1) increases (decreases), and when $\mu_1 = 0$ they become degenerate at $\mathbf{k} = \mathbf{0}$. For $\mu_1 < 0$, the second condition can

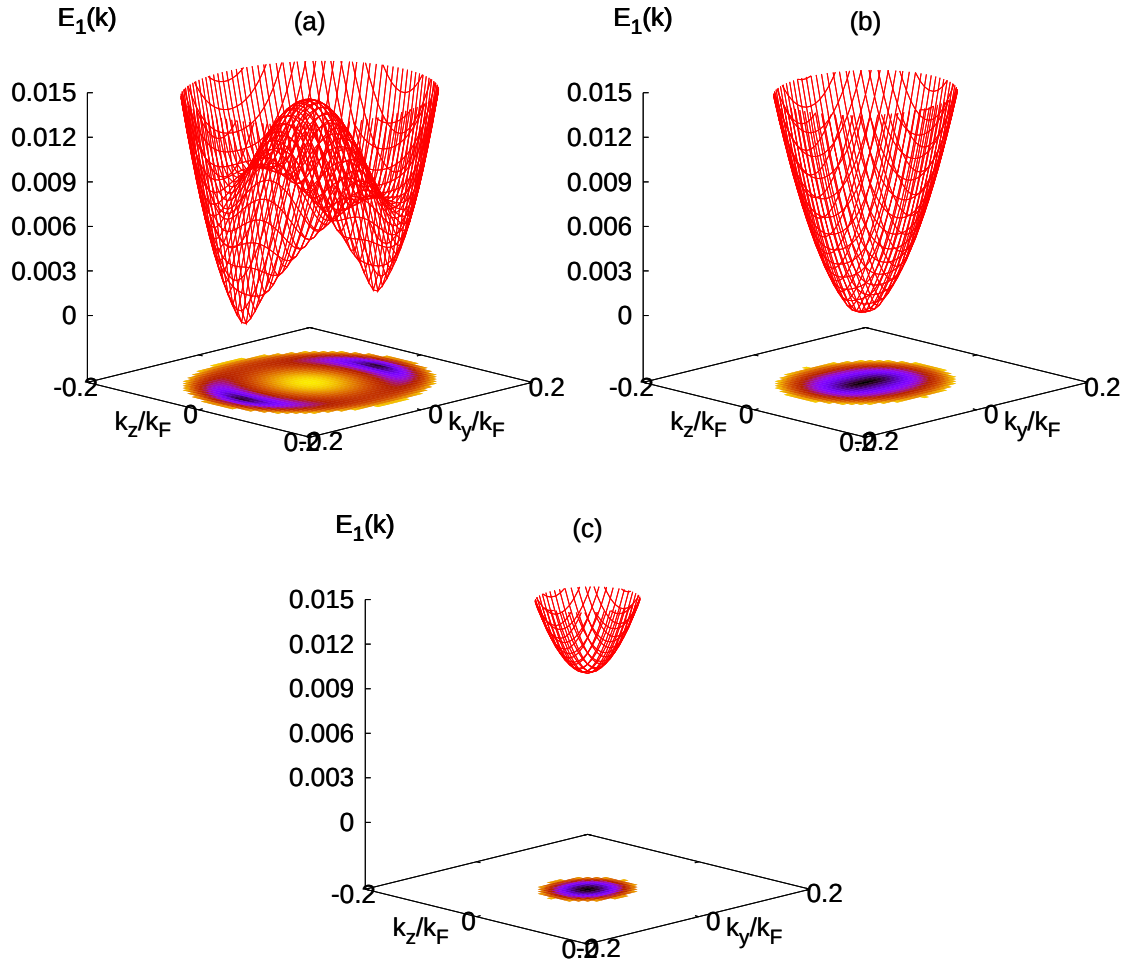

Figure 2.7: Plots of quasiparticle excitation spectrum $E_1(k_x = 0, k_y, k_z)$ in (a) $\mu_1 > 0$ (BCS side) for $1/(k_F^3 a_1) = -1$, (b) $\mu_1 = 0$ (intermediate regime) for $1/(k_F^3 a_1) \approx 0.48$, and (c) $\mu_1 < 0$ (BEC side) for $1/(k_F^3 a_1) = 1$ versus momentum k_y/k_F and k_z/k_F. For $\ell = 1$ pairing, I show that the quasiparticle excitation spectrum changes from gapless in the BCS side ($\mu_0 > 0$) to fully gapped in the BEC side ($\mu_0 < 0$) as a function of interaction strength.

not be satisfied, and thus, a gap opens in the excitation spectrum of quasiparticles as shown in Fig. 2.7c.

The spectrum of quasiparticles plays an important role in the thermodynamic properties of the evolution from BCS to BEC regime at low temperatures. For $\ell = 0$, thermodynamic quantities depend exponentially on T throughout the evolution. Thus, a smooth crossover occurs at $\mu_0 = 0$. However, for $\ell \neq 0$, thermodynamic quantitites depend exponentially on T only in the BEC side, while they have a power law dependence on T in the BCS side. Thus, a non-analytic evolution occurs at $\mu_{\ell \neq 0} = 0$. This can be seen best in the momentum distribution which is discussed next.

2.4.3 Momentum Distribution

In this section, I analyze the momentum distribution

$$n_\ell(\mathbf{k}) = \frac{1}{2} - \frac{\xi_\ell(\mathbf{k})}{2E_\ell(\mathbf{k})} \tag{2.60}$$

in the BCS ($\mu_\ell > 0$) and BEC sides ($\mu_\ell < 0$), which reflect the gapless to gapped phase transition for nonzero angular momentum superfluids.

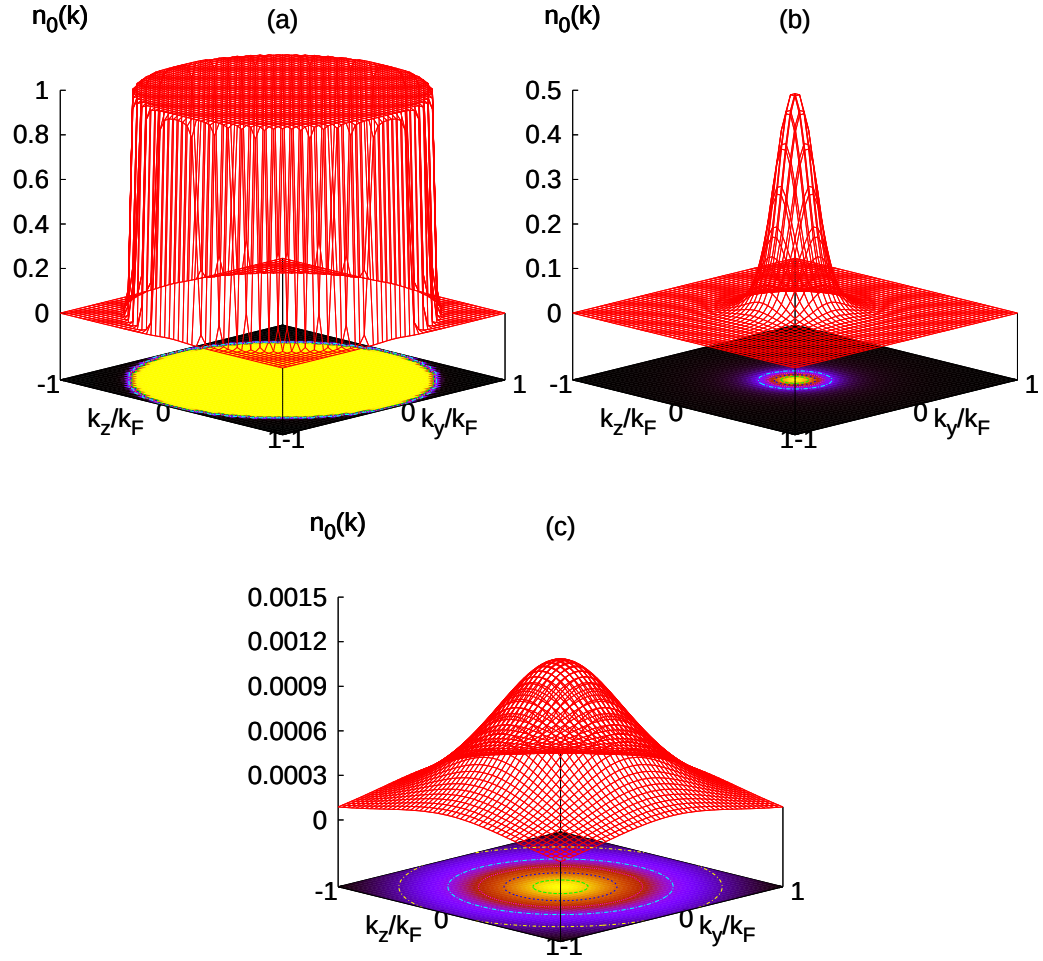

Figure 2.8: Contour plots of momentum distribution $n_0(k_x = 0, k_y, k_z)$ when (a) $\mu_0 > 0$ (BCS side) for $1/(k_F a_0) = -1$, (b) $\mu_0 = 0$ (intermediate regime) for $1/(k_F a_0) \approx 0.55$, and (c) $\mu_0 < 0$ (BEC side) for $1/(k_F a_0) = 1$ versus momentum k_y/k_F and k_z/k_F. For $\ell = 0$ pairing, I show that the evolution of momentum distribution is analytic for all interaction strengths.

In Fig. 2.8, I show $n_0(k_x = 0, k_y, k_z)$ for an s-wave ($\ell = 0, m_\ell = 0$) superfluid when (a) $\mu_0 > 0$ (BCS side) for $1/(k_F a_0) = -1$, (b) $\mu_0 = 0$ (intermediate regime) for $1/(k_F a_0) \approx 0.55$, and (c) $\mu_0 < 0$ (BEC side) for $1/(k_F a_0) = 1$. As the interaction increases the Fermi sea

with locus $\xi_0(\mathbf{k}) = 0$ is suppressed, and pairs of atoms with opposite momenta become more tightly bound. As a result, $n_0(\mathbf{k})$ broadens in the BEC side since fermions with larger momentum participate in the formation of bound states. Notice that, the evolution is a crossover without any qualitative change. Furthermore, $n_0(k_x, k_y = 0, k_z)$ and $n_0(k_x, k_y, k_z = 0)$ can be trivially obtained from $n_0(k_x = 0, k_y, k_z)$, since $n_0(k_x, k_y, k_z)$ is symmetric in k_x, k_y and k_z.

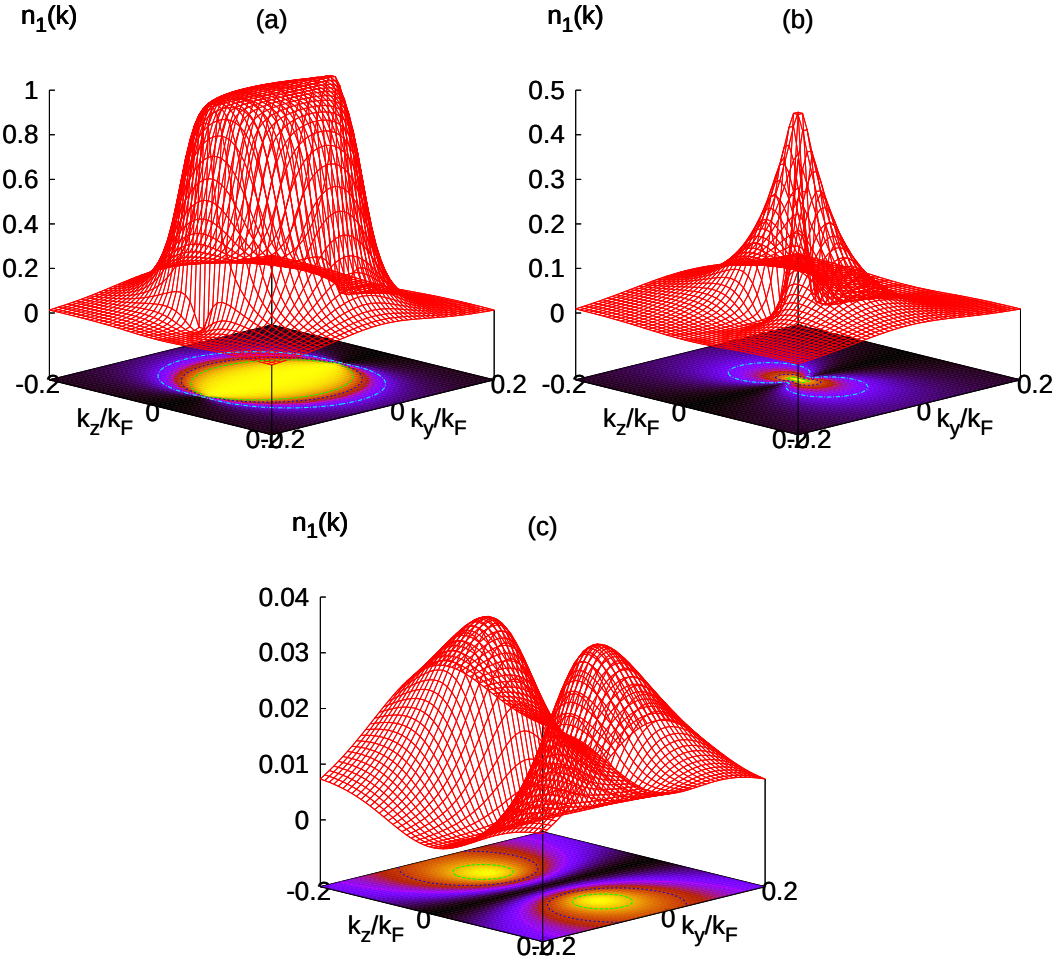

Figure 2.9: Contour plots of momentum distribution $n_1(k_x = 0, k_y, k_z)$ in (a) $\mu_1 > 0$ (BCS side) for $1/(k_F^3 a_1) = -1$, (b) $\mu_1 = 0$ (intermediate regime) for $1/(k_F^3 a_1) \approx 0.48$, and (c) $\mu_1 < 0$ (BEC side) for $1/(k_F^3 a_1) = 1$ versus momentum k_y/k_F and k_z/k_F. For $\ell = 1$ pairing, I show that the momentum distribution has a major rearrangement when μ_1 changes from positive values in the BCS side to negative values in the BEC side as a function of interaction strength.

In Fig. 2.9, I show $n_1(k_x = 0, k_y, k_z)$ for a p-wave ($\ell = 1, m_\ell = 0$) superfluid when (a) $\mu_1 > 0$ (BCS side) for $1/(k_F^3 a_1) = -1$, (b) $\mu_1 = 0$ (intermediate regime) for $1/(k_F^3 a_1) \approx 0.48$,

and (c) $\mu_1 < 0$ (BEC side) for $1/(k_{\rm F}^3 a_1) = 1$. Notice that $n_1(k_x = 0, k_y, k_z)$ is largest in the BCS side when $k_z/k_{\rm F} = 0$, but it vanishes along $k_z/k_{\rm F} = 0$ for any $k_y/k_{\rm F}$ in the BEC side. As the interaction increases the Fermi sea with locus $\xi_1(\mathbf{k}) = 0$ is suppressed, and pairs of atoms with opposite momenta become more tightly bound. As a result, the large momentum distribution in the vicinity of $\mathbf{k} = \mathbf{0}$ splits into two peaks around finite $\mathbf{k}$ reflecting the p-wave symmetry of these tightly bound states. Furthermore, $n_1(k_x, k_y, k_z = 0) = [1-{\rm sgn}(\xi_1(\mathbf{k}))]/2$ for any μ_1, and $n_1(k_x, k_y = 0, k_z)$ is trivially obtained from $n_1(k_x = 0, k_y, k_z)$, since $n_1(\mathbf{k})$ is symmetric in k_x, k_y. Here, sgn is the Sign function.

Thus, $n_1(\mathbf{k})$ for the p-wave case has a major rearrangement in $\mathbf{k}$-space with increasing interaction, in sharp contrast to s-wave. This qualitative difference between p-wave and s-wave symmetries around $\mathbf{k} = \mathbf{0}$ explicitly shows a direct measurable consequence of the gapless to gapped quantum phase transition when $\mu_1 = 0$, since $n_1(\mathbf{k})$ depends explicitly on $E_1(\mathbf{k})$. These quantum phase transitions are present in all nonzero angular momentum states, and can be further characterized through the atomic compressibility as discussed in the next section.

2.4.4 Atomic Compressibility

At finite temperatures, the isothermal atomic compressibility is defined by

$$\kappa_\ell^T(T) = -\frac{1}{\mathcal{V}}\left(\frac{\partial \mathcal{V}}{\partial \mathcal{P}}\right)_{T,N_\ell} \tag{2.61}$$

where $\mathcal{V}$ is the volume and $\mathcal{P}$ is the pressure of the gas. This can be rewritten as

$$\kappa_\ell^T(T) = -\frac{1}{N_\ell^2}\left(\frac{\partial^2 \Omega_\ell}{\partial \mu_\ell^2}\right)_{T,\mathcal{V}} = \frac{1}{N_\ell^2}\left(\frac{\partial N_\ell}{\partial \mu_\ell}\right)_{T,\mathcal{V}}, \tag{2.62}$$

where the partial derivative $\partial N_\ell/\partial \mu_\ell$ at $T \approx 0$ is given by

$$\frac{\partial N_\ell}{\partial \mu_\ell} \approx \frac{\partial N_\ell^{\rm sp}}{\partial \mu_\ell} = \sum_{\mathbf{k},s} \frac{|\Delta_\ell(\mathbf{k})|^2}{2E_\ell^3(\mathbf{k})}. \tag{2.63}$$

The expression above leads to $\kappa_0^T(0) = 2N(\epsilon_{\rm F})/N_0^2$ in weak coupling BCS and $\kappa_0^T(0) = 2N(\epsilon_{\rm F})\epsilon_{\rm F}/(3|\mu_0|N_0^2)$ in strong coupling BEC limit for $\ell = 0$, where $N(\epsilon_{\rm F}) = M\mathcal{V}k_{\rm F}/(2\pi^2)$ is the density of states per spin at the Fermi energy. Notice that $\kappa_0^T(0)$ decreases as a_0^2 in strong coupling since $|\mu_0| = 1/(2Ma_0^2)$. However, I only present the strong coupling results

for higher angular momentum states since they exhibit an interesting dependence on a_ℓ and k_0. In the case of THS pseudo-spin singlet, I obtain $\kappa^T_{\ell>1}(0) = 4N(\epsilon_{\rm F})\epsilon_{\rm F}\bar{\phi}_\ell/(\epsilon_0\phi_\ell N_\ell^2)$ for $\ell > 1$, while in the case of SHS states I obtain $\kappa^T_1(0) = N(\epsilon_{\rm F})\epsilon_{\rm F}/(\sqrt{\epsilon_0|\mu_1|}N_\ell^2)$ for $\ell = 1$ and $\kappa^T_{\ell>1}(0) = 2N(\epsilon_{\rm F})\epsilon_{\rm F}\bar{\phi}_\ell/(\epsilon_0\phi_\ell N_\ell^2)$ for $\ell > 1$. Here $\phi_\ell = \Gamma(\ell - 1/2)/\Gamma(\ell + 1)$ and $\bar{\phi}_\ell = \Gamma(\ell-3/2)/\Gamma(\ell+1)$, where $\Gamma(x)$ is the Gamma function. Notice that $\kappa^T_1(0)$ decreases as $\sqrt{a_1}$ for $\ell = 1$ since $|\mu_1| = 1(Mk_0a_1)$ and $\kappa^T_{\ell>1}(0)$ is a constant for $\ell > 1$ in strong coupling.

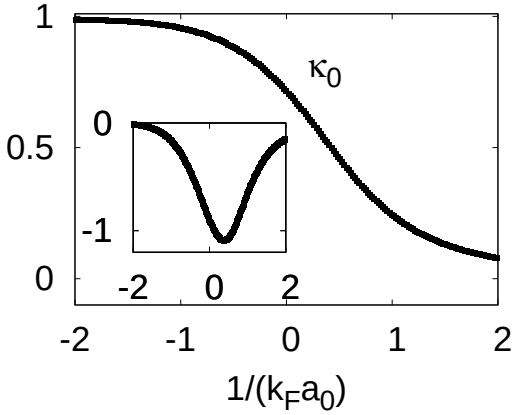

Figure 2.10: Plot of isothermal atomic compressibility $\kappa_{\rm r} = \kappa^T_0(0)/\widetilde{\kappa}_0$ versus interaction strength $1/(k_{\rm F}a_0)$ for $k_0 \approx 200k_{\rm F}$. The inset shows the numerical derivative of $d\kappa_{\rm r}/d[(k_{\rm F}a_0)^{-1}]$ versus $1/(k_{\rm F}a_0)$. Here, $\widetilde{\kappa}_0$ is the weak coupling compressibility. For $\ell = 0$ pairing, I show that the isothermal atomic compressibility is analytic for all interaction strengths, suggesting that the BCS to BEC evolution is just a crossover.

In Fig. 2.10, I show the evolution of $\kappa^T_0(0)$ for a s-wave ($\ell = 0, m_\ell = 0$) superfluid from the BCS to the BEC regime. $\kappa^T_0(0)$ decreases continuously, and thus the evolution is a crossover (smooth) as can be seen in the inset where the numerical derivative of $\kappa^T_0(0)$ with respect to $1/(k_{\rm F}a_0)$ is shown $\{d\kappa^T_0(0)/d[(k_{\rm F}a_0)^{-1}]\}$. This decrease is associated with the increase of the gap of the excitation spectrum as a function of $1/(k_{\rm F}a_0)$. In this approximation, the gas is incompressible $[\kappa^T_0(0) \to 0]$ in the extreme BEC limit.

In Fig. 2.11, I show the evolution of $\kappa^T_1(0)$ for a p-wave ($\ell = 1, m_\ell = 0$) superfluid from the BCS to the BEC regime. Notice that, there is a change in qualitative behavior when $\mu_1 = 0$ at $1/(k_{\rm F}^3a_1) \approx 0.48$ as can be seen in the inset where the numerical derivative of $\kappa^T_1(0)$ with respect to $1/(k_{\rm F}^3a_1)$ is shown $\{d\kappa^T_1(0)/d[(k_{\rm F}^3a_1)^{-1}]\}$. Thus, the evolution from BCS to BEC is not a crossover, but a quantum phase transition occurs when $\mu_1 =$

0 [121, 123, 122, 114].

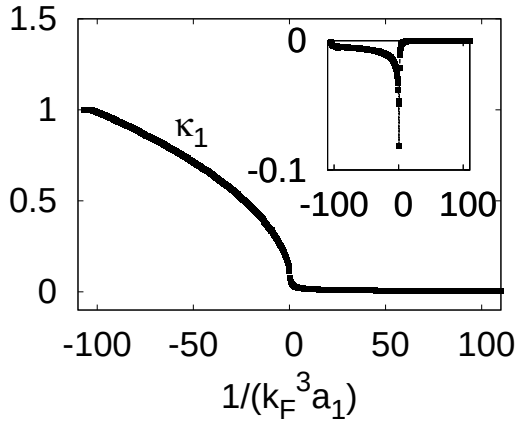

Figure 2.11: Plot of isothermal atomic compressibility $\kappa_{\rm r} = \kappa_1^T(0)/\widetilde{\kappa}_1$ versus interaction strength $1/(k_{\rm F}^3 a_1)$ for $k_0 \approx 200 k_{\rm F}$. The inset shows the numerical derivative of $d\kappa_{\rm r}/d[(k_{\rm F}^3 a_1)^{-1}]$ versus $1/(k_{\rm F}^3 a_1)$. Here $\widetilde{\kappa}_1$ is the weak coupling compressibility. For $\ell = 1$ pairing, I show that the isothermal atomic compressibility is non-analytic when μ_1 changes from positive values in the BCS side to negative values in the BEC side, suggesting that the BCS to BEC evolution is not a crossover but a quantum phase transition.

The non-analytic behavior occurring when $\mu_{\ell\neq 0} = 0$ can be understood from higher derivatives of κ_ℓ with respect to μ_ℓ

$$\left[\frac{\partial \kappa_\ell^T(T)}{\partial \mu_\ell}\right]_{T,\mathcal{V}} = -2N_\ell[\kappa_\ell^T(T)]^2 + \frac{1}{N_\ell^2}\left(\frac{\partial^2 N_\ell}{\partial \mu_\ell^2}\right)_{T,\mathcal{V}}. \tag{2.64}$$

For instance, the second derivative $\partial^2 N_\ell^{\rm sp}/\partial\mu_\ell^2 = 3\sum_{\mathbf{k},s}|\Delta_\ell(\mathbf{k})|^2\xi_\ell(\mathbf{k})/[2E_\ell^5(\mathbf{k})]$ tends to zero in the weak ($\mu_\ell \approx \epsilon_{\rm F} > 0$) and strong ($\mu_\ell \approx E_{{\rm b},\ell}/2 < 0$) coupling limits. On the other hand, when $\mu_\ell = 0$, $\partial^2 N_\ell^{\rm sp}/\partial\mu_\ell^2$ is finite only for $\ell = 0$, and it diverges for $\ell \neq 0$. This divergence is logarithmic for $\ell = 1$, and of higher order for $\ell > 1$. Thus, I conclude again that higher derivatives of $N_\ell^{\rm sp}$ are nonanalytic when $\mu_{\ell\neq 0} = 0$, and that a quantum phase transition occurs for $\ell \neq 0$.

Theoretically, the calculation of the isothermal atomic compressibility $\kappa_\ell^T(T)$ is easier than the isentropic atomic compressibility $\kappa_\ell^{\mathcal{S}}(T)$. However, performing measurements of $\kappa_\ell^{\mathcal{S}}(T)$ may be simpler in cold Fermi gases, since the gas expansion upon release from the trap is expected to be nearly isentropic. Fortunately, $\kappa_\ell^{\mathcal{S}}(T)$ is related to $\kappa_\ell^T(T)$ via the thermodynamic relation

$$\kappa_\ell^{\mathcal{S}}(T) = \frac{C_\ell^{\mathcal{V}}(T)}{C_\ell^{\mathcal{P}}(T)}\kappa_\ell^T(T), \tag{2.65}$$

where $\kappa_\ell^T(T) > \kappa_\ell^{\mathcal{S}}(T)$ since specific heat capacitites $C_\ell^{\mathcal{P}}(T) > C_\ell^{\mathcal{V}}(T)$. Furthermore, at low temperatures ($T \approx 0$) the ratio $C_\ell^{\mathcal{P}}(T)/C_\ell^{\mathcal{V}}(T) \approx$ const, and therefore, $\kappa_\ell^S(T \approx 0) \propto \kappa_\ell^T(T \approx 0)$. Thus, I expect qualitatively similar behavior in both the isentropic and isothermal compressibilities at low temperatures ($T \approx 0$).

The measurement of the atomic compressibility could also be performed via an analysis of particle density fluctuations [133, 134]. As it is well know from thermodynamics [3], $\kappa_\ell^T(T)$ is connected to density fluctuations via the relation

$$\langle n_\ell^2 \rangle - \langle n_\ell \rangle^2 = T \langle n_\ell \rangle^2 \kappa_\ell^T(T), \tag{2.66}$$

where $\langle n_\ell \rangle$ is the average density of atoms. From the measurement of density fluctuations $\kappa_\ell^T(T)$ can be extracted at any temperature T.

It is important to emphasize that in this quantum phase transition at $\mu_{\ell \neq 0} = 0$, the symmetry of the order parameter does not change as is typical in the Landau classification of phase transitions. However, a clear thermodynamic signature occurs in derivatives of the compressibility suggesting that the phase transition is higher than second order according to Ehrenfest's classification. Therefore, if the symmetry of the order parameter does not change when μ_ℓ changes sign, what is changing? To address this question, the topology of momentum space is discussed next.

2.4.5 Topological Quantum Phase Transitions

In what follows, I discuss the role of momentum space topology [135, 117] in the non-analytic behavior of the thermodynamic potential, when $\mu_{\ell \neq 0} = 0$. To investigate the role of topology, I make an immediate connection to the Lifshitz transition [136] in the context of ordinary metals at $T = 0$ and high pressure. In the conventional Lifshitz transition, the Fermi surface $\epsilon(\mathbf{k}, \mathcal{P}) = \epsilon_{\rm F}$ changes its topology as the pressure $\mathcal{P}$ is changed. For an isotropic pressure $\mathcal{P}$, the deviation $\Delta\mathcal{P} = \mathcal{P} - \mathcal{P}_{\rm c}$ from the critical pressure $\mathcal{P}_{\rm c}$ is proportional to $\Delta\mu = \mu - \mu_{\rm c}$ where $\mu_{\rm c}$ is the critical chemical potential at the transition point. A typical example of the Lifshitz transition is the disruption of a neck of the Fermi surface which leads to a non-analytic behavior of the number of states $\mathcal{N}(\mu)$ inside the Fermi surface. In this case, $\mathcal{N}(\mu)$ behaves as $\mathcal{A}(\mu_{\rm c}) + \mathcal{B}|\mu - \mu_{\rm c}|^{3/2}$ for $\mu < \mu_{\rm c}$, and as $\mathcal{A}(\mu_{\rm c})$ for $\mu > \mu_{\rm c}$, in

the vicinity of $\mu_{\rm c}$. Here, $\mathcal{K} = (3/2)\mathcal{B}|\mu - \mu_{\rm c}|^{1/2}/n_{\rm c}^2$ is the electronic compressibility, where $n_{\rm c} = N_{\rm c}/\mathcal{V}$ is the critical density of electrons at the transition point. Notice that $\mathcal{K}$ is nonanalytic, but it is not singular. The quantity that signals a phase transition in this case is not $\mathcal{K}$, but the thermopower $\mathcal{Q}$, which is proportional to $-\partial \ln(n^2\mathcal{K})/\partial\mu$, thus leading to $\mathcal{Q} \propto -|\Delta\mu|^{-1/2}$. In the conventional Lifshitz transition, the system lowers its energy by $\Delta\mathcal{E} \propto -|\Delta\mu|^{5/2} \propto -|\Delta\mathcal{P}|^{5/2}$, and the transition is said to be of second and half order [137].

The topological transition proposed here is analogous to the Lifshitz transition in the sense that the surface in momentum space corresponding to $E_{\ell\neq 0}(\mathbf{k}) = E_{\ell\neq 0}(\mathbf{k}, \mu_\ell) = 0$ changes from a well defined set of $\mathbf{k}$ points for $\mu_{\ell\neq 0} > 0$ to a null set for $\mu_{\ell\neq 0} < 0$. Here, $E_{\ell\neq 0}(\mathbf{k}, \mu_\ell)$ plays the role of $\epsilon(\mathbf{k}, \mathcal{P})$ and $\mu_{\ell\neq 0} = \mu_{\rm c} = 0$ plays the role of the critical pressure $\mathcal{P}_{\rm c}$.

For the Lifshitz transition in $\ell \neq 0$ superfluids, there is a non-analytic behavior in $\partial^2 N_{\ell\neq 0}/\partial\mu_\ell^2$, and thus in $\partial\kappa^T_{\ell\neq 0}(0)/\partial\mu_\ell$. This behavior in $\kappa^T_{\ell\neq 0}(0)$ is due to the collapse of all order parameter nodes at $\mathbf{k} = 0$, which produce a gap in the excitation spectrum $E_{\ell\neq 0}(\mathbf{k})$ and a massive discontinuous rearrangement of the momentum distribution $n_{\ell\neq 0}(\mathbf{k})$ in the ground state as $\mu_{\ell\neq 0} \to \mu^{\rm c}_{\ell\neq 0} = 0$. A direct topological analogy with the standard Lifshitz transition can be made by noticing the collapse of locus of zero quasiparticle excitation energy at $\mu_{\ell\neq 0} = \mu^{\rm c}_{\ell\neq 0}$ in the excitation spectrum of the system. Generalized topological invariants can be invented along the lines of Ref. [117, 135], however, I do not discuss them here. Instead, I analyze next the phase diagram at zero temperature.

2.4.6 Phase Diagram

To have a full picture of the evolution from the BCS to the BEC limit at $T = 0$, it is important to analyze thermodynamic quantities at low temperatures. In particular, it is important to determine the quantum critical region (QCR) where a qualitative change occurs in quantities such as the specific heat, compressibility and spin susceptibility. Here, I do not discuss in detail the QCR, but I analyze the contributions from quasiparticle excitations to thermodynamic properties. However, the discussion can be extended to include collective excitations [117] (see Section 2.5).

Next, I point out a major difference between $\ell = 0$ and $\ell \neq 0$ states in connection with the spectrum of the quasiparticle excitations (see Section 2.4.2) and their contribution to low temperature thermodynamics.

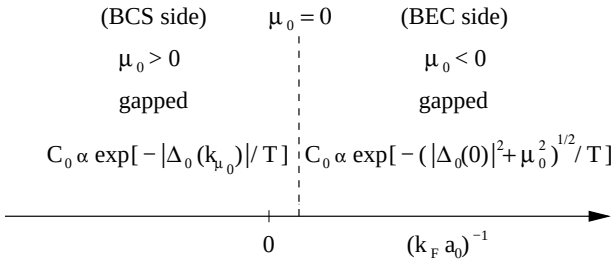

Figure 2.12: The phase diagram of s-wave superfluids as a function of $1/(k_{\rm F}a_0)$. For $\ell = 0$ pairing, since the quasiparticle excitations are always fully gapped, the thermodynamic quantities have an exponential dependence on the temperature and the minimum energy of quasiparticle excitations for all interaction strengths.

For $\ell = 0$, quasiparticle excitations are gapped for all couplings, and therefore, thermodynamic quantities such as atomic compressibility, specific heat and spin susceptibility have an exponential dependence on the temperature and the minimum energy of quasiparticle excitations $\sim \exp[-\min\{E_0(\mathbf{k})\}/T]$. Using Eqs. (2.56) and (2.57) leads to $\sim \exp[-|\Delta_0(k_{\mu_0})|/T]$ in the BCS side ($\mu_0 > 0$) and $\sim \exp[-\sqrt{|\Delta_0(0)|^2 + \mu_0^2}/T]$ in the BEC side ($\mu_0 < 0$) as shown in Fig. 2.12, where $k_{\mu_\ell} = \sqrt{2M\mu_\ell}$. Notice that, there is no qualitative change across $\mu_0 = 0$ at small but finite temperatures. This indicates the absence of a QCR and confirms there is only a crossover for s-wave ($\ell = 0$) superfluids at $T = 0$.

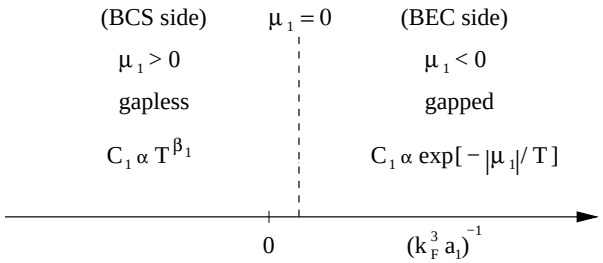

Figure 2.13: The phase diagram of p-wave superfluids as a function of $1/(k_{\rm F}^3 a_1)$. For $\ell = 1$ pairing, since the quasiparticle excitations are gapless in the BCS side and are only gapped in the BEC side, the thermodynamic quantities have a power law dependence in the BCS side while an exponential dependence in the BEC side on the temperature and the minimum energy of quasiparticle excitations for all interaction strengths.

For $\ell \neq 0$, quasiparticle excitations are gapless in the BCS side and are only gapped in

the BEC side, and therefore, while thermodynamic quantities such as atomic compressibility, specific heat and spin susceptibility have power law dependences on the temperature $\sim T^{\beta_{\ell\neq 0}}$ in the BCS side, they have exponential dependences on the temperature and the minimum energy of quasiparticle excitations $\sim \exp[-\min\{E_{\ell\neq 0}(\mathbf{k})\}/T]$ in the BEC side. Here, $\beta_{\ell\neq 0}$ is a real number which depends on particular ℓ state. For $\ell = 1$, using Eqs. (2.58) and (2.59) leads to $\sim T^{\beta_1}$ in the BCS side ($\mu_1 > 0$) and $\sim \exp(-|\mu_1|/T)$ in the BEC side ($\mu_1 < 0$) as shown in Fig. 2.13. Notice the change in qualitative behavior across $\mu_1 = 0$ (as well as other $\ell \neq 0$ states) at small but finite temperatures. This change occurs within the QCR and signals the existence of a quantum phase transition ($T = 0$) for $\ell \neq 0$ superfluids.

Having analyzed the low temperature phase diagrams, I discuss next the thermodynamic potential in the BCS and BEC limits.

2.4.7 Thermodynamic Potential

Now, I discuss the thermodynamic potential Ω_ℓ at $T = 0$ in the asymptotic BCS and BEC limits. In the weak coupling limit, from Eq. (2.23) I obtain

$$\Omega_\ell^{\rm sp} = -\frac{2}{5} N_\ell \epsilon_{\rm F}, \tag{2.67}$$

which is identical to the full thermodynamic potential Ω_ℓ. This indicates that $\Omega_\ell^{\rm fluct}$ is negligible in the BCS limit.

However, in the strong coupling limit, from Eq. (2.23) I obtain

$$\Omega_\ell^{\rm sp} = -\frac{1}{2} N_\ell (2\mu_\ell - E_{{\rm b},\ell}). \tag{2.68}$$

Notice that, $\mu_{{\rm B},\ell} = 2\mu_\ell - E_{{\rm b},\ell} > 0$ is the Bosonic chemical potential and $N_{{\rm B},\ell} = N_\ell/2$ is the number of bosons. To evaluate $\mu_{{\rm B},\ell}$, it is necessary to find the first nonvanishing correction for $2\mu_\ell - E_{{\rm b},\ell}$. In the specific case of $\ell = 0$, I obtain $\mu_{\rm B,0} = 4\epsilon_{\rm F} k_{\rm F} a_0/(3\pi) = 4\pi a_{\rm B,0}/M_{\rm B,0}$ for the chemical potential and $\Omega_\ell^{\rm sp} = -\pi N_0^2 a_0/(M\mathcal{V}) = -N_{\rm B,0}\mu_{\rm B,0}$ for the thermodynamic potential of the pairs. Here $a_{\rm B,0} = 2a_0$ and $M_{\rm B,0} = 2M$ is the scattering length and mass of the corresponding bosons. A better estimate for $a_{\rm B,0} \approx 0.6a_0$ can be found in the literature [138, 63, 139, 140], by taking into account higher order processes. The main reason for this difference is that my theory does not include possible intermediate

(virtual) scattering processes which renormalize $a_{\mathrm{B},0}$. This is also the case when I analyze the collective modes in Section 2.5.3 and the TDGL equation in Section 2.7.2.

Using $\mu_\ell = (\mu_{\mathrm{B},\ell} + E_{\mathrm{b},\ell})/2$ and the thermodynamic relation $\mu_\ell = (\partial E_\ell/\partial N_\ell)_{\mathcal{V}}$, where E_ℓ is the ground state energy, I obtain

$$\Omega_\ell = -\frac{1}{2} N_{\mathrm{B},\ell}\mu_{\mathrm{B},\ell}. \tag{2.69}$$

Notice that this expression is identical to the thermodynamic potential of bosons $\Omega_{\mathrm{B},\ell} = E_{\mathrm{B},\ell} - N_{\mathrm{B},\ell}\mu_{\mathrm{B},\ell}$, where $E_{\mathrm{B},\ell}$ is the ground state energy. Therefore, the fermionic thermodynamic potential in the strong coupling limit should lead to the thermodynamic potential of real bosons ($\Omega_\ell \equiv \Omega_{\mathrm{B},\ell}$). Since $\Omega_\ell = \Omega_\ell^{\mathrm{sp}} + \Omega_\ell^{\mathrm{fluct}}$, I conclude from this thermodynamic argument that

$$\Omega_\ell^{\mathrm{fluct}} = \frac{1}{2} N_{\mathrm{B},\ell}\mu_{\mathrm{B},\ell} \tag{2.70}$$

in the strong coupling limit. Therefore, $E_\ell - N_\ell E_{\mathrm{b},\ell}/2 \equiv E_{\mathrm{B},\ell}$, or $E_\ell/N_\ell - \mu_\ell \equiv (E_{\mathrm{B},\ell}/N_{\mathrm{B},\ell} - \mu_{\mathrm{B},\ell})/2$ which is consistent with quantum Monte Carlo calculations [142].

The fluctuation contribution to $\Omega_\ell^{\mathrm{fluct}}$ comes from the zero point energy of the collective excitations, which is discussed next.

2.5 Gaussian Fluctuations

The pole structure of $\mathbf{F}_\ell(\mathbf{q}, iv_j)$ defined in Eqs. (2.21) and (2.22) determines the two-particle excitation spectrum of the superconducting state with $iv_j \to w + i0^+$, and has to be taken into account to derive $\Omega_\ell^{\mathrm{fluct}}$. The matrix elements of $\mathbf{F}_\ell(\mathbf{q}, iv_j)$ are $\mathbf{F}_{\ell,m_\ell,m'_\ell}(\mathbf{q}, iv_j)$ for a given ℓ. I focus here only on the zero temperature limit and analyse the collective phase modes. In this limit, I separate the diagonal matrix elements of $\mathbf{F}^{-1}_{\ell,m_\ell,m'_\ell}(q)$ into even and odd contributions with respect to iv_j

$$\begin{aligned}
(\mathbf{F}^{-1}_{\ell,m_\ell,m'_\ell})^E_{11} &= \sum_{\mathbf{k}} \frac{(\xi_+\xi_- + E_+E_-)(E_+ + E_-)}{2E_+E_-[(iv_j)^2 - (E_+ + E_-)^2]} \Gamma^2_\ell(k) Y_{\ell,m_\ell}(\widehat{\mathbf{k}}) Y^*_{\ell,m'_\ell}(\widehat{\mathbf{k}}) \\
&- \frac{\delta_{m_\ell,m'_\ell}\mathcal{V}}{4\pi\lambda_\ell}, \qquad (2.71) \\
(\mathbf{F}^{-1}_{\ell,m_\ell,m'_\ell})^O_{11} &= -\sum_{\mathbf{k}} \frac{(\xi_+E_- + \xi_-E_+)(iv_j)}{2E_+E_-[(iv_j)^2 - (E_+ + E_-)^2]} \Gamma^2_\ell(k) Y_{\ell,m_\ell}(\widehat{\mathbf{k}}) Y^*_{\ell,m'_\ell}(\widehat{\mathbf{k}}). \qquad (2.72)
\end{aligned}$$

The off-diagonal term is even in iv_j, and it reduces to

$$(\mathbf{F}^{-1}_{\ell,m_\ell,m'_\ell})_{12} = -\sum_{\mathbf{k}} \frac{\Delta_+\Delta_-(E_+ + E_-)}{2E_+E_-[(iv_j)^2 - (E_+ + E_-)^2]}\Gamma^2_\ell(k)Y_{\ell,m_\ell}(\widehat{\mathbf{k}})Y^*_{\ell,m'_\ell}(\widehat{\mathbf{k}}). \tag{2.73}$$

Here the labels $\pm$ denote that the corresponding variables are functions of $\mathbf{k} \pm \mathbf{q}/2$.

In order to obtain the collective mode spectrum, I express $\Lambda_{\ell,m_\ell}(q) = \tau_{\ell,m_\ell}(q)e^{i\vartheta_{\ell,m_\ell}(q)} = [\rho_{\ell,m_\ell}(q) + i\theta_{\ell,m_\ell}(q)]/\sqrt{2}$ where $\tau_{\ell,m_\ell}(q)$, $\vartheta_{\ell,m_\ell}(q)$, $\rho_{\ell,m_\ell}(q)$ and $\theta_{\ell,m_\ell}(q)$ are all real. Notice that the new fields $\rho_{\ell,m_\ell}(q) = \tau_{\ell,m_\ell}(q)\cos[\vartheta_{\ell,m_\ell}(q)]$, and $\theta_{\ell,m_\ell}(q) = \tau_{\ell,m_\ell}(q)\sin[\vartheta_{\ell,m_\ell}(q)]$ can be regarded essentially as the amplitude and phase fields respectively, when $\vartheta_{\ell,m_\ell}(q)$ is small. This change of basis can be described by the following unitary transformation

$$\Lambda_{\ell,m_\ell}(q) = \frac{1}{\sqrt{2}}\begin{pmatrix} 1 & i \\ 1 & -i \end{pmatrix}\begin{bmatrix} \rho_{\ell,m_\ell}(q) \\ \theta_{\ell,m_\ell}(q) \end{bmatrix}. \tag{2.74}$$

From now on, I take Δ_{ℓ,m_ℓ} as real without loss of generality. The diagonal elements of the fluctuation matrix in the rotated basis are $(\widetilde{\mathbf{F}}^{-1}_{\ell,m_\ell,m'_\ell})_{11} = (\mathbf{F}^{-1}_{\ell,m_\ell,m'_\ell})^E_{11} + (\mathbf{F}^{-1}_{\ell,m_\ell,m'_\ell})_{12}$, and $(\widetilde{\mathbf{F}}^{-1}_{\ell,m_\ell,m'_\ell})_{22} = (\mathbf{F}^{-1}_{\ell,m_\ell,m'_\ell})^E_{11} - (\mathbf{F}^{-1}_{\ell,m_\ell,m'_\ell})_{12}$; and the off-diagonal elements are $(\widetilde{\mathbf{F}}^{-1}_{\ell,m_\ell,m'_\ell})_{12} = (\widetilde{\mathbf{F}}^{-1}_{\ell,m_\ell,m'_\ell})^*_{21} = i(\mathbf{F}^{-1}_{\ell,m_\ell,m'_\ell})^O_{11}$ with the q dependence being implicit.

2.5.1 Collective (Goldstone) Modes

The collective modes are determined by the poles of the propagator matrix $\mathbf{F}_\ell(q)$ for the pair fluctuation fields $\Lambda_{\ell,m_\ell}(q)$, which describe the Gaussian deviations about the saddle point order parameter. The poles of $\mathbf{F}_\ell(q)$ are determined by the condition

$$\det \mathbf{F}^{-1}_\ell(q) = 0, \tag{2.75}$$

which leads to $2(2\ell+1)$ collective (amplitude and phase) modes, when the usual analytic continuation $iv_j \to w + i0^+$ is performed. Among them, there are $2\ell+1$ amplitude modes which I do not discuss here.

The easiest way to get the phase collective modes is to integrate out the amplitude fields to obtain a phase-only effective action. Notice that, for $\ell \neq 0$ channels at any temperature, and for $\ell = 0$ channel at finite temperature, a well defined low frequency expansion is not possible for $\mu_\ell > 0$ due to Landau damping which causes the collective modes to decay

into the two quasiparticle continuum. A well defined expansion [collective mode dispersion w] must satisfy the following condition $w \ll \min\{E_+ + E_-\}$. Thus, a zero temperature expansion is always possible when Landau damping is subdominant (underdamped regime). To obtain the long wavelength dispersions for the collective modes at $T = 0$, I expand the matrix elements of $\widetilde{\mathbf{F}}^{-1}_{\ell,m_\ell,m'_\ell}$ to second order in $|\mathbf{q}|$ and w to get

$$(\widetilde{\mathbf{F}}^{-1}_{\ell,m_\ell,m'_\ell})_{11} = A_{\ell,m_\ell,m'_\ell} + \sum_{i,j} C^{i,j}_{\ell,m_\ell,m'_\ell} q_i q_j - D_{\ell,m_\ell,m'_\ell} w^2, \tag{2.76}$$

$$(\widetilde{\mathbf{F}}^{-1}_{\ell,m_\ell,m'_\ell})_{22} = P_{\ell,m_\ell,m'_\ell} + \sum_{i,j} Q^{i,j}_{\ell,m_\ell,m'_\ell} q_i q_j - R_{\ell,m_\ell,m'_\ell} w^2, \tag{2.77}$$

$$(\widetilde{\mathbf{F}}^{-1}_{\ell,m_\ell,m'_\ell})_{12} = iB_{\ell,m_\ell,m'_\ell} w. \tag{2.78}$$

The expressions for the expansion coefficients are given in App. A.1.

For $\ell = 0$, the coefficients $C^{i,j}_{0,0,0} = C_{0,0,0}\delta_{i,j}$ and $Q^{i,j}_{0,0,0} = Q_{0,0,0}\delta_{i,j}$ are diagonal and isotropic in (i,j), and $P_{0,0,0} = 0$ vanishes. Here, $\delta_{i,j}$ is the Kronecker delta. Thus, the collective mode is the isotropic Goldstone mode with dispersion

$$W_{0,0}(\mathbf{q}) = \mathcal{C}_{0,0}|\mathbf{q}|, \tag{2.79}$$

$$\mathcal{C}_{0,0} = \left(\frac{A_{0,0,0}Q_{0,0,0}}{A_{0,0,0}R_{0,0,0} + B^2_{0,0,0}}\right)^{\frac{1}{2}}, \tag{2.80}$$

where $\mathcal{C}_{0,0}$ is the speed of sound. Notice that the quasiparticle excitations are always fully gapped from weak to strong coupling, and thus, the Goldstone mode is not damped at $T = 0$ for all couplings.

For $\ell \neq 0$, the dispersion for collective modes is not easy to extract in general, and therefore, I consider the case when only one of the spherical harmonics $Y_{\ell,m_\ell}(\widehat{\mathbf{k}})$ is dominant and characterizes the order parameter. In this case, $P_{\ell,m_\ell,m_\ell} = 0$ due to the order parameter equation, and the collective mode is the anisotropic Goldstone mode with dispersion

$$W_{\ell\neq 0,m_\ell}(\mathbf{q}) = \left[\sum_{i,j} (\mathcal{C}^{i,j}_{\ell,m_\ell})^2 q_i q_j\right]^{\frac{1}{2}}, \tag{2.81}$$

$$\mathcal{C}^{i,j}_{\ell\neq 0,m_\ell} = \left(\frac{A_{\ell,m_\ell,m_\ell}Q^{i,j}_{\ell,m_\ell,m_\ell}}{A_{\ell,m_\ell,m_\ell}R_{\ell,m_\ell,m_\ell} + B^2_{\ell,m_\ell,m_\ell}}\right)^{\frac{1}{2}}. \tag{2.82}$$

Notice that the speed of sound has a tensor structure and is anisotropic. Furthermore, the quasiparticle excitations are gapless when $\mu_{\ell\neq 0} > 0$, and thus, the Goldstone mode

is damped even at $T = 0$. However, Landau damping is subdominant and the real part of the pole dominates for small momenta. In addition, quasiparticle excitations are fully gapped when $\mu_{\ell\neq 0} < 0$, and thus, the Goldstone mode is not damped. Therefore, the pole contribution to $\Omega^{\rm fluct}_{\ell\neq 0}$ comes from the Goldstone mode for all couplings. In addition, there is also a branch cut representing the continuum of two particle scattering states, but the contribution from the Goldstone mode dominates at sufficiently low temperatures.

It is also illustrative to analyze the eigenvectors of $\widetilde{\mathbf{F}}^{-1}_{\ell}(q)$ in the amplitude-phase representation corresponding to small $W_{\ell,m_\ell}(\mathbf{q})$ mode

$$\begin{bmatrix} \rho_{\ell,m_\ell}(q) \\ \theta_{\ell,m_\ell}(q) \end{bmatrix} = \begin{bmatrix} -i\frac{B_{\ell,m_\ell,m_\ell}}{A_{\ell,m_\ell,m_\ell}} W_{\ell,m_\ell}(\mathbf{q}) \\ 1 \end{bmatrix}. \tag{2.83}$$

Notice that, when $B_{\ell,m_\ell,m_\ell} \to 0$ the amplitude and phase modes are not mixed.

Next, I discuss the dispersion of collective modes in the weak and strong coupling limits, where the expansion coefficients are analytically tractable for a fixed (ℓ, m_ℓ) state.

2.5.2 Weak Coupling (BCS) Regime

The s-wave ($\ell = 0, m_\ell = 0$) weak coupling limit is characterized by the criteria $\mu_0 > 0$ and $\mu_0 \approx \epsilon_{\rm F} \gg |\Delta_{0,0}|$. The expansion of the matrix elements to order $|\mathbf{q}|^2$ and w^2 is performed under the condition $[w, |\mathbf{q}|^2/(2M)] \ll |\Delta_{0,0}|$. Analytic calculations are particularly simple in this case since all integrals for the coefficients needed to calculate the collective mode dispersions are peaked near the Fermi surface. I first introduce a shell about the Fermi energy $|\xi_0(\mathbf{k})| \leq w_{\rm D}$ such that $\epsilon_{\rm F} \gg w_{\rm D} \gg \Delta_0(\mathbf{k}_{\rm F})$, inside of which one may ignore the 3D density of states factor $\sqrt{\epsilon/\epsilon_{\rm F}}$ and outside of which one may ignore $\Delta_0(\mathbf{k})$. In addition, I make use of the nearly perfect particle-hole symmetry, which forces integrals to vanish when their integrands are odd under the transformation $\xi_0(\mathbf{k}) \to -\xi_0(\mathbf{k})$. For instance, the coefficient that couple phase and amplitude modes vanish ($B_{0,0,0} = 0$) in this limit. Thus, there is no mixing between phase and amplitude fields in weak coupling, as can be seen by inspection of the fluctuation matrix $\widetilde{\mathbf{F}}_0(q)$.

For $\ell = 0$, the zeroth order coefficient is

$$A_{0,0,0} = \frac{N(\epsilon_{\rm F})}{4\pi}, \tag{2.84}$$

and the second order coefficients are

$$C^{i,j}_{0,0,0} = \frac{Q^{i,j}_{0,0,0}}{3} = \frac{N(\epsilon_{\rm F})v_{\rm F}^2}{36|\Delta_{0,0}|^2}\delta_{i,j}, \tag{2.85}$$

$$D_{0,0,0} = \frac{R_{0,0,0}}{3} = \frac{N(\epsilon_{\rm F})}{12|\Delta_{0,0}|^2}. \tag{2.86}$$

Here, $v_{\rm F} = k_{\rm F}/M$ is the Fermi velocity and $N(\epsilon_{\rm F}) = M\mathcal{V}k_{\rm F}/(2\pi^2)$ is the density of states per spin at the Fermi energy.

In weak coupling, since $B^2_{\ell,m_\ell,m_\ell} \ll A_{\ell,m_\ell,m_\ell}R_{\ell,m_\ell,m_\ell}$, the sound velocity is simplified to $C^{i,j}_{\ell,m_\ell} \approx [Q^{i,j}_{\ell,m_\ell,m_\ell}/A_{\ell,m_\ell,m_\ell}]$ for any ℓ. Using the coefficients above in Eq. (2.80), for $\ell = 0$, I obtain

$$\mathcal{C}_{0,0} = \frac{v_{\rm F}}{\sqrt{3}} \tag{2.87}$$

which is the well known Anderson-Bogoliubov relation. For $\ell \neq 0$, the expansion coefficients require more detailed and lengthy analysis, and therefore, I do not discuss here. On the other hand, the expansion coefficients can be calculated for any ℓ in the strong coupling BEC regime, which is discussed next.

2.5.3 Strong Coupling (BEC) Regime

The strong coupling limit is characterized by the criteria $\mu_\ell < 0$, $|\mu_\ell| \ll \epsilon_0 = k_0^2/(2M)$ and $|\xi_\ell(\mathbf{k})| \gg |\Delta_\ell(\mathbf{k})|$. The expansion of the matrix elements to order $|\mathbf{q}|^2$ and w^2 is performed under the condition $[w, |\mathbf{q}|^2/(2M)] \ll |\mu_\ell|$. The situation encountered here is very different from the weak coupling limit, because one can no longer invoke particle-hole symmetry to simplify the calculation of many of the coefficients appearing in the fluctuation matrix $\widetilde{\mathbf{F}}_\ell(q)$. In particular, the coefficient $B_{\ell,m_\ell,m'_\ell} \neq 0$ indicates that the amplitude and phase fields are mixed. Furthermore, $P_{\ell,m_\ell,m'_\ell} = 0$, since this coefficient reduces to the order parameter equation in this limit.

For $\ell = 0$, the zeroth order coefficient is

$$A_{0,0,0} = \frac{\kappa|\Delta_{0,0}|^2}{8\pi|\mu_0|}, \tag{2.88}$$

the first order coefficient is

$$B_{0,0,0} = \kappa, \tag{2.89}$$

and the second order coefficients are

$$C^{i,j}_{0,0,0} = Q^{i,j}_{0,0,0} = \frac{\kappa}{4M}\delta_{i,j}, \tag{2.90}$$

$$D_{0,0,0} = R_{0,0,0} = \frac{\kappa}{8|\mu_0|}, \tag{2.91}$$

where $\kappa = N(\epsilon_{\rm F})/(32\sqrt{|\mu_0|\epsilon_F})$.

Using the expressions above in Eq. (2.80), I obtain the sound velocity

$$\mathcal{C}_{0,0} = \left(\frac{|\Delta_{0,0}|}{32M|\mu_0|\pi}\right)^{\frac{1}{2}} = v_{\rm F}\sqrt{\frac{k_{\rm F}a_0}{3\pi}}. \tag{2.92}$$

Notice that the sound velocity is very small and its smallness is controlled by the scattering length a_0. Furthermore, in the theory of weakly interacting dilute Bose gas, the sound velocity is given by $\mathcal{C}_{\rm B,0} = 4\pi a_{\rm B,0}n_{\rm B,0}/M^2_{\rm B,0}$. Making the identification that the density of pairs is $n_{\rm B,0} = n_0/2$, the mass of the pairs is $M_{\rm B,0} = 2M$ and that the Bose scattering length is $a_{\rm B,0} = 2a_0$, it follows that Eq. (2.92) is identical to the Bogoliubov result $\mathcal{C}_{\rm B,0}$. Therefore, my result for the fermionic system represents in fact a weakly interacting Bose gas in the strong coupling limit. A better estimate for $a_{\rm B,0} \approx 0.6a_0$ can be found in the literature [138, 63, 139, 140], by taking into account higher order processes. This is also the case when I construct the TDGL equation in Section 2.7.2.

For $\ell \neq 0$, the zeroth order coefficient is

$$A_{\ell\neq 0,m_\ell,m_\ell} = \frac{15\widehat{\phi}_\ell\widetilde{\kappa}}{2\epsilon_0\sqrt{\pi}}|\Delta_{\ell,m_\ell}|^2\gamma_{\ell,\{m_\ell\}}, \tag{2.93}$$

the first order coefficient is

$$B_{\ell\neq 0,m_\ell,m'_\ell} = \frac{\phi_\ell\widetilde{\kappa}}{\sqrt{\pi}}\delta_{m_\ell,m'_\ell}, \tag{2.94}$$

and the second order coefficients are

$$C^{i,i}_{\ell\neq 0,m_\ell,m'_\ell} = Q^{i,i}_{\ell\neq 0,m_\ell,m'_\ell} = \frac{\phi_\ell\widetilde{\kappa}}{4M\sqrt{\pi}}\delta_{m_\ell,m'_\ell}, \tag{2.95}$$

$$D_{1,m_\ell,m'_\ell} = R_{1,m_\ell,m'_\ell} = \frac{3\widetilde{\kappa}}{8\sqrt{\epsilon_0|\mu_1|}}\delta_{m_\ell,m'_\ell}, \tag{2.96}$$

$$D_{\ell>1,m_\ell,m'_\ell} = R_{\ell>1,m_\ell,m'_\ell} = \frac{3\bar{\phi}_\ell\widetilde{\kappa}}{4\sqrt{\pi}\epsilon_0}\delta_{m_\ell,m'_\ell}, \tag{2.97}$$

where $\widetilde{\kappa} = N(\epsilon_{\rm F})/(32\sqrt{\epsilon_0\epsilon_F})$, $\phi_\ell = \Gamma(\ell-1/2)/\Gamma(\ell+1)$, $\bar{\phi}_\ell = \Gamma(\ell-3/2)/\Gamma(\ell+1)$ and $\widehat{\phi}_\ell = \Gamma(2\ell-3/2)/\Gamma(2\ell+2)$. Here $\Gamma(x)$ is the Gamma function, and γ_{ℓ,m_ℓ} is an angular averaged quantity defined in App. A.2.

In strong coupling, since $B^2_{\ell,m_\ell,m_\ell} \gg A_{\ell,m_\ell,m_\ell}R_{\ell,m_\ell,m_\ell}$, the sound velocity is simplified to $C^{i,j}_{\ell,m_\ell} \approx [A_{\ell,m_\ell,m_\ell}Q^{i,j}_{\ell,m_\ell,m_\ell}/B^2_{\ell,m_\ell,m_\ell}]^{1/2}$ for any ℓ. Using the expressions above in Eq. (2.82), for $\ell \neq 0$, I obtain

$$\mathcal{C}^{i,i}_{\ell\neq 0,m_\ell} = \left(\frac{15\gamma_{\ell,\{m_\ell\}}|\Delta_{\ell,m_\ell}|^2\widehat{\phi}_\ell}{8M\phi_\ell\epsilon_0}\right)^{\frac{1}{2}} \tag{2.98}$$

$$= v_{\rm F}\left(\frac{20\gamma_{\ell,\{m_\ell\}}\sqrt{\pi}\widehat{\phi}_\ell}{\phi^2_\ell}\frac{k_{\rm F}}{k_0}\right)^{\frac{1}{2}}. \tag{2.99}$$

Therefore, the sound velocity is also very small and its smallness is controlled by the interaction range k_0 through the diluteness condition i.e. $(k_0/k_F)^3 \gg 1$, for $\ell \neq 0$. Notice that, the sound velocity is independent of the scattering parameter for $\ell \neq 0$.

Now, I turn my attention to a numerical analysis of the phase collective modes during the evolution from weak coupling BCS to strong coupling BEC limits.

2.5.4 Evolution from BCS to BEC Regime

I focus only on s-wave ($\ell = 0, m_\ell = 0$) and p-wave ($\ell = 1, m_\ell = 0$) cases, since they may be the most relevant to current experiments involving ultracold atoms.

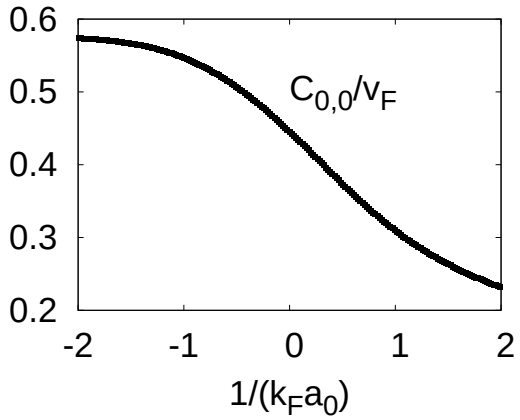

Figure 2.14: Plot of Goldstone (sound) velocity $(\mathcal{C}_{0,0})_r = \mathcal{C}_{0,0}/v_{\rm F}$ versus interaction strength $1/(k_{\rm F}a_0)$ for $k_0 \approx 200k_{\rm F}$. For $\ell = 0$ pairing, I show that the evolution of sound velocity is analytic for all interaction strengths.

In Fig. 2.14, I show the evolution of $\mathcal{C}_{0,0}$ as a function of $1/(k_{\rm F}a_0)$ for s-wave case. The weak coupling Anderson-Bogoliubov velocity $\mathcal{C}_{0,0} = v_{\rm F}/\sqrt{3}$ evolves continuously to the strong coupling Bogoliubov velocity $\mathcal{C}_{0,0} = v_{\rm F}\sqrt{k_{\rm F}a_0/(3\pi)}$. Notice that the sound velocity is a monotonically decreasing function of $1/(k_{\rm F}a_0)$, and the evolution across $\mu_0 = 0$ is a crossover.

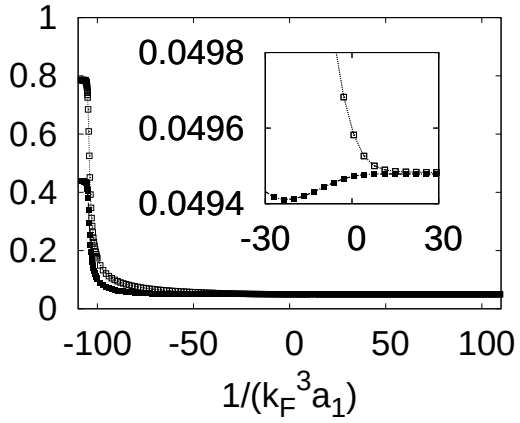

Figure 2.15: Plots of Goldstone (sound) velocity $(\mathcal{C}^{x,x}_{1,0})_r = \mathcal{C}^{x,x}_{1,0}/v_{\rm F}$ (solid squares) and $(\mathcal{C}^{z,z}_{1,0})_r = \mathcal{C}^{z,z}_{1,0}/v_{\rm F}$ (hollow squares) versus interaction strength $1/(k_{\rm F}^3 a_1)$ for $k_0 \approx 200 k_{\rm F}$. The inset zooms into the unitarity region. For $\ell = 1$ pairing, I show that the sound velocity is anisotropic (isotropic) in the BCS (BEC) side, and the evolution of sound velocity is non-analytic when μ_1 changes from positive values in the BCS side to negative values in the BEC side as a function of interaction strength.

In Fig. 2.15, I show the evolution of $\mathcal{C}^{i,j}_{1,0}$ as a function of $1/(k_{\rm F}^3 a_1)$ for p-wave case. Notice that $\mathcal{C}^{i,i}_{1,0}$ is strongly anisotropic in weak coupling, since $\mathcal{C}^{x,x}_{1,0} = \mathcal{C}^{y,y}_{1,0} \approx 0.44 v_{\rm F}$ and $\mathcal{C}^{z,z}_{1,0} = \sqrt{3}\mathcal{C}^{x,x}_{1,0} \approx 0.79 v_{\rm F}$, thus reflecting the order parameter symmetry. In addition, $\mathcal{C}^{i,i}_{1,0}$ is isotropic in strong coupling, since $\mathcal{C}^{i,i}_{1,0} = v_{\rm F}\sqrt{3k_{\rm F}/(2\pi k_0)} \approx 0.049 v_{\rm F}$ for $k_0 \approx 200 k_{\rm F}$, thus revealing the secondary role of the order parameter symmetry in this limit. The anisotropy is very small in the intermediate regime beyond $\mu_1 < 0$. Notice also that, $\mathcal{C}^{z,z}_{1,0}$ is a monotonically decreasing function of $1/(k_{\rm F}^3 a_1)$ in BCS side until $\mu_1 = 0$, where it saturates. However, $\mathcal{C}^{x,x}_{1,0} = \mathcal{C}^{y,y}_{1,0}$ is a nonmonotonic function of $1/(k_{\rm F}a_1)^3$, and it also saturates beyond $\mu_1 = 0$. Therefore, the behavior of $\mathcal{C}^{i,i}_{1,0}$ reflects the disapperance of nodes of the quasiparticle energy $E_1(\mathbf{k})$ as μ_1 changes sign.

These collective excitations may contribute significantly to the thermodynamic potential, which is discussed next.

2.5.5 Corrections to $\Omega_\ell^{\rm sp}$ due to Collective Modes

In this section, I analyze corrections to the saddle point thermodynamic potential $\Omega_\ell^{\rm sp}$ due to low energy collective excitations. The evaluation of bosonic Matsubara frequency sums in Eq. (2.24) leads to $\Omega_\ell^{\rm fluct} \to \Omega_\ell^{\rm coll}$, where

$$\Omega_\ell^{\rm coll} = \sum_{\mathbf{q}}{}' \big\{ W_\ell(\mathbf{q}) + \frac{2}{\beta} \ln\left[1 - \exp(-\beta W_\ell(\mathbf{q}))\right] \big\} \tag{2.100}$$

is the collective mode contribution to the thermodynamic potential. Here, $W_\ell(\mathbf{q})$ is the dispersion of the collective mode defined in Eqs. (2.80) and (2.82) for the $\ell = 0$ and $\ell \neq 0$ cases, respectively. The prime on the summation indicates that a momentum cutoff is required since a long wavelength and low frequency approximation is used to derive the collective mode dispersion. Notice that the first term in Eq. (2.100) contributes to the ground state energy of the interacting Fermi system. This contribution is necessary to recover the ground state energy of the effective Bose system in the strong coupling limit as discussed in Sec 2.4.7.

The corrections to the saddle point number equation $N_\ell^{\rm coll} = -\partial\Omega_\ell^{\rm coll}/\partial\mu_\ell$ are due to the zero point motion ($N_\ell^{\rm zp}$) and thermal excitation ($N_\ell^{\rm te}$) of the collective modes

$$N_\ell^{\rm zp} = -\frac{\partial}{\partial\mu_\ell} \sum_{\mathbf{q}}{}' W_\ell(\mathbf{q}), \tag{2.101}$$

$$N_\ell^{\rm te} = -\sum_{\mathbf{q}}{}' \frac{\partial W_\ell(\mathbf{q})}{\partial\mu_\ell} n_{\rm B}[W_\ell(\mathbf{q})]. \tag{2.102}$$

Here $n_{\rm B}(x) = 1/[\exp(\beta x) - 1]$ is the Bose distribution. For $\ell = 0$, the last equation can be solved to obtain $N_0^{\rm te} = -6(\partial\mathcal{C}_{0,0}/\partial\mu_0)\zeta(4)T^4/(\pi^2\mathcal{C}_{0,0}^2)$, which vanishes at $T = 0$. Here $\zeta(x)$ is the Zeta function. Similarly, $N_{\ell\neq 0}^{\rm te}$ has a power law dependence on T, and therefore, vanishes at $T = 0$ since the collective modes are not excited. $N_\ell^{\rm zp}$ gives small contributions to the number equation in weak and strong couplings, but may lead to significant contributions in the intermediate regime for all ℓ. The impact of $N_\ell^{\rm zp}$ on the order parameter and chemical potential in the intermediate regime may require a careful analysis of the full fluctuation contributions [132].

Until now, I discussed the evolution of superfluidity from the BCS to the BEC regime at zero temperature. In the rest of this chapter, I analyze the evolution of superfluidity from the BCS to the BEC limit at finite temperatures.

2.6 BCS to BEC Evolution near $T = T_{c,\ell}$

In this section, I concentrate on physical properties near critical temperatures $T = T_{c,\ell}$. To calculate $T_{c,\ell}$, the self-consistency (order parameter and number) equations have to be solved simultaneously. At $T = T_{c,\ell}$, then $\Delta_{\ell,m_\ell} = 0$, and the saddle point order parameter equation Eq. (2.38) reduces to

$$\frac{M\mathcal{V}}{4\pi k_0^{2\ell} a_\ell} = \sum_{\mathbf{k}} \Gamma_\ell^2(k) \left[\frac{1}{2\epsilon(\mathbf{k})} - \frac{\tanh[\xi_\ell(\mathbf{k})/(2T_{c,\ell})]}{2\xi_\ell(\mathbf{k})} \right]. \tag{2.103}$$

This expression is independent of m_ℓ since the interaction amplitude λ_ℓ depends only on ℓ. Similarly, the saddle point number equation reduces to

$$N_\ell^{\rm sp} = \sum_{\mathbf{k},s} n_{\rm F}[\xi_\ell(\mathbf{k})], \tag{2.104}$$

where $n_{\rm F}(x) = 1/[\exp(\beta x) + 1]$ is the Fermi distribution. Notice that the summation over spins (s) is not present in the SHS case. It is important to emphasize that the inclusion of $N_\ell^{\rm fluct}$ around $T_\ell = T_{c,\ell}$ is essential to produce the qualitatively correct physics with increasing coupling, as discussed next.

2.6.1 Gaussian Fluctuations

To evaluate the gaussian contribution to the thermodynamic potential, I sum over the fermionic Matsubara frequencies in Eq. (2.24), and obtain the action

$$S_\ell^{\rm fluct} = \beta \sum_{q,m_\ell,m'_\ell} \Lambda^\dagger_{\ell,m_\ell}(q) L^{-1}_{\ell,m_\ell,m'_\ell}(q) \Lambda_{\ell,m'_\ell}(q), \tag{2.105}$$

where $L^{-1}_{\ell,m_\ell,m'_\ell}(q) = (\mathbf{F}^{-1}_{\ell,m_\ell,m'_\ell})_{11}$ is the element of the fluctuation propagator given by

$$L^{-1}_{\ell,m_\ell,m'_\ell}(q) = \frac{\delta_{m_\ell,m'_\ell}}{4\pi\mathcal{V}^{-1}\lambda_\ell} - \sum_{\mathbf{k}} \frac{1 - n_{\rm F}(\xi_+) - n_{\rm F}(\xi_-)}{\xi_+ + \xi_- - iv_j} \Gamma_\ell^2(k) Y_{\ell,m_\ell}(\widehat{\mathbf{k}}) Y^*_{\ell,m'_\ell}(\widehat{\mathbf{k}}). \tag{2.106}$$

This is the generalization of the $\ell = 0$ case to $\ell \neq 0$, where $\xi_\pm = \xi_\ell(\mathbf{k} \pm \mathbf{q}/2)$. From $S_\ell^{\rm fluct}$, I obtain the thermodynamic potential $\Omega_\ell^{\rm gauss} = \Omega_\ell^{\rm sp} + \Omega_\ell^{\rm fluct}$, where $\Omega_\ell^{\rm sp}$ is the saddle point

contribution with $\Delta_\ell(\mathbf{k}) = 0$, and

$$\Omega_\ell^{\text{fluct}} = -\frac{1}{\beta}\sum_q \ln\det[L_\ell(q)/\beta] \tag{2.107}$$

is the fluctuation contribution.

I evaluate the bosonic Matsubara frequency (iv_j) sums by using contour integration, and determine the branch cut and pole terms. I use the phase shift

$$\varphi_\ell^{\text{fluct}}(\mathbf{q}, w) = \text{Arg}[\det L_\ell(\mathbf{q}, iv_j \to w + i0^+)] \tag{2.108}$$

to replace $\det L_\ell(q)$ in Eq. (2.107), leading to

$$\Omega_\ell^{\text{fluct}} = -\sum_{\mathbf{q}}\int_{-\infty}^{\infty}\frac{dw}{\pi} n_{\text{B}}(w)\widetilde{\varphi}_\ell^{\text{fluct}}(\mathbf{q}, w), \tag{2.109}$$

where $\widetilde{\varphi}_\ell^{\text{fluct}}(\mathbf{q}, w) = \varphi_\ell^{\text{fluct}}(\mathbf{q}, w) - \varphi_\ell^{\text{fluct}}(\mathbf{q}, 0)$ and $n_{\text{B}}(x) = 1/\left[\exp(\beta x) - 1\right]$ is the Bose distribution. Notice that, this equation is the generalization of the s-wave ($\ell = 0$) case [41, 44] for $\ell \neq 0$. Furthermore, the phase shift can be written as $\widetilde{\varphi}_\ell^{\text{fluct}}(\mathbf{q}, w) = \widetilde{\varphi}_\ell^{\text{sc}}(\mathbf{q}, w) + \widetilde{\varphi}_\ell^{\text{bs}}(\mathbf{q}, w)$, where

$$\widetilde{\varphi}_\ell^{\text{sc}}(\mathbf{q}, w) = \widetilde{\varphi}_\ell(\mathbf{q}, w)\Theta(w - w_{\mathbf{q}}^*), \tag{2.110}$$

is the branch cut (scattering) and $\widetilde{\varphi}_\ell^{\text{bs}}(\mathbf{q}, w)$ is the pole (bound state) contribution. Here, $\Theta(x)$ is the Heaviside function, $w_{\mathbf{q}}^* = w_{\mathbf{q}} - 2\mu_\ell$ with $w_{\mathbf{q}} = |\mathbf{q}|^2/(4M)$ is the branch frequency and μ_ℓ is the fermionic chemical potential.

The branch cut (scattering) contribution to the thermodynamic potential becomes

$$\Omega_\ell^{\text{sc}} = -\sum_{\mathbf{q}}\int_{-\infty}^{\infty}\frac{dw}{\pi} n_{\text{B}}(w)\widetilde{\varphi}_\ell^{\text{sc}}(\mathbf{q}, w). \tag{2.111}$$

For each $\mathbf{q}$, the integrand is nonvanishing only for $w > w_{\mathbf{q}}^*$ since $\widetilde{\varphi}_\ell^{\text{sc}}(\mathbf{q}, w) = 0$ otherwise. Thus, the branch cut (scattering) contribution to the number equation $N_\ell^{\text{sc}} = -\partial\Omega_\ell^{\text{sc}}/\partial\mu_\ell$ is given by

$$N_\ell^{\text{sc}} = \sum_{\mathbf{q}}\int_0^{\infty}\frac{dw}{\pi}\left[\frac{\partial n_{\text{B}}(\widetilde{w})}{\partial\mu_\ell} - n_{\text{B}}(\widetilde{w})\frac{\partial}{\partial\mu_\ell}\right]\widetilde{\varphi}_\ell(\mathbf{q}, \widetilde{w}), \tag{2.112}$$

where $\widetilde{w} = w + w_{\mathbf{q}}^*$.

When $a_\ell < 0$, there are no bound states above $T_{c,\ell}$ and N_ℓ^{sc} represents the correction due to scattering states. However, when $a_\ell > 0$, there are bound states represented by poles at $w < w_{\mathbf{q}}^*$. The pole (bound state) contribution to the number equation is

$$N_\ell^{bs} = -\sum_{\mathbf{q}} n_B[\mathcal{W}_\ell(\mathbf{q})]\eta_\ell[\mathbf{q}, \mathcal{W}_\ell(\mathbf{q})], \tag{2.113}$$

where $\mathcal{W}_\ell(\mathbf{q})$ corresponds to the poles of $L_\ell^{-1}(q)$ and

$$\eta_\ell[\mathbf{q}, \mathcal{W}_\ell(\mathbf{q})] = \mathrm{Res}\Big\{\frac{\partial \det L_\ell^{-1}[\mathbf{q}, \mathcal{W}_\ell(\mathbf{q})]/\partial\mu_\ell}{\det L_\ell^{-1}[\mathbf{q}, \mathcal{W}_\ell(\mathbf{q})]}\Big\} \tag{2.114}$$

is the residue. Heavy numerical calculations are necessary to find the poles as a function of $\mathbf{q}$ for all couplings. However, in sufficiently strong coupling, when $n_F(\xi_\pm) \ll 1$ in Eq. (2.106), the pole (bound state) contribution can be evaluated analytically by eliminating λ_ℓ in favor of the two-body bound state energy $\widetilde{E}_{b,\ell}$ in vacuum. Notice that, $\widetilde{E}_{b,\ell}$ is related to the $E_{b,\ell}$ obtained from the T-matrix approach, where multiple scattering events are included. However, they become identical in the dilute limit.

A relation between λ_ℓ and $\widetilde{E}_{b,\ell}$ can be obtained by solving the Schroedinger equation for two fermions interacting via a pairing potential $V(r)$. After Fourier transforming from real to momentum space, the Schroedinger equation for the pair wave function $\psi(\mathbf{k})$ is

$$2\epsilon(\mathbf{k})\psi(\mathbf{k}) + \frac{1}{\mathcal{V}}\sum_{\mathbf{k}'} V(\mathbf{k}, \mathbf{k}')\psi(\mathbf{k}') = \widetilde{E}_b\psi(\mathbf{k}). \tag{2.115}$$

Using the Fourier expansion of $V(\mathbf{k}, \mathbf{k}')$ given in Eq. (2.113) and choosing only the ℓth angular momentum channel, I obtain

$$\frac{1}{\lambda_\ell} = \frac{1}{\mathcal{V}}\sum_{\mathbf{k}} \frac{\Gamma_\ell^2(k)}{2\epsilon(\mathbf{k}) - \widetilde{E}_{b,\ell}}. \tag{2.116}$$

This expression relates $\widetilde{E}_{b,\ell} < 0$ to λ_ℓ in order to express Eq. (2.119) in terms of binding energy $\widetilde{E}_{b,\ell} < 0$. Notice that, this equation is similar to the order parameter equation in the strong coupling limit ($\mu_\ell < 0$ and $|\mu_\ell| \gg T_{c,\ell}$), where

$$\frac{1}{\lambda_\ell} = \frac{1}{\mathcal{V}}\sum_{\mathbf{k}} \frac{\Gamma_\ell^2(k)}{2\epsilon(\mathbf{k}) - 2\mu_\ell}. \tag{2.117}$$

Therefore, $\mu_\ell \to \widetilde{E}_{b,\ell}/2$ as the coupling increases.

Substitution of Eq. (2.116) in Eq. (2.114) yields the pole contribution which is given by $\mathcal{W}_\ell(\mathbf{q}) = w_\mathbf{q} + \widetilde{E}_{\mathrm{b},\ell} - 2\mu_\ell$, and the residue at this pole is $\eta_\ell[\mathbf{q}, \mathcal{W}_\ell(\mathbf{q})] = -2\sum_{m_\ell}$. Therefore, the bound state contribution to the phase shift in the sufficiently strong coupling limit is given by

$$\widetilde{\varphi}_\ell^{\mathrm{bs}}(\mathbf{q}, w) = \pi\Theta(w - w_\mathbf{q} + \mu_{\mathrm{B},\ell}), \tag{2.118}$$

which leads to the bound state number equation

$$N_\ell^{\mathrm{bs}} = 2\sum_{\mathbf{q},m_\ell} n_{\mathrm{B}}[w_\mathbf{q} - \mu_{\mathrm{B},\ell}], \tag{2.119}$$

where $\mu_{\mathrm{B},\ell} = 2\mu_\ell - \widetilde{E}_{\mathrm{b},\ell} \leq 0$ is the chemical potential of the bosonic molecules. Notice that, Eq. (2.119) is only valid for interaction strengths where $\mu_{\mathrm{B},\ell} \leq 0$. Thus, this expression can not be used over a region of coupling strengths where $\mu_{\mathrm{B},\ell}$ is positive.

2.6.2 Critical Temperature and Chemical Potential

To obtain the evolution from BCS to BEC, the total number equation [Eqs. (2.104), (2.112) and (2.119)]

$$N_\ell \approx N_\ell^{\mathrm{gauss}} = N_\ell^{\mathrm{sp}} + N_\ell^{\mathrm{sc}} + N_\ell^{\mathrm{bs}} \tag{2.120}$$

and order parameter [Eq. (2.103)] equations have to be solved self-consistently for $T_{\mathrm{c},\ell}$ and μ_ℓ. First, I analyze the number of unbound, scattering and bound fermions as a function of the scattering parameter for the s-wave ($\ell = 0$) and p-wave ($\ell = 1$) cases.

In Fig. 2.16, I plot different contributions to the number equation as a function of $1/(k_{\mathrm{F}}a_0)$ for the s-wave ($\ell = 0, m_\ell = 0$) case. Notice that, N_0^{sp} (N_0^{bs}) dominates in weak (strong) coupling, while N_0^{sc} is the highest for intermediate couplings. Thus, all fermions are unbound in the strictly BCS limit (not shown in the figure), while all fermions are bound in the strictly BEC limit.

In Fig. 2.17, I present plots of different contributions to the number equation as a function of $1/(k_{\mathrm{F}}^3 a_1)$ for the p-wave ($\ell = 1, m_\ell = 0$) case. Notice also that, N_1^{sp} (N_1^{bs}) dominates in weak (strong) coupling, while N_1^{sc} is the highest for intermediate couplings. Thus, again all fermions are unbound in the strictly BCS limit, while all fermions are bound in the strictly BEC limit.

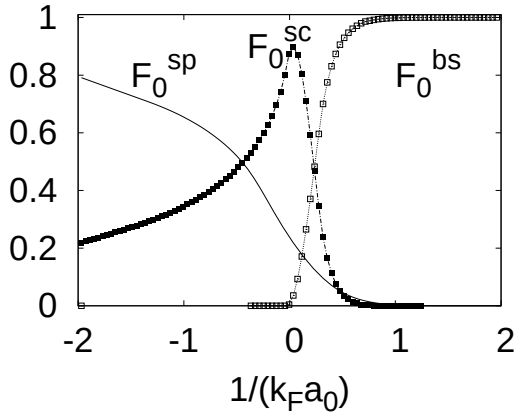

Figure 2.16: Fractions of unbound $F_0^{\rm sp} = N_0^{\rm sp}/N_0$, scattering $F_0^{\rm sc} = N_0^{\rm sc}/N_0$, bound $F_0^{\rm bs} = N_0^{\rm bs}/N_0$ fermions at $T = T_{\rm c,0}$ versus $1/(k_{\rm F}a_0)$ for $k_0 \approx 200k_{\rm F}$. For $\ell = 0$ pairing, I show that all fermions are unbound (bound) in the BCS (BEC) limit, while the scattering contribution dominates in the intermediate region.

Therefore, the total fluctuation contribution $N_\ell^{\rm sc}+N_\ell^{\rm bs}$ is negligible in weak coupling and $N_\ell^{\rm sp}$ is sufficient. However, the inclusion of fluctuations is necessary for strong coupling to recover the physics of BEC. However, in the vicinity of the unitary limit $[1/(k_{\rm F}^{2\ell+1}a_\ell) \to 0]$, my results are not quantitatively strictly applicable and should be regarded as qualitative only.

Next, I discuss the chemical potential and critical temperature. In weak coupling, I introduce a shell about the Fermi energy $|\xi_\ell(\mathbf{k})| \leq w_{\rm D}$, such that $\mu_\ell \approx \epsilon_{\rm F} \gg w_{\rm D} \gg T_{{\rm c},\ell}$. Then, in Eq. (2.103), I set $\tanh[|\xi_\ell(\mathbf{k})|/(2T_{{\rm c},\ell})] = 1$ outside the shell and treat the integration within the shell as usual in the BCS theory. In strong coupling, I use that $\min[\xi_\ell(\mathbf{k})] = |\mu_\ell| \gg T_{{\rm c},\ell}$ and set $\tanh[\xi_\ell(\mathbf{k})/(2T_{{\rm c},\ell})] = 1$. Therefore, in strictly weak and strong coupling, the self-consistency equations are decoupled, and play reversed roles. In weak (strong) coupling the order parameter equation determines $T_{{\rm c},\ell}$ (μ_ℓ) and the number equation determines μ_ℓ ($T_{{\rm c},\ell}$).

In weak coupling, the number equation $N_\ell \approx N_\ell^{\rm sp}$ leads to

$$\mu_\ell \approx \epsilon_{\rm F} \tag{2.121}$$

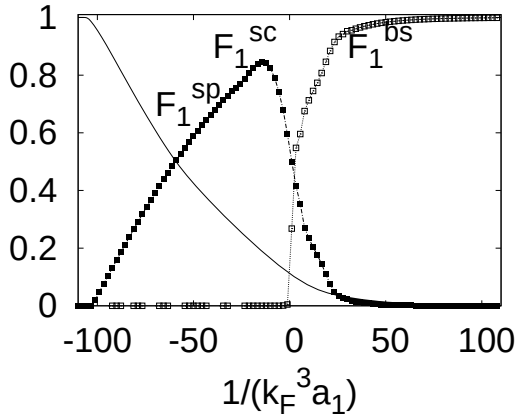

Figure 2.17: Fractions of unbound $F_1^{\rm sp} = N_1^{\rm sp}/N_1$, scattering $F_1^{\rm sc} = N_1^{\rm sc}/N_1$, bound $F_1^{\rm bs} = N_1^{\rm bs}/N_1$ fermions at $T = T_{\rm c,1}$ versus $1/(k_{\rm F}^3 a_1)$ for $k_0 \approx 200 k_{\rm F}$. For $\ell = 1$ pairing, I show that all fermions are unbound (bound) in the BCS (BEC) limit, while the scattering contribution dominates in the intermediate region.

for any ℓ. In strong coupling, the order parameter equation leads to

$$\mu_0 = -\frac{1}{2Ma_0^2}, \tag{2.122}$$

$$\mu_{\ell\neq 0} = -\frac{\sqrt{\pi}}{Mk_0^{2\ell-1}a_\ell\phi_\ell}, \tag{2.123}$$

where $\phi_\ell = \Gamma(\ell-1/2)/\Gamma(\ell+1)$ and $\Gamma(x)$ is the Gamma function. This calculation requires $a_0 k_0 > 1$ for $\ell = 0$, and $k_0^{2\ell+1} a_\ell \phi_\ell > (\ell+1)\sqrt{\pi}$ for $\ell \neq 0$ for the order parameter equation to have a solution with $\mu_\ell < 0$. Furthermore, I assume $|\mu_\ell| \ll \epsilon_0 = k_0^2/(2M)$ to obtain Eqs. (2.122) and (2.123). Notice that, $\mu_\ell = E_{{\rm b},\ell}/2$ in this limit.

On the other hand, the solution of the order parameter equation in weak coupling is

$$T_{\rm c,0} = \frac{8}{\pi}\epsilon_{\rm F} \exp\left[\gamma - 2 + \frac{\pi}{2}\frac{k_{\rm F}}{k_0} - \frac{\pi}{2k_{\rm F}|a_0|}\right], \tag{2.124}$$

$$T_{{\rm c},\ell} \sim \epsilon_{\rm F} \exp\left[t_\ell \left(\frac{k_0}{k_{\rm F}}\right)^{2\ell-1} - \frac{\pi}{2k_{\rm F}^{2\ell+1}|a_\ell|}\right], \tag{2.125}$$

where $\gamma \approx 0.577$ is the Euler's constant, $t_1 = \pi/4$ and $t_{\ell>1} = \pi 2^{\ell+1}(2\ell-3)!!/\ell!$. These expressions are valid only when the exponential terms are small. Therefore, they suggest that the range of BCS to unitarity region in terms of $1/(2k_F^{2\ell+1}|a_\ell|)$ is of order 1 for $\ell = 0$ and of order $(k_0/k_{\rm F})^{2\ell-1}$ for $\ell \neq 0$. In strong coupling, the number equation $N_\ell \approx N_\ell^{\rm bs}$

leads to

$$T_{\mathrm{c},\ell}^{\mathrm{THS}} = \frac{2\pi}{M_{\mathrm{B},\ell}} \left[\frac{n_\ell}{\sum_{m_\ell} \zeta(3/2)} \right]^{\frac{2}{3}} = \frac{0.218}{(\sum_{m_\ell})^{\frac{2}{3}}} \epsilon_{\mathrm{F}}, \tag{2.126}$$

where $M_{B,\ell} = 2M$ is the mass of the bosonic molecules. Here, $n_\ell = k_{\mathrm{F}}^3/(3\pi^2)$ is the density of fermions. For THS Fermi gases, I conclude that the BEC critical temperature of s-wave superfluids is the highest, and this temperature is reduced for higher angular momentum states. However, for SHS Fermi gases

$$T_{\mathrm{c},\ell\neq 0}^{\mathrm{SHS}} = \frac{2\pi}{M_{\mathrm{B},\ell}} \left[\frac{n_\ell}{\sum_{m_\ell} \zeta(3/2)} \right]^{\frac{2}{3}} = \frac{0.137\epsilon_{\mathrm{F}}}{(\sum_{m_\ell})^{\frac{2}{3}}}. \tag{2.127}$$

where $n_\ell = k_{\mathrm{F}}^3/(6\pi^2)$ and $\zeta(x)$ is the Zeta function. Here, the summation over m_ℓ is over degenerate spherical harmonics involved in the order parameter of the system, and can be at most $\sum_{m_\ell} = 2\ell+1$. For SHS states, I conclude that the BEC critical temperature of p-wave superfluids is the highest, and this temperature is reduced for higher angular momentum states.

For completeness, it is also possible to relate a_ℓ and $T_{\mathrm{c},\ell}$ when the chemical potential vanishes. When $\mu_\ell = 0$, the solution of the number equation Eq. (2.120) is highly non-trivial and it is difficult to find the value of the scattering parameter a_ℓ^* at $\mu_\ell = 0$. However, the critical temperature in terms of a_ℓ^* can be found analytically from Eq. (2.103) as

$$\left(\frac{T_{\mathrm{c},\ell}}{\epsilon_{\mathrm{F}}} \right)^{\ell+\frac{1}{2}} = \frac{\pi/(k_{\mathrm{F}}^{2\ell+1} a_\ell^*)}{(2-2^{-\ell+\frac{3}{2}})\Gamma(\ell+\frac{1}{2})\zeta(\ell+\frac{1}{2})}. \tag{2.128}$$

to order $T_{\mathrm{c},\ell}/\epsilon_0$, where $\epsilon_0 = k_0^2/(2M) \gg T_{\mathrm{c},\ell}$. Notice that, this relation depends on k_0 only through a_ℓ^*.

On the other hand, if temporal fluctuations are neglected, the solution for $T_{0,\ell}$ from the saddle point self-consistency equations is $|\widetilde{E}_{\mathrm{b},\ell}| = 2T_{0,\ell} \ln\left[3\sqrt{\pi}(T_{0,\ell}/\epsilon_{\mathrm{F}})^{3/2}/4\right]$ and $\mu_\ell = \widetilde{E}_{\mathrm{b},\ell}/2$ which leads to

$$T_{0,\ell} \sim \frac{|\widetilde{E}_{\mathrm{b},\ell}|}{2\ln\left(|\widetilde{E}_{\mathrm{b},\ell}|/\epsilon_{\mathrm{F}}\right)^{\frac{3}{2}}}. \tag{2.129}$$

up to logarithmic accuracy. Therefore, $T_{0,\ell}$ grows without bound as the coupling increases. Within this calculation, the normal state for $T > T_{0,\ell}$ is described by unbound and non-degenerate fermions since $\Delta_\ell(\mathbf{k}) = 0$ and $|\mu_\ell|/T_{0,\ell} \sim \ln(|\widetilde{E}_{\mathrm{b},\ell}|/\epsilon_{\mathrm{F}})^{3/2} \gg 1$. Notice that the

saddle point approximation becomes progressively worse with increasing coupling, since the formation of bound states is neglected.

I emphasize that, there is no phase transition across $T_{0,\ell}$ in strong coupling. However, this temperature is related to the pair breaking or dissociation energy scale [44]. To see this connection, I consider the chemical equilibrium between nondegenerate unbound fermions (f) and bound pairs (b) such that

$$b(\uparrow\downarrow) \leftrightarrow f(\uparrow) + f(\downarrow) \tag{2.130}$$

for THS singlet states and

$$b(\uparrow\uparrow) \leftrightarrow f(\uparrow) + f(\uparrow) \tag{2.131}$$

for SHS triplet states.

Notice that $T_{0,\ell}$ is sufficiently high that the chemical potential of the bosons and the fermions satisfy $|\mu_{\rm b}| \gg T$ and $|\mu_{\rm f}| \gg T$ at the temperature T of interest. Thus, both the unbound fermions (f) and molecules (b) can be treated as classical ideal gases. The equilibrium condition $\mu_{\rm b} = 2\mu_{\rm f}$ for these non-degenerate gases may be written as

$$T \ln\left[n_{\rm b}\left(\frac{2\pi}{M_{\rm b}T}\right)^{3/2}\right] - \widetilde{E}_{{\rm b},\ell} = 2T \ln\left[n_{\rm f}\left(\frac{2\pi}{M_{\rm f}T}\right)^{3/2}\right], \tag{2.132}$$

where $n_{\rm b}$ ($n_{\rm f}$) is the boson (fermion) density, $M_{\rm b}$ ($M_{\rm f}$) is the boson (fermion) mass, and $\widetilde{E}_{{\rm b},\ell}$ is the binding energy of a bosonic molecule. The dissociation temperature above which some fraction of the bound pairs (molecules) are dissociated, is then found to be

$$T_{{\rm dissoc},\ell} \approx \frac{|\widetilde{E}_{{\rm b},\ell}|}{\ln\left(|\widetilde{E}_{{\rm b},\ell}|/\epsilon_{\rm F}\right)^{\frac{3}{2}}}, \tag{2.133}$$

where I dropped a few constants of order unity. Therefore, the logarithmic term is an entropic contribution which favors broken pairs and leads to a dissociation temperature considerably lower than the absolute value of binding energy $|\widetilde{E}_{{\rm b},\ell}|$. The analysis above gives insight into the logarithmic factor appearing in Eq. (2.129) since $T_{0,\ell} \sim T_{{\rm dissoc},\ell}/2$. Thus, $T_{0,\ell}$ is essentially the pair dissociation temperature of bound pairs (molecules), while $T_{{\rm c},\ell}$ is the phase coherence temperature corresponding to BEC of bound pairs (bosonic molecules).

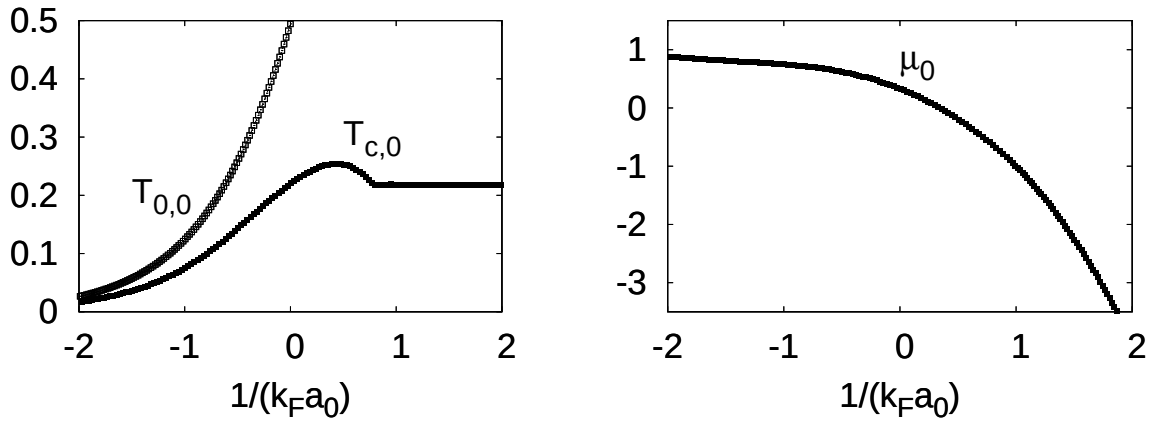

Figure 2.18: Plots of (a) critical temperature $T_{\rm r} = T_{\rm c,0}/\epsilon_{\rm F}$ and (b) chemical potential $\mu_{\rm r} = \mu_0/\epsilon_{\rm F}$ versus interaction strength $1/(k_{\rm F}a_0)$ at $T = T_{\rm c,0}$ for $k_0 \approx 200k_{\rm F}$. For $\ell = 0$ pairing, I show that the critical transition temperature grows from an exponential dependence in the BCS limit to a saturation in the BEC limit, while the mean field temperature characterizing the formation of pairs grows without limit.

In Fig. 2.18(a), I show $T_{\rm c,0}$ for the s-wave ($\ell = 0, m_\ell = 0$) case. Notice that $T_{\rm c,0}$ grows from an exponential dependence in weak coupling to a constant in strong coupling with increasing interaction. Furthermore, the mean field $T_{0,0}$ and gaussian $T_{\rm c,0}$ are similar only in weak coupling, while $T_{0,0}$ increases without bound as $T_{0,0} \sim 1/[(Ma_0^2)|\ln(k_{\rm F}a_0)|]$ in strong coupling. When $\mu_0 = 0$, I also obtain analytically $T_{\rm c,0}/\epsilon_{\rm F} \approx 2.15/(k_{\rm F}a_0^*)^2$ from Eq. (2.128). The hump in $T_{\rm c,0}$ around $1/(k_{\rm F}a_0) \approx 0.5$ is similar to the those in Ref. [44], and might be an artifact of the approximations used here. Thus, a more detailed self-consistent numerical analysis is needed to determine if this hump is real.

In Fig. 2.18(b), I show μ_0 for the s-wave case, where it changes from $\epsilon_{\rm F}$ in weak coupling to $E_{\rm b,0}/2 = -1/(2Ma_0^2)$ in strong coupling. Notice that, μ_0 at $T_{\rm c,0}$ is qualitatively similar to μ_0 at $T = 0$, however, it is reduced at $T_{\rm c,0}$ in weak coupling. Furthermore, μ_0 changes sign at $1/(k_{\rm F}a_0) \approx 0.32$.

In Fig. 2.19(a), I show $T_{\rm c,1}$ for the p-wave ($\ell = 1, m_\ell = 0$) case. $T_{\rm c,1}$ grows from an exponential dependence in weak coupling to a constant in strong coupling with increasing

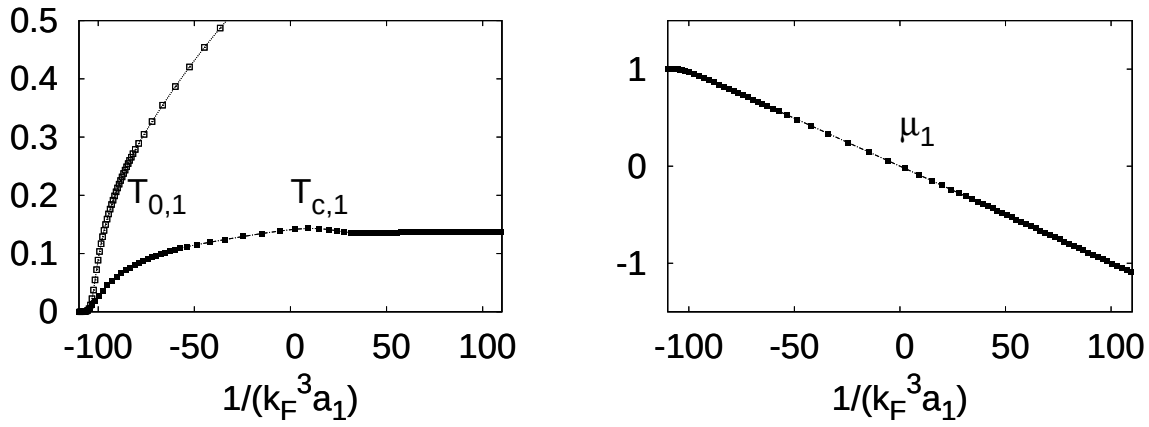

Figure 2.19: Plots of (a) critical temperature $T_{\rm r} = T_{c,1}/\epsilon_{\rm F}$ and (b) chemical potential $\mu_{\rm r} = \mu_1/\epsilon_{\rm F}$ versus interaction strength $1/(k_{\rm F}^3 a_1)$ at $T = T_{c,1}$ for $k_0 \approx 200 k_{\rm F}$. For $\ell = 1$ pairing, I show that the critical transition temperature grows from an exponential dependence in the BCS limit to a saturation in the BEC limit, while the mean field temperature characterizing the formation of pairs grows without limit.

interaction. For completeness, I present the limiting expressions

$$T_{\rm c,1} = \frac{8}{\pi}\epsilon_{\rm F} \exp\left[\gamma - \frac{8}{3} + \frac{\pi k_0}{4k_{\rm F}} - \frac{\pi}{2k_{\rm F}^3|a_1|}\right], \tag{2.134}$$

$$T_{\rm c,1} = \frac{2\pi}{M_{\rm B,1}}\left[\frac{n_1}{\zeta(3/2)}\right]^{\frac{2}{3}} = 0.137\epsilon_{\rm F}, \tag{2.135}$$

in the weak and strong coupling limits, respectively. Furthermore, the mean field $T_{0,1}$ and gaussian $T_{\rm c,1}$ are similar only in weak coupling, while $T_{0,1}$ increases without bound as $T_{0,1} \sim 1/[(Mk_0a_1)|\ln(k_{\rm F}^2 k_0 a_1)|]$ in strong coupling. When $\mu_1 = 0$, I also obtain analytically $T_{\rm c,1}/\epsilon_{\rm F} \approx 1.75/(k_{\rm F}^3 a_1^*)^{2/3}$ from Eq. (2.128). The hump in the intermediate regime is similar to the one found in fermion-boson model [128]. But to determine if this hump is real, it may be necessary to develop a fully self-consistent numerical calculation.

In Fig. 2.19(b), I show μ_1 for the p-wave case, where it changes from $\epsilon_{\rm F}$ in weak coupling to $E_{\rm b,1}/2 = -1/(Mk_0a_1)$ in strong coupling. Notice that, μ_1 at $T_{\rm c,1}$ is both qualitatively and quantitatively similar to μ_1 at $T = 0$. Furthermore, μ_1 changes sign at $1/(k_{\rm F}^3 a_1) \approx 0.02$.

For any given ℓ, mean field and gaussian theories lead to similar results for $T_{{\rm c},\ell}$ and $T_{0,\ell}$ in the BCS regime, while they are very different in the BEC side. In the latter case, $T_{0,\ell}$ increases without bound, however, the gaussian theory predicts in a constant critical

temperature which coincides with the BEC temperature of bosons. Notice that the temperature region between the pair formation $T_{c,\ell}$ and the pair condensation $T_{0,\ell}$ for $\ell = 0$ state is much larger than $\ell \neq 0$ states since $T_{0,\ell\neq 0}$ grows faster than $T_{0,\ell\neq 0}$. Furthermore, similar humps in $T_{c,\ell}$ around $1/(k_F^{2\ell+1}a_\ell) = 0$ are expected for any ℓ as shown for the s-wave and p-wave cases, however, whether these humps are physical or not may require a fully self-consistent numerical approach.

As shown in this section, the frequency (temporal) dependence of fluctuations about the saddle point is crucial to describe adequately the bosonic degrees of freedom that emerge with increasing coupling. In the next section, I derive the TDGL functional near $T_{c,\ell}$ to emphasize further the importance of these fluctuations.

2.7 Time-Dependent Ginzburg-Landau (TDGL) Functional near $T_{c,\ell}$

My basic motivation here is to investigate the low frequency and long wavelength behavior of the order parameter near $T_{c,\ell}$. To study the evolution of the time-dependent Ginzburg-Landau (TDGL) functional near $T_{c,\ell}$, I need to expand the effective action $S_\ell^{\rm eff}$ in Eq. (2.14) around $\Delta_{\ell,m_\ell} = 0$ leading to

$$S_\ell^{\rm eff} = S_\ell^{\rm sp} + S_\ell^{\rm gauss} + \frac{\beta}{2}\sum_{\{q_n,m_{\ell_n}\}} b_{\ell,\{m_{\ell_n}\}}(\{q_n\})\Lambda^\dagger_{\ell,m_{\ell_1}}(q_1)\Lambda_{\ell,m_{\ell_2}}(q_2) \Lambda^\dagger_{\ell,m_{\ell_3}}(q_3)\Lambda_{\ell,m_{\ell_4}}(q_1-q_2+q_3). \quad (2.136)$$

Here, $\Lambda_{\ell,m_\ell}(q)$ is the pairing fluctuation field.

I first consider the static part of $L^{-1}_{\ell,m_\ell,m'_\ell}(q)$, and expand it in powers of q_i to get

$$L^{-1}_{\ell,m_\ell,m'_\ell}(\mathbf{q},0) = a_{\ell,m_\ell,m'_\ell} + \sum_{i,j} c^{i,j}_{\ell,m_\ell,m'_\ell}\frac{q_i q_j}{2M} + ... \quad (2.137)$$

Next, I consider the time-dependence of the TDGL equation, where it is necessary to expand $L^{-1}_{\ell,m_\ell,m'_\ell}(0,iv_j) - L^{-1}_{\ell,m_\ell,m'_\ell}(0,0)$ in powers of w after analytic continuation $iv_j \to w + i0^+$.

In the $x = (\mathbf{x},t)$ representation, the calculation above leads to the TDGL equation

$$\sum_{m_{\ell_2}}\Bigg[a_{\ell,m_{\ell_1},m_{\ell_2}} - \sum_{i,j} c^{i,j}_{\ell,m_{\ell_1},m_{\ell_2}}\frac{\nabla_i\nabla_j}{2M} + \sum_{m_{\ell_3},m_{\ell_4}} b_{\ell,\{m_{\ell_n}\}}(0)\Lambda^\dagger_{\ell,m_{\ell_3}}(x)\Lambda_{\ell,m_{\ell_4}}(x) - id_{\ell,m_{\ell_1},m_{\ell_2}}\frac{\partial}{\partial t}\Bigg]\Lambda_{\ell,m_{\ell_2}}(x) = 0, \quad (2.138)$$

which is the generalization of the TDGL equation to higher momentum channels of THS singlet and SHS triplet states. Notice that, for THS triplet states, there may be extra gradient mixing textures and fourth order terms in the expansion [131], which are not discussed here. All static and dynamic expansion coefficients are presented in Appendix A.2. The condition $\det a_\ell = 0$ with matrix elements $a_{\ell,m_{\ell_1},m_{\ell_2}}$ is the Thouless criterion, which leads to the order parameter equation given in Eq. (2.103). The coefficient $c^{i,j}_{\ell,m_{\ell_1},m_{\ell_2}}$ reflects a major difference between $\ell = 0$ and $\ell \neq 0$ cases. While $c^{i,j}_{0,0,0} = c_{0,0,0}\delta_{i,j}$ is isotropic in space, $c^{i,j}_{\ell\neq 0,m_{\ell_1},m_{\ell_2}}$ is anisotropic, thus characterizing the anisotropy of the order parameter. The coefficient $b_{\ell,\{m_{\ell_n}\}}(0)$ is positive and guarantees the stability of the theory. The coefficient $d_{\ell,m_{\ell_1},m_{\ell_2}}$ is a complex number. Its imaginary part reflects the decay of Cooper pairs into the two-particle continuum for $\mu_\ell > 0$. However, for $\mu_\ell < 0$, imaginary part of $d_{\ell,m_{\ell_1},m_{\ell_2}}$ vanishes and the behavior of the order parameter is propagating reflecting the presence of stable bound states.

Next, I present the asymptotic forms of $a_{\ell,m_{\ell_1},m_{\ell_2}}$; $b_{\ell,\{m_{\ell_n}\}}(0)$; $c^{i,j}_{\ell,m_{\ell_1},m_{\ell_2}}$ and $d_{\ell,m_{\ell_1},m_{\ell_2}}$ which are used to recover the usual Ginzburg-Landau (GL) equation for BCS superfluids in weak coupling and the Gross-Pitaevskii (GP) equation for a weakly interacting dilute Bose gas in strong coupling.

2.7.1 Weak Coupling (BCS) Regime

The weak coupling BCS regime is characterized by $\mu_\ell > 0$ and $\mu_\ell \approx \epsilon_{\rm F} \gg T_{{\rm c},\ell}$. For any given ℓ, I find the following values for the coefficients

$$a_{\ell,m_{\ell_1},m_{\ell_2}} = \kappa^{\rm w}_\ell \ln\left(\frac{T}{T_{{\rm c},\ell}}\right)\delta_{m_{\ell_1},m_{\ell_2}}, \tag{2.139}$$

$$b_{\ell,\{m_{\ell_n}\}}(0) = 7\gamma_{\ell,\{m_{\ell_n}\}}\frac{\kappa^{\rm w}_\ell\zeta(3)}{8T^2_{{\rm c},\ell}}\left(\frac{\epsilon_{\rm F}}{\epsilon_0}\right)^\ell, \tag{2.140}$$

$$c^{i,j}_{\ell,m_{\ell_1},m_{\ell_2}} = 7\alpha^{i,j}_{\ell,m_{\ell_1},m_{\ell_2}}\frac{\kappa^{\rm w}_\ell\epsilon_{\rm F}\zeta(3)}{4\pi^2T^2_{{\rm c},\ell}}, \tag{2.141}$$

$$d_{\ell,m_{\ell_1},m_{\ell_2}} = \kappa^{\rm w}_\ell\left(\frac{1}{4\epsilon_{\rm F}} + i\frac{\pi}{8T_{{\rm c},\ell}}\right)\delta_{m_{\ell_1},m_{\ell_2}}, \tag{2.142}$$

where $\kappa^{\rm w}_\ell = N(\epsilon_{\rm F})(\epsilon_{\rm F}/\epsilon_0)^\ell/(4\pi)$ with $N(\epsilon_{\rm F}) = M\mathcal{V}k_{\rm F}/(2\pi^2)$ is the density of states per spin at the Fermi energy. Here $\delta_{m_{\ell_1},m_{\ell_2}}$ is the Kronecker delta, and $\alpha^{i,j}_{\ell,m_{\ell_1},m_{\ell_2}}$ and $\gamma_{\ell,\{m_\ell\}}$

are angular averaged quantities defined in App. A.2. Notice that the critical transition temperature is determined by $\det a_\ell = 0$.

In the particular case, where only one of the spherical harmonics $Y_{\ell,m_\ell}(\widehat{\mathbf{k}})$ is dominant and characterizes the order parameter, I can rescale the pairing field as

$$\Psi^{\mathrm{w}}_{\ell,m_\ell}(x) = \sqrt{\frac{b_{\ell,\{m_\ell\}}(0)}{\kappa^{\mathrm{w}}_\ell}}\Lambda_{\ell,m_\ell}(x) \tag{2.143}$$

to obtain the conventional TDGL equation [141]

$$\left[-\varepsilon_\ell + |\Psi^{\mathrm{w}}_{\ell,m_\ell}|^2 - \sum_i (\xi^{\mathrm{GL}}_{\ell,m_\ell})_i^2\nabla_i^2 + \tau^{\mathrm{GL}}_{\ell,m_\ell}\frac{\partial}{\partial t}\right]\Psi^{\mathrm{w}}_{\ell,m_\ell} = 0. \tag{2.144}$$

Here, $\varepsilon_\ell = (T_{\mathrm{c},\ell} - T)/T_{\mathrm{c},\ell}$ with $|\varepsilon_\ell| \ll 1$, $(\xi_{\ell,m_\ell})_i^2(T) = c^{i,i}_{\ell,m_\ell,m_\ell}/[2Ma_{\ell,m_\ell,m_\ell}] = (\xi^{\mathrm{GL}}_{\ell,m_\ell})_i^2/\varepsilon_\ell$ is the characteristic GL length and $\tau_{\ell,m_\ell} = -id_{\ell,m_\ell,m_\ell}/a_{\ell,m_\ell,m_\ell} = \tau^{\mathrm{GL}}_{\ell,m_\ell}/\varepsilon_\ell$ is the characteristic GL time.

In this limit, the GL coherence length is given by $k_{\mathrm{F}}(\xi^{\mathrm{GL}}_{\ell,m_\ell})_i = [7\alpha^{i,i}_{\ell,m_\ell,m_\ell}\zeta(3)/(4\pi^2)]^{1/2}(\epsilon_{\mathrm{F}}/T_{\mathrm{c},\ell})$, which makes $(\xi^{\mathrm{GL}}_{\ell,m_\ell})_i$ much larger than the interparticle spacing k_{F}^{-1}. There is a major difference between $\ell = 0$ and $\ell \neq 0$ pairings regarding $(\xi^{\mathrm{GL}}_{\ell,m_\ell})_i$. While $c^{i,j}_{0,0,0} = c_{0,0,0}\delta_{i,j}$ is isotropic, $c^{i,j}_{\ell\neq 0,m_{\ell_1},m_{\ell_2}} = c^{i,i}_{\ell,m_{\ell_1},m_{\ell_2}}\delta_{i,j}$ is in general anisotropic in space (see App. A.2). Thus, $(\xi^{\mathrm{GL}}_{0,0})_i$ is isotropic and $(\xi^{\mathrm{GL}}_{\ell\neq 0,m_\ell})_i$ is not.

Furthermore, $\tau^{\mathrm{GL}}_{\ell,m_\ell} = -i/(4\epsilon_{\mathrm{F}}) + \pi/(8T_{\mathrm{c},\ell})$ showing that the dynamics of $\Psi^{\mathrm{w}}_{\ell,m_\ell}(x)$ is overdamped reflecting the continuum of fermionic excitations into which a pair can decay. In addition, there is a small propagating term since there is no perfect particle-hole symmetry. As the coupling grows, the coefficient of the propagating term increases while that of the damping term vanishes for $\mu_\ell \leq 0$. Thus, the mode is propagating in strong coupling reflecting the stability of the bound states against the two particle continuum.

2.7.2 Strong Coupling (BEC) Regime

The strong coupling BEC regime is characterized by $\mu_\ell < 0$ and $\epsilon_0 = k_0^2/(2M) \gg |\mu_\ell| \gg T_{\mathrm{c},\ell}$. For $\ell = 0$, I find the following coefficients

$$
\begin{aligned}
a_{0,0,0} &= 2\kappa_0^{\mathrm{s}} \left(2|\mu_0| - |\widetilde{E}_{\mathrm{b},0}|\right), && (2.145)\\
b_{0,\{0\}}(0) &= \frac{\kappa_0^{\mathrm{s}}}{8\pi|\mu_0|}, && (2.146)\\
c_{0,0,0}^{i,j} &= \kappa_0^{\mathrm{s}}\delta_{i,j}, && (2.147)\\
d_{0,0,0} &= 2\kappa_0^{\mathrm{s}}, && (2.148)
\end{aligned}
$$

where $\kappa_0^{\mathrm{s}} = N(\epsilon_{\mathrm{F}})/(64\sqrt{\epsilon_{\mathrm{F}}|\mu_0|})$. Similarly, for $\ell \neq 0$, I obtain

$$
\begin{aligned}
a_{\ell\neq 0,m_{\ell_1},m_{\ell_2}} &= 2\kappa_\ell^{\mathrm{s}}\phi_\ell \left(2|\mu_\ell| - |\widetilde{E}_{\mathrm{b},\ell}|\right)\delta_{m_{\ell_1},m_{\ell_2}}, && (2.149)\\
b_{\ell\neq 0,\{m_{\ell_n}\}}(0) &= 15\gamma_{\ell,\{m_{\ell_n}\}}\frac{\kappa_\ell^{\mathrm{s}}\widehat{\phi}_\ell}{2\epsilon_0}, && (2.150)\\
c_{\ell\neq 0,m_{\ell_1},m_{\ell_2}}^{i,j} &= \kappa_\ell^{\mathrm{s}}\phi_\ell\delta_{m_{\ell_1},m_{\ell_2}}\delta_{i,j}, && (2.151)\\
d_{\ell\neq 0,m_{\ell_1},m_{\ell_2}} &= 2\kappa_\ell^{\mathrm{s}}\phi_\ell\delta_{m_{\ell_1},m_{\ell_2}}, && (2.152)
\end{aligned}
$$

where $\kappa_{\ell\neq 0}^{\mathrm{s}} = N(\epsilon_{\mathrm{F}})/(64\sqrt{\pi\epsilon_{\mathrm{F}}\epsilon_0})$. Here $\phi_\ell = \Gamma(\ell-1/2)/\Gamma(\ell+1)$ and $\widehat{\phi}_\ell = \Gamma(2\ell-3/2)/\Gamma(2\ell+2)$, where $\Gamma(x)$ is the Gamma function. Notice that, $c_{\ell\neq 0,m_{\ell_1},m_{\ell_2}}^{i,j}$ is isotropic in space for any ℓ. Thus, the anisotropy of the order parameter plays a secondary role in the TDGL theory in this limit.

In the particular case, where only one of the spherical harmonics $Y_{\ell,m_\ell}(\widehat{\mathbf{k}})$ is dominant and characterizes the order parameter, I can rescale the pairing field as

$$
\Psi_{\ell,m_\ell}^{\mathrm{s}}(x) = \sqrt{d_{\ell,m_\ell,m_\ell}}\Lambda_{\ell,m_\ell}(x), \tag{2.153}
$$

to obtain the conventional Gross-Pitaevskii (GP) equation

$$
\left[-\mu_{\mathrm{B},\ell} + U_{\ell,m_\ell}|\Psi_{\ell,m_\ell}^{\mathrm{s}}|^2 - \frac{\nabla^2}{2M_{\mathrm{B},\ell}} - i\frac{\partial}{\partial t}\right]\Psi_{\ell,m_\ell}^{\mathrm{s}} = 0 \tag{2.154}
$$

for a dilute gas of bosons. Here, $\mu_{\mathrm{B},\ell} = -a_{\ell,m_\ell,m_\ell}/d_{\ell,m_\ell,m_\ell} = 2\mu_\ell - \widetilde{E}_{\mathrm{b},\ell}$ is the chemical potential, $M_{\mathrm{B},\ell} = Md_{\ell,m_\ell,m_\ell}/c_{\ell,m_\ell,m_\ell}^{i,i} = 2M$ is the mass, and $U_{\ell,m_\ell} = b_{\ell,\{m_\ell\}}(0)/d_{\ell,m_\ell,m_\ell}^2$ is the repulsive interactions of the bosons. I obtain, $U_{0,0} = 4\pi a_0/M$ and $U_{\ell\neq 0,m_\ell} =$

$240\pi^2\sqrt{\pi}\widehat{\phi}_\ell\gamma_{\ell,\{m_\ell\}}/(M\phi_\ell^2 k_0)$ for $\ell = 0$ and $\ell \neq 0$, respectively. Notice that the mass of the composite bosons is independent of the anisotropy and symmetry of the order parameter for any given ℓ. However, this is not the case for the repulsive interactions between bosons, which explicitly depends on ℓ.

For $\ell = 0$, $U_{0,0} = 4\pi a_{\mathrm{B},0}/M_{\mathrm{B},0}$ is directly proportional to the fermion (boson) scattering length a_0 ($a_{\mathrm{B},0}$), where $a_{\mathrm{B},0} = 2a_0$ is the boson-boson scattering lenth. A better estimate for $a_{\mathrm{B},0} \approx 0.6a_0$ can be found in the literature [138, 63, 139, 140], by taking into account higher order processes. While for $\ell \neq 0$, U_{ℓ,m_ℓ} is a constant (independent of the scattering parameter a_ℓ) depending only on the interaction range k_0 and the particular (ℓ, m_ℓ) state. For a finite range potential, $n_{\mathrm{B},\ell}U_{\ell,m_\ell}$ is small compared to ϵ_{F}, where $n_{\mathrm{B},\ell} = n_\ell/2$ is the density of bosons. In the $\ell = 0$ case $n_{\mathrm{B},0}U_{0,0}/\epsilon_{\mathrm{F}} = 4k_{\mathrm{F}}a_0/(3\pi)$ is much smaller than unity. For $\ell \neq 0$ and even, $n_{\mathrm{B},\ell}U_{\ell,m_\ell}/\epsilon_{\mathrm{F}} = 80\sqrt{\pi}\widehat{\phi}_\ell\gamma_{\ell,\{m_\ell\}}/\phi_\ell^2(k_{\mathrm{F}}/k_0)$. In the case of SHS states where $\ell \neq 0$ and odd, $n_{\mathrm{B},\ell}U_{\ell,m_\ell}/\epsilon_{\mathrm{F}} = 40\sqrt{\pi}\widehat{\phi}_\ell\gamma_{\ell,\{m_\ell\}}/\phi_\ell^2(k_{\mathrm{F}}/k_0)$. The results for higher angular momentum channels reflect the diluteness condition $(k_{\mathrm{F}}/k_0)^3 \ll 1$.

To calculate $(\xi^{\mathrm{GL}}_{\ell,m_\ell})_i$ in the strong coupling limit, I need to know $\partial\mu_\ell/\partial T$ evaluated at $T_{\mathrm{c},\ell}$ (see below). The temperature dependence of μ_ℓ in the vicinity of $T_{\mathrm{c},\ell}$ can be obtained by noticing that $\mu_{\mathrm{B},\ell} = \widetilde{n}(T)U_{\ell,m_\ell}$, where $\widetilde{n}(T) = n_{\mathrm{B},\ell}\left[1 - (T/T_{\mathrm{c},\ell})^{3/2}\right]$. This leads to $k_{\mathrm{F}}(\xi^{\mathrm{GL}}_{\ell,m_\ell})_i = [\pi^2/(2Mk_{\mathrm{F}}U_{\ell,m_\ell})]^{1/2}$ in the BEC regime. Using the asymptotic values of U_{ℓ,m_ℓ}, I obtain $k_{\mathrm{F}}(\xi^{\mathrm{GL}}_{0,0})_i = [\pi/(8k_{\mathrm{F}}a_0)]^{1/2}$ for $\ell = 0$ and $k_{\mathrm{F}}(\xi^{\mathrm{GL}}_{\ell\neq 0,m_\ell})_i = \left[\phi_\ell^2/(480\sqrt{\pi}\gamma_{\ell,\{m_\ell\}}\widehat{\phi}_\ell)\right]^{1/2}(k_0/k_{\mathrm{F}})^{1/2}$ for $\ell \neq 0$. Therefore, $(\xi^{\mathrm{GL}}_{\ell,m_\ell})_i$ is also much larger than the interparticle spacing k_{F}^{-1} in this limit, since $k_{\mathrm{F}}a_0 \to 0$ for $\ell = 0$ and $k_0 \gg k_{\mathrm{F}}$ for any ℓ.

2.7.3 Ginzburg-Landau Coherence Length versus Average Cooper Pair Size

In the particular case, where only one of the spherical harmonics $Y_{\ell,m_\ell}(\widehat{\mathbf{k}})$ is dominant and characterizes the order parameter, I can define the GL coherence length as $(\xi_{\ell,m_\ell})_i^2(T) = c^{i,i}_{\ell,m_\ell,m_\ell}/(2Ma_{\ell,m_\ell,m_\ell})$. An expansion of the parameters a_{ℓ,m_ℓ,m_ℓ} and $c^{i,i}_{\ell,m_\ell,m_\ell}$ in the vicinity of $T_{\mathrm{c},\ell}$ leads to

$$(\xi_{\ell,m_\ell})_i^2(T) \approx (\xi^{\mathrm{GL}}_{\ell,m_\ell})_i^2\frac{T_{\mathrm{c},\ell}}{T_{\mathrm{c},\ell} - T}, \tag{2.155}$$

where the prefactor is the GL coherence length and given by

$$(\xi^{\rm GL}_{\ell,m_\ell})^2_i = \frac{c^{i,i}_{\ell,m_\ell,m_\ell}}{2MT_{{\rm c},\ell}} \left[\frac{\partial a_{\ell,m_\ell,m_\ell}}{\partial T}\right]^{-1}_{T=T_{{\rm c},\ell}}. \tag{2.156}$$

The slope of the coefficient a_{ℓ,m_ℓ,m_ℓ} with respect to T is given by

$$\frac{\partial a_{\ell,m_\ell,m_\ell}}{\partial T} = \sum_{\mathbf{k}} \left[\frac{\mathcal{Y}_\ell(\mathbf{k})}{2T^2} + \frac{\partial \mu_\ell}{\partial T}\left(\frac{\mathcal{Y}_\ell(\mathbf{k})}{2T\xi_\ell(\mathbf{k})} - \frac{\mathcal{X}_\ell(\mathbf{k})}{\xi^2_\ell(\mathbf{k})}\right)\right] \frac{\Gamma^2_\ell(k)}{8\pi}. \tag{2.157}$$

Here $\mathcal{X}_\ell(\mathbf{k})$ and $\mathcal{Y}_\ell(\mathbf{k})$ are defined in App. A.2. Notice that, while $\partial\mu_\ell/\partial T$ vanishes at $T_{c,\ell}$ in weak coupling, it plays an important role in strong coupling. Furthermore, while $(\xi^{\rm GL}_{\ell,m_\ell})_i$ representing the phase coherence length is large compared to interparticle spacing in both BCS and BEC limits, it should have a minimum near $\mu_\ell \approx 0$.

The prefactor $(\xi^{\rm GL}_{\ell,m_\ell})_i$ of the GL coherence length must be compared with the average Cooper pair size $\xi^{\rm pair}_\ell$ defined by

$$(\xi^{\rm pair}_\ell)^2 = \frac{\langle \mathcal{Z}_\ell(\mathbf{k})|r^2|\mathcal{Z}_\ell(\mathbf{k})\rangle}{\langle \mathcal{Z}_\ell(\mathbf{k})|\mathcal{Z}_\ell(\mathbf{k})\rangle} = -\frac{\langle \mathcal{Z}_\ell(\mathbf{k})|\nabla^2_{\mathbf{k}}|\mathcal{Z}_\ell(\mathbf{k})\rangle}{\langle \mathcal{Z}_\ell(\mathbf{k})|\mathcal{Z}_\ell(\mathbf{k})\rangle}, \tag{2.158}$$

where $\mathcal{Z}_\ell(\mathbf{k}) = \Delta_\ell(\mathbf{k})/[2E_\ell(\mathbf{k})]$ is the zero temperature pair wave function [117]. In the BCS limit, $\xi^{\rm pair}_\ell$ is much larger than the interparticle distance $k_{\rm F}^{-1}$ since the Cooper pairs are weakly bound. Furthermore, for $\mu_\ell < 0$, I expect that $\xi^{\rm pair}_\ell$ is a decreasing function of interaction for any ℓ, since Cooper pairs become more tightly bound as the interaction increases. Next, I compare $(\xi^{\rm GL}_{\ell,m_\ell})_i$ and $\xi^{\rm pair}_\ell$ for s-wave ($\ell = 0$) and p-wave ($\ell = 1$) states.

In Fig. 2.20, a comparison between $(\xi^{\rm GL}_{0,0})_i$ and $\xi^{\rm pair}_0$ is shown for s-wave ($\ell = 0, m_\ell = 0$). $\xi^{\rm pair}_0$ changes from $k_{\rm F}\xi^{\rm pair}_0 = [e^\gamma/\sqrt{2}\pi](\epsilon_{\rm F}/T_{c,0})$ in the BCS limit to $k_{\rm F}\xi^{\rm pair}_0 = [\epsilon_{\rm F}/(2|\mu_0|)]^{1/2} = k_{\rm F}a_0/\sqrt{2}$ in the BEC limit as the interaction increases. Here $\gamma \approx 0.577$ is the Euler's constant. Furthermore, when $\mu_0 = 0$, I obtain $k_{\rm F}\xi^{\rm pair}_0 = \sqrt{7}[\Gamma^2(1/4)/\sqrt{\pi}]^{1/3}/4 \approx 1.29$, where $\Gamma(x)$ is the Gamma function. Notice that, $\xi^{\rm pair}_0$ is continuous at $\mu_0 = 0$, and monotonically decreasing function of $1/(k_{\rm F}a_0)$ with a limiting value controlled by a_0 in strong coupling. However, $(\xi^{\rm GL}_{0,0})_i$ is a non-monotonic function of $1/(k_{\rm F}a_0)$ having a minimum around $1/(k_{\rm F}a_0) \approx 0.32$ ($\mu_0 = 0$). It changes from $k_{\rm F}(\xi^{\rm GL}_{0,0})_i = [7\zeta(3)/(12\pi^2)]^{1/2}(\epsilon_{\rm F}/T_{c,0})$ in the BCS to $k_{\rm F}(\xi^{\rm GL}_{0,0})_i = [\pi/(8k_{\rm F}a_0)]^{1/2}$ in the BEC limit as the coupling increases, where $\zeta(x)$ is the Zeta function. Notice that, $(\xi^{\rm GL}_{0,0})_i$ grows as $1/\sqrt{k_{\rm F}a_0}$ in strong coupling limit.

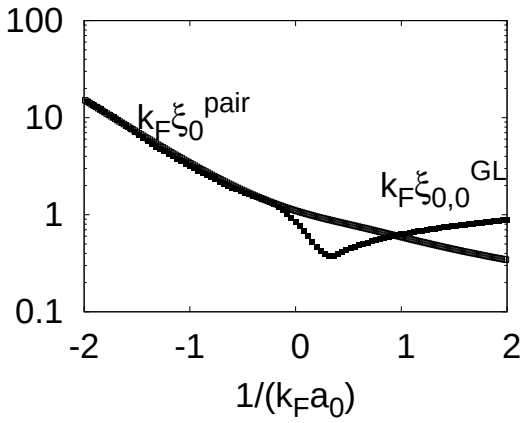

Figure 2.20: Plots of GL coherence length $k_{\rm F}\xi_{0,0}^{\rm GL}$ (solid squares), and zero temperature Cooper pair size $k_{\rm F}\xi_{0,0}^{\rm pair}$ (hollow squares) versus interaction strength $1/(k_{\rm F}a_0)$ at $T = T_{\rm c,0}$ for $k_0 \approx 200k_{\rm F}$. For $\ell = 0$ pairing, compared to the interparticle distance, I show that both Cooper pair size and GL coherence length are large in the BCS limit, and while Cooper pair size continue to decrease as a function of interaction strength, the GL coherence length increases after having a minimum in the intermediate region. Notice that the evolution of Cooper pair size is analytic for all interaction strengths.

In Fig. 2.21, a comparison between $(\xi_{1,0}^{\rm GL})_z$ and $\xi_1^{\rm pair}$ is shown for p-wave ($\ell = 1, m_\ell = 0$). Notice that, $\xi_1^{\rm pair}$ is nonanalytic at $\mu_1 = 0$, and is a monotonically decreasing function of $1/(k_{\rm F}^3 a_1)$ with a limiting value controlled by $k_{\rm F}/k_0$ in strong coupling. This nonanalytic behavior is associated with the change in $E_1(\mathbf{k})$ from gapless (with line nodes) in the BCS to fully gapped in the BEC side. However, $(\xi_{1,0}^{\rm GL})_z$ is a non-monotonic function of $1/(k_{\rm F}^3 a_1)$ having a minimum around $1/(k_{\rm F}^3 a_1) \approx 0.02$ ($\mu_1 = 0$). It changes from $k_{\rm F}(\xi_{1,0}^{\rm GL})_x = k_{\rm F}(\xi_{1,0}^{\rm GL})_y = k_{\rm F}(\xi_{1,0}^{\rm GL})_z/\sqrt{3} = [7\zeta(3)/(20\pi^2)]^{1/2}(\epsilon_{\rm F}/T_{\rm c,1})$ in the BCS to $k_{\rm F}(\xi_{1,0}^{\rm GL})_i = [\pi k_0/(36k_{\rm F})]^{1/2}$ in the BEC limit as the coupling increases. Notice that, $\xi_{1,0}^{\rm GL}$ saturates in strong coupling limit reflecting the finite range of interactions.

It is important to emphasize that $(\xi_{\ell,m_\ell}^{\rm GL})_z$ shown in Figs. (2.20) and (2.21) is only qualitative in the intermediate regime around unitarity $1/(k_{\rm F}^{2\ell+1}a_\ell) = 0$ since my theory may not be strictly applicable in that region, but it converges and provides a good qualitative interpolation between BCS and BEC regimes.

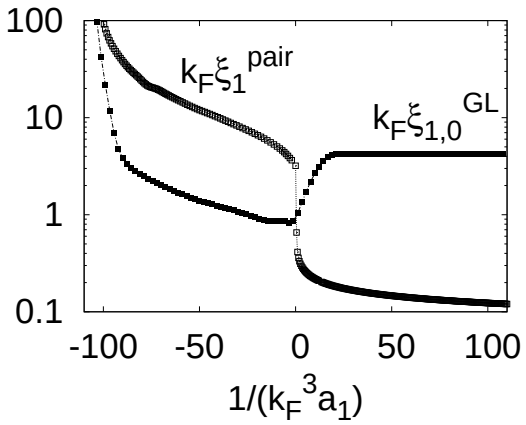

Figure 2.21: Plots of GL coherence length $k_{\rm F}(\xi^{\rm GL}_{1,0})_z$ (solid squares), and zero temperature Cooper pair size $k_{\rm F}\xi^{\rm pair}_{1,0}$ (hollow squares) versus interaction strength $1/(k_{\rm F}^3 a_1)$ at $T = T_{\rm c,1}$ for $k_0 \approx 200 k_{\rm F}$. For $\ell = 1$ pairing, compared to the interparticle distance, I show that both Cooper pair size and GL coherence length are large in the BCS limit, and while Cooper pair size continue to decrease as a function of interaction strength, the GL coherence length grovs and saturates after having a minimum in the intermediate region. Notice that the evolution of Cooper pair size is non-analytic when μ_1 changes from positive values in the BCS side to negative values in the BEC side as a function of interaction strength. Furthermore, GL coherence length is anisotropic in the BCS limit, which becomes isotropic only in the BEC limit (not shown).

2.8 Summary

In this chapter, I extended the s-wave ($\ell = 0$) functional integral formalism to finite angular momentum ℓ including two hyperfine states (THS) pseudo-spin singlet and single hyperfine states (SHS) pseudo-spin triplet channels. I analyzed analytically superfluid properties of dilute Fermi gases in the ground state ($T = 0$) and near critical temperatures ($T \approx T_{\rm c,\ell}$) from the weak fermion attraction BCS limit to the strong fermion attraction BEC limit as a function of scattering parameter (a_ℓ) for arbitrary ℓ. However, I presented numerical results only for THS s-wave and SHS p-wave symmetries which may be relevant for current experiments involving atomic Fermi gases. The main results of this chapter are as follows.

First, I analyzed the low energy scattering amplitude within a T-matrix approach. I found that bound states occur only when $a_\ell > 0$ for any ℓ. The energy of the bound states $E_{\rm b,\ell}$ involves only the scattering parameter a_0 for $\ell = 0$. However, another parameter related to the interaction range $1/k_0$ is necessary to characterize $E_{\rm b,\ell}$ for $\ell \neq 0$. Therefore, all superfluid properties for $\ell \neq 0$ depend strongly on k_0 and a_ℓ, while for $\ell = 0$ they depend

strongly only on a_0 but weakly on k_0.

Then, I discussed the order parameter, chemical potential, quasiparticle excitations, momentum distribution, atomic compressibility, ground state energy, collective modes and average Cooper pair size at $T = 0$. There I showed that the evolution from BCS to BEC is just a crossover for $\ell = 0$, while the same evolution for $\ell \neq 0$ exhibits a quantum phase transition characterized by a gapless superfluid on the BCS side to a fully gapped superfluid on the BEC side. This transition is a many-body effect and takes place exactly when chemical potential $\mu_{\ell\neq 0}$ crosses the bottom of the fermion band ($\mu_{\ell\neq 0} = 0$), and is best reflected as non-analytic behavior in the ground state atomic compressibility, momentum distribution and average Cooper pair size.

Lastly, I discussed the critical temperature, chemical potential, and the number of unbound, scattering and bound fermions at $T = T_{\mathrm{c},\ell}$. I found that the critical BEC temperature is the highest for $\ell = 0$. I also derived the time-dependent Ginzburg-Landau functional (TDGL) near $T_{\mathrm{c},\ell}$ and extracted the Ginzburg-Landau (GL) coherence length and time. I recovered the usual TDGL equation for BCS superfluids in the weak fermion attraction BCS limit, whereas in the strong fermion attraction BEC limit I recovered the Gross-Pitaevskii (GP) equation for a weakly interacting dilute Bose gas. The TDGL equation exhibits anisotropic coherence lengths for $\ell \neq 0$ which become isotropic only in the BEC limit, in sharp contrast to the $\ell = 0$ case, where the coherence length is isotropic for all interaction strengths. Furthermore, the GL time is a complex number with a larger imaginary component for $\mu_\ell > 0$ reflecting the decay of Cooper pairs into the two particle continuum. However, for $\mu_\ell < 0$ the imaginary component vanishes and Cooper pairs become stable above $T_{\mathrm{c},\ell}$.

In summary, the BCS to BEC evolution in higher angular momentum ($\ell \neq 0$) states exhibit quantum phase transitions and is much richer than in conventional $\ell = 0$ s-wave systems, where there is only a crossover. Signatures of this quantum phase transition can be found in measurable quantities such as momentum distribution, atomic compressibility, collective excitations, etc. as discussed in this chapter. These $\ell \neq 0$ states might be found not only in atomic Fermi gases, but also in nuclear (pairing in nuclei), astrophysics (neutron

stars) and condensed matter (high-T_c and organic superconductors) systems.

In addition, similar topological quantum phase transitions with much richer phase diagram occur in two-species fermion mixtures with mass and population imbalance as discussed in the next chapter.

CHAPTER III

TWO-SPECIES FERMION MIXTURES WITH MASS AND POPULATION IMBALANCE

In the previous chapter, I analyzed zero and nonzero orbital angular momentum pairing effects, and show that a quantum phase transition occurs for nonzero angular momentum pairing, unlike the s-wave case where the BCS to BEC evolution is just a crossover. I showed that this quantum phase transition was topological in its nature, characterized by a gapless superfluid on the BCS side to a fully gapped superfluid on the BEC side. Several quantum phase transitions with much richer phase diagram also occur in two-component fermion mixtures with different masses and/or different populations as discussed next in this chapter.

3.1 Introduction

Major experimental breakthroughs have been made recently involving one-species trapped fermions (^{6}Li) in two hyperfine states with different populations. The superfluid to normal phase transition and the vortex state [76], as well as phase separation between paired and unpaired fermions [77] were identified as a function of population imbalance and scattering parameter. These studies are important extensions of the so-called BCS to BEC evolution for equal populations, which were studied via the use of Feshbach resonances [71, 72, 73, 75].

In contrast with the crossover physics found in the symmetric case (equal masses and equal spin populations) [37, 38, 41, 44, 110], these experiments [76, 77] have demonstrated the existence of phase transitions between normal and superfluid phases, as well as phase separation between superfluid (paired) and normal (excess) fermions as a function of population imbalance [111, 112, 143, 144]. These one-species experiments with population imbalance are ideal candidates for the observation of uniform and non-uniform superfluid phases, which may be present not only in atomic, but also in nuclear (pairing in nuclei),

astrophysics (neutron stars), and condensed matter (superconductors) systems. Following these experiments, the problem of fermion superfluidity with population imbalance has been revisited recently in several theoretical works in continuum and trapped systems [145, 146, 147, 148, 149, 150, 151].

Arguably one of the next frontiers of exploration in cold Fermi gases is the study of asymmetric two-component fermion superfluidity (unequal masses, and equal or unequal populations) in two-species fermion mixtures from the BCS to the BEC limit. Earlier works on two-species fermion mixtures with unequal masses were limited to the BCS regime [152, 153, 154]. However, very recently, the evolution from BCS to BEC was preliminarily addressed in homogenous systems as a function of population imbalance and scattering length especially for ^{6}Li and ^{40}K mixtures as well as other mixtures including ^{6}Li and ^{87}Sr or ^{40}K and ^{87}Sr [155, 156, 157]. In addition, the superfluid phase diagram of trapped systems at unitarity was also analyzed as a function of population imbalance and mass anisotropy [158] (see also Ref. [159]).

In this chapter, I study the BCS to BEC evolution of asymmetric two-component fermion superfluids as a function of scattering parameter, population imbalance and mass anisotropy. My main results are as follows.

For homogeneous systems, I analyze the ground state *saddle point* phase diagrams for two-species fermion mixtures as a function of scattering parameter, mass anisotropy and population imbalance. I identify regions corresponding to normal, uniform or non-uniform superfluid phases, and discuss topological quantum phase transitions in the BCS, unitarity and BEC limits. I derive the Ginzburg-Landau theory near the critical temperature, and show that it describes a dilute mixture of weakly interacting paired and unpaired fermions in the BEC limit. I also derive the zero temperature low frequency and long wavelength collective excitation spectrum for zero population imbalance, and recover the Bogoliubov relation for weakly interacting dilute bosons in the BEC limit. In addition, I describe analytically phase separation boundaries of the resulting Bose-Fermi mixture of paired fermions and unpaired fermions in the BEC limit. Lastly, I discuss the effects of harmonic traps and the resulting density profiles of paired and unpaired fermions in the BEC regime.

Furthermore, in the BEC limit, I analyze the *exact* superfluid phase diagram of two-species dilute Fermi-Fermi mixtures with equal or unequal masses. I first calculate the exact boson-fermion scattering length as a function of mass anisotropy, and then construct the exact phase diagrams. In addition to the normal and uniform superfluid phases, I find two different non-uniform phase separated (PS) states: (1) phase separation between pure unpaired (excess) and pure tightly paired fermions (molecular bosons), and (2) phase separation between pure excess fermions and a mixture of excess fermions and molecular bosons. For equal mass mixtures, the results for the phase boundary between phase separation and uniform superfluid phases is quantitative agreement with the saddle point results, however, there are important qualitative and quantitative differences for unequal mass mixtures showing the importance of fluctuations.

For optical lattices, I used an attractive Fermi-Hubbard Hamiltonian to describe fermion mixtures, and obtain the ground state phase diagram consisting of normal, phase-separated and coexisting superfluid/excess-fermions, and insulating regions as a function of interaction strength and density of fermions. I show that when molecular bosons are formed (in the strong attraction limit), they interact with each other strongly and repulsively. Furthermore, when there are excess fermions, the resulting system corresponds to a strongly interacting (repulsive) mixture of molecular bosons and fermions, in sharp contrast with homogenous systems where the resulting boson-fermion mixture is weakly interacting. This result is a direct manifestation of the Pauli exclusion principle in the lattice case, since each molecular boson consists of two fermions, and more than one identical fermion on the same lattice site is not allowed. Lastly, several insulating phases appear in the strong attraction limit depending on fermion filling fractions. For instance, I find a molecular Bose-Mott insulator (superfluid) for molecular filling fraction equal to (less than) one when fermion filling fractions are identical, which is in qualitative agreement with a recent experiment from MIT [87]. Furthermore, when the filling fraction of one type of fermion is one and the filling fraction of the other is one-half (corresponding to molecular boson and excess fermion filling fractions of one-half), I also find either a phase-separated state consisting of a Fermi-Pauli insulator (FPI) of the excess fermions and a molecular Bose-Mott insulator

(BMI) or a Bose-Fermi checkerboard (BFC) phase depending on the tunneling anisotropy.

The rest of this chapter is organized as follows. After introducing the Hamiltonian in Section 3.2, I introduce the imaginary-time functional integration formalism in Section 3.3, and obtain the self-consistency (order parameter and number) equations. In Section 3.4, I discuss the evolution from BCS to BEC superfluidity at zero temperature within the saddle point approximation, and analyze the order parameter, chemical potential, quasiparticle excitation spectrum and momentum distribution. In addition, I obtain the ground state phase diagrams by analyzing the stability of the saddle point solutions. In Section 3.5, I discuss gaussian fluctuations near the critical temperature to derive the time-dependent Ginzburg-Landau (TDGL) equations, and at zero temperature to obtain the low energy collective excitations. In addition, I discuss the effects of harmonic traps on the density profile of paired and unpaired fermions at zero temperature. In Section 3.6, I discussed corrections to the ground state phase diagrams which are beyond the saddle point approximation in the BEC regime. Then, I analyzed the superfluid and insulating phases of mass and population imbalanced fermion mixtures in Section 3.7. A summary of my conclusions is given in Section 3.8. Lastly, I present in Appendices B.1, B.5, and B.3 the elements of the inverse fluctuation matrix, and their low frequency and long wavelength expansion coefficients at zero and finite temperatures.

3.2 Two-Species Hamiltonian

To describe a dilute two-species Fermi gas in three dimensions, I start from the Hamiltonian ($\hbar = 1$)

$$H = \sum_{\mathbf{k},\sigma} \xi_{\mathbf{k},\sigma} a^\dagger_{\mathbf{k},\sigma} a_{\mathbf{k},\sigma} + \sum_{\mathbf{k},\mathbf{k}',\mathbf{q}} U(\mathbf{k},\mathbf{k}') b^\dagger_{\mathbf{k},\mathbf{q}} b_{\mathbf{k}',\mathbf{q}}, \tag{3.1}$$

where the pseudo-spin σ labels both the type and hyperfine states of atoms represented by the creation operator $a^\dagger_{\mathbf{k},\sigma}$, and by the pair creation operator $b^\dagger_{\mathbf{k},\mathbf{q}} = a^\dagger_{\mathbf{k}+\mathbf{q}/2,\uparrow} a^\dagger_{-\mathbf{k}+\mathbf{q}/2,\downarrow}$. Here, $\xi_{\mathbf{k},\sigma} = \epsilon_{\mathbf{k},\sigma} - \mu_\sigma$, where $\epsilon_{\mathbf{k},\sigma} = k^2/(2m_\sigma)$ is the energy and μ_σ is the chemical potential of the fermions.

Notice that, to describe mass and population imbalanced fermion mixtures, I allow for the fermions to have different masses m_σ and different populations controlled by independent

chemical potentials μ_σ. The attractive fermion-fermion interaction $U(\mathbf{k},\mathbf{k}')$ can be written in a separable form as

$$U(\mathbf{k},\mathbf{k}') = -g\Gamma^*_{\mathbf{k}}\Gamma_{\mathbf{k}'}, \tag{3.2}$$

where $g > 0$. For the s-wave symmetry discussed, $\Gamma_{\mathbf{k}} = 1$ for $k < k_0$ and $\Gamma_{\mathbf{k}} = 0$ for $k > k_0$, where k_0 is an ultraviolet cut-off for the s-wave interaction. This cutoff is eliminated in the following sections, when I express the interaction strength g in terms of the s-wave scattering length a_F. It is important to emphasize that my final results depend only on a_F and are independent of the specific value of k_0.

3.3 Functional Integral Formalism

In this section, I extend the functional integral formalism to describe two-species fermion mixtures with mass and population imbalance. My generalized formalism and results reduce to the usual expressions when fermion masses and populations are equal.

3.3.1 Effective Action

In the imaginary-time functional integral formalism ($\beta = 1/T$ and unit $k_B = 1$) [99], the partition function for the Hamiltonian in Eq. (3.1) can be written as

$$\mathcal{Z} = \int \mathcal{D}[a^\dagger, a] e^{-S[a^\dagger,a]}, \tag{3.3}$$

where S is the action, given by

$$S = \int_0^\beta d\tau \left[\sum_{\mathbf{k},\sigma} a^\dagger_{\mathbf{k},\sigma}(\tau)\frac{\partial}{\partial\tau} a_{\mathbf{k},\sigma}(\tau) + H(\tau) \right]. \tag{3.4}$$

Here, τ is the imaginary time and $a^\dagger_{\mathbf{k},\sigma}(\tau)$ and $a_{\mathbf{k},\sigma}(\tau)$ are Grassmann variables [100, 124]. The Hamiltonian can be rewritten in the form

$$H(\tau) = \sum_{\mathbf{k},\sigma} \xi_{\mathbf{k},\sigma} a^\dagger_{\mathbf{k},\sigma}(\tau) a_{\mathbf{k},\sigma}(\tau) - g\sum_{\mathbf{q}} B^\dagger_{\mathbf{q}}(\tau) B_{\mathbf{q}}(\tau), \tag{3.5}$$

where I define the operator $B_{\mathbf{q}}(\tau) = \sum_{\mathbf{k}} \Gamma(\mathbf{k}) b_{\mathbf{k},\mathbf{q}}(\tau)$. I first introduce the Nambu spinor $\psi^\dagger(p) = (a^\dagger_{p,\uparrow}, a_{-p,\downarrow})$, where $p = (\mathbf{k}, iw_\ell)$ denotes both momentum and fermionic Matsubara frequency $w_\ell = (2\ell+1)\pi/\beta$, and use the Hubbard-Stratonovich transformation [125, 126]

$$e^{gB^\dagger(q)B(q)} = \int \mathcal{D}[\Phi^\dagger, \Phi] e^{-\frac{\Phi^\dagger(q)\Phi(q)}{g} + [B^\dagger(q)\Phi(q) + h.c.]} \tag{3.6}$$

to decouple the fermionic degrees of freedom at the expense of introducing the bosonic complex field $\Phi(q)$. Here, $q = (\mathbf{q}, iv_\ell)$ denotes both momentum and bosonic Matsubara frequency $v_\ell = 2\pi\ell/\beta$. I write

$$\Phi(q) = \Delta_0 \delta_{q,0} + \Lambda(q), \tag{3.7}$$

where Δ_0 is the τ-independent saddle point and $\Lambda(q)$ is the τ-dependent fluctuation.

Performing a Gaussian integration over the fermionic degrees of freedom and an expansion of S to quadratic order in $\Lambda(q)$, I obtain the gaussian effective action

$$S_{\text{Gauss}} = S_0 + \frac{\beta}{2} \sum_q \bar{\Lambda}^\dagger(q) \mathbf{F}^{-1}(q) \bar{\Lambda}(q), \tag{3.8}$$

the vector $\bar{\Lambda}^\dagger(q)$ is such that $\bar{\Lambda}^\dagger(q) = [\Lambda^\dagger(q), \Lambda(-q)]$. Here, the saddle point action is given by

$$S_0 = \beta \frac{|\Delta_0|^2}{g} - \sum_p \text{Tr} \ln[\mathbf{G}^{\text{sp}}(\text{p})/\beta]^{-1}, \tag{3.9}$$

where $(\mathbf{G}^{\text{sp}})^{-1}(p)$ is the inverse fermion propagator, and

$$\Delta_{\mathbf{k}} = \Delta_0 \Gamma_{\mathbf{k}}. \tag{3.10}$$

is the order parameter. The matrix $(\mathbf{G}^{\text{sp}})^{-1}(p)$ is defined by

$$(\mathbf{G}^{\text{sp}})^{-1}(p) = \begin{pmatrix} iw_\ell - \xi_{\mathbf{k},\uparrow} & \Delta_{\mathbf{k}} \\ \Delta^*_{\mathbf{k}} & iw_\ell + \xi_{\mathbf{k},\downarrow} \end{pmatrix}. \tag{3.11}$$

Furthermore, the vector $\bar{\Lambda}^\dagger(q)$ is the order parameter fluctuation field and $\mathbf{F}^{-1}(q)$ is the inverse fluctuation propagator. The matrix elements of $\mathbf{F}^{-1}(q)$ are given by

$$\mathbf{F}^{-1}_{1,1}(q) = \frac{1}{g} - \frac{1}{\beta} \sum_p \mathbf{G}^{\text{sp}}_{\uparrow,\uparrow}(\frac{q}{2} + p) \mathbf{G}^{\text{sp}}_{\downarrow,\downarrow}(\frac{q}{2} - p) |\Gamma_{\mathbf{k}}|^2, \tag{3.12}$$

$$\mathbf{F}^{-1}_{1,2}(q) = \frac{1}{\beta} \sum_p \mathbf{G}^{\text{sp}}_{\uparrow,\downarrow}(\frac{q}{2} + p) \mathbf{G}^{\text{sp}}_{\uparrow,\downarrow}(\frac{q}{2} - p) |\Gamma_{\mathbf{k}}|^2. \tag{3.13}$$

Notice that $\mathbf{F}^{-1}_{2,1}(q) = (\mathbf{F}^{-1}_{1,2})^*(q)$ and $\mathbf{F}^{-1}_{2,2}(q) = \mathbf{F}^{-1}_{1,1}(-q)$. These matrix elements are described further in appendix B.1. The fluctuation term in the action leads to a correction to the thermodynamic potential, which can be written as $\Omega_{\text{Gauss}} = \Omega_0 + \Omega_{\text{fluct}}$ with $\Omega_0 = S_0/\beta$ and

$$\Omega_{\text{fluct}} = \frac{1}{\beta} \sum_q \ln \det[\mathbf{F}^{-1}(q)/\beta]. \tag{3.14}$$

The action and thermodynamic potentials defined above are used to derive the self-consistency equations, as discussed next.

3.3.2 Self-consistency Equations

The saddle point condition $\delta S_0/\delta\Delta_0^* = 0$ imposed on Eq. (3.9) or the relation

$$\Delta_{\mathbf{k}'} = -\frac{1}{\beta}\lim_{\tau\to 0}\sum_p U(\mathbf{k},\mathbf{k}')\mathbf{G}^{\rm sp}_{\uparrow,\downarrow}(p)\exp(iw_\ell\tau) \tag{3.15}$$

leads to an equation for the order parameter

$$\frac{1}{g} = \sum_{\mathbf{k}}\frac{|\Gamma_{\mathbf{k}}|^2}{2E_{\mathbf{k},+}}\mathcal{X}_{\mathbf{k},+}, \tag{3.16}$$

where $\mathcal{X}_{\mathbf{k},\pm} = (\mathcal{X}_{\mathbf{k},1} \pm \mathcal{X}_{\mathbf{k},2})/2$ with $\mathcal{X}_{\mathbf{k},s} = \tanh(\beta E_{\mathbf{k},s}/2)$. Notice that, at low temperatures $T \approx 0$, $\theta(-E_{\mathbf{k},\mathbf{s}}) = \lim_{\beta\to\infty}\mathcal{X}_{\mathbf{k},s}$, where $\theta(x)$ is the Heaviside function. Here, $E_{\mathbf{k},\pm} = (E_{\mathbf{k},1} \pm E_{\mathbf{k},2})/2$ and $\xi_{\mathbf{k},\pm} = (\xi_{\mathbf{k},\uparrow} \pm \xi_{\mathbf{k},\downarrow})/2 = k^2/(2m_\pm) - \mu_\pm$, where

$$E_{\mathbf{k},1} = (\xi^2_{\mathbf{k},+} + |\Delta_{\mathbf{k}}|^2)^{1/2} + \xi_{\mathbf{k},-}, \tag{3.17}$$

$$E_{\mathbf{k},2} = (\xi^2_{\mathbf{k},+} + |\Delta_{\mathbf{k}}|^2)^{1/2} - \xi_{\mathbf{k},-} \tag{3.18}$$

are the quasiparticle and negative of the quasihole energies respectively, $m_\pm = 2m_\uparrow m_\downarrow/(m_\downarrow \pm m_\uparrow)$ and $\mu_\pm = (\mu_\uparrow \pm \mu_\downarrow)/2$. Notice that m_+ is twice the reduced mass of the $\uparrow$ and $\downarrow$ fermions, and that the equal mass case corresponds to $|m_-| \to \infty$. As usual, I eliminate g in favor of the scattering length a_F via the relation

$$\frac{1}{g} = -\frac{m_+ V}{4\pi a_F} + \sum_{\mathbf{k}}\frac{|\Gamma_{\mathbf{k}}|^2}{2\epsilon_{\mathbf{k},+}}, \tag{3.19}$$

where V is the volume and $\epsilon_{\mathbf{k},\pm} = (\epsilon_{\mathbf{k},\uparrow} \pm \epsilon_{\mathbf{k},\downarrow})/2$.

The order parameter equation has to be solved self-consistently with number equations $N_\sigma = -\partial\Omega/\partial\mu_\sigma$ which have two contributions $N_\sigma = N_{0,\sigma} + N_{\rm fluct,\sigma}$. The first term $N_{0,\sigma} = -\partial\Omega_0/\partial\mu_\sigma$ or the relation

$$N_{0,\sigma} = \frac{\gamma_\sigma}{\beta}\lim_{\tau\to 0}\sum_p \mathbf{G}^{\rm sp}_{\sigma,\sigma}(p)\exp(i\gamma_\sigma w_\ell\tau) \tag{3.20}$$

leads to the saddle point contribution, and is given by

$$N_{0,\sigma} = \sum_{\mathbf{k}}\left(\frac{1-\gamma_\sigma\mathcal{X}_{\mathbf{k},-}}{2} - \frac{\xi_{\mathbf{k},+}}{2E_{\mathbf{k},+}}\mathcal{X}_{\mathbf{k},+}\right). \tag{3.21}$$

Here, $\gamma_\uparrow = +1$ and $\gamma_\downarrow = -1$. Similarly, the second term $N_{\text{fluct},\sigma} = -\partial\Omega_{\text{fluct}}/\partial\mu_\sigma$ leads to the fluctuation contribution, and is given by

$$N_{\text{fluct},\sigma} = -\frac{1}{\beta}\sum_q \frac{\partial[\det \mathbf{F}^{-1}(q)]/\partial\mu_\sigma}{\det \mathbf{F}^{-1}(q)}. \tag{3.22}$$

While the saddle point contribution is sufficient for a semi-quantitative analysis at zero temperature ($T \approx 0$), inclusion of the fluctuation contribution is necessary to recover BEC physics at finite temperatures ($T \to T_c$).

When populations of the pseudo-spin components are balanced ($N_\uparrow = N_\downarrow$), the results for $|\Delta_0|$ and μ_+ (μ_- is irrelevant in this case) in the $m_\uparrow \neq m_\downarrow$ case can be obtained from the results for $|\Delta_0|$ and μ in the $m = m_\uparrow = m_\downarrow$ case via the substitution of $m \to m_+$. However, when populations of the pseudo-spin components are imbalanced ($N_\uparrow \neq N_\downarrow$), I need to solve all three self-consistency equations, since population imbalance is achieved when either $E_{\mathbf{k},1}$ or $E_{\mathbf{k},2}$ is negative in some regions of momentum space, as discussed next.

3.4 Saddle Point Results

At low temperatures $T \approx 0$, the saddle point self-consistency (order parameter and number) equations are sufficient to describe qualitatively the evolution of superfluidity from the BCS to the BEC limit. In this section, I analyze the amplitude of the order parameter $|\Delta_0|$ and chemical potentials μ_σ as a function of scattering parameter $1/(k_{F,+}a_F)$, population imbalance

$$P = \frac{N_-}{N_+} = \frac{N_\uparrow - N_\downarrow}{N_\uparrow + N_\downarrow}, \tag{3.23}$$

and mass anisotropy $m_r = m_\uparrow/m_\downarrow$. Here $N_\pm = (N_\uparrow \pm N_\downarrow)/2$ and $k^3_{F,\pm} = (k^3_{F,\uparrow} \pm k^3_{F,\downarrow})/2$. Because of the parabolic dispersion relation, the density of $\uparrow$ fermions is $n_\uparrow = k^3_{F,\uparrow}/(6\pi^2)$ and the density of $\downarrow$ fermions is $n_\downarrow = k^3_{F,\downarrow}/(6\pi^2)$. Here, the Fermi momenta $k_{F,\uparrow}$ and $k_{F,\downarrow}$ are determined from the Fermi energies $\epsilon_{F,\sigma} = k^2_{F,\sigma}/(2m_\sigma)$. Therefore,

$$n = n_\uparrow + n_\downarrow = \frac{k^3_{F,+}}{3\pi^2}, \tag{3.24}$$

which is the total fermion density.

Using the notations described in the preceeding paragraph, I can solve the self-consistency Eqs. (3.16), (3.19) and (3.21). For instance, in Fig. 3.1, I plot self-consistent solutions of

$|\Delta_0|$, μ_+ and μ_- (in units of $\epsilon_{F,+}$) at $T = 0$ for two cases: (a) as a function of $1/(k_{F,+}a_F)$ when $P = 0.5$ (or $N_\uparrow = 3N_\downarrow$) and (b) as a function of P when $1/(k_{F,+}a_F) = 0$ (or on resonance).

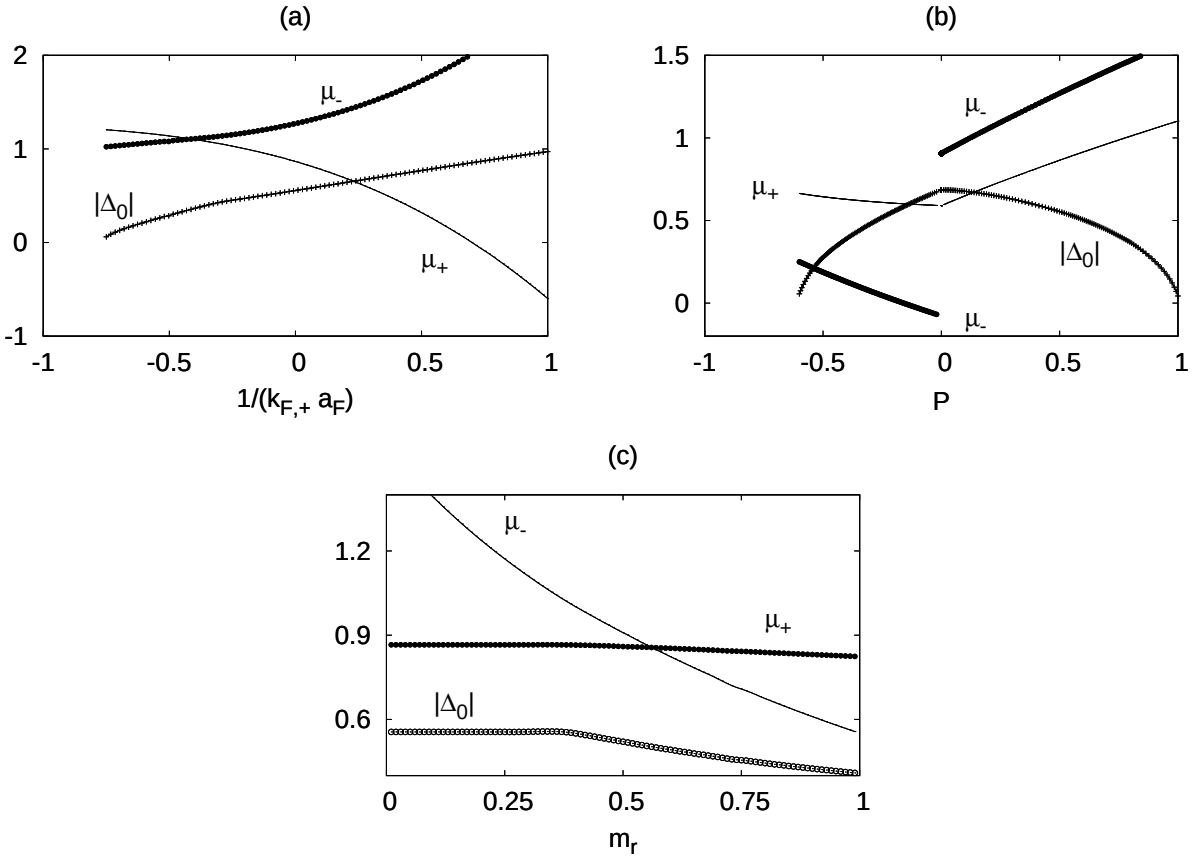

Figure 3.1: Plots of $|\Delta_0|$, μ_+ and μ_- (units of $\epsilon_{F,+}$) for $m_\uparrow = 0.15m_\downarrow$ (a) as a function of $1/(k_{F,+}a_F)$ when $P = 0.5$ and (b) as a function of P when $1/(k_{F,+}a_F) = 0$. (c) Plots of $|\Delta_0|$, μ_+ and μ_- (in units of $\epsilon_{F,+}$) as a function of m_r, when $P = 0.5$ and $1/(k_{F,+}a_F) = 0$ (unitarity limit). Notice the presence of small cusps in $|\Delta_0|$ and μ_+ which signal a topological quantum phase transition discussed below. These cusps are more pronounced for higher $|P|$ (not shown), but are best seen in these figures at small grazing angles.

In Fig. 3.1(a), the BCS $\mu_\pm \approx (\epsilon_{F,\uparrow} \pm \epsilon_{F,\downarrow})/2$ changes continuously to the BEC $|\mu_\pm| \to |\epsilon_b|/2$, where

$$\epsilon_b = -\frac{1}{m_+ a_F^2} \tag{3.25}$$

is the binding energy which follows from

$$\frac{1}{g} = \sum_{\mathbf{k}} \frac{|\Gamma_{\mathbf{k}}|^2}{2\epsilon_{\mathbf{k},+} - \epsilon_b}. \tag{3.26}$$

Since $P > 0$ and the $\uparrow$ fermions are in excess, all $\downarrow$ fermions pair to form $N_\downarrow$ bosons and the remaining $\uparrow$ fermions are unpaired. The amplitude $|\Delta_0|$ evolves continuously from the BCS to the BEC limit with a cusp around $1/(k_{F,+}a_F) \approx -0.27$. This cusp in $|\Delta_0|$ is more pronounced for higher $|P|$ and signals a quantum phase transition discussed below.

In Fig. 3.1(b), I show (on resonance) that $|\Delta_0| = 0$ (normal phase) for $P < -0.61$, where $\mu_+ \approx 0.64\epsilon_{F,+}$ and $\mu_- \approx 0.28\epsilon_{F,+}$. I notice that the evolution of $|\Delta_0|$, μ_+ and μ_- as a function of P is non-analytic when $|P| \to 0$, and also signals a quantum phase transition discussed below. I obtain similar results when $m_\uparrow = m_\downarrow$, where the plot is symmetric around $P = 0$. Therefore, this quantum phase transition may be studied in current experiments involving only one-species of fermions [76, 77].

In Fig. 3.1(c), I show self-consistent solutions of $|\Delta_0|$, μ_+ and μ_- (in units of $\epsilon_{F,+}$) as a function of m_r when $P = 0.5$ and $1/(k_{F,+}a_F) = 0$. Here, $\epsilon_{F,\pm} = k_{F,\pm}^2/(2m_\pm)$. With increasing mass anisotropy (or decreasing m_r), I find that both $|\Delta_0|$ and μ_+ increase until $m_r \approx 0.4$. However, further decrease in m_r beyond $m_r \approx 0.4$ leads to a saturation of both $|\Delta_0|$ and μ_+ with a small cusp in both quantities. The cusp is best seen in Fig. 3.1(c) at small grazing angles. Therefore, the evolution from $m_r = 1$ to $m_r \to 0$ is non-analytic when $m_r \approx 0.4$, and the evolution is not a crossover. These cusps in $|\Delta_0|$ and μ_+ are more pronounced for higher $|P|$, and they signal a topological quantum phase transition discussed below. Notice that, for $P = 0$, the evolution of $|\Delta_0|$ and μ_+ is analytic for all m_r, and the evolution is just a crossover.

Next, I discuss the stability of uniform superfluidity using two criteria [111, 160, 161, 162, 163]: positive definite compressibility matrix $\kappa(T)$ and positive definite superfluid density matrix $\rho(T)$.

3.4.1 Stability of Uniform Superfluidity

In order to analyze the phase diagram at $T = 0$, I solve the saddle point self-consistency (order parameter and number) equations for all P and m_r for a set of $1/(k_{F,+}a_F)$, and check the stability of saddle point solutions for the uniform superfluid phase using two criteria.

The first criterion requires that the compressibility matrix $\kappa(T)$ is positive definite,

where the elements of $\kappa(T)$ are

$$\kappa_{\sigma,\sigma'}(T) = -\frac{\partial^2\Omega_0}{\partial\mu_\sigma\partial\mu_{\sigma'}}. \tag{3.27}$$

This criterion is related (identical) to the condition that the curvature

$$\frac{\partial^2\Omega_0}{\partial\Delta_0^2} = \sum_{\mathbf{k}} |\Delta_{\mathbf{k}}|^2 \left(\frac{\mathcal{X}_{\mathbf{k},+}}{E_{\mathbf{k},+}^3} - \beta \frac{\mathcal{Y}_{\mathbf{k},+}}{2E_{\mathbf{k},+}^2} \right). \tag{3.28}$$

of the saddle point thermodynamic potential Ω_0 with respect to the saddle point parameter Δ_0 needs to be positive [161, 163]. Here, $\mathcal{Y}_{\mathbf{k},\pm} = (\mathcal{Y}_{\mathbf{k},\uparrow} \pm \mathcal{Y}_{\mathbf{k},\downarrow})/2$ with $\mathcal{Y}_{\mathbf{k},s} = \mathrm{sech}^2(\beta E_{\mathbf{k},s}/2)$. Notice that, at low temperatures $T \approx 0$, $\delta(E_{\mathbf{k},\mathbf{s}}) = \lim_{\beta\to\infty} \beta\mathcal{Y}_{\mathbf{k},s}/4$ where $\delta(x)$ is the delta function. When at least one of the eigenvalues of $\kappa(T)$, or the curvature $\partial^2\Omega_0/\partial\Delta_0^2$ is negative, the uniform saddle point solution does not correspond to a minimum of Ω_0, and a non-uniform superfluid phase is favored. I would like to mention that the positivity of the compressibility matrix guarantees the stability of the minima of the free energy in connection with a particular choice of symmetry or functional form of the order parameter. Within this restriction, when the compressibility becomes negative the free energy changes from a minimum to a maximum. In the present case, I restricted myself only to order parameters with zero center of mass (CM) momentum. However, if one is interested in a different class of superfluid states such that the order parameter describes a Cooper pair with finite CM momentum, then one needs to compare energies, and two separate energy calculations are necessary: one for the zero-CM-momentum case and the other for the finite-CM-momentum [Fulde-Ferrel-Larkin-Ovchinnikov (FFLO)] case [163, 164, 165]. However, in this chapter, I study only the stability of the zero-CM-momentum case.

The second criterion requires the superfluid density matrix $\rho(T)$ to be positive definite, where the elements of $\rho(T)$ are defined by

$$\rho_{i,j}(T) = \frac{1}{\beta}\sum_p \{\mathrm{Tr}[\mathbf{G}^{\mathrm{sp}}(p)\widetilde{\mathbf{M}}]\delta_{i,j} + k_i k_j \mathrm{Tr}[\mathbf{G}^{\mathrm{sp}}(p)\mathbf{G}^{\mathrm{sp}}(p)]\}, \tag{3.29}$$

where $\widetilde{\mathbf{M}}$ is a diagonal mass matrix with elements $\widetilde{\mathbf{M}}_{i,j} = \gamma_\sigma m_\sigma \delta_{i,j}$ with $\gamma_\uparrow = 1$ and $\gamma_\downarrow = -1$, and $\delta_{i,j}$ is the Kronecker delta. After the evaluation of the fermionic Matsubara frequency, I obtain

$$\rho_{ij}(T) = (m_\uparrow N_\uparrow + m_\downarrow N_\downarrow)\delta_{i,j} - \frac{\beta}{2}\sum_{\mathbf{k}} k_i k_j \mathcal{Y}_{\mathbf{k},+}. \tag{3.30}$$

When at least one of the eigenvalues of $\rho(T)$ is negative, a spontaneously generated gradient of the phase of the order parameter appears, leading to a non-uniform superfluid phase. Notice that the $\rho(T)$ matrix is reducible to the scalar

$$\rho_0(T) = m_\uparrow N_\uparrow + m_\downarrow N_\downarrow - \frac{\beta}{6}\sum_{\mathbf{k}} k^2 \mathcal{Y}_{\mathbf{k},+}, \tag{3.31}$$

in the s-wave case.

Eventhough, I use these two criteria, I have found that the compressibility criterion is the most restrictive over the entire phase space explored. This indicates that non-uniform phases with spontaneously generated phase gradients are not present. The non-uniform phases that can be obtained using the dominant compressibility criterium correspond to phase separated (PS) states, where normal and superfluid states do not mix. However, allowing for Cooper pairs to have CM momenta produces FFLO phases [164, 165] near the BCS regime, and allows for the possibility of generalized FFLO phases with several wavevectors close to unitarity. However, I have not performed these calculations in connection with generalized FFLO states, and thus limited myself only to the stability of the zero CM momentum (uniform) superfluid states. In addition, I did not specifically consider the phase boundary between FFLO and PS since it was shown that the standard FFLO phases exist only a very small region on the BCS side of the phase diagram [112].

Before discussing ground state phase diagrams, I would like to add an additional criterion to fine tune the classification of the various phases that emerge as a result of unequal masses, interactions, and population imbalance. For this purpose I discuss next, the quasiparticle excitation spectrum and its connection to topological quantum phase transitions.

3.4.2 Topological Quantum Phase Transitions

The excitation spectrum of quasiparticles is determined by energies $E_{\mathbf{k},1}$ and $E_{\mathbf{k},2}$ defined in Eq. (3.17). Using these relations, one can identify surfaces in momentum space where these energies have zeros, indicating that the quasiparticle excitation spectrum changes from a gapped to a gapless phase, with a corresponding change in the momentum distribution as well. These changes in the Fermi surfaces of quasiparticles are topological in nature. Thus,

I identify topological quantum phase transitions associated with the disappearance or appearance of momentum space regions of zero quasiparticle energies when either $1/(k_{F,+}a_F)$, P, and/or m_r is changed. These topological transitions are shown as dotted lines in Figs. 3.4 through 3.7.

These phases are characterized by the number of zeros of $E_{\mathbf{k},1}$ and $E_{\mathbf{k},2}$ (zero energy surfaces in momentum space) such that I) $E_{\mathbf{k},1}$ has no zeros and $E_{\mathbf{k},2}$ has only one, and II) $E_{\mathbf{k},1}$ has no zeros and $E_{\mathbf{k},2}$ has two zeros. I first define $B_\pm = m_\uparrow\mu_\uparrow \pm m_\downarrow\mu_\downarrow$ to establish general constraints on the magnitude $|\Delta_0|$ of the order parameter for the s-wave pairing in the presence of population imbalance. The zeros of $E_{\mathbf{k},s}$ occur at real momenta

$$k_\pm^2 = B_+ \pm (B_-^2 - 4m_\uparrow m_\downarrow |\Delta_0|^2)^{1/2} \tag{3.32}$$

provided that the following conditions

$$|\Delta_0|^2 < \frac{|B_-|^2}{4m_\uparrow m_\downarrow}, \qquad B_+ \geq 0 \tag{3.33}$$

$$|\Delta_0|^2 < -\mu_\uparrow\mu_\downarrow, \qquad B_+ < 0 \tag{3.34}$$

are satisfied. Notice that, the Fermi sea of the lower quasiparticle band is a sphere of radius k_+ in phase I, and is a spherical shell $k_- \leq k \leq k_+$ in phase II, and the transition from phase II to I occurs when $k_- \to 0$. The superfluid has gapless quasiparticle excitations in both phases I and II, when there is population imbalance, e.g., $N_\uparrow \neq N_\downarrow$. I illustrate these cases in Figs. 3.2(b) and 3.2(c), respectively, for $N_\uparrow > N_\downarrow$. The case of no population imbalance $P = 0$ ($N_\uparrow = N_\downarrow$) corresponds to case III, where $E_{\mathbf{k},1}$ and $E_{\mathbf{k},2}$ have no zeros and are always positive, and thus the superfluid has always gapped quasiparticle excitations which is shown in Fig. 3.2(a). In these figures, the parameters used are (a) $|\Delta_0| = 0.495\epsilon_{F,+}$, $\mu_+ = 0.779\epsilon_{F,+}$ and $\mu_- = 0.0$; (b) $|\Delta_0| = 0.811\epsilon_{F,+}$, $\mu_+ = 0.167\epsilon_{F,+}$ and $\mu_- = 1.162\epsilon_{F,+}$, and (c) $|\Delta_0| = 0.499\epsilon_{F,+}$, $\mu_+ = 0.751\epsilon_{F,+}$ and $\mu_- = 0.633$.

The transitions among phases I, II and III indicate a change in topology in the lowest quasiparticle band, similar to the Lifshitz transition in ordinary metals [136] and non-swave superfluids [135, 116, 117, 123, 129]. The topological transition here is unique, because it involves an s-wave superfluid, and could be potentially observed for the first time through

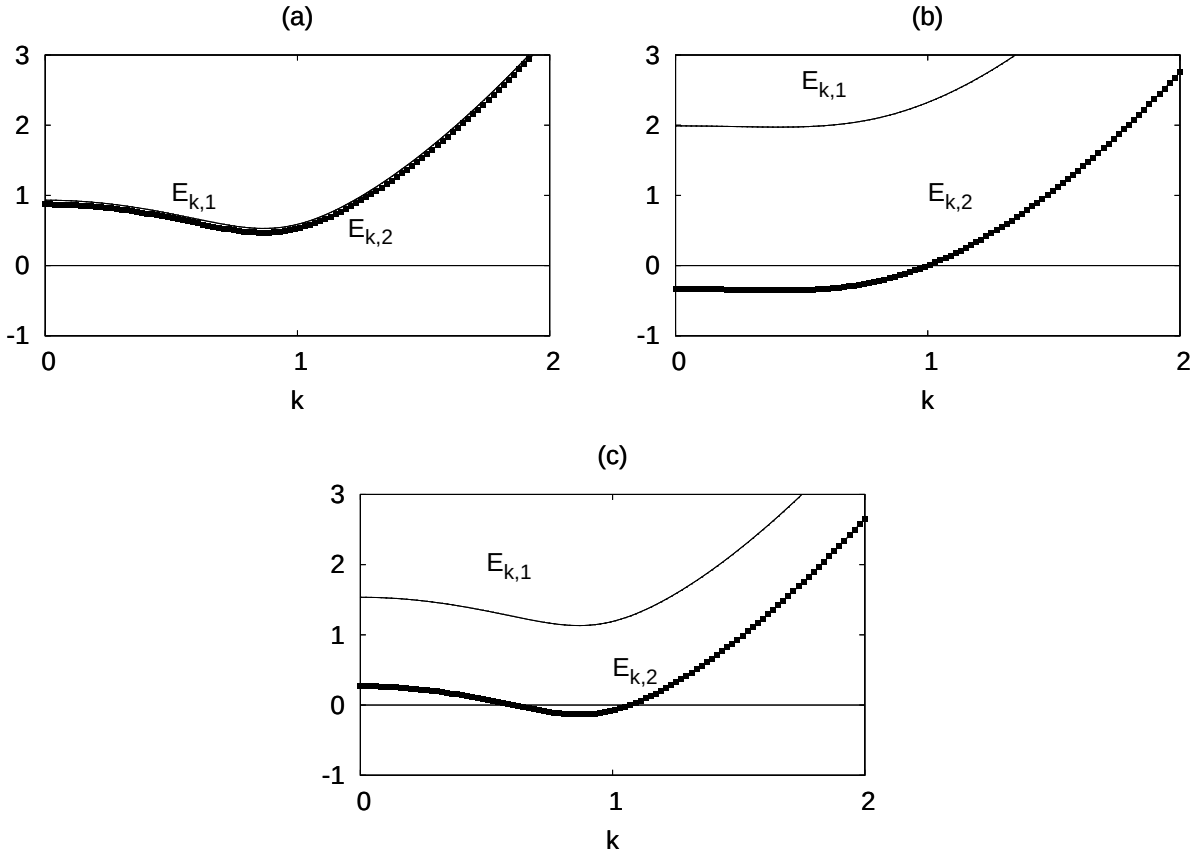

Figure 3.2: Schematic plots of $E_{\mathbf{k},1}$ (thin lines) and $E_{\mathbf{k},2}$ (thick lines) versus k for (a) phase III, (b) phase I, and (c) phase II. Here, $E_{\mathbf{k},s}$ and k are in units of $\epsilon_{F,+}$ and $k_{F,+}$, respectively. The transitions among phases I, II and III indicate a change in topology in the lowest quasiparticle band, and they are characterized by the number of zeros of $E_{\mathbf{k},1}$ and $E_{\mathbf{k},2}$ (zero energy surfaces in momentum space) such that (a) in phase III, $E_{\mathbf{k},1}$ and $E_{\mathbf{k},2}$ have no zeros; (b) in phase I, $E_{\mathbf{k},1}$ has no zeros and $E_{\mathbf{k},2}$ has only one; and (c) in phase II, $E_{\mathbf{k},1}$ has no zeros and $E_{\mathbf{k},2}$ has two zeros.

the measurement of the momentum distribution or thermodynamic properties. Notice that the topological transition occurs without changing the symmetry of the order parameter as the Landau classification demands for ordinary phase transitions. However, thermodynamic signatures of the topological transition are present at low temperatures in the compressibility, specific heat, superfluid density, etc., because the quasiparticle excitation spectrum changes dramatically. The temperature dependence of the quasiparticle contributions to these properties are exponentially activated [$\sim \exp(-E_g/T)$] for the gapped phase (III), or have a power law behavior (with different powers of T) in the gapless phases (I and II).

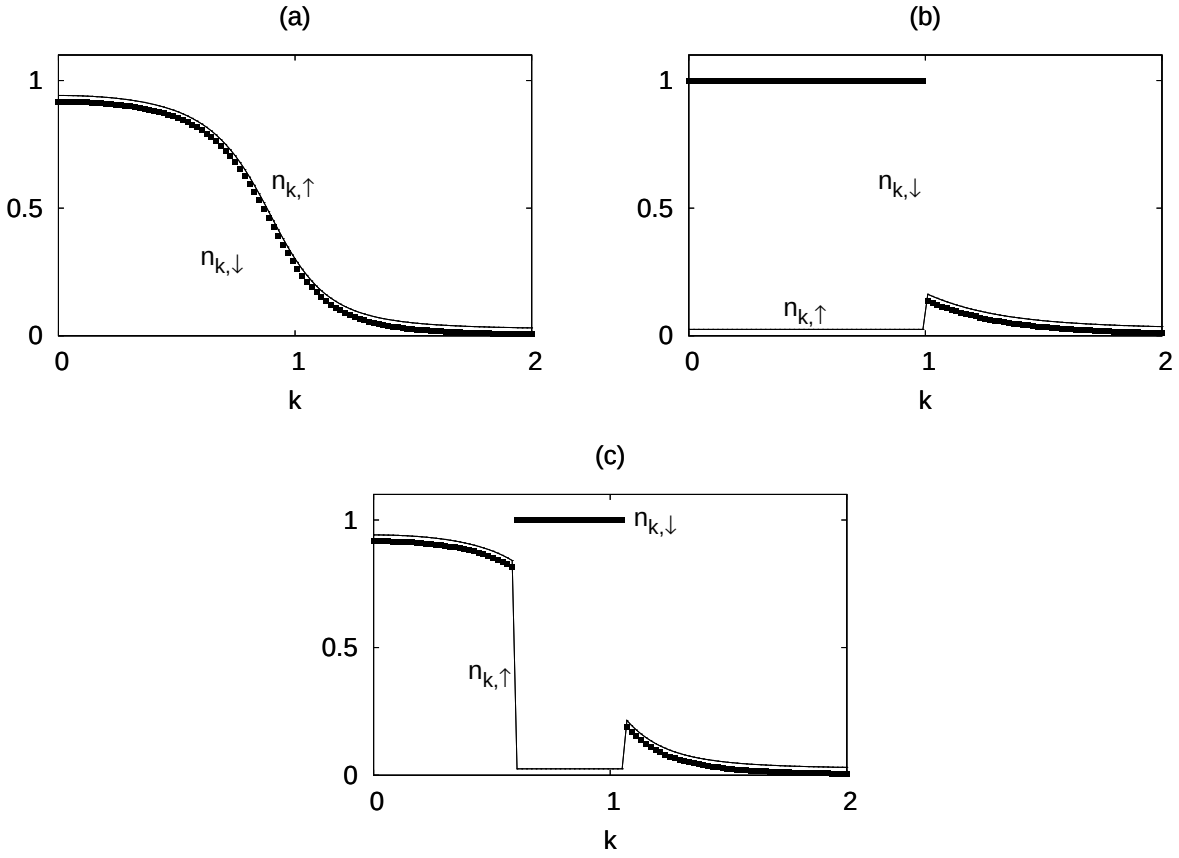

Figure 3.3: Corresponding plots of momentum distributions $n_{\mathbf{k},\uparrow}$ (thin lines) and $n_{\mathbf{k},\downarrow}$ (thick lines) are shown in (a) phase III, (b) phase I and (c) phase II. For momentum space regions where $E_{\mathbf{k},1} > 0$ and $E_{\mathbf{k},2} > 0$, the corresponding momentum distributions are equal $n_{\mathbf{k},\uparrow} = n_{\mathbf{k},\downarrow}$. However, when $E_{\mathbf{k},1} > 0$ and $E_{\mathbf{k},2} < 0$, then $n_{\mathbf{k},\uparrow} = 0$ and $n_{\mathbf{k},\downarrow} = 1$. Notice that the zero of $n_{\mathbf{k},\uparrow}$ is slightly shifted upwards from the zero of $n_{\mathbf{k},\downarrow}$, for better visualization.

The zero temperature momentum distributions

$$n_{\mathbf{k},\sigma} = \frac{1 - \gamma_\sigma \mathcal{X}_{\mathbf{k},-}}{2} - \frac{\xi_{\mathbf{k},+}}{2E_{\mathbf{k},+}} \mathcal{X}_{\mathbf{k},+} \tag{3.35}$$

for phases I and II are extracted from Eq. (3.21). For momentum space regions where $E_{\mathbf{k},1} > 0$ and $E_{\mathbf{k},2} > 0$, the corresponding momentum distributions are equal $n_{\mathbf{k},\uparrow} = n_{\mathbf{k},\downarrow}$. However, when $E_{\mathbf{k},1} > 0$ and $E_{\mathbf{k},2} < 0$, then $n_{\mathbf{k},\uparrow} = 0$ and $n_{\mathbf{k},\downarrow} = 1$. I illustrate these cases in Figs. 3.3(a), 3.3(b) and 3.3(c) for parameters of Figs. 3.2(a), 3.2(b) and 3.2(c), respectively. Notice that the zero of $n_{\mathbf{k},\uparrow}$ is shifted slightly upwards to distinguish it from $n_{\mathbf{k},\downarrow}$ in the regions of momentum space where $n_{\mathbf{k},\uparrow} = n_{\mathbf{k},\downarrow}$. Although this topological transition is quantum ($T = 0$) in nature, signatures of the transition should still be observed at

finite temperatures within the quantum critical region, where the momentum distributions are smeared out due to thermal effects. Although the primary signature of this topological transition is seen in the momentum distribution, the isentropic κ_S or isothermal κ_T compressibilities and the speed of sound c_s would have a cusp at the topological transition line similar to that encountered in $|\Delta_0|$ (see Fig. 3.1) as a function of the mass anisotropy m_r. The cusp (discontinuous change in slope) in κ_S, κ_T or c_s gets larger with increasing population imbalance.

Having discussed the finer topological classification of possible superfluid phases, I take all the criteria together (positive compressibility, positive curvature of thermodynamic potential, positive superfluid density, and topological character) to present next the resulting ground state phase diagrams.

3.4.3 Saddle Point Phase Diagrams

Based on all the previous criteria, I construct the the P versus $1/(k_{F,+}a_F)$ phase diagram for the mass ratios: $m_\uparrow = m_\downarrow$ ($m_r = 1$) for equal mass mixtures and $m_\uparrow = 0.15 m_\downarrow$ ($m_r = 0.15$) for ^{6}Li and ^{40}K mixture. In addition, I construct the P versus m_r phase diagram for seven sets of interaction strengths: $1/(k_{F,+}a_F) = -2$, -1 and -0.25 on the BCS side shown in Fig. 3.5; $1/(k_{F,+}a_F) = 0$ at unitarity shown in Fig. 3.6; and $1/(k_{F,+}a_F) = 0.25$, 1 and 2 on the BEC side shown in Fig. 3.7. In these diagrams, the $\uparrow$ ($\downarrow$) label always corresponds to lighter (heavier) mass such that lighter (heavier) fermions are in excess when $P > 0$ ($P < 0$). Notice that this choice spans all possible population imbalances and mass ratios.

In Figs. 3.4 through 3.7, I indicate the regions of normal (N), and uniform (U) or non-uniform (NU) superfluid phases. The black squares indicate the transition line that separates topological phases I and II. In all phase diagrams, phase I (II) always appears to the left (right) of the dotted lines for $P > 0$, while phase I (II) always appears to the right (left) of the dotted lines for $P < 0$.

The normal phase is characterized by a vanishing order parameter ($\Delta_0 = 0$), while the uniform superfluid phase is characterized by $\rho_0(0) > 0$ and $\partial^2\Omega_0/\partial\Delta_0^2 > 0$. The non-uniform superfluid phase is characterized by $\rho_0(0) < 0$ and/or $\partial^2\Omega_0/\partial\Delta_0^2 < 0$, and it should be of the

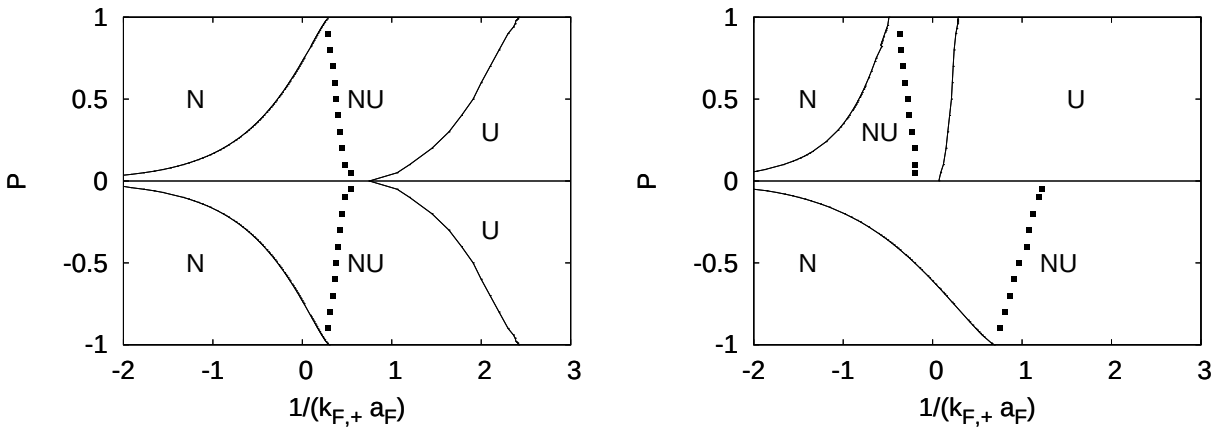

Figure 3.4: Phase diagram of $P = (N_\uparrow - N_\downarrow)/(N_\uparrow + N_\downarrow)$ versus $1/(k_{F,+}a_F)$ for (a) equal ($m_\uparrow = m_\downarrow$) and (b) unequal masses ($m_\uparrow = 0.15m_\downarrow$). I show normal (N), non-uniform (NU) or uniform (U) superfluid phases. The dotted and $P = 0$ lines separate topologically distinct regions. In b) the U phase also occurs for $P < 0$ when $1/(k_{F,+}a_F) > 4.8$ (not shown).

FFLO-type having one wavevector modulation only near the BCS limit [164, 165], although closer to unitarity, I expect the non-uniform phase to be substantially different from the FFLO phases either having spatial modulation that would encompass several wavevectors or presenting complete phase separation between paired and unpaired fermions. However, from numerical calculations, the superfluid density criterion seems to be weaker for all parameter space and the non-uniform superfluid phase is characterized by $\partial^2\Omega_0/\partial\Delta_0^2 < 0$, which indicates possible phase separation, since at least one of the eigenvalues of the compressibility matrix $\kappa_{\sigma,\sigma'}$ also becomes negative. Therefore, for homogeneous systems, paired (superfluid) fermions and unpaired (excess) fermions coexist in the uniform superfluid regions, but are phase separated in non-uniform superfluid regions, such that the topological transition from phase I to phase II may not be accessible. However, in a harmonic trap with a large superfluid region at the center, the topological phases should be observable since the central region is essentially a "uniform superfluid" with the excess fermions at the edge [129]. The peculiar momentum distribution of different topological phases would be smeared out by the trapping potential, but their marked signatures should still be present. Furthermore, these topological phases may be accessible in trapped systems at finite temperature [166], or in optical lattices [167].

As shown in Fig. 3.4(a), when $m_\uparrow = m_\downarrow$, the phase diagram is symmetric around $P = 0$.

A continuous quantum phase transition occurs from the NU to the N phase beyond a critical population imbalance on the BCS side. In addition, a discontinous transition from the NU to the U phase of topological type (I) also occurs. In contrast, as shown in Fig. 3.4(b), when $m_\uparrow = 0.15 m_\downarrow$, the phase diagram is asymmetric around $P = 0$,having a larger stability region for uniform superfluidity when the population $N_\uparrow$ of lighter fermions is larger than the population $N_\downarrow$ of heavier fermions. A continuous quantum phase transition occurs from the NU to the N phase beyond a critical population imbalance on the BCS side. Furthermore, it is found that the U phase has a larger stability region when light fermions are in excess, and that a discontinuous transition from the NU to the U phase occurs. The U phase also exists for $P < 0$ when $1/(k_{F,+}a_F) > 4.8$ (not shown). Lastly, one of the topological quantum phase transitions (dotted lines) is very close to the NU/U boundary for $P > 0$ in contrast to the equal mass case. This line indicates a change in quasiparticle Fermi surface topology from type (I) to type (II), and may lie in the U region when $m_\uparrow/m_\downarrow < 0.15$.

Next I discuss the P versus m_r phase diagram for seven sets of interaction strengths: $1/(k_{F,+}a_F) = -2$, -1 and -0.25 on the BCS side shown in Fig. 3.5; $1/(k_{F,+}a_F) = 0$ at unitarity shown in Fig. 3.6; and $1/(k_{F,+}a_F) = 0.25$, 1 and 2 on the BEC side shown in Fig. 3.7.

As shown in Fig. 3.5(a) and 3.5(b), I find a small region of uniform superfluidity on the BCS side only when the mass anisotropy is small and the lighter fermions are in excess ($P > 0$). Thus, to probe the largest amount of phases on the BCS side, mixtures consisting of ^{6}Li and ^{40}K ($m_r \approx 0.15$) or ^{6}Li and ^{87}Sr ($m_r \approx 0.07$) are good candidates. In the rest of the phase diagram, I find a quantum phase transition from the non-uniform superfluid to the normal phase beyond a critical population imbalance for both positive and negative P. The phase space of uniform superfluidity expands while that of the normal phase shrinks with increasing interaction strength as shown in Figs. 3.5(b) and 3.5(c).

This general trend continues into the unitarity limit [$1/(k_{F,+}a_F) = 0$] as shown in Fig. 3.6. Since this limit is theoretically important as well as experimentally accessible, it is useful to analyze the phase diagram as a function of population imbalance and mass anisotropy. Notice that Fermi mixtures corresponding to mass ranges $0 < m_r < 0.23$, like

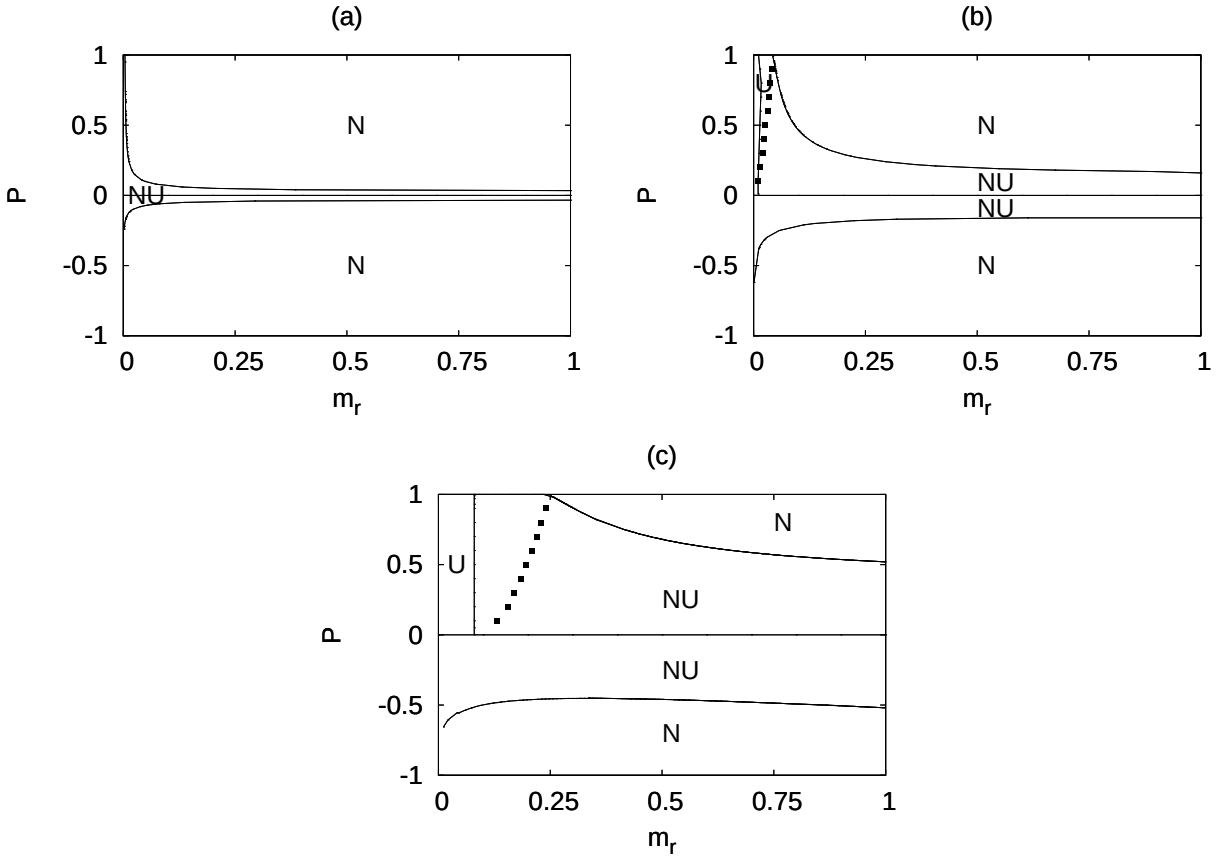

Figure 3.5: Phase diagram of $P = (N_\uparrow - N_\downarrow)/(N_\uparrow + N_\downarrow)$ versus $m_r = m_\uparrow/m_\downarrow$ on the BCS side when (a) $1/(k_{F,+}a_F) = -2$ (b) $1/(k_{F,+}a_F) = -1$ and (c) $1/(k_{F,+}a_F) = -0.25$. I show normal (N), uniform (U) or non-uniform (NU) superfluid phases. The dotted line separates topologically distinct superfluid phases. For $P > 0$ topological phase I (II) corresponds to the region to the left (right) region of the dotted line, and for $P < 0$ the topological phase is always of type II.

^{6}Li and ^{87}Sr ($m_r \approx 0.07$) and ^{6}Li and ^{40}K ($m_r \approx 0.15$) have phase diagrams which are qualitatively different from those corresponding to mass ratios $0.23 < m_r < 0.45$ like ^{6}Li and ^{25}Mg ($m_r \approx 0.24$) and ^{6}Li and ^{2}H ($m_r \approx 0.33$), since a topological transition line may be accessible in the second range. Furthermore, only NU and N phases are accessible at unitarity for Fermi mixtures in the range of mass ratios $0.45 < m_r < 1$ like ^{40}K and ^{87}Sr ($m_r \approx 0.64$) or any equal mass mixtures. Notice that the results for the case of equal masses ($m_r = 1$) are in close agreement with recent MIT experiments [76] in a trap. At unitarity, my non-uniform superfluid to normal state boundary occurs at $P \approx \pm 0.73$, and the MIT group obtains $P \approx \pm 0.70(4)$ for their superfluid to normal boundary. This agreement is

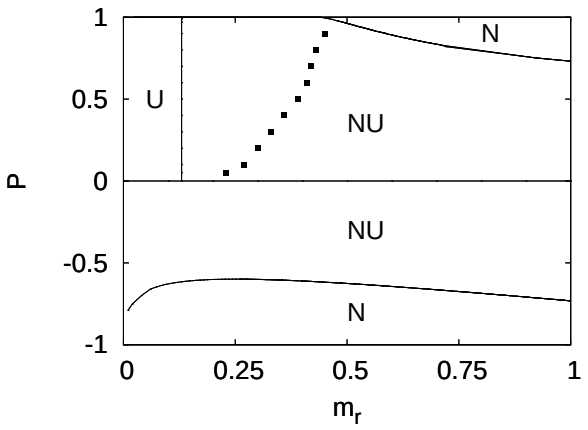

Figure 3.6: Phase diagram of $P = (N_\uparrow - N_\downarrow)/(N_\uparrow + N_\downarrow)$ versus $m_r = m_\uparrow/m_\downarrow$ at the unitarity limit when $1/(k_{F,+}a_F) = 0$. I show normal (N), uniform (U) or non-uniform (NU) superfluid phases. The dotted line separates topologically distinct superfluid phases. For $P > 0$ topological phase I (II) corresponds to the region to the left (right) region of the dotted line, and for $P < 0$ the topological phase is always of type II.

perhaps coincidental, since my calculations do not include the trapping potential, while the experiments do. In recent Monte Carlo calculations [168] the population imbalance for the homogeneous system at the disappearance of superfluidity is $P = 0.44$. However when the trap is considered the Monte Carlo method leads to $P = 0.77$. However, it is not presently clear why the finite-sized Monte Carlo results and my thermodynamic calculations differ by a factor of 1.66 for the superfluid to normal phase boundary at unitarity.

Additional increase of interaction strength beyond unitarity on the BEC side leads to further expansion (shrinkage) of the uniform superfluid (normal) region as shown in Fig. 3.7(a) and 3.7(b). When heavier fermions are in excess ($P < 0$), a uniform superfluid phase is not possible for any mass anisotropy until a critical interaction strength is reached. The critical interaction strength corresponds to $1/(k_{F,+}a_F) \approx 0.8$ for $m_r = 1$. Further increase of interaction strength towards the BEC limit [$1/(k_{F,+}a_F) > 1$], leads to further expansion (shrinkage) of the uniform (non-uniform) superfluid region as shown in Fig. 3.7(c), and only the uniform superfluid phase exists in the extreme BEC limit [$1/(k_{F,+}a_F) \gg 1$] even for $P < 0$ (not shown).

Having discussed the ground state phase diagrams, I present next fluctuation effects beyond the saddle point approximation.

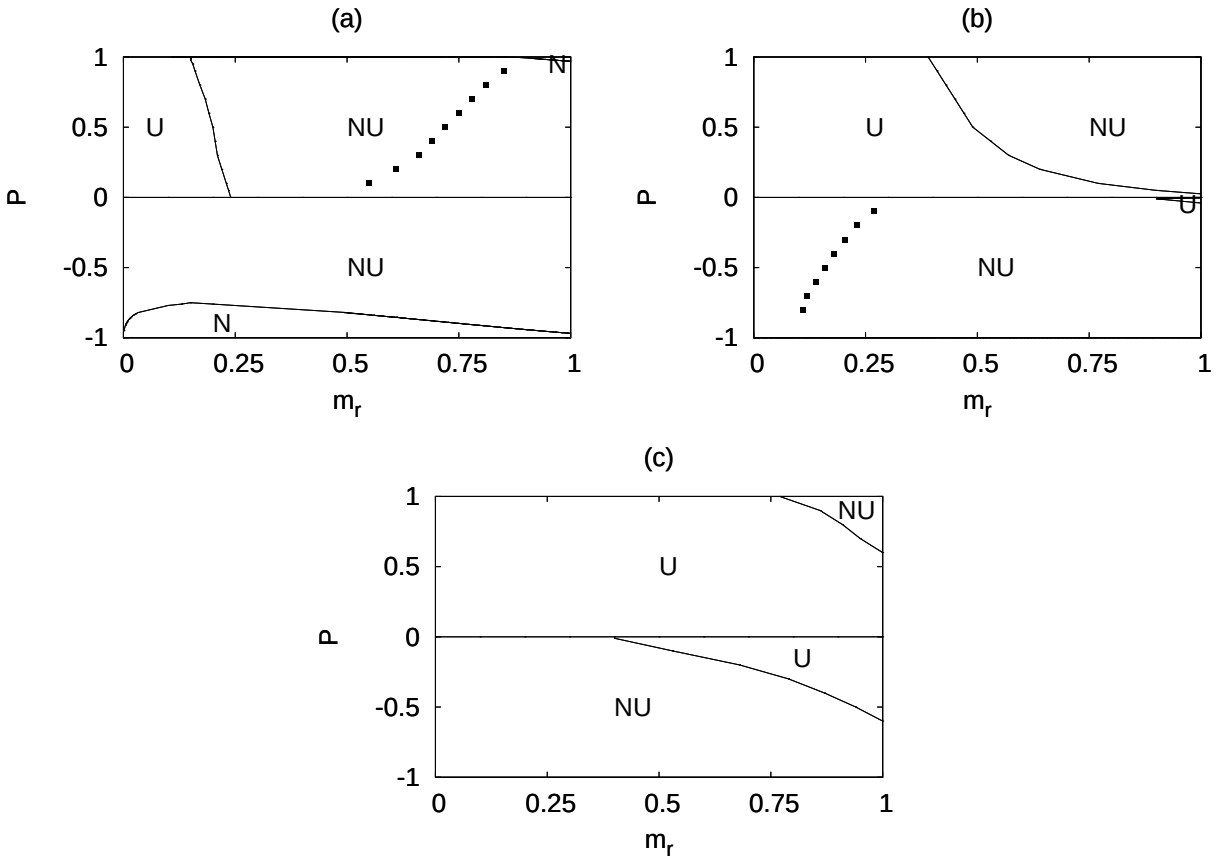

Figure 3.7: Phase diagram of $P = (N_\uparrow - N_\downarrow)/(N_\uparrow + N_\downarrow)$ versus $m_r = m_\uparrow/m_\downarrow$ on the BEC side when (a) $1/(k_{F,+}a_F) = 0.25$, (b) $1/(k_{F,+}a_F) = 1$ and (c) $1/(k_{F,+}a_F) = 2$. I show normal (N), uniform (U) or non-uniform (NU) superfluid phases. The dotted lines separate topologically distinct superfluid phases. In (a) phase I (II) corresponds to the region to the left (right) of the dotted line, and for $P < 0$ phase is always of type II. In (b) phase I (II) corresponds to the region to the right (left) of the dotted line, and for $P > 0$ the phase is always of type I. In (c) the entire superfluid region corresponds to phase I.

3.5 Gaussian Fluctuations

In this section, I discuss the (gaussian) fluctuation effects around the saddle point solutions at finite and zero temperatures. Near the critical temperature ($T \approx T_c$) I discuss the time-dependent Ginzburg-Landau (TDGL) equation, and at zero temperature ($T = 0$) I analyse the collective phase (or Goldstone) mode as well as the effects of harmonic trap in the BEC limit, which are discussed next.

3.5.1 Time-Dependent Ginzburg-Landau (TDGL) Equation near T_c

My basic motivation here is to investigate the low frequency and long wavelength behavior of the order parameter near T_c where $\Delta_0 = 0$, and derive the TDGL equation [44]. The TDGL equations can be obtained from the GL action

$$S_{GL} = S_{Gauss} + S_4, \tag{3.36}$$

where S_{Gauss} is the Gaussian effective action of Eq. (3.8) with $\Delta_0 = 0$ and $S_4 = b|\Lambda(x)|^4/2$. Here, b is a four-point Green's function defined in Appendix B.

The quadratic part of the Ginzburg-Landau action can be obtained from a long wavelength, small frequency expansion of S_{Gauss} when the order parameter vanishes ($\Delta_0 = 0$). In this case, $\mathbf{F}^{-1}_{1,2}(q) = 0$ and $\mathbf{F}^{-1}_{1,1}(q) = L^{-1}(q)$, where

$$L^{-1}(q) = \frac{1}{g} - \sum_{\mathbf{k}} \frac{1 - n_f(\xi_{\mathbf{q}/2+\mathbf{k},\uparrow}) - n_f(\xi_{\mathbf{q}/2-\mathbf{k},\downarrow})}{\xi_{\mathbf{q}/2+\mathbf{k},\uparrow} + \xi_{\mathbf{q}/2-\mathbf{k},\downarrow} - iv_\ell} |\Gamma_{\mathbf{k}}|^2,$$

where $n_f(\xi) = 1/[\exp(\beta\xi) + 1]$ is the Fermi distribution.

Minimization of the action S_{GL} leads to the TDGL equation

$$\left[a + b|\Lambda(x)|^2 - \sum_{i,j} \frac{c_{ij}}{2} \nabla_i \nabla_j - id\frac{\partial}{\partial t} \right] \Lambda(x) = 0 \tag{3.37}$$

in the real space $x = (\mathbf{x}, t)$ representation. Notice that these equations are nothing but the Euler-Lagrange equations for the field $\Lambda(x)$ appearing in S_{GL}.

Expressions for the coefficients a, b, c_{ij} and d are presented in appendix B.3. The condition $a = 0$ corresponds to the Thouless criterion, and the coefficient of the nonlinear term is positive ($b > 0$) guaranteeing the stability of the effective theory. The kinetic energy coefficient c_{ij} is an effective inverse mass tensor which reduces to a scalar c in the s-wave case. The time-dependent coefficient d is a complex number, and its imaginary part reflects the decay of Cooper pairs into the two-particle continuum for $\mu_+ > 0$. However, for $\mu_+ < 0$, the imaginary part of d vanishes and the behavior of the order parameter $\Lambda(x)$ is propagating reflecting the presence of stable (long lived) bound states.

Since a uniform superfluid phase is more stable in the BEC side, I calculate analytically all coefficients in the BEC limit where $|\mu_\pm| \sim |\epsilon_b|/2 \gg T_c$. I obtain $a = a_1 + a_2 =$

$-Vm_+^2(2\mu_+ - \epsilon_b)a_F/(8\pi) + Vm_+ n_e a_F^2$, $b = b_1 + b_2 = Vm_+^3 a_F^3/(16\pi) - Vm_+^2(\partial n_e/\partial\mu_e)a_F^4$, $c = Vm_+^2 a_F/[8\pi(m_\uparrow + m_\downarrow)]$, and $d = Vm_+^2 a_F/(8\pi)$. Here, e labels the excess type of fermions and n_e is the density of unpaired fermions. Through the rescaling

$$\Psi(x) = \sqrt{d}\Lambda(x), \tag{3.38}$$

I obtain the equation of motion for a dilute mixture of weakly interacting bosons and fermions

$$-\mu_B\Psi(x) + \left[U_{BB}|\Psi(x)|^2 + U_{BF}n_e(x)\right]\Psi(x) - \frac{\nabla^2\Psi(x)}{2m_B} - i\frac{\partial\Psi(x)}{\partial t} = 0, \tag{3.39}$$

with bosonic chemical potential $\mu_B = -a_1/d = 2\mu_+ - \epsilon_b$, mass $m_B = d/c = m_\uparrow + m_\downarrow$, and repulsive boson-boson $U_{BB} = Vb_1/d^2 = 4\pi a_F/m_+$ and boson-fermion $U_{BF} = Va_2/(dn_e) = 8\pi a_F/m_+$ interactions. This procedure also yields the spatial density of unpaired fermions given by

$$\begin{aligned} n_e(x) &= [a_2/d + b_2|\Psi(x)|^2/d^2]/U_{BF} \\ &= n_e - U_{BF}(\partial n_e/\partial\mu_e)|\Psi(x)|^2. \end{aligned} \tag{3.40}$$

Since $\partial n_e/\partial\mu_e > 0$ the unpaired fermions avoid regions where the boson field $|\Psi(x)|$ is large. Thus, in a harmonic trap, the bosons condense at the center and the unpaired fermions tend to be at the edges. Notice that, Eq. (3.39) reduces to the Gross-Pitaevskii equation for equal masses with $P = 0$ [44], and to the equation of motion for equal masses with $P \neq 0$ [146].

Next, I recall the standard definitions of the interactions in terms of the scattering lenghts $U_{BB} = 4\pi a_{BB}/m_B$ and $U_{BF} = 4\pi a_{BF}/m_{BF}$, where m_B is the mass of the bosons and $m_{BF} = 2m_e m_B/(m_B + m_e)$ is twice the reduced mass of a boson of mass m_B and an excess fermion of mass m_e. Combining these definitions with the results for U_{BB} and U_{BF} in terms of the fermion-fermion scattering length a_F, I can directly relate the boson-boson scattering parameter

$$a_{BB} = \frac{m_B}{m_+}a_F = \left[1 + \frac{m_\uparrow}{2m_\downarrow} + \frac{m_\downarrow}{2m_\uparrow}\right]a_F \tag{3.41}$$

and the boson-fermion scattering parameter

$$a_{BF} = \frac{2m_{BF}}{m_+}a_F = \frac{4m_B m_e}{m_+(m_B + m_e)}a_F \tag{3.42}$$

to a_F. Notice that these expressions reduce to $a_{BB} = 2a_F$ and $a_{BF} = 8a_F/3$ for equal masses [44, 146]. A better estimate for a_{BB} can be found in the literature [63].

Since the effective boson-fermion system is weakly interacting, the BEC temperature is

$$T_c = \frac{2\pi}{m_B}\left[\frac{n_B}{\zeta(3/2)}\right]^{2/3}, \tag{3.43}$$

where $\zeta(x)$ is the Zeta function and $n_B = (n - n_e)/2$.

Notice that, the effective total number equation for the boson-fermion mixture can be written as

$$N \approx \sum_{\mathbf{k}} n_f(\xi_{\mathbf{k},e}) + 2\sum_{\mathbf{q}} n_b\left[\frac{|\mathbf{q}|^2}{2m_B} - \widetilde{\mu}_B\right], \tag{3.44}$$

where $n_b(\varepsilon) = 1/[\exp(\beta\varepsilon)-1]$ is the Bose distribution and $\widetilde{\mu}_B \to 0^-$ includes also the Hartree shift. In the limit when $T_c \to 0$, I obtain the critical chemical potential for unpaired fermions at the normal-to-stable uniform superfluid boundary as given by

$$\mu_e = 2^{2/3}(m_+/m_e)\epsilon_{F,+}, \tag{3.45}$$

where $e = (\uparrow, \downarrow)$ labels excess type of atoms. Since, $\mu_+ \to \epsilon_b/2$ in this limit, the critical chemical potential imbalance is given by $\mu_- = \gamma_e[-\epsilon_b/2 + 2^{2/3}(m_+/m_e)\epsilon_{F,+}]$, where $\epsilon_b = -1/(m_+ a_F^2)$ is the binding energy, and $\gamma_\uparrow = +1$ and $\gamma_\downarrow = -1$.

This concludes my analysis for the homogenous mixture of two types of ultra-cold fermions at finite temperatures. Next I discuss collective excitations at zero temperature.

3.5.2 Sound Velocity at Zero Temperature

In order to obtain the collective mode spectrum, I use the effective action defined in Eq. (3.8) and express

$$\Lambda(q) = \frac{\lambda(q) + i\theta(q)}{\sqrt{2}} \tag{3.46}$$

in terms of the amplitude $\lambda(q)$ and phase $\theta(q)$ fields, respectively. Using the matrix elements of $\mathbf{F}^{-1}$ defined in Eqs. (3.12) and (3.13) and described in appendix B.1, I can obtain the matrix elements of the fluctuation matrix in the rotated basis $(\lambda(q), \theta(q))$. The diagonal elements of the fluctuation matrix in the rotated basis become $\mathbf{M}^{-1}_{\lambda,\lambda}(q) = [\mathbf{F}^{-1}_{1,1} + \mathbf{F}^{-1}_{1,2} + \mathbf{F}^{-1}_{2,1} + \mathbf{F}^{-1}_{2,2}]/2$ and $\mathbf{M}^{-1}_{\theta,\theta}(q) = [\mathbf{F}^{-1}_{1,1} - \mathbf{F}^{-1}_{1,2} - \mathbf{F}^{-1}_{2,1} + \mathbf{F}^{-1}_{2,2}]/2$, while the off-diagonal elements become $\mathbf{M}^{-1}_{\lambda,\theta}(q) = i[\mathbf{F}^{-1}_{1,1} - \mathbf{F}^{-1}_{1,2} + \mathbf{F}^{-1}_{2,1} - \mathbf{F}^{-1}_{2,2}]/2$ with $\mathbf{M}^{-1}_{\theta,\lambda}(q) = (\mathbf{M}^{-1}_{\lambda,\theta})^*(q)$.

The collective modes are found from the poles of the fluctuation matrix $\mathbf{M}(q)$ determined by the condition

$$\det \mathbf{M}^{-1}(q) = 0, \tag{3.47}$$

when the usual analytic continuation $iv_\ell \to w + i0^+$ is performed. The easiest way to get the phase collective modes is to integrate out the amplitude fields to obtain a phase-only effective action. To obtain the long wavelength dispersions for the collective modes at $T = 0$, I consider $|P| \to 0$ or $k_{F,+} = k_{F,\uparrow} = k_{F,\downarrow}$ limit, and expand the matrix elements of $\mathbf{F}^{-1}(q)$ to second order in $|\mathbf{q}|$ and w to get $\mathbf{M}^{-1}_{\lambda,\lambda}(q) = A + C|\mathbf{q}|^2 - Dw^2$, $\mathbf{M}^{-1}_{\theta,\theta}(q) = Q|\mathbf{q}|^2 - Rw^2$ and $\mathbf{M}^{-1}_{\lambda,\theta}(q) = iBw$, such that

$$\mathbf{M}^{-1}(\mathbf{q}, w) = \begin{pmatrix} A + C|\mathbf{q}|^2 - Dw^2 & iBw \\ -iBw & Q|\mathbf{q}|^2 - Rw^2 \end{pmatrix}.$$

The expansion coefficients are given in the Appendix B.3. Thus, there are two branches for the collective excitations, but I focus only on the lowest energy one correponding to the Goldstone mode with dispersion $w(\mathbf{q}) = v|\mathbf{q}|$, where

$$v = \sqrt{\frac{AQ}{AR + B^2}} \tag{3.48}$$

is the speed of sound. Extra care is required when $P \neq 0$ since Landau damping causes collective excitations to decay into the two-quasiparticle continuum even for the s-wave case, since gapless fermionic (quasiparticle) excitations are present (see Fig. 3.2).

The BCS limit is characterized by the criteria $\mu_+ > 0$ and $\mu_+ \approx \epsilon_{F,+} \gg |\Delta_0|$. The expansion of the matrix elements to order $|\mathbf{q}|^2$ and w^2 is performed under the condition $[w, |\mathbf{q}|^2/(2m_+)] \ll |\Delta_0|$. The coefficient that couples phase and amplitude fields vanish ($B = 0$) in this limit. Thus, there is no mixing between the phase and amplitude modes. The zeroth order coefficient is $A = \mathcal{D}$, and the second order coefficients are $C = Q/3 = \mathcal{D}v_{F,\uparrow}v_{F,\downarrow}/(36|\Delta_0|^2)$, and $D = R/3 = \mathcal{D}/(12|\Delta_0|^2)$. Here, $v_{F,\sigma} = k_{F,\sigma}/m_\sigma$ is the Fermi velocity and $\mathcal{D} = m_+ V k_{F,+}/(2\pi^2)$ is the density of states per spin at the Fermi energy. Thus, I obtain

$$v = \sqrt{\frac{v_{F,\uparrow}v_{F,\downarrow}}{3}} = \sqrt{v_\uparrow v_\downarrow}, \tag{3.49}$$

with $v_\sigma = v_{F,\sigma}/\sqrt{3}$, which reduces to the Anderson-Bogoliubov relation when the masses are equal.

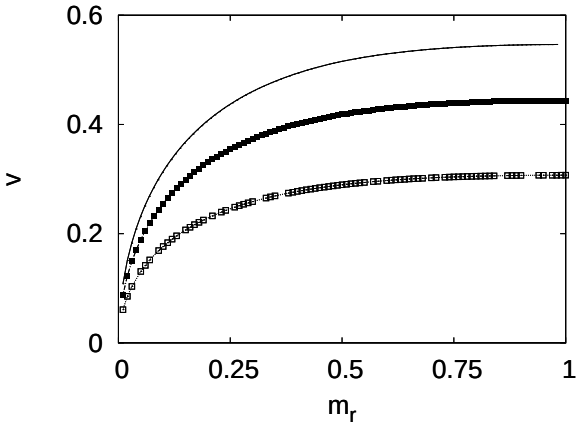

Figure 3.8: Sound velocity v (in units of $v_{F,+} = k_{F,+}/m_+$) versus m_r for $1/(k_{F,+}a_F) = -1$ (solid line), $1/(k_{F,+}a_F) = 0$ (solid squares) and $1/(k_{F,+}a_F) = 1$ (hollow squares). Here, populations are equal ($P = 0$).

On the other hand, the BEC limit is characterized by the criteria $\mu_+ < 0$ and $\xi_{\mathbf{k},+} \gg |\Delta_0|$. The expansion of the matrix elements to order $|\mathbf{q}|^2$ and w^2 is performed under the condition $[w, |\mathbf{q}|^2/(2m_+)] \ll |\mu_+|$. The coefficient $B \neq 0$ indicates that the amplitude and phase fields are mixed. The zeroth order coefficient is $A = \kappa|\Delta_0|^2/(2|\mu_+|)$, the first order coefficient is $B = \kappa$, and the second order coefficients are $C = Q = \kappa/[2(m_\uparrow + m_\downarrow)]$ and $D = R = \kappa/(8|\mu_+|)$, where $\kappa = \mathcal{D}/(32\sqrt{|\mu_+|\epsilon_{F,+}})$. Thus, I obtain

$$v = \frac{|\Delta_0|}{\sqrt{4(m_\uparrow + m_\downarrow)|\mu_+|}} = \sqrt{v_\uparrow v_\downarrow} \tag{3.50}$$

with $v_\sigma = \sqrt{2\pi n_\sigma a_F/m_\sigma^2}$. Notice that the sound velocity is very small and its smallness is controlled by the scattering length a_F. Furthermore, in the theory of weakly interacting dilute Bose gas, the sound velocity is given by $v_B = \sqrt{4\pi a_{BB} n_B/m_B^2}$. Making the identification that the density of pairs is $n_B = n_+$, the mass of the bound pairs is $m_B = m_\uparrow + m_\downarrow$ and that the Bose scattering length is

$$a_{BB} = \frac{m_B}{m_+} a_F = \left[1 + \frac{m_\uparrow}{2m_\downarrow} + \frac{m_\downarrow}{2m_\uparrow}\right] a_F, \tag{3.51}$$

v_B reduces to the well known Bogoliubov relation when the masses are equal. Therefore, the strongly interacting Fermi gas with two species can be described as a weakly interacting

Bose gas at zero temperature as well as at finite temperatures [155]. Notice that a_{BB} reduces to $a_{BB} = 2a_F$ for equal masses [110] in the Born approximation. A better estimate for a_{BB} can be found in the literature [63, 139, 140].

In Fig. 3.8, I show the sound velocity as a function of the mass ratio m_r for three values of the scattering parameter $1/(k_{F,+}a_F) = -1, 0$ and 1 corresponding to the BCS side $[1/(k_{F,+}a_F) = -1]$, unitarity $[1/(k_{F,+}a_F) = 0]$, and to the BEC side $[1/(k_{F,+}a_F) = 1]$. Notice that the speed of sound could be measured for a given m_r using similar techniques as in the single species case $m_r = 1$ [72].

This concludes my analysis of collective excitations in the continuum mixture for two types of fermions at zero temperature. I discuss next the effective field theory between paired and unpaired fermions.

3.5.3 Weakly Interacting Paired and Excess Fermions at Zero Temperature

In this section, I concentrate on the BEC regime, where the paired and unpaired (excess) fermions can be described by a mixture of molecular bosons and fermions. In this limit, the resulting equation of motion is identical to Eq. (3.39) near the critical temperature, except that all parameters are evaluated at zero temperature. Thus, at low temperatures the system continues to behave as a dilute mixture of weakly interacting bosons (formed from paired fermions) and unpaired fermions, and can be described by the free energy density

$$\mathcal{F}(\mathbf{x}) = E(\mathbf{x}) - \mu_e n_e(\mathbf{x}) - \mu_B |\Psi(\mathbf{x})|^2, \tag{3.52}$$

where the energy density is

$$E(\mathbf{x}) = K_B + K_F + \frac{1}{2} U_{BB} |\Psi(\mathbf{x})|^4 + U_{BF} n_e(\mathbf{x}) |\Psi(\mathbf{x})|^2.$$

Here, K_B is the kinetic energy density of bosons (assumed to be much smaller than all the other energies) and K_F is the kinetic energy density of fermions. Averaging these energy densities over the spatial coordinates $F = \int d\mathbf{x} \mathcal{F}(\mathbf{x})/V$ leads to a ground state average free energy density

$$F = \frac{1}{2} U_{BB} n_B^2 + U_{BF} n_e n_B + \frac{3}{5} \epsilon_{F,e} n_e - \mu_e n_e - \mu_B n_B,$$

where n_e (n_B) is the average density of fermions (bosons), and $\epsilon_{F,e}$ is the fermi energy of the excess fermions. Using the positivity of the Bose-Fermi compressibility matrix $\kappa_{\alpha,\beta} = \partial\mu_\alpha/\partial n_\beta$, where $\alpha, \beta = e, B$, one can show that bosons and fermions phase separate when the condition

$$n_e \geq \frac{4\pi}{3}\left(\frac{\pi}{m_e}\right)^3\left(\frac{U_{BB}}{U_{BF}^2}\right)^3 \tag{3.53}$$

is satisfied [171].

Using the boson-boson and boson-fermion interactions $U_{BB} = 4\pi a_{BB}/m_B$ and $U_{BF} = 4\pi a_{BF}/m_{BF}$, the scattering paramaters indicated in Eqs. (3.41) and (3.42), as well as the relations $|P| = n_e/n$, $n = n_\uparrow + n_\downarrow = k_{F,+}^3/(3\pi^2)$ and $n_B = (n - n_e)/2$, then phase separation occurs when

$$|P| \geq \frac{1}{2}\left(\frac{\pi}{8}\right)^3\left(\frac{m_+/m_e}{k_{F,+}a_F}\right)^3. \tag{3.54}$$

Here e labels excess type of fermions, and m_e is the mass of the unpaired fermions, and m_+ is twice the reduced mass of the $\uparrow$ and $\downarrow$ fermions. This expression is quantitatively correct in its region of validity, i.e., when $1/(k_{F,+}a_F) \gg 1$, however, it still gives semi-quantitative results for $1/(k_{F,+}a_F) \gtrsim 2$. For instance, in the case of an equal mass mixture, this expression would suggest that the resulting Bose-Fermi mixture is uniform when $1/(k_{F,+}a_F) > 2.5$ for $|P| \to 0.5$, and when $1/(k_{F,+}a_F) > 3.2$ for $|P| \to 1$. From the numerical calculations I find $1/(k_{F,+}a_F) > 1.9$ for $|P| \to 0.5$, and when $1/(k_{F,+}a_F) > 2.4$ for $|P| \to 1$.

The analytic expression given in Eq. (3.54) may be used as a guide for the boundary between phase separation (non-uniform) and the mixed phase (uniform) for any mixture of fermions. In particular, this relation serves as an estimator for the phase boundary for future experiments performed in the BEC limit of unequal mass fermions with population imbalance. This relation can be rewritten in terms of the mass ratio $m_r = m_\uparrow/m_\downarrow$ by realizing that the ratio $m_+/m_e = 2m_r/(1 + m_r)$ when $\downarrow$ (heavier) fermions are in excess, and that $m_+/m_e = 2/(1 + m_r)$ when $\uparrow$ (lighter) fermions are in excess. Thus, when $\downarrow$ (heavier) fermions are in excess, the critical polarization below which phase separation (non-uniform phase) occurs is

$$P_{c,\downarrow}^{(1)} = -\frac{1}{2}\left(\frac{\pi}{4k_{F,+}a_F}\right)^3\left(\frac{m_r}{1+m_r}\right)^3, \tag{3.55}$$

while, when ↑ (lighter) fermions are in excess, the critical polarization above which phase separation (non-uniform phase) occurs is

$$P_{c,\uparrow}^{(1)} = +\frac{1}{2}\left(\frac{\pi}{4k_{F,+}a_F}\right)^3\left(\frac{1}{1+m_r}\right)^3. \tag{3.56}$$

Notice that in the equal mass ($m_r = 1$) case $P_{c,\downarrow}^{(1)} = -P_{c,\uparrow}^{(1)}$ as required by symmetry.

In addition, I can also describe analytically a finer structure of non-uniform (phase separated) superfluid phases deep into the BEC regime. For a weakly interacting Bose-Fermi mixture, the phase separated region consists of two regions: PS(1), where there is phase separation between pure fermions and pure bosons (tightly paired fermions), and PS(2), where there is phase separation between pure fermions and a mixture of fermions and bosons (tighly bound fermions). Following the method of Ref. [171], I obtain analytically the condition

$$n_e \geq \frac{1125\pi^4}{128m_e^4}\frac{U_{BB}^3}{U_{BF}^6} - \frac{5}{4}\frac{U_{BB}}{U_{BF}}n_B, \tag{3.57}$$

for the transition from the PS(2) to the PS(1) phase.

Using the effective boson-boson (U_{BB}) and effective boson-fermion U_{BF} interactions, I can rewrite this relation as

$$|P| \geq \frac{8}{11}\left(\frac{15\pi}{64}\right)^3\left(\frac{m_+/m_e}{k_{F,+}a_F}\right)^3 - \frac{5}{11}, \tag{3.58}$$

where I used $n_B = (n-n_e)/2$ as the boson density and $|P| = n_e/n$. These phase boundaries can also be expressed in terms of m_r and $1/(k_{F,+}a_F)$ as follows. When ↓ (heavier) fermions are in excess, the critical polarization below which the transition from PS(2) to PS(1) occurs is

$$P_{c,\downarrow}^{(2)} = -\frac{1}{11}\left(\frac{15\pi}{16k_{F,+}a_F}\right)^3\left(\frac{m_r}{1+m_r}\right)^3 + \frac{5}{11}, \tag{3.59}$$

while, when ↑ (lighter) fermions are in excess, the critical polarization above which the transition from PS(2) to PS(1) occurs is

$$P_{c,\uparrow}^{(2)} = +\frac{1}{11}\left(\frac{15\pi}{16k_{F,+}a_F}\right)^3\left(\frac{1}{1+m_r}\right)^3 - \frac{5}{11}. \tag{3.60}$$

Notice that in the equal mass ($m_r = 1$) case $P_{c,\downarrow}^{(2)} = -P_{c,\uparrow}^{(2)}$ as required by symmetry.

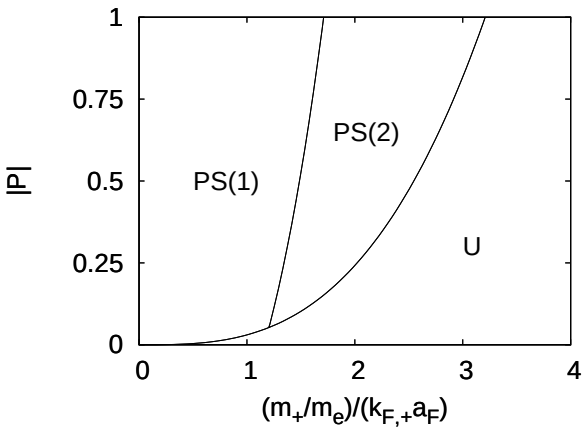

Figure 3.9: Phase diagram of $|P| = |N_\uparrow - N_\downarrow|/(N_\uparrow + N_\downarrow)$ versus $(m_+/m_e)/(k_{F,+}a_F)$ in the BEC limit. I show the uniform superfluid (U) phase where paired and unpaired fermions coexist, and the phase separated non-uniform superfluid phases PS(1) and PS(2). The PS(1) region labels phase separation between pure unpaired (excess) and pure tightly paired fermions (bosons), while the PS(2) region labels phase separation between pure unpaired (excess) fermions and a mixture of unpaired and tightly paired fermions.

In Fig. 3.9, I show phase diagram of uniform and non-uniform superfluidity as a function of population imbalance $|P|$ and $(m_+/m_e)/(k_{F,+}a_F)$, which is strictly valid in the BEC limit when $1/(k_{F,+}a_F) \gg 1$. In this figure, I show the uniform superfluid (U) phase where tightly paired and unpaired fermions coexist, and phase separated (non-uniform) superfluid (PS) phases. The PS(1) region labels phase separation between pure unpaired (excess) and pure tightly paired fermions (bosons), while the PS(2) region labels phase separation between pure unpaired (excess) fermions and a mixture of unpaired and tightly paired fermions. The phase boundary between U and PS(2) phases is determined from Eq. (3.54), and the phase boundary between PS(2) and PS(1) phases is determined from Eq. (3.58). For a fixed mass anisotropy m_r, when $|P|$ is large, I find phase transitions from PS(1) to PS(2) to U phase as the interaction strength $1/(k_{F,+}a_F)$ increases as shown in Fig. 3.10. However, when $|P|$ is small, I find a direct phase transition from the PS(1) to the U phase as $1/(k_{F,+}a_F)$ increases. Notice that the phase diagrams given in Fig. 3.10 are very similar to the ones given in Fig. 3.4, with the added refinement of the non-uniform superfluid phases PS(1) and PS(2).

In Fig. 3.11, I show the phase diagram of population imbalance P versus mass anisotropy

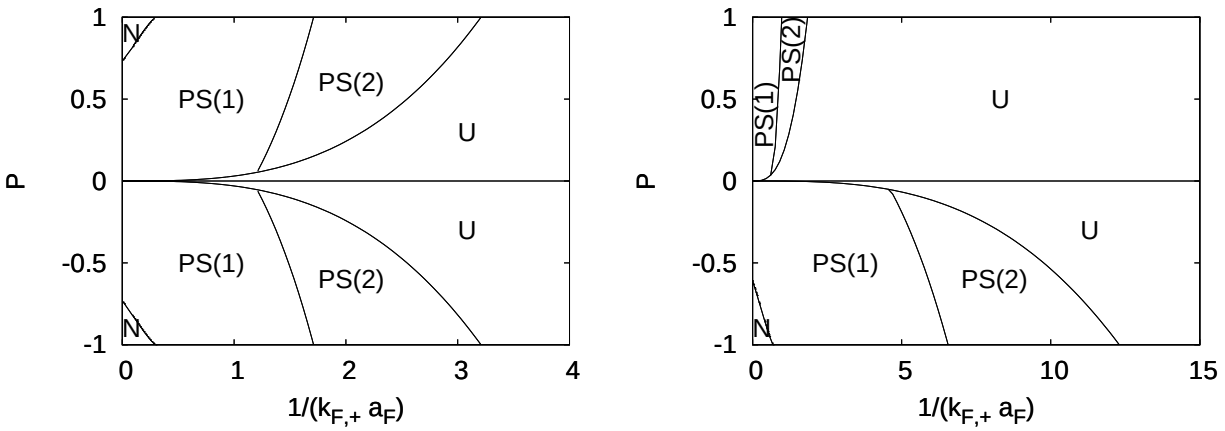

Figure 3.10: Phase diagram of $P = (N_\uparrow - N_\downarrow)/(N_\uparrow + N_\downarrow)$ versus $1/(k_{F,+}a_F)$ for (a) equal masses when $m_\uparrow = m_\downarrow$, and (b) unequal masses when $m_\uparrow = 0.15m_\downarrow$ in the BEC side. I show normal(N), uniform superfluid (U) and phase separated non-uniform superfluid phases PS(1) and PS(2).

$m_r = m_\uparrow/m_\downarrow$ in the BEC limit when (a) $1/(k_{F,+}a_F) = 3$ and (b) $1/(k_{F,+}a_F) = 4$. I indicate the uniform superfluid (U) phase where paired and unpaired fermion coexist, and phase separated non-uniform superfluid phases PS(1) and PS(2). The phase boundary between U and PS(2) phases is determined from Eq. (3.55) when $P < 0$, and from Eq. (3.56) when $P > 0$. In addition, the phase boundary between PS(2) and PS(1) phases is determined from Eq. (3.59) when $P < 0$, and PS(1) phase does not exist when $P > 0$. Notice that these phase diagrams are very similar to the one given in Fig. 3.7(c), with the added refinement of the non-uniform superfluid phases PS(1) and PS(2). For a fixed interaction strength $1/(k_{F,+}a_F)$, when $|P|$ is large, I find phase transitions from PS(1) to PS(2) to U phase as the mass anisotropy m_r increases. However, when $|P|$ is small, I find a phase transition from the PS(1) to the U phase as m_r increases.

To summarize, I studied analytically the structure of non-uniform (phase separated) superfluid phases in the BEC regime. However to understand experiments on ultracold atoms, I need to consider the trapping potential, which is discussed next.

3.5.4 Effects of a Trapping Potential

For simplicity, I approximate the trapping potential by an isotropic harmonic function where the potential energy is $V_\sigma(\mathbf{x}) = \alpha_\sigma|\mathbf{x}|^2/2$ such that the local chemical potentials are given

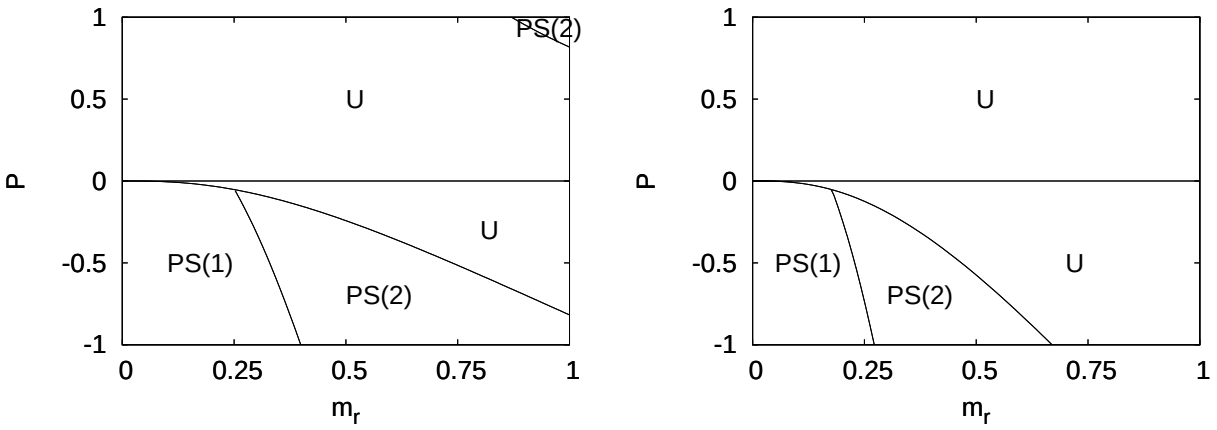

Figure 3.11: Phase diagram of $P = (N_\uparrow - N_\downarrow)/(N_\uparrow + N_\downarrow)$ versus $m_r = m_\uparrow/m_\downarrow$ in the BEC limit when (a) $1/(k_{F,+}a_F) = 3$ and (b) $1/(k_{F,+}a_F) = 4$. I show the uniform superfluid (U) phase where paired and unpaired fermion coexist, and phase separated non-uniform superfluid phases PS(1) and PS(2).

by

$$\mu_\sigma(\mathbf{x}) = \mu_\sigma - \frac{1}{2}\alpha_\sigma|\mathbf{x}|^2. \tag{3.61}$$

Here, α_σ is proportional to the trapping frequency of the σ type fermion, which is typically different for each kind of atom. In general, it is quite difficult to make completely isotropic traps and harmonic traps are typically elongated such that

$$V_\sigma(\mathbf{x}) = \frac{\alpha_{\sigma,x}}{2}x^2 + \frac{\alpha_{\sigma,y}}{2}y^2 + \frac{\alpha_{\sigma,z}}{2}z^2 \tag{3.62}$$

with $\alpha_{\sigma,x} = \alpha_{\sigma,y} \gg \alpha_{\sigma,z}$. However, the same qualitative behavior occurs in the elongated or spherically symmetric (isotropic) traps, and I confine myself for simplicity to the isotropic case. When experimental data becomes available and all the numbers are known, one can revisit this problem for detailed comparison between theory and experiment.

Again, I confine the discussion to the BEC regime, and obtain the equation of motion for a dilute mixture of weakly interacting bosons and fermions at zero temperature

$$\begin{aligned} - \quad & \mu_B\Psi(x) + \left[U_{BB}|\Psi(x)|^2 + U_{BF}n_e(x)\right]\Psi(x) \\ + \quad & [V_\uparrow(\mathbf{x}) + V_\downarrow(\mathbf{x})]\Psi(x) - \frac{\nabla^2\Psi(x)}{2m_B} = i\frac{\partial\Psi(x)}{\partial t}, \end{aligned} \tag{3.63}$$

where the spatial density of unpaired fermions is

$$n_e(x) = n_{ex}(\mathbf{x}) - U_{BF}\frac{\partial n_{ex}(\mathbf{x})}{\partial\mu_e}|\Psi(x)|^2. \tag{3.64}$$

These results are quite similar to the case of equal masses [146]. Notice that setting $V_\sigma = 0$ reduces the problem to the free space case discussed in the previous subsection. Here,

$$n_e(\mathbf{x}) = \frac{1}{V}\sum_{\mathbf{k}} n_f\left[\epsilon_{\mathbf{k},e} - \mu_e(\mathbf{x})\right], \tag{3.65}$$

where $n_f(\varepsilon) = 1/[\exp(\beta\varepsilon)+1]$ is the Fermi distribution. In the BEC limit when $a_F \to 0^+$, I can approximate the local density of unpaired fermions as

$$n_e(x) \approx \frac{1}{V}\sum_{\mathbf{k}} n_f\left[\epsilon_{\mathbf{k},e} - \mu_e(\mathbf{x}) + U_{BF}|\Psi(x)|^2\right], \tag{3.66}$$

which at zero temperature leads to

$$n_e(\mathbf{x}) = \frac{1}{6\pi^2}\{2m_e\left[\mu_e(\mathbf{x}) - U_{BF}n_B(\mathbf{x})\right]\}^{3/2}. \tag{3.67}$$

Notice that the density of bosons at zero temperature is given by

$$n_B(\mathbf{x}) = |\Psi(\mathbf{x})|^2. \tag{3.68}$$

Therefore, I need to solve Eq. (3.63) self-consistently with the number of unpaired (excess) $N_e = \int d\mathbf{x} n_e(\mathbf{x})$ and paired (bound) $N_{bf} = 2\int d\mathbf{x} n_B(\mathbf{x})$ fermions such that the total number of fermions is $N = N_e + N_{bf}$.

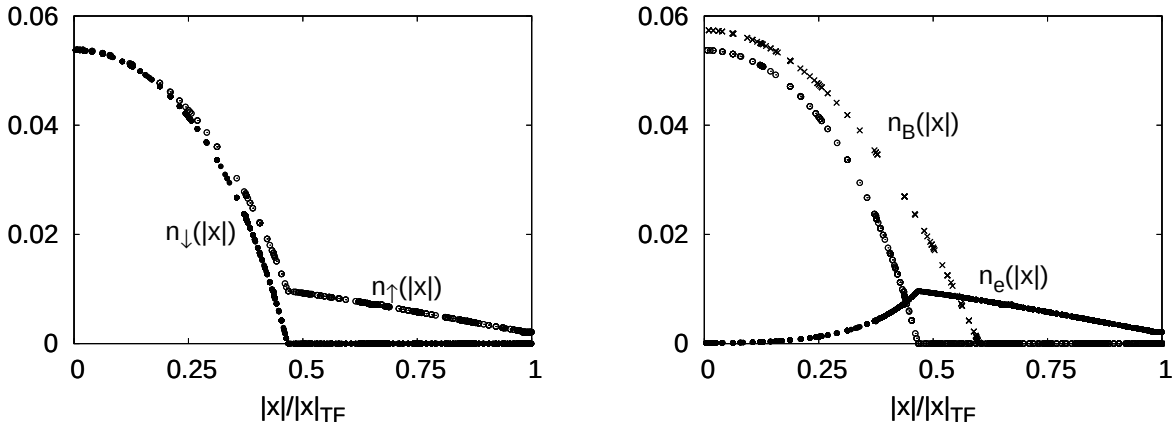

Figure 3.12: (a) Density $n_\sigma(|\mathbf{x}|)$ of fermions (in units of $k_{F,+}^3$), and (b) density of molecular bosons $n_B(|\mathbf{x}|)$ (hollow circles) and unpaired fermions $n_e(|\mathbf{x}|)$ (solid circles) versus trap radius $|\mathbf{x}|/|\mathbf{x}|_{TF}$. Here $P = 0.5$ and $1/(k_{F,+}a_F) = 2$. In (b), I also compare $n_B(|\mathbf{x}|)$ for $P = 0$ when $1/(k_{F,+}a_F) = 2$ (crosses).

Next I solve the self-consistency equations for a ^{6}Li and ^{40}K mixture ($m_r = 0.15$) within the Thomas-Fermi (TF) approximation, where the kinetic energy term in Eq. (3.63) is

neglected. This leads to coupled equations for the density of paired and unpaired fermions

$$n_B(\mathbf{x}) \approx \frac{\mu_B - V_\uparrow(\mathbf{x}) - V_\downarrow(\mathbf{x}) - U_{BF} n_e(\mathbf{x})}{U_{BB}}. \tag{3.69}$$

In the numerical analysis, I choose for convenience $\alpha_\uparrow = \alpha_\downarrow = \alpha$, $1/(k_{F,+}a_F) = 2$ and $P = 0.2, 0.5$ and 0.8. However, in a more realistic case $\alpha_\uparrow \neq \alpha_\downarrow = \alpha$, since atoms with different masses may experience different trapping potentials due to their different polarizabilities.

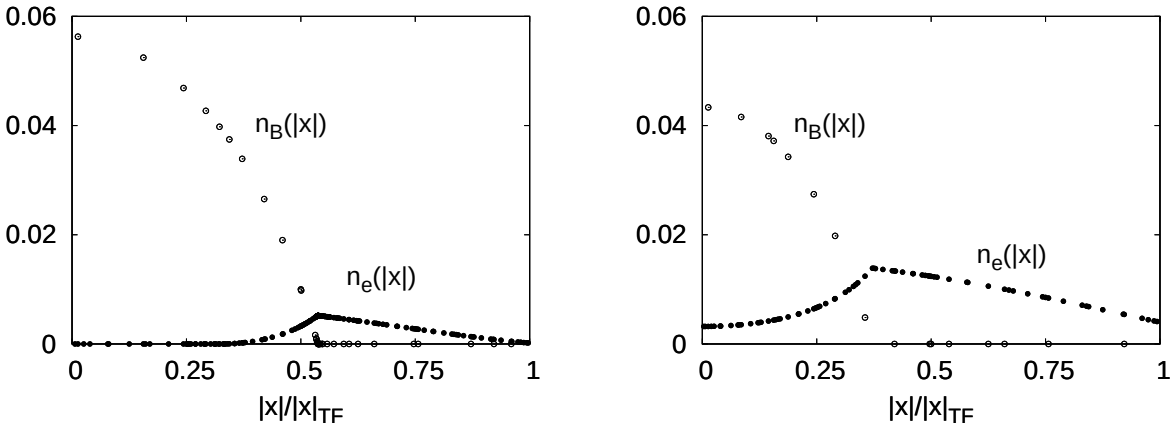

Figure 3.13: Density of molecular bosons $n_B(|\mathbf{x}|)$ (hollow circles) and unpaired fermions $n_e(|\mathbf{x}|)$ (solid circles) versus trap radius $|\mathbf{x}|/|\mathbf{x}|_{TF}$ for (a) $P = 0.2$, and (b) $P = 0.8$ when $1/(k_{F,+}a_F) = 2$.

In Fig. 3.12(a), I show the density $n_\sigma(|\mathbf{x}|)$ of σ type fermion (in units of $k_{F,+}^3$) as a function of $|\mathbf{x}|/|\mathbf{x}|_{TF}$, where $|\mathbf{x}|_{TF}$ is the TF radius defined by $\epsilon_{F,+} = k_{F,+}^2/(2m_+) = \alpha|\mathbf{x}|_{TF}^2/2$. I also scale the total number of fermions with

$$N = \frac{k_{F,+}^3 |\mathbf{x}|_{TF}^3}{24}. \tag{3.70}$$

I find that the density of $\uparrow$ and $\downarrow$ fermions are similar close to the center of the trapping potential, while most of the excess fermions are close to the edges. In Figs. 3.12(b) and 3.13, I show the density of molecular bosons $n_B(|\mathbf{x}|) = [n(|\mathbf{x}|) - n_e(|\mathbf{x}|)]/2$ as well as unpaired fermions $n_e(|\mathbf{x}|) = n_\uparrow(|\mathbf{x}|) - n_\downarrow(|\mathbf{x}|)$. In both figures, I find a clear indication of phase separation between paired and unpaired fermions. In Fig. 3.12(b), I also compare the total density of fermions $n(|\mathbf{x}|)$ for the same parameters when the populations are balanced $N_\uparrow = N_\downarrow$. When $P \neq 0$, the total local density of fermions at the center of the trap is reduced in comparison to the $P = 0$ case for the same fermion scattering parameter, since the unpaired

fermions are pushed away from the center of the trap due to U_{BF}. These findings for unequal masses are similar to previous results on equal mass mixtures [146, 147, 148, 149, 150, 151]. However, in Figs. 3.12(b) and 3.13(a), I find three regions within the TF approximation and parameters used. For instance, in Fig. 3.12(b), (i) bosons only for $|\mathbf{x}| \leq 0.23|\mathbf{x}|_{TF}$; (ii) bosons and excess fermions for $0.23|\mathbf{x}|_{TF} < |\mathbf{x}| \leq 0.45|\mathbf{x}|_{TF}$; and (iii) excess fermions only for $|\mathbf{x}| > 0.45|\mathbf{x}|_{TF}$. While in Fig. 3.13(b), I find two regions within the TF approximation and parameters used. (i) bosons and excess fermions for $0 \leq |\mathbf{x}| \leq 0.35|\mathbf{x}|_{TF}$; and (ii) excess fermions only for $|\mathbf{x}| > 0.35|\mathbf{x}|_{TF}$.

Lastly, for the parameters used, the harmonic trap tends to favor phase separation into a PS(1)-type phase where one has almost pure fermion and almost pure boson regions. This is simply because the excess fermions feel effectively a repulsive trapping potential at the center of the trap, while they feel an attractive trapping potential towards the edges of the trap, as can be directly shown from Eqs. (3.67) and (3.69). In a harmonic trap it may be still possible to realize the PS(2)-type phase where one has an almost pure fermion region and an almost pure mixed phase of bosons and fermions, provided that good control over the trapping potentials is possible [172].

Having concluded discussion of saddle point ground state phase diagrams and the effects of a trapping potential, I present next the exact ground state phase diagrams in the BEC limit.

3.6 Phase Diagrams in the BEC Limit beyond the Born Approximation

In this section, I use the effective weakly interacting Bose-Fermi mixture description to analyze the superfluid phase diagram beyond the Born approximation for two-species dilute Fermi-Fermi mixtures with equal and unequal masses in the BEC limit. I first calculate the exact boson-fermion scattering length as a function of mass anisotropy and then construct the phase diagrams. My main results are as follows. In addition to the normal and uniform superfluid phases, I find two different non-uniform phase separated (PS) states: (1) a phase separation between pure unpaired (excess) and pure tightly paired fermions (molecular bosons), and (2) a phase separation between pure excess fermions and a mixture of excess

fermions and molecular bosons. For equal mass mixtures, the improved results for the PS(2) to U phase boundary is quantitatively in agreement with the previous saddle-point or mean-field results, however, there are important qualitative and quantitative differences for unequal mass mixtures showing the larger effects of fluctuations in the latter case.

3.6.1 Weakly Interacting Molecular Bosons and Fermions

In the BEC limit, I showed in Section 3.5 that Fermi-Fermi mixtures behave as a dilute mixture of weakly interacting molecular bosons (formed from paired fermions) and unpaired excess fermions. Using the positive definiteness of the Bose-Fermi compressibility matrix $\kappa_{i,j} = \partial\mu_i/\partial n_j$, where $\{i,j\} \equiv \{B,F\}$, I find that molecular bosons and excess fermions phase separate when the condition $n_F \geq 4\pi^4 U_{BB}^3/(3m_F^3 U_{BF}^6)$ is satisfied [171]. Defining the boson-boson and boson-fermion interaction strengths $U_{BB} = 4\pi a_{BB}/m_B$ and $U_{BF} = 4\pi a_{BF}/m_{BF}$ as well as the relations $|P| = n_F/n$ and $n = k_{F,+}^3/(3\pi^2)$ where $k_{F,+}$ is the Fermi momentum, phase separation occurs when

$$|P| \geq \frac{\pi^3 \gamma_B^3 m_{BF}^6}{16\beta_F^6 m_B^3 m_F^3}\lambda^3. \tag{3.71}$$

Here a_F, $a_{BB} = \gamma_B a_F$ and $a_{BF} = \beta_F a_F$ are the fermion-fermion, boson-boson and boson-fermion scattering lengths where γ_B and β_F are constants, $\lambda = 1/(k_{F,+}a_F)$ is the interaction strength, $m_B = m_\uparrow + m_\downarrow$ is the mass of the molecular bosons, $m_{BF} = 2m_B m_F/(m_B + m_F)$ is twice the reduced mass of a molecular boson and an excess fermion, and m_F is the mass of the excess-type fermions.

In addition, I can also describe analytically a finer structure of non-uniform phase separated superfluid phases. For a weakly interacting Bose-Fermi mixture, the phase separation consists of two regions [171]: (I) PS(1) where there is phase separation between pure excess fermions and pure molecular bosons, and (II) PS(2) where there is phase separation between pure excess fermions and a mixture of excess fermions and molecular bosons. I obtain analytically the condition $n_F \geq 1125\pi^4 U_{BB}^3/(128m_F^4 U_{BF}^6) - 5U_{BB}n_B/(4U_{BF})$ for the transition from the PS(2) to the PS(1) phase. Using the definitions of boson-boson and

boson-fermion interactions, I can rewrite this relation as

$$|P|\left(1-\frac{5\gamma_B m_{BF}}{8\beta_F m_B}\right)\geq\frac{3375\pi^3\gamma_B^3 m_{BF}^6}{8192\beta_F^6 m_B^3 m_F^3}\lambda^3-\frac{5\gamma_B m_{BF}}{8\beta_F m_B},\tag{3.72}$$

where $\gamma_B = a_{BB}/a_F$, $\beta_F = a_{BF}/a_F$ and $\lambda = 1/(k_{F,+}a_F)$.

The analytic expressions given in Eqs. (3.71) and (3.72) are exact in their region of validity, i.e., when $1/(k_{F,+}a_F) \gg 1$, however, they may still give semi-quantitative results for $1/(k_{F,+}a_F) \gtrsim 1$. Therefore, these expressions may be used as a guide for the boundary between phase separated (non-uniform) and the mixed (uniform) phases for any mixture of fermions. In particular, they serve as an estimator for the phase bounday for future experiments performed in the BEC limit for unequal mass fermions with population imbalance.

In order to make quantitative predictions for future experiments, I need to know the exact boson-boson and boson-fermion scattering lengths as a function of mass anisotropy. While I calculated the boson-boson and boson-fermion scattering lengths within the Born approximation in Section 3.5.1, it is known that one needs to go beyond this approximation to calculate the exact scattering lengths [170]. This is true even for equal mass mixtures, that is

$$a_{BB} = 0.60a_F, \qquad a_{BF} = 1.18a_F \qquad \text{(exact)},\tag{3.73}$$

$$a_{BB} = 2.00a_F, \qquad a_{BF} = 2.67a_F \qquad \text{(Born)},\tag{3.74}$$

are the exact and the Born approximation values. For my purposes, I need to calculate the exact values for a_{BB} and a_{BF} as a function of mass anisotropy as discussed next.

3.6.2 Boson-Boson and Boson-Fermion Scattering Length

For equal mass mixtures, a diagrammatic approach has been recently used to calculate exact values for a_{BB} and a_{BF} [139, 140], and the results are in agreement with earlier works [169, 170]. Next, I generalize this approach and analyze only the boson-fermion scattering length of three fermions when two of the fermions have different mass from the third one.

This problem was first solved by Skorniakov and Ter-Martirosian in the context of

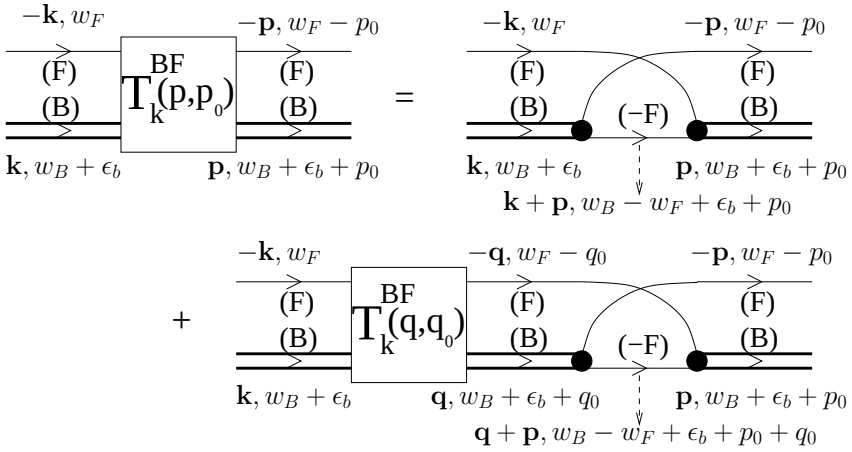

Figure 3.14: Diagrammatic representation of the integral equation for the boson-fermion scattering t-matrix $T_{\mathbf{k}}^{BF}(\mathbf{p}, p_0)$, where the single lines represent the σ-type fermion propagators, and the double lines represent the dressed molecular boson propagators. Notice that the first diagram on the right represents a fermion exchange process, and all other possible processes are included in the second diagram.

nuclear physics when all three fermions had the same mass [169]. The diagrammatic representation for the equation of the boson-fermion scattering t-matrix $T_{\mathbf{k}}^{BF}(\mathbf{p}, p_0)$ is shown in Fig. 3.14, where $w_F = k^2/(2m_F)$ and $w_B = k^2/(2m_B)$ are the kinetic energies for the excess-type fermions and molecular bosons, respectively, and $\epsilon_b = -1/(m_{\uparrow\downarrow}a_F^2) < 0$ is the binding energy of the $\uparrow$- and $\downarrow$-type fermions. Here, $m_{\uparrow\downarrow} = 2m_\uparrow m_\downarrow/(m_\uparrow + m_\downarrow)$ is twice the reduced mass of the $\uparrow$- and $\downarrow$-type fermions. In this figure, single lines represent the σ-type fermion propagators given by

$$G_{0,\sigma}(\mathbf{k}, w) = \frac{1}{w - w_\sigma + \mu_\sigma + i0^+}, \tag{3.75}$$

where $w_\sigma = k^2/(2m_\sigma)$ is the energy and μ_σ is the chemical potential of the σ-type fermions. Similarly double lines represent the dressed molecular boson propagators given by

$$D_0(\mathbf{k}, w) = \frac{4\pi}{m_{\uparrow\downarrow}^{3/2}} \frac{1}{|\epsilon_b|^{1/2} - (w_B - w - \mu_\uparrow - \mu_\downarrow - i0^+)^{1/2}}, \tag{3.76}$$

which is derived in Appendix B.4. Notice that, on the right hand side of Fig. 3.14, the first diagram represents a fermion exchange process, and all other (infinitely many) possible processes are included in the second diagram. In the following, I set $\mu_\sigma = 0$ since all of the calculations are performed for three-body interactions in vacuum.

Therefore, in the analytical form, the t-matrix $T_{\mathbf{k}}^{BF}(\mathbf{p}, p_0)$ satisfies the following integral

equation

$$
\begin{aligned}
T^{BF}_{\mathbf{k}}(\mathbf{p},p_0) = \; & - \; G_{0,F}(\mathbf{k}+\mathbf{p}, w_B - w_F + \epsilon_b + p_0) \\
& - \; \sum_{\mathbf{q},q_0} D_0(\mathbf{q}, w_B + \epsilon_b + q_0) G_{0,F}(-\mathbf{q}, w_F - q_0) \\
& \quad T^{BF}_{\mathbf{k}}(\mathbf{q},q_0) G_{0,-F}(\mathbf{p}+\mathbf{q}, w_B - w_F + \epsilon_b + p_0 + q_0), \qquad (3.77)
\end{aligned}
$$

where I used $(-\uparrow) \equiv \downarrow$ and vice versa. On the right hand side, I can sum over frequency q_0 by closing the integration contour in the upper half-plane, where $T^{BF}_{\mathbf{k}}(\mathbf{q},q_0)$ and $D_0(\mathbf{q}, w_B + \epsilon_b + q_0)$ are analytic functions of q_0. Since this integration sets $q_0 = k^2/(2m_F) - q^2/(2m_F)$, I set $p_0 = k^2/(2m_F) - p^2/(2m_F)$ in order to have the same frequency dependence for the t-matrix on both sides [140]. Since I are interested in zero-range low energy s-wave scattering, I average out the angular dependences of $\mathbf{k}$ and $\mathbf{p}$. When $k \to 0$, the resultant equation is the generalized integral equation for the boson-fermion scattering and it is given by

$$
\begin{aligned}
& \frac{m_{\uparrow\downarrow} a_0^{BF}(p)/m_{BF}}{a_F^{-1} + (m_{\uparrow\downarrow} p^2/m_{BF} + a_F^{-2})^{1/2}} = \frac{1}{p^2 + a_F^{-2}} - \frac{m_B}{2\pi m_F} \\
& \int_0^\infty \frac{dq}{qp} \ln\left(\frac{q^2 + 2m_F qp/m_B + p^2 + a_F^{-2}}{q^2 - 2m_F qp/m_B + p^2 + a_F^{-2}} \right) a_0^{BF}(q). \qquad (3.78)
\end{aligned}
$$

Here, I define the boson-fermion scattering length

$$
a_k^{BF}(p) = \frac{m_{BF}}{m_{\uparrow\downarrow}^{3/2}} \left[|\epsilon_b|^{1/2} + \left(\frac{p^2 - k^2}{m_{BF}} - \epsilon_b \right)^{1/2} \right] T_k^{BF}(p) \qquad (3.79)
$$

with its full momentum dependence. The integral equation given above as well as the scattering length expression reduces to the well-known identities for equal masses, i.e. when $m_\uparrow = m_\downarrow = m$. Notice that, only the fermion exchange process is taken into account in the Born approximation, and neglecting the second term on the right hand side of Eq. (3.78) leads to $a_0^{BF}(0) = 2(m_{BF}/m_{\uparrow\downarrow}) a_F$ which is consistent with my previous results given in Section 3.5.1. However, I need to include both terms in order to find exact boson-fermion scattering length.

Next, I solve Eq. (3.78) numerically for $a_0^{BF}(p)$ as a function of mass anisotropy $m_\uparrow/m_\downarrow$, and exact results for $a_0^{BF}(0)$ as well as the Born approximation values are shown in Fig. 3.15(a). In the diagrams, I choose $\uparrow$ ($\downarrow$) to label lighter (heavier) fermions such that lighter (heavier)

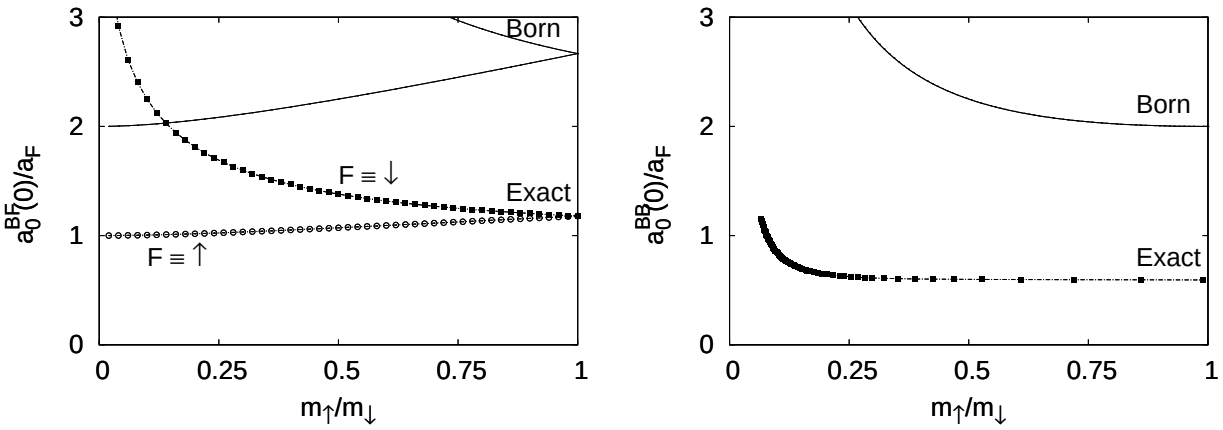

Figure 3.15: In (a), boson-fermion scattering length $a_0^{BF}(0)/a_F$ versus mass anisotropy $m_\uparrow/m_\downarrow$ is shown when lighter $\uparrow$-type (hollow circles) or heavier (solid circles) $\downarrow$-type fermions are in excess. In (b), boson-boson scattering length $a^{BB}(0)/a_F$ versus mass anisotropy $m_\uparrow/m_\downarrow$ is shown.

fermions are in excess when $F \equiv\uparrow$ ($F \equiv\downarrow$). This choice spans all possible mass ratios. I find that while $a_0^{BF}(0) = 1.179a_F$ when $m_\uparrow = m_\downarrow$, $a_0^{BF}(0)$ decreases (increases) from this value with increasing mass anisotropy when the lighter (heavier) fermions are in excess. In addition, in the limit of $m_\uparrow/m_\downarrow \to 0$, while $a_0^{BF}(0) \to a_F$ when the lighter fermions are in excess, $a_0^{BF}(0)$ diverges when the heavier fermions are in excess. Notice also that the Born approximation values for $a_0^{BF}(0)$ are not in agreement with the exact values for any mass anisotropy.

In Fig. 3.15(b), I present exact results for $a^{BB}(0)$ which are extracted from Ref. [170], together with the Born approximation values $a^{BB}(0) = (m_B/m_{\uparrow\downarrow})a_F$ which is derived in Section 3.5.1 as a function of mass anisotropy $m_\uparrow/m_\downarrow$. I again find that the Born approximation values for $a^{BB}(0)$ are not in agreement with the exact values for any mass anisotropy. Since I now have the exact values for the boson-boson as well as the boson-fermion scattering lengths, I analyze next the superfluid phase diagrams of two-species Fermi-Fermi mixtures in the BEC limit.

3.6.3 Superfluid Phase Diagrams in the BEC Limit

As discussed in the introduction, atomic gases of fermionic ^{6}Li, ^{40}K, ^{87}Sr, and ^{171}Yb atoms have been cooled down below their Fermi degeneracy temperatures, and the superfluid

properties of two-component mixtures of the same atom species have been intensely analyzed [76, 77, 111, 112]. Anticipating future experiments, I analyze in this section the superfluid phase diagrams of two-species fermion mixtures. The boson-boson and boson-fermion scattering lengths for some of the possible mixtures are given in Table 3.1. Among these possibilities, next I confine the analysis to a population imbalanced mixture of ^{6}Li and ^{40}K atoms where $m_\uparrow = 0.15 m_\downarrow$.

Table 3.1: Exact boson-boson (a_{BB}) and boson-fermion (a_{BF}) scattering lengths for a list of two-species Fermi-Fermi mixtures. Here, $a_{B\uparrow}$ ($a_{B\downarrow}$) corresponds to excess-type of $\uparrow$ ($\downarrow$) fermions.

$\uparrow$	$\downarrow$	$m_\uparrow/m_\downarrow$	a_{BB}/a_F	$a_{B\uparrow}/a_F$	$a_{B\downarrow}/a_F$
^{6}Li	^{6}Li	1.000	0.599	1.179	1.179
^{6}Li	^{40}K	0.150	0.695	1.010	1.984
^{6}Li	^{87}Sr	0.068	-	1.003	2.512
^{6}Li	^{171}Yb	0.035	-	1.001	3.023
^{40}K	^{87}Sr	0.460	0.599	1.064	1.411
^{40}K	^{171}Yb	0.234	0.629	1.022	1.723
^{87}Sr	^{171}Yb	0.508	0.599	1.073	1.374

In Fig. 3.16, I show phase diagrams of uniform and non-uniform superfluidity as a function of population imbalance $P = (N_\uparrow - N_\downarrow)/(N_\uparrow + N_\downarrow)$ and interaction strength $1/(k_{F,+}a_F)$ for equal mass mixtures when $m_\uparrow = m_\downarrow$ and for unequal mass mixtures when $m_\uparrow = 0.15 m_\downarrow$. In the diagrams, I choose $\uparrow$ ($\downarrow$) to label lighter (heavier) fermions such that lighter (heavier) fermions are in excess when $P > 0$ ($P < 0$). Although these diagrams are strictly valid in the BEC limit when $1/(k_{F,+}a_F) \gg 1$, they may be qualitatively correct when $1/(k_{F,+}a_F) \gtrsim 1$.

In Fig. 3.16, I show the uniform superfluid (U) phase where tightly paired and unpaired fermions coexist, and phase separated (non-uniform) superfluid (PS) phases. The PS(1) region labels phase separation between pure excess fermions and molecular bosons, while the PS(2) region labels phase separation between pure excess fermions and a mixture of excess fermions and molecular bosons. It is important to emphasize that the possibility of a PS(1) region has not been proposed before for the population imbalanced fermion mixtures. The phase boundary between U and PS(2) phases is determined from Eq. (3.71), and the phase boundary between PS(2) and PS(1) phases is determined from Eq. (3.72). For a fixed

mass anisotropy, when $|P|$ is large, I find phase transitions from PS(1) to PS(2) to U phase as the interaction strength $1/(k_{F,+}a_F)$ increases. However, when $|P|$ is very small, I find a phase transition from the PS(1) to the U phase as $1/(k_{F,+}a_F)$ increases.

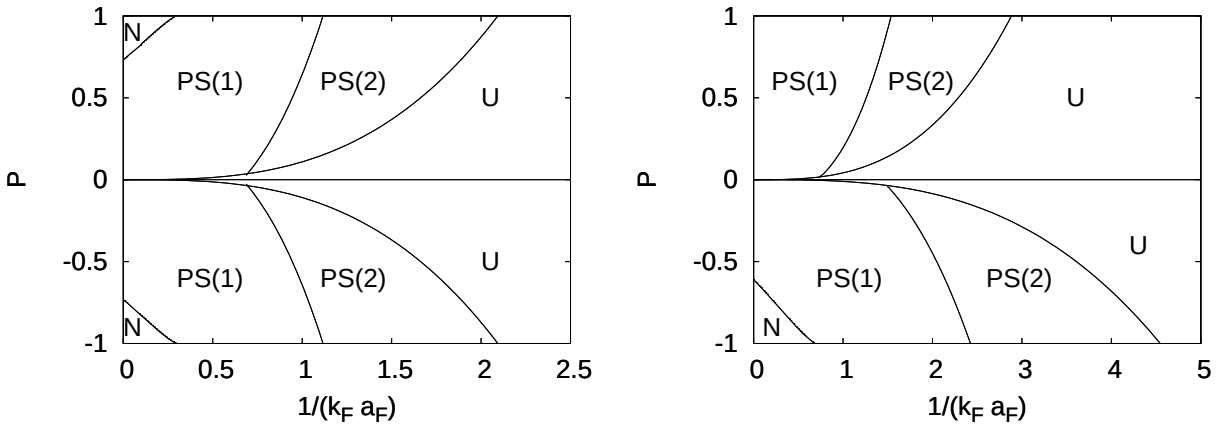

Figure 3.16: Phase diagram of $P = (N_\uparrow - N_\downarrow)/(N_\uparrow + N_\downarrow)$ versus $1/(k_{F,+}a_F)$ for (a) equal masses when $m_\uparrow = m_\downarrow$, and (b) unequal masses when $m_\uparrow = 0.15m_\downarrow$ in the BEC side. I show normal(N), uniform superfluid (U) and phase separated non-uniform superfluid phases PS(1) and PS(2).

It is also important to emphasize that these phase diagrams include fluctuation corrections beyond the mean-field approach in the BEC limit since I use the exact boson-boson and boson-fermion scattering lengths. The improved results for equal mass mixtures for the PS(2) to U phase boundary is quantitatively in agreement with the previous saddle-point or mean-field results [111, 112] shown in Fig. 3.4(a), however, there are important qualitative and quantitative differences for unequal mass mixtures shown in Fig. 3.4(b), showing the larger effects of fluctuations in the latter case. In addition, the presence of a trapping potential tends to favor PS(2) type phase separation [76], however, it may be still possible to realize the PS(2) phase provided that good control over the trapping potentials is possible [77].

Having concluded the analysis of two-species fermion mixtures with mass and population imbalance in continuum and trapped systems, next I analyze mass and population imbalanced fermion mixtures in optical lattices, which is one of the next research frontiers in ultracold atomic Fermi gases.

3.7 Mass and Population Imbalanced Fermion Mixtures in Optical Lattices

In a very recent paper, the MIT group produced preliminary experimental evidence for superfluid and insulating phases of ultracold ^{6}Li atoms in optical lattices [87]. This last experiment overcame some earlier difficulties of producing Fermi superfluids in optical lattices from an atomic Fermi gas or from molecules of Fermi atoms [88, 84, 85, 86]. Unlike in homogeneous or harmonically trapped systems, optical lattices offer an enormous degree of control since phase diagrams may be studied as a function of atom transfer energy t_σ between adjacent lattice sites, on-site atom-atom interactions g, filling fraction n_σ, lattice dimensionality $\mathcal{D}$ and tunnelling anisotropy $\eta = t_\downarrow/t_\uparrow$, where σ labels the type of fermion state.

Arguably, mixtures of two-hyperfine states of the same type of Fermi atoms or mixtures of two different types of Fermi atoms loaded into optical lattices are one of the next frontiers in ultracold atom research because of their richer phase diagrams and greater tunability. Thus, I analyze next the ground state phase diagram containing normal, phase-separated and coexisting superfluid/excess-fermions, and insulating regions as a function of interaction strength and density of fermions.

My main results are as follows. By using an attractive Fermi-Hubbard Hamiltonian to describe fermion mixtures in optical lattices, I show that when fermion-fermion (Bose) molecules are formed, they interact with each other strongly and repulsively. Furthermore, when there are excess fermions, the resulting system corresponds to a strongly interacting (repulsive) mixture of bosons and fermions in the molecular limit, in sharp contrast with homogenous and trapped systems where the resulting Bose-Fermi mixtures are weakly interacting as discussed in Secs. 3.5.3 and 3.5.4. This result is a direct manifestation of the Pauli exclusion principle in the lattice case, since each Bose molecule consists of two fermions, and more than one identical fermion on the same lattice site is not allowed. Lastly, several insulating phases appear in the strong attraction limit depending on fermion filling fractions. For instance, I find a molecular Bose-Mott insulator (superfluid) for molecular filling fraction equal to (less than) one when fermion filling fractions are identical, which is in

qualitative agreement with the MIT experiment [87]. Furthermore, when the filling fraction of one type of fermion is one and the filling fraction of the other is one-half (corresponding to molecular boson and excess fermion filling fractions of one-half), I also find either a phase-separated state consisting of a Fermi-Pauli insulator (FPI) of the excess fermions and a molecular Bose-Mott insulator (BMI) or a Bose-Fermi checkerboard (BFC) phase depending on the tunneling anisotropy η.

3.7.1 Lattice Hamiltonian

To describe mixtures of fermions loaded into optical lattices, I start with a single-band Fermi-Hubbard Hamiltonian in momentum space

$$H = \sum_{\mathbf{k},\sigma} \xi_{\mathbf{k},\sigma} a^{\dagger}_{\mathbf{k},\sigma} a_{\mathbf{k},\sigma} - \frac{g}{2} \sum_{\mathbf{k},\mathbf{k}',\mathbf{q},\sigma} b^{\dagger}_{\mathbf{k},\mathbf{q},\sigma} b_{\mathbf{k}',\mathbf{q},\sigma}, \tag{3.80}$$

with an on-site attractive interaction $g > 0$. Here, the pseudo-spin σ labels the trapped hyperfine states of a given species of fermions, or labels different types of fermions in a two-species mixture, where $a^{\dagger}_{\mathbf{k},\sigma}$ is the fermion creation operator and $b^{\dagger}_{\mathbf{k},\mathbf{q},\sigma} = a^{\dagger}_{\mathbf{k}+\mathbf{q}/2,\sigma} a^{\dagger}_{-\mathbf{k}+\mathbf{q}/2,-\sigma} \Gamma^{*}_{\mathbf{k}}$ is the pair creation operator. The factor $\Gamma_{\mathbf{k}}$ is the symmetry of the pairing interaction, and it is $\Gamma_{\mathbf{k}} = 1$ for the s-wave interaction considered in this manuscript. In addition, $\xi_{\mathbf{k},\sigma} = \epsilon_{\mathbf{k},\sigma} - \widetilde{\mu}_{\sigma}$ describes the nearest neighbor tight-binding dispersion $\epsilon_{\mathbf{k},\sigma} = 2t_{\sigma}\theta_{\mathbf{k}}$ with $\widetilde{\mu}_{\sigma} = \mu_{\sigma} - V_{H,\sigma}$ and

$$\theta_{\mathbf{k}} = \sum_{i=\{x,y,z\}} [1 - \cos(k_i a_c)], \tag{3.81}$$

where t_{σ} is the tunelling matrix element, μ_{σ} is the chemical potential and $V_{H,\sigma}$ is a possible Hartree energy shift.

Notice that, I allow fermions to be of different species through t_{σ}, and to have different populations controlled by independent $\widetilde{\mu}_{\sigma}$. Furthermore, unlike recent work of BCS pairing of fermions in optical lattices [173, 174], I discuss the evolution from BCS to BEC pairing and the emergence of insulating phases. I ignore multi-band effects since a single-band Hamiltonian may be sufficient to describe the evolution from BCS to BEC physics in optical lattices [175]. However, these effects can be easily incorporated into the theory.

For the Hamiltonian given in Eq. (3.80), the saddle point order parameter equation is

given by

$$\frac{1}{g} = \frac{1}{M}\sum_{\mathbf{k}} \frac{1 - f(E_{\mathbf{k},1}) - f(E_{\mathbf{k},2})}{2E_{\mathbf{k},+}} |\Gamma_{\mathbf{k}}|^2, \tag{3.82}$$

where M is the number of lattice sites, $f(x) = 1/[\exp(x/T) + 1]$ is the Fermi function, $E_{\mathbf{k},s} = (\xi_{\mathbf{k},+}^2 + |\Delta_{\mathbf{k}}|^2)^{1/2} + \gamma_s \xi_{\mathbf{k},-}$ is the quasiparticle energy when $\gamma_1 = 1$ or the negative of the quasihole energy when $\gamma_2 = -1$, and $E_{\mathbf{k},\pm} = (E_{\mathbf{k},1} \pm E_{\mathbf{k},2})/2$. Here, $\Delta_{\mathbf{k}} = \Delta_0 \Gamma_{\mathbf{k}}$ is the order parameter and $\xi_{\mathbf{k},\pm} = \epsilon_{\mathbf{k},\pm} - \widetilde{\mu}_{\pm}$, where $\epsilon_{\mathbf{k},\pm} = 2t_{\pm}\theta_{\mathbf{k}}$ with $t_{\pm} = (t_{\uparrow} \pm t_{\downarrow})/2$ and $\widetilde{\mu}_{\pm} = (\widetilde{\mu}_{\uparrow} \pm \widetilde{\mu}_{\downarrow})/2$. Notice that, the symmetry between quasiparticles and quasiholes is broken when $\xi_{\mathbf{k},-} \neq 0$. The order parameter equation has to be solved self-consistently with number equations

$$N_{\uparrow} = \sum_{\mathbf{k}} \left[|u_{\mathbf{k}}|^2 f(E_{\mathbf{k},1}) + |v_{\mathbf{k}}|^2 f(-E_{\mathbf{k},2}) \right], \tag{3.83}$$

$$N_{\downarrow} = \sum_{\mathbf{k}} \left[|u_{\mathbf{k}}|^2 f(E_{\mathbf{k},2}) + |v_{\mathbf{k}}|^2 f(-E_{\mathbf{k},1}) \right], \tag{3.84}$$

where $|u_{\mathbf{k}}|^2 = (1 + \xi_{\mathbf{k},+}/E_{\mathbf{k},+})/2$, and $|v_{\mathbf{k}}|^2 = (1 - \xi_{\mathbf{k},+}/E_{\mathbf{k},+})/2$. The number of σ-type fermions per lattice site is given by

$$0 \leq n_{\sigma} = \frac{N_{\sigma}}{M} \leq 1. \tag{3.85}$$

Thus, when $n_{\uparrow} \neq n_{\downarrow}$, I need to solve all three self-consistency equations, since population imbalance is achieved when either $E_{\mathbf{k},1}$ or $E_{\mathbf{k},2}$ is negative in some regions of momentum space, as discussed next.

3.7.2 Saddle Point Phase Diagrams

In order to analyze the ground state phase diagrams, I solve Eqs. (3.82) and (**??**) as a function of interaction strength g, population imbalance and total filling fraction

$$-1 \leq P = \frac{n_{\uparrow} - n_{\downarrow}}{n_{\uparrow} + n_{\downarrow}} \leq 1, \tag{3.86}$$

$$0 \leq F = \frac{n_{\uparrow} + n_{\downarrow}}{2} \leq 1, \tag{3.87}$$

respectively, and consider two sets of tunneling ratios $\eta = t_{\downarrow}/t_{\uparrow}$ as follows. The case of $\eta = 1$ ($t_{\sigma} = t$) is shown in Fig. 3.17, and the case of $\eta = 0.15$ is shown in Fig. 3.18. While $\eta = 1$ corresponds to one-species (two-hyperfine-state) mixture such as ^{6}Li or ^{40}K, $\eta = 0.15$

corresponds to a two-species mixture (one-hyperfine-state of each type of atom) such as ^{6}Li and ^{40}K.

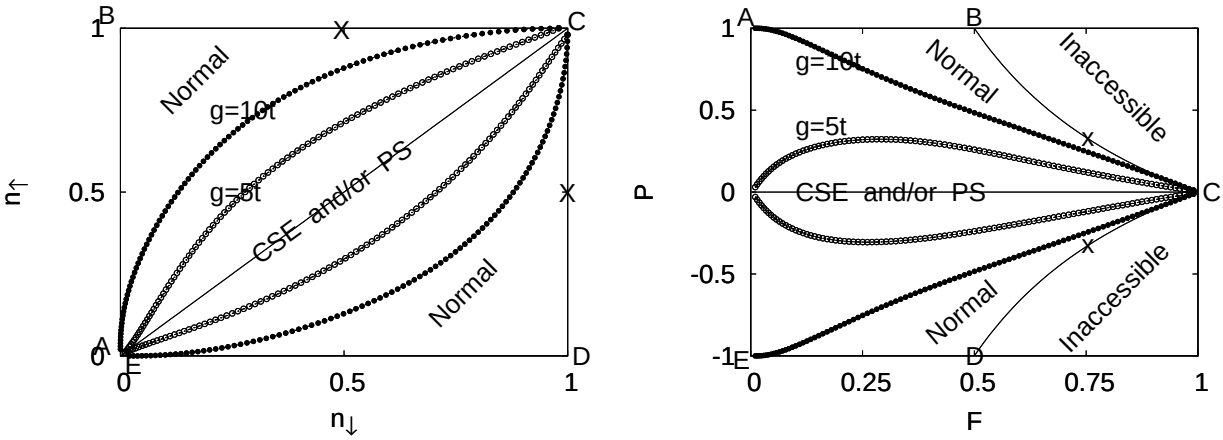

Figure 3.17: Phase diagrams for a one-species (^{6}Li or ^{40}K) mixture of two-hyperfine states with $\eta = 1$: (a) $n_\uparrow$ versus $n_\downarrow$, and (b) P versus F, for $g = 5t$ and $g = 10t$. The normal regions (outside the "football" boundaries) and coexistence of superfluidity with excess fermions (CSE) and/or phase separation (PS) (inside the "football" boundaries) are indicated. The CSE/PS (normal) region expands (shrinks) with increasing attraction.

In the phase diagrams shown in Figs. 3.17 and 3.18, I indicate the regions of normal (N) phase where $|\Delta_0| = 0$, and group together the regions of coexistence of superfluidity and excess fermions (CSE) and/or phase separation (PS), where $|\Delta_0| \neq 0$. When $F \ll 1$, the phase diagrams are similar to the homogenous case analyzed in Section 3.4.3, and the P versus F phase diagram is symmetric for equal tunnelings as shown in Fig. 3.17(b), and is asymmetric for unequal tunnelings having a smaller normal region when the lighter band mass fermions are in excess as shown in Fig. 3.18(b). Here, I do not discuss separately the CSE and PS regions since they have already been discussed in homogeneous and harmonically trapped systems in Secs. 3.4.3 and 3.5.4, and experimentally observed [76, 77]. Thus, I concentrate next on the emergence of insulating phases which are present only in optical lattices.

In Figs. 3.17 and 3.18, the lines AB ($0 < n_\uparrow < 1$; $n_\downarrow = 0$) and ED ($n_\uparrow = 0$; $0 < n_\downarrow < 1$) correspond to normal σ-type Fermi gases for all interactions, while points B ($n_\uparrow = 1, n_\downarrow = 0$) and D ($n_\uparrow = 0, n_\downarrow = 1$) correspond to a Fermi-Pauli (band) insulator since there is only one type of fermion in a fully occupied band. The only option for additional fermions ($\uparrow$ in case

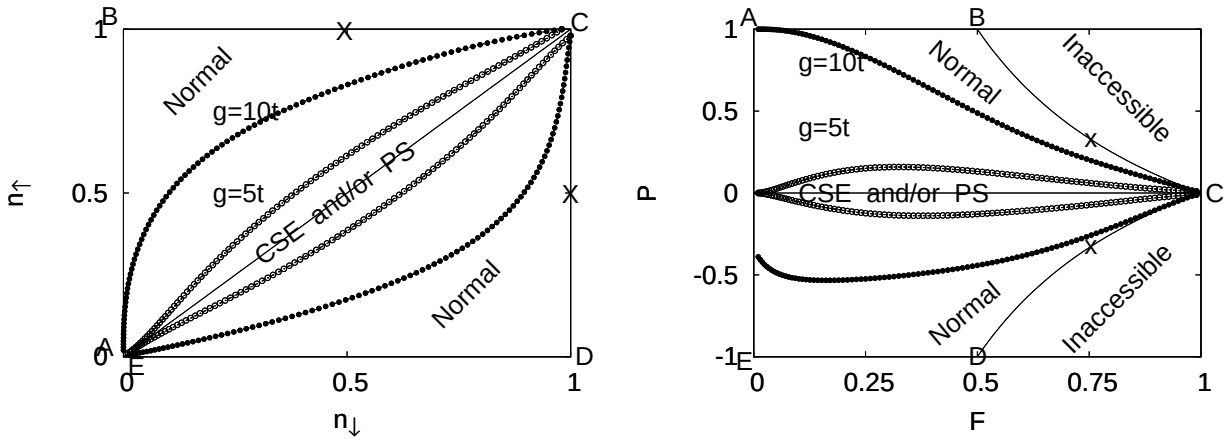

Figure 3.18: Phase diagrams for a two-species (^{6}Li and ^{40}K) mixture of two-hyperfine states with $\eta = 0.15$: (a) $n_\uparrow$ versus $n_\downarrow$, and (b) P versus F, for $g = 5t$ and $g = 10t$. The normal regions (outside the "football" boundaries) and coexistence of superfluidity with excess fermions (CSE) and/or phase separation (PS) (inside the "football" boundaries) are indicated. The CSE/PS (normal) region expands (shrinks) with increasing attraction.

B and $\downarrow$ in case D) is to start filling higher energy bands if the optical potential supports it, otherwise the extra fermions are not trapped. For the case where no additional bands are occupied we label the corresponding phase diagram regions as 'Inaccessible' in Figs. 3.17(b) and 3.18(b), since either $n_\uparrow > 1$ or $n_\downarrow > 1$ in these regions.

In addition, the population balanced line 0C ends at the special point C, where $n_\uparrow = n_\downarrow = 1$. This point is a Fermi-Pauli (band) insulator for weak attraction since both fermion bands are fully occupied, and a Bose-Mott Insulator (BMI) in the strong attraction limit, since at each lattice site there is exactly one molecular boson (consisting of a pair of $\uparrow$ and $\downarrow$ fermions) which has a strong repulsive on-site interaction with any additional molecular boson due to the Pauli exclusion principle.

Furthermore, for very weak fermion attraction, lines BC ($n_\uparrow = 1, 0 < n_\downarrow < 1$) and DC ($0 < n_\uparrow < 1, n_\downarrow = 1$) correspond essentially to a fully polarized ferromagnetic metal (or half-metal), where only the fermion with filling fraction less then one can move around. However, when the fermion attraction is sufficiently strong these lines describe insulators, as molecular bosons and excess fermions are strongly repulsive due to the Pauli exclusion principle. The crosses in Figs. 3.17 and 3.18 at points $n_\uparrow = 1, n_\downarrow = 1/2$ or $n_\uparrow = 1/2, n_\downarrow = 1$ indicate the case where the molecular boson filling fraction $n_B = 1/2$ and the excess fermion filling fraction

is $n_e = 1/2$. At these high symmetry points, molecular bosons and excess fermions tend to segregate, either producing a domain wall type of phase separation with a molecular Bose-Mott insulator (BMI) and a Fermi-Pauli insulator (FPI) region or a checkerboard phase of alternating molecular bosons and excess fermions (BFC). A two dimensional schematic diagram of these two phases are shown in Fig. 3.19(a).

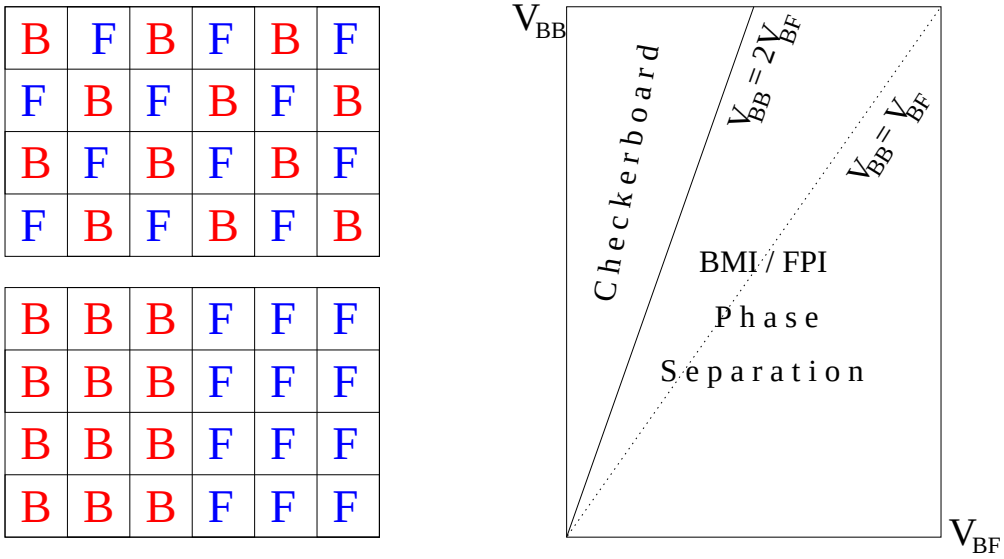

Figure 3.19: (a) On top is the schematic diagram for the Bose-Fermi checkerboard (BFC) phase, and at the bottom is the Bose-Mott insulator/Fermi-Pauli insulator (BMI/FPI) phase separation, and (b) nearest neighbor boson-boson interaction (V_{BB}) versus nearest neighbor boson-fermion interaction (V_{BF}) phase diagram. In (a), F and B represent unpaired and paired fermions, respectively.

The strong attraction limit in optical lattices brings additional physics which is not present in homogenous or purely harmonically trapped systems, and deserves special attention. However, before I analyze this limit, I would like to make two quick remarks. First, the phase diagram characterized by normal, non-normal (CSE or PS), and insulating regions may be explored experimentally by tuning the ratio g/t_+, total filling fraction F, and population imbalance P as done in harmonic traps [76, 77]. Second, topological phases characterized by the number (I and II) of simply connected zero-energy surfaces of $E_{\mathbf{k},\sigma}$ may lie in the stable region of CSE, unlike in the homogeneous case where the topological phase II always lies in the phase separated region for all parameter space as discussed in Section 3.4.3. Next, I analyze the strong attraction (molecular) limit, since it reveals several

additional phases which are only present in optical lattices.

3.7.3 Strong Attraction (Molecular) Limit

First, I derive a time dependent Ginzburg-Landau theory involving molecular bosons and excess fermions near the critical temperature T_c of the possible superfluid phase leading to

$$\left[a+b|\Lambda(x)|^2-\sum_{i,j}\frac{c_{i,j}}{2}\nabla_i\nabla_j-id\frac{\partial}{\partial t}\right]\Lambda(x)=0 \tag{3.88}$$

in the $x=(\mathbf{x},t)$ representation. Here, $\Lambda(x)$ is the fluctuation of the order parameter around its saddle point value $|\Delta_0|=0$, and the expansion coefficients are given in Appendix B.5.

For the s-wave symmetry considered, in the strong attraction (molecular) limit $|\widetilde{\mu}_+|\approx|\epsilon_b|(1-p_e)/2\gg 2\mathcal{D}t_+$, I obtain $a=a_1+a_2=-[2\widetilde{\mu}_+-\epsilon_b(1-p_e)]/[g^2(1-p_e)]+p_e/[g(1-p_e)]$, $b=b_1+b_2=2/[g^3(1-p_e)^2]-(\partial p_e/\partial\widetilde{\mu}_e)/[g^2(1-p_e)]$, $c_{i,j}=c\delta_{i,j}$ with $c=4a_c^2t_\uparrow t_\downarrow/[g^3(1-p_e)^2]$, and $d=1/[g^2(1-p_e)]$. Here, $\epsilon_b=-g$ is the binding energy defined by $1/g=\sum_{\mathbf{k}}1/(2\epsilon_{\mathbf{k},+}-\epsilon_b)$, and e $(-e)$ labels the excess (non-excess) type of fermions and $p_e=|n_\uparrow-n_\downarrow|$ is the number of unpaired fermions per lattice site.

Through the rescaling $\Psi(x)=\sqrt{d}\Lambda(x)$, I obtain the equation of motion for a mixture of bound pairs (molecular bosons) and unpaired (excess) fermions

$$-\mu_B\Psi(x)+\left[U_{BB}|\Psi(x)|^2+U_{BF}p_e(x)\right]\Psi(x)-\frac{\nabla^2\Psi(x)}{2m_B}-i\frac{\partial\Psi(x)}{\partial t}=0, \tag{3.89}$$

with pair chemical potential $\mu_B=-a_1/d=2\widetilde{\mu}_+-\epsilon_b(1-p_e)$, mass $m_B=d/c=g/(4a_c^2t_\uparrow t_\downarrow)$, and repulsive pair-pair $U_{BB}=b_1a_c^3/d^2=2ga_c^3$ and pair-fermion $U_{BF}=a_2a_c^3/(dp_e)=ga_c^3$ interactions. This procedure also yields the spatial density $p_e(x)\geq 0$ of unpaired fermions

$$\begin{aligned} p_e(x) &= [a_2/d+b_2|\Psi(x)|^2/d^2]/U_{BF}, & (3.90)\\ &= p_e-ga_c^3(\partial p_e/\partial\mu_e)(1-p_e)|\Psi(x)|^2. & (3.91)\end{aligned}$$

In contrast with homogeneous or harmonically trapped systems, the boson-boson and boson-fermion interactions are strongly repulsive due to the important role played by the Pauli exclusion principle in the lattice. This role is discussed next, where I analyze some aspects of the phase diagram in the strong attraction limit in terms of an effective Bose-Fermi mixture.

3.7.4 Effective Lattice Bose-Fermi Action

In the limit of strong attractions between fermions $g/t_+ \gg 1$, I obtain an effective Bose-Fermi lattice action

$$S_{BF}^{eff} = \int_0^\beta d\tau \left[\sum_i (f_i^\dagger \partial_\tau f_i + b_i^\dagger \partial_\tau b_i) + K_F + K_B + H_{BF} + H_{BB} \right], \tag{3.92}$$

where K_F and K_B of the effective Hamiltonian are given by

$$K_F = -\mu_F \sum_i f_i^\dagger f_i - t_F \sum_{\langle i,j \rangle} f_i^\dagger f_j, \tag{3.93}$$

$$K_B = -\mu_B \sum_i b_i^\dagger b_i - t_B \sum_{\langle i,j \rangle} b_i^\dagger b_j, \tag{3.94}$$

which are the kinetic part of the excess fermions and molecular bosons, respectively. While H_{BF} and H_{BB} of the effective Hamiltonian are given by

$$H_{BF} = U_{BF} \sum_i f_i^\dagger f_i b_i^\dagger b_i, \tag{3.95}$$

$$H_{BB} = U_{BB} \sum_i b_i^\dagger b_i b_i^\dagger b_i, \tag{3.96}$$

which are the interaction between molecular bosons and excess fermions, and two molecular bosons, respectively.

The total number of fermions is fixed by the constraint $n = 2n_B + p_e$, where $n_B = N_B/M$ is the number of bosons per lattice site. The important parameters of this effective Hamiltonian are the excess fermion transfer energy $t_F = t_e$, the molecular boson transfer energy $t_B = 2t_\uparrow t_\downarrow/g$, the boson-fermion effective repulsion $U_{BF} = g$ and the boson-boson effective repulsion $U_{BB} = 2g$. Notice that, on-site interactions U_{BB} and U_{BF} become infinite (hard-core) when $g \to \infty$ as a manifestation of the Pauli exclusion principle. In addition, there are weak and repulsive nearest neighbor boson-boson $V_{BB} \propto (t_\uparrow^2 + t_\downarrow^2)/g$ and boson-fermion $V_{BF} \propto t_e^2/g$ interactions. These repulsive interactions in optical lattices lead to several insulating phases, depending on fermion filling fractions. In the following analysis, I discuss only two high symmetry cases: (a) $n_\uparrow = n_\downarrow$; and (b) $n_\uparrow = 1$ and $n_\downarrow = 1/2$ or $n_\uparrow = 1/2$ and $n_\downarrow = 1$.

In case (a) indicated as point C in Figs. 3.17, 3.18 and 3.20 where $p_e = 0$, the effective Hamiltonian reduces to a molecular Bose-Hubbard Hamiltonian with the molecular Bose

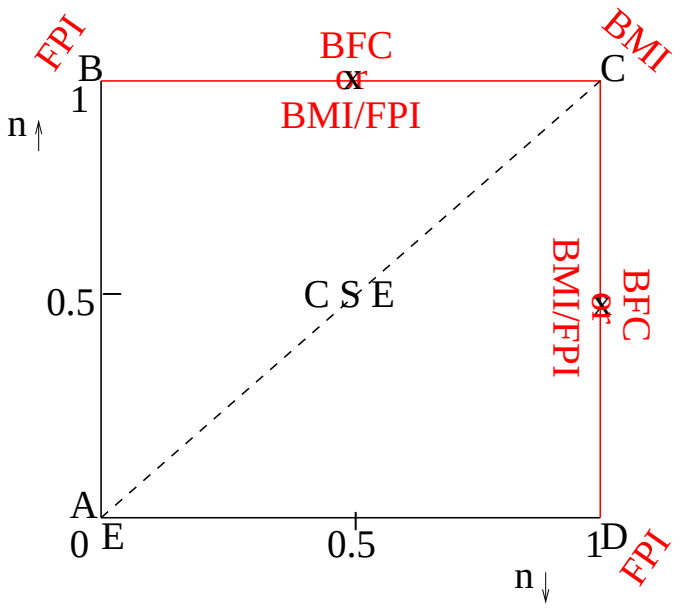

Figure 3.20: The filling fractions $n_\uparrow$ versus $n_\downarrow$ phase diagram in the strong attraction limit ($g/t_+ \to \infty$), indicating the coexisting of superfluid and excess fermions (CSE) phase, and several insulating phases including Fermi-Pauli (FPI), Bose-Fermi checkerboard (BFC), Bose-Mott (BMI), and BMI/FPI phase separation.

filling fraction $n_B = n/2 = F$, thus leading to a molecular BMI when $n_B = 1$ beyond a critical value of U_{BB}. The critical value U^c_{BB} needed to attain the BMI phase can be estimated using the approach of Ref. [176] leading to $U^c_{BB} = 3(3+\sqrt{8})t_B$, which can be translated in terms of the underlying fermion parameters as $g_c = 4.18\sqrt{t_\uparrow t_\downarrow}$. The prefactor should be regarded only as a lower bound estimate of the critical value where the superfluid-to-insulator transition occurs, since the effective Hamiltonian is only valid in the $g \gg t_+$ limit. Thus, these results suggest the existence of a superfluid-to-insulator transition occuring at g_c. The existence of this molecular boson insulating phase which is realized only in optical lattices may have already been observed in the very recent experiments of fermions in optical lattices [87].

In case (b) indicated as crosses in Figs. 3.17, 3.18 and 3.20, the ground state of the effective molecular-boson/excess-fermion system corresponds to either a checkerboard phase of alternating bosons and fermions or to a phase separated BMI/FPI system depending on the ratio V_{BB}/V_{BF}. The checkerboard phase shown in Fig 3.19(a) is favored when $V_{BB} > 2V_{BF}$, leading to the phase diagram of Fig. 3.19(b). At the current level of approximation, I

find that when $t_\uparrow = t_\downarrow$ phase separation is always favored, however when $\uparrow$ ($\downarrow$) fermions are in excess the checkerboard phase is favored when $t_\downarrow > \sqrt{3}t_\uparrow$ ($t_\downarrow < t_\uparrow/\sqrt{3}$). This result is quite interesting since phase separation gives room for the observation of a checkerboard phase if the tunneling ratio η can be controlled experimentally in optical lattices. Furthermore, this checkerboard phase present in the lattice case is completely absent in homogeneous or harmonically trapped systems as discussed in Section 3.4.3.

3.8 Summary

In this chapter, I analyzed the phase diagram of ultra cold mixtures of two types of fermions (e.g., ^{6}Li and ^{40}K; ^{6}Li and ^{87}Sr; or ^{40}K and ^{87}Sr) from the BCS to the BEC limit as a function of scattering parameter, population imbalance, and mass anisotropy. At zero temperature, in addition to the standard superfluid phase, I found phase separated or coexisting superfluid/excess fermion phases depending on the population imbalance and scattering parameter. The phase diagram of population imbalance versus scattering parameter is asymmetric for unequal masses, having a larger stability region for uniform superfluidity when the lighter fermions are in excess. This result is in sharp contrast with the symmetric phase diagram for equal masses.

In addition, I discussed topological quantum phase transitions associated with the disappearance or appearance of momentum space regions of zero quasiparticle energies when either the scattering parameter or population imbalance are changed. These quantum phase transitions are reflected in the momentum distribution as well as in thermodynamic properties, however they seem to lie in the non-uniform region of the phase diagram, but may survive at the center of a harmonic trap. Furthermore this phase may be observable at finite temperatures in trapped systems [166], or in optical lattices, but requires further investigation.

I also analyzed gaussian fluctuations around the saddle point order parameter both at finite and zero temperatures. Near the critical temperature, I derived the Ginzburg-Landau equation, and showed that it describes a dilute mixture of composite bosons (tightly bound fermions) and excess (unpaired) fermions in the BEC limit. At zero temperature, I obtained

analytically the dispersion of collective excitations in the BCS and BEC limits, and described numerically the evolution of the sound velocity from the BCS to the BEC regime for zero population imbalance. In addition, I discussed analytically how phase separation between paired fermions and excess fermions emerges at zero temperature in the BEC limit. I discussed the effects of harmonic trapping potential, and concluded that phase separation between paired and unpaired fermions is favored even in the BEC limit.

In addition, I used an effective weakly interacting Bose-Fermi mixture description to analyze the superfluid phase diagram of two-species dilute Fermi-Fermi mixtures with equal or unequal masses in the strong fermion attraction limit. I first calculated the exact boson-fermion scattering length as a function of mass anisotropy, and then constructed the exact phase diagram. In addition to the normal (N) and uniform (U) superfluid phases, I found two different non-uniform phase separated (PS) states: (1) phase separation between pure unpaired (excess) and pure tightly paired fermions (molecular bosons), and (2) phase separation between pure excess fermions and a mixture of excess fermions and molecular bosons. For equal mass mixtures, the results for the PS(2) to U phase boundary is quantitatively in agreement with the previous saddle-point or mean-field results, however, there are important qualitative and quantitative differences for unequal mass mixtures showing the larger effects of fluctuations in the latter case.

Finally, I analyzed the ground state phase diagram of fermion mixtures in optical lattices as a function of interaction strength, fermion filling factor, and tunneling parameters. In addition to standard superfluid, phase separated or coexisting superfluid/excess fermion phases, I found several insulating phases including a molecular Bose-Mott insulator (BMI), a Fermi-Pauli (band) insulator (FPI), a phase separated BMI/FPI mixture, and a Bose-Fermi checkerboard phase depending on fermion filling fractions. All of these additional phases make the physics of Fermi mixtures much richer than those of atomic bosons or Bose-Fermi mixtures in optical lattices, and of harmonically trapped fermions. Lastly, the molecular BMI phase discussed here has been preliminarily observed in a very recent MIT experiment [87], opening up the experimental exploration of the rich phase diagram of fermion mixtures in optical lattices in the near future.

In summary, the BCS to BEC evolution in two-species fermion mixtures with mass and/or population imbalance exhibits several quantum phase transitions, and are much richer than conventional (mass and population balanced) s-wave systems, where there is only a crossover. Signatures of these quantum phase transition can be found in measurable quantities such as momentum distribution, atomic compressibility, collective excitations etc. as discussed in this chapter.

CHAPTER IV

CONCLUSIONS AND OUTLOOK

In this thesis, I focused on the evolution from Bardeen-Cooper-Schrieffer (BCS) to Bose-Einstein condensation (BEC) evolution in ultracold superfluid Fermi gases as a function of interaction strength. The tuning of attractive interactions permits the ground state of the system to evolve from the weak fermion attraction (BCS) limit of loosely bound and largely overlapping Cooper pairs to the strong fermion attraction limit of tightly bound small bosonic molecules which undergo BEC. This evolution is accompanied by anomalous behavior of many superfluid properties, and reveals several quantum phase transitions.

4.1 Conclusions

The systems analyzed in Chapter II corresponds to zero and nonzero orbital angular momentum fermion pairing, and in Chapter III corresponds to mixtures of two types of fermions with mass and population imbalance in continuum, trap and lattice models.

In Chapter II, I extended the s-wave ($\ell = 0$) functional integral formalism to finite angular momentum ℓ including two-hyperfine-state (THS) pseudo-spin singlet and single-hyperfine-state (SHS) pseudo-spin triplet channels. I obtained analytically superfluid properties of dilute Fermi gases in the ground state ($T = 0$) and near their critical temperatures ($T \approx T_{c,\ell}$) from the weak fermion attraction (BCS) to the strong fermion attraction BEC limit as a function of the scattering parameter (a_ℓ) for arbitrary ℓ. However, I presented numerical results only for THS s-wave and SHS p-wave symmetries which may be relevant for current experiments involving atomic Fermi gases. The main results of Chapter II are as follows.

First, I analyzed the low energy scattering amplitude within a T-matrix approach. I found that bound states occur only when $a_\ell > 0$ for any ℓ. The energy of the bound states $E_{b,\ell}$ involves only the scattering parameter a_0 for $\ell = 0$. However, another parameter related to the interaction range $1/k_0$ is necessary to characterize $E_{b,\ell}$ for $\ell \neq 0$. Therefore,

all superfluid properties for $\ell \neq 0$ depend strongly on k_0 and a_ℓ, while for $\ell = 0$ they depend strongly only on a_0 but weakly on k_0.

Then, I discussed the order parameter, chemical potential, quasiparticle excitations, momentum distribution, atomic compressibility, ground state energy, collective modes and average Cooper pair size at $T = 0$. There I showed that the evolution from BCS to BEC is just a crossover for $\ell = 0$, while the same evolution for $\ell \neq 0$ exhibits a quantum phase transition characterized by a gapless superfluid on the BCS side to a fully gapped superfluid on the BEC side. This transition is a many body effect and takes place exactly when the chemical potential $\mu_{\ell\neq 0}$ crosses the bottom of the fermion band ($\mu_{\ell\neq 0} = 0$), and is best reflected as a non-analytic behavior in the ground state atomic compressibility, momentum distribution and average Cooper pair size.

I also discussed the critical temperature, chemical potential, and the number of unbound, scattering and bound fermions at $T = T_{c,\ell}$. I found that the critical BEC temperature is the highest for $\ell = 0$. I also derived the time-dependent Ginzburg-Landau functional (TDGL) near $T_{c,\ell}$ and extracted the Ginzburg-Landau (GL) coherence length and time. I recovered the usual TDGL equation for BCS superfluids in the weak fermion attraction (BCS) limit, whereas in the strong fermion attraction (BEC) limit, I recovered the Gross-Pitaevskii (GP) equation for a weakly interacting dilute Bose gas. The TDGL equation exhibits anisotropic coherence lengths for $\ell \neq 0$ which become isotropic only in the BEC limit, in sharp contrast to the $\ell = 0$ case, where the coherence length is isotropic for all interaction strengths. Furthermore, the GL time is a complex number with a larger imaginary component for $\mu_\ell > 0$ reflecting the decay of Cooper pairs into the two particle continuum. However, for $\mu_\ell < 0$ the imaginary component vanishes and Cooper pairs become stable above $T_{c,\ell}$.

Having concluded that a quantum phase transition occurs for nonzero angular momentum pairing unlike the $\ell = 0$ case where the BCS to BEC evolution is just a crossover, in Chapter III I discussed several quantum phase transitions in two-species fermion mixtures with mass and population imbalance.

In Chapter III, I analyzed the phase diagram of ultra cold mixtures of two types of fermions (e.g., ^{6}Li and ^{40}K; ^{6}Li and ^{87}Sr; or ^{40}K and ^{87}Sr) from the BCS to the BEC

limit as a function of scattering parameter, population imbalance, and mass anisotropy in continuum, trap and lattice models. The main results of Chapter III are as follows.

At zero temperature, in addition to the standard superfluid phase, I found phase separated or coexisting superfluid/excess fermion phases depending on the population imbalance and the scattering parameter. The phase diagram of population imbalance versus scattering parameter is asymmetric for unequal masses, having a larger stability region for uniform superfluidity when the lighter fermions are in excess. This result is in sharp contrast with the symmetric phase diagram for equal masses.

I also discussed topological quantum phase transitions associated with the disappearance or appearance of momentum space regions of zero quasiparticle energies when either the scattering parameter or population imbalance are changed. These quantum phase transitions are reflected in the momentum distribution as well as in thermodynamic properties, however they seem to lie in the non-uniform region of the phase diagram, but may survive at the center of a harmonic trap. Furthermore this phase may be observable at finite temperatures in trapped systems, or in optical lattices, and requires further investigation.

Then, I analyzed gaussian fluctuations around the saddle point order parameter both at finite and zero temperatures. Near the critical temperature, I derived the Ginzburg-Landau equation, and showed that it describes a dilute mixture of composite bosons (tightly bound fermions) and excess (unpaired) fermions in the BEC limit. At zero temperature, I obtained analytically the dispersion of collective excitations in the BCS and BEC limits, and showed numerically the evolution from the BCS to BEC regimes in the case of zero population imbalance. In addition, I discussed analytically how phase separation between paired fermions and excess fermions emerges analytically at zero temperature in the BEC limit. Furthermore, I discussed the effects of harmonic trapping potential, and concluded that phase separation between paired and unpaired fermions is favored even in the BEC limit.

I also used an effective weakly interacting Bose-Fermi mixture description to analyze the superfluid phase diagram of dilute Fermi mixtures od two types of fermions with equal or unequal masses in the BEC limit. I first calculated the exact boson-fermion scattering length

as a function of mass anisotropy, and then constructed the phase diagram. In addition to the normal (N) and uniform (U) superfluid phases, I found two different non-uniform phase separated (PS) states: (1) phase separation between pure unpaired (excess) and pure tightly paired fermions (molecular bosons), and (2) phase separation between pure excess fermions and a mixture of excess fermions and molecular bosons. For equal mass mixtures, results for the PS(2) to U phase boundary are in quantitative agreement with previous saddle-point or mean-field results, however, there are important qualitative and quantitative differences for unequal mass mixtures showing the larger effects of fluctuations in the latter case.

In addition, I analyzed the ground state phase diagram of fermion mixtures in optical lattices as a function of interaction strength, fermion filling factor, and tunneling parameters. In addition to standard superfluid, phase separated or coexisting superfluid/excess fermion phases, I found several insulating phases including a molecular Bose-Mott insulator (BMI), a Fermi-Pauli (band) insulator (FPI), a phase separated BMI/FPI mixture, and a Bose-Fermi checkerboard phase depending on fermion filling fractions. All these additional phases make the physics of Fermi mixtures much richer than those of atomic bosons or Bose-Fermi mixtures in optical lattices, and of harmonically trapped fermions. Lastly, the molecular BMI phase discussed here has been preliminarily observed in a very recent MIT experiment [87], opening up the experimental exploration of the rich phase diagram of fermion mixtures in optical lattices in the near future.

To conclude, the BCS to BEC evolution in higher angular momentum ($\ell \neq 0$) states and in mixtures of two types of fermions with mass and/or population imbalance exhibit several quantum phase transitions, and are much richer than the conventional (mass and population balanced) $\ell = 0$ s-wave systems, where there is only a crossover. Signatures of these quantum phase transition can be found in measurable quantities such as momentum distribution, atomic compressibility, collective excitations, etc. as discussed in this thesis.

In both problems presented in Chapters II and III, I tried to provide a comprehensive analysis. However, descriptions of these problems are still incomplete, and can be further studied in several ways as discussed next.

4.2 Outlook

The nonzero angular momentum, and mass or population imbalanced superfluidity might be found not only in atomic Fermi gases, but also in nuclear (pairing in nuclei), astrophysics (neutron stars) and condensed matter (high-T_c and organic superconductors) systems. Therefore, it is important and necessary to extend the analysis given in this thesis as follows.

For instance, in Chapter II, I discussed pseudo-spin singlet pairing in two-hyperfine-state systems and pseudo-spin triplet pairing in single-hyperfine-state systems, but the analysis of pseudo-spin triplet pairing can be extended to two-hyperfine-state systems. While I do not expect to find different physics with regards to the topological quantum phase transitions discussed, the pseudo-spin triplet pairing in two-hyperfine-state systems is more relevant to condensed and nuclear matter.

In Chapter II, I also discussed only the BCS to BEC evolution in homogenous systems, and did not consider the effects of a trapping potential. The natural next step is to include trapping effects in the description of nonzero angular momentum superfluidity of ultracold Fermi gases, and calculate the momentum distribution, density profile, etc. In contrast to isotropic properties found for the $\ell = 0$ s-wave case, such quantities are expected to be anisotropic in the BCS limit with much richer features for the $\ell \neq 0$ systems.

There are also several ways to extend the analysis of two-species fermion mixtures with mass and population imbalance. For instance, in Chapter III, I discussed only the ground state (zero temperature) phase diagrams, but it is certainly important to construct phase diagrams at finite temperatures. This is especially crucial for quantitative understanding of current experiments, which are conducted at low but finite temperatures.

In Chapter III, I discussed briefly the possibility of non-uniform FFLO-type superfluidity [164, 165], but did not really calculate the phase boundaries for such pairing. While this phase exists in a very narrow region for equal mass mixtures [112], it is expected to exist in a larger region for unequal mass mixtures. The FFLO phase was proposed more than forty years ago, but convincing evidence has not been found in standard condensed matter systems. The possible observation of such unconventional superfluid phase with mass

and population imbalanced fermion mixtures in traps or optical lattices might provide the missing evidence, and needs to be further analyzed both theoretically and experimentally.

Furthermore, in Chapter III, I used the Thomas-Fermi (or local density) approximation (TFA) to analyze the effects of a trapping potential on the density profiles. While TFA is known to be a good approximation for systems with large number of fermions, a fully self-consistent Bogoliubov-de Gennes (BdG) calculation is necessary to understand better current experiments, and to make quantitative predictions for future experiments.

As a final remark, it is worth emphasizing that ultracold Fermi gases has been very fruitful for the understanding of novel superfluid phases across different branches of physics, ranging from condensed matter and nuclear to atomic and molecular physics. I believe that this field will continue to flourish over the next several years, and that it will open doors to study new and exotic phenomena.

APPENDIX A

LONG-WAVELENGTH AND LOW-FREQUENCY EXPANSION FOR CHAPTER II

I used the following expansion coefficients in Chapter 2 for analyzing the Gaussian fluctuations at zero and finite temperatures to derive the collective mode spectrum and the time-dependent Ginzburg-Landau equations, respectively.

A.1 Expansion Coefficients at $T = 0$

In this appendix, I obtain the expansion coefficients necessary to calculate the collective modes at $T = 0$ from the rotated fluctuation matrix $\widetilde{\mathbf{F}}_\ell^{-1}(q)$ expressed in the amplitude-phase basis. In the long wavelength ($|\mathbf{q}| \to 0$), and low frequency limit ($w \to 0$) the condition

$$\{w, \frac{q_i q_j}{2M}\} \ll \min\{2E_\ell(\mathbf{k})\}, \tag{A.1}$$

is used. While there is no Landau damping and a well defined expansion is possible for $\ell = 0$ case for all couplings, extra care is necessary for $\ell \neq 0$ when $\mu_\ell > 0$ since Landau damping is present.

In all the expressions below I use the following simplifying notation $\dot{\xi}_\ell^i = \partial\xi_\ell(\mathbf{k} + \mathbf{q}/2)/\partial q_i$, $\ddot{\xi}_\ell^{i,j} = \partial\xi_\ell(\mathbf{k} + \mathbf{q}/2)/(\partial q_i \partial q_j)$, $\dot{\Delta}_\ell^i = \partial\Delta_\ell(\mathbf{k} + \mathbf{q}/2)/\partial q_i$ and $\ddot{\Delta}_\ell^{i,j} = \partial^2\Delta_\ell(\mathbf{k} + \mathbf{q}/2)/(\partial q_i \partial q_j)$, which are evaluated at $\mathbf{q} = 0$.

The coefficients necessary to obtain the matrix element $(\widetilde{\mathbf{F}}^{-1}_{\ell,m_\ell,m'_\ell})_{11}$ are

$$A_{\ell,m_\ell,m'_\ell} = \frac{\delta_{m_\ell,m'_\ell}}{4\pi\mathcal{V}^{-1}\lambda_\ell} - \sum_{\mathbf{k}} \frac{\xi_\ell^2}{2E_\ell^3}\Gamma_\ell^2(k) Y_{\ell,m_\ell}(\widehat{\mathbf{k}}) Y^*_{\ell,m'_\ell}(\widehat{\mathbf{k}}), \tag{A.2}$$

corresponding to the $(\mathbf{q} = 0, w = 0)$ term,

$$\begin{aligned} C^{i,j}_{\ell,m_\ell,m'_\ell} &= \sum_{\mathbf{k}} \frac{\xi_\ell(\mathbf{k})}{4E_\ell^7(\mathbf{k})} \{ \ddot{\xi}_\ell^{i,j} E_\ell^2(\mathbf{k}) \left[\xi_\ell^2(\mathbf{k}) - 2\Delta_\ell^2(\mathbf{k})\right] + 3\ddot{\Delta}_\ell^{i,j} E_\ell^2(\mathbf{k})\xi_\ell(\mathbf{k})\Delta_\ell(\mathbf{k}) \\ &+ 5\dot{\xi}_\ell^i\dot{\xi}_\ell^j\Delta_\ell^2(\mathbf{k})\xi_\ell^2(\mathbf{k}) + \dot{\Delta}_\ell^i\dot{\Delta}_\ell^j\xi_\ell(\mathbf{k})\left[\xi_\ell^2(\mathbf{k}) - 4\Delta_\ell^2(\mathbf{k})\right] \\ &+ (\dot{\xi}_\ell^i\dot{\Delta}_\ell^j + \dot{\xi}_\ell^j\dot{\Delta}_\ell^i)\Delta_\ell(\mathbf{k})\left[2\Delta_\ell^2(\mathbf{k}) - 3\xi_\ell^2(\mathbf{k})\right] \}\Gamma_\ell^2(k) Y_{\ell,m_\ell}(\widehat{\mathbf{k}}) Y^*_{\ell,m'_\ell}(\widehat{\mathbf{k}}), \end{aligned} \tag{A.3}$$

corresponding to the $q_i q_j$ term, and

$$D_{\ell,m_\ell,m'_\ell} = \sum_{\mathbf{k}} \frac{\xi_\ell^2(\mathbf{k})}{8E_\ell^5(\mathbf{k})} \Gamma_\ell^2(k) Y_{\ell,m_\ell}(\widehat{\mathbf{k}}) Y^*_{\ell,m'_\ell}(\widehat{\mathbf{k}}), \tag{A.4}$$

corresponding to the w^2 term. Here δ_{m_ℓ,m'_ℓ} is the Kronecker delta.

The coefficients necessary to obtain the matrix element $(\widetilde{\mathbf{F}}^{-1}_{\ell,m_\ell,m'_\ell})_{22}$ are

$$P_{\ell,m_\ell,m'_\ell} = \frac{\delta_{m_\ell,m'_\ell}}{4\pi \mathcal{V}^{-1}\lambda_\ell} - \sum_{\mathbf{k}} \frac{1}{2E_\ell(\mathbf{k})} \Gamma_\ell^2(k) Y_{\ell,m_\ell}(\widehat{\mathbf{k}}) Y^*_{\ell,m'_\ell}(\widehat{\mathbf{k}}), \tag{A.5}$$

corresponding to the $(\mathbf{q}=0, w=0)$ term,

$$\begin{aligned} Q^{i,j}_{\ell,m_\ell,m'_\ell} &= \sum_{\mathbf{k}} \frac{1}{4E_\ell^5(\mathbf{k})} \{ \ddot{\xi}^{i,j}_\ell E_\ell^2(\mathbf{k}) \xi_\ell(\mathbf{k}) + \ddot{\Delta}^{i,j}_\ell E_\ell^2(\mathbf{k}) \Delta_\ell(\mathbf{k}) + 3\dot{\xi}^i_\ell \dot{\xi}^j_\ell \Delta_\ell^2(\mathbf{k}) \\ &+ 3\dot{\Delta}^i_\ell \dot{\Delta}^j_\ell \xi_\ell^2(\mathbf{k}) - 3(\dot{\xi}^i_\ell \dot{\Delta}^j_\ell + \dot{\xi}^j_\ell \dot{\Delta}^i_\ell) \xi_\ell(\mathbf{k}) \Delta_\ell(\mathbf{k}) \} \Gamma_\ell^2(k) Y_{\ell,m_\ell}(\widehat{\mathbf{k}}) Y^*_{\ell,m'_\ell}(\widehat{\mathbf{k}}), \end{aligned} \tag{A.6}$$

corresponding to the $q_i q_j$ term, and

$$R_{\ell,m_\ell,m'_\ell} = \sum_{\mathbf{k}} \frac{1}{8E_\ell^3(\mathbf{k})} \Gamma_\ell^2(k) Y_{\ell,m_\ell}(\widehat{\mathbf{k}}) Y^*_{\ell,m'_\ell}(\widehat{\mathbf{k}}), \tag{A.7}$$

corresponding to the w^2 term.

The coefficients necessary to obtain the matrix element $(\widetilde{\mathbf{F}}^{-1}_{\ell,m_\ell,m'_\ell})_{12}$ is

$$B_{\ell,m_\ell,m'_\ell} = \sum_{\mathbf{k}} \frac{\xi_\ell(\mathbf{k})}{4E_\ell^3(\mathbf{k})} \Gamma_\ell^2(k) Y_{\ell,m_\ell}(\widehat{\mathbf{k}}) Y^*_{\ell,m'_\ell}(\widehat{\mathbf{k}}), \tag{A.8}$$

corresponding to the w term.

A.2 Expansion Coefficients near $T = T_{\mathrm{c},\ell}$

In this Appendix, I perform a small $\mathbf{q}$ and $iv_j \to w + i0^+$ expansion near $T_{\mathrm{c},\ell}$, where I assumed that the fluctuation field $\Lambda_{\ell,m_\ell}(\mathbf{x},t)$ is a slowly varying function of $\mathbf{x}$ and t.

The zeroth order coefficient $L^{-1}_{\ell,m_\ell,m'_\ell}(0,0)$ is diagonal in m_ℓ and m'_ℓ, and is given by

$$a_{\ell,m_\ell,m'_\ell} = \frac{\delta_{m_\ell,m'_\ell}}{4\pi} \left[\frac{\mathcal{V}}{\lambda_\ell} - \sum_{\mathbf{k}} \frac{\mathcal{X}_\ell(\mathbf{k})}{2\xi_\ell(\mathbf{k})} \Gamma_\ell^2(k) \right], \tag{A.9}$$

where $\mathcal{X}_\ell(\mathbf{k}) = \tanh[\beta\xi_\ell(\mathbf{k})/2]$. The second order coefficient $M\partial^2 L^{-1}_{\ell,m_\ell,m'_\ell}(\mathbf{q},0)/(\partial q_i \partial q_j)$ evaluated at $\mathbf{q}=0$ is given by

$$\begin{aligned} c^{i,j}_{\ell,m_\ell,m'_\ell} &= \frac{1}{4\pi} \sum_{\mathbf{k}} \{ \left[\frac{\mathcal{X}_\ell(\mathbf{k})}{8\xi_\ell^2(\mathbf{k})} - \frac{\beta \mathcal{Y}_\ell(\mathbf{k})}{16\xi_\ell(\mathbf{k})} \right] \delta_{m_\ell,m'_\ell} \delta_{i,j} \\ &+ \alpha^{i,j}_{\ell,m_\ell,m'_\ell} \frac{\beta^2 k^2 \mathcal{X}_\ell(\mathbf{k}) \mathcal{Y}_\ell(\mathbf{k})}{16M\xi_\ell(\mathbf{k})} \} \Gamma_\ell^2(k), \end{aligned} \tag{A.10}$$

where $\mathcal{Y}_\ell(\mathbf{k}) = \mathrm{sech}^2[\beta\xi_\ell(\mathbf{k})/2]$ and the angular average

$$\alpha^{i,j}_{\ell,m_\ell,m'_\ell} = \int d\widehat{\mathbf{k}}\widehat{k}_i\widehat{k}_j Y_{\ell,m_\ell}(\widehat{\mathbf{k}})Y^*_{\ell,m'_\ell}(\widehat{\mathbf{k}}). \tag{A.11}$$

Here, $d\widehat{\mathbf{k}} = \sin(\theta_\mathbf{k})d\theta_\mathbf{k}d\phi_\mathbf{k}$, $\widehat{k}_x = \sin(\theta_\mathbf{k})\cos(\phi_\mathbf{k})$, $\widehat{k}_y = \sin(\theta_\mathbf{k})\sin(\phi_\mathbf{k})$ and $\widehat{k}_z = \cos(\theta_\mathbf{k})$. In general, $\alpha^{i,j}_{\ell,m_\ell,m'_\ell}$ is a fourth order tensor for fixed ℓ. However, in the particular case where only one of the spherical harmonics $Y_{\ell,m_\ell}(\widehat{\mathbf{k}})$ is dominant and characterizes the order parameter, $\alpha^{i,j}_{\ell,m_\ell,m'_\ell} = \alpha^{i,j}_{\ell,m_\ell,m_\ell}\delta_{m_\ell,m'_\ell}$ is diagonal in m_ℓ and m'_ℓ. In this case, I use Gaunt coefficients [177] to show that $\alpha^{i,j}_{\ell,m_\ell,m_\ell}$ is also diagonal in i and j leading to $\alpha^{i,j}_{\ell,m_\ell,m'_\ell} = \alpha^{i,i}_{\ell,m_\ell,m_\ell}\delta_{m_\ell,m'_\ell}\delta_{i,j}$.

The coefficient of fourth order term is approximated at $q_n = 0$, and given by

$$b_{\ell,\{m_{\ell_n}\}}(0) = \frac{\gamma_{\ell,\{m_{\ell_n}\}}}{4\pi}\sum_\mathbf{k}\left[\frac{\mathcal{X}_\ell(\mathbf{k})}{4\xi^3_\ell(\mathbf{k})} - \frac{\beta\mathcal{Y}_\ell(\mathbf{k})}{8\xi^2_\ell(\mathbf{k})}\right]\Gamma^4_\ell(k), \tag{A.12}$$

where the angular average

$$\gamma_{\ell,\{m_{\ell_n}\}} = \int d\widehat{\mathbf{k}}Y_{\ell,m_{\ell_1}}(\widehat{\mathbf{k}})Y^*_{\ell,m_{\ell_2}}(\widehat{\mathbf{k}})Y_{\ell,m_{\ell_3}}(\widehat{\mathbf{k}})Y^*_{\ell,m_{\ell_4}}(\widehat{\mathbf{k}}). \tag{A.13}$$

To extract the time-dependence, I expand $Q_{\ell,m_\ell,m'_\ell}(iv_j) = L^{-1}_{\ell.m_\ell,m'_\ell}(\mathbf{q}=0,iv_j) - L^{-1}_{\ell,m_\ell,m'_\ell}(0,0)$ in powers of w after the analytic continuation $iv_j \to w + i0^+$. I use the relation $(x \pm i0^+)^{-1} = \mathcal{P}(1/x) \mp i\pi\delta(x)$, where $\mathcal{P}$ is the principal value and $\delta(x)$ is the Delta function, to obtain

$$Q_{\ell,m_\ell,m'_\ell}(iv_j) = -\frac{\delta_{m_\ell,m'_\ell}}{4\pi}\left[\sum_\mathbf{k}\frac{\mathcal{X}_\ell(\mathbf{k})}{4\xi^2_\ell(\mathbf{k})}\Gamma^2_\ell(k) - i\pi\sum_\mathbf{k}\mathcal{X}_\ell(\mathbf{k})\delta[2\xi_\ell(\mathbf{k}) - w]\Gamma^2_\ell(k)\right] \tag{A.14}$$

Keeping only the first order terms in w leads to $Q_{\ell,m_\ell,m'_\ell}(w + i0^+) = -d_{\ell,m_\ell,m'_\ell}w + ...$, where

$$d_{\ell,m_\ell,m'_\ell} = \frac{\delta_{m_\ell,m'_\ell}}{4\pi}\left[\sum_\mathbf{k}\frac{\mathcal{X}_\ell(\mathbf{k})}{4\xi^2_\ell(\mathbf{k})}\Gamma^2_\ell(k) + i\frac{\pi\beta}{8}N(\epsilon_\mathrm{F})\sqrt{\frac{\mu_\ell}{\epsilon_\mathrm{F}}}\Gamma^2_\ell(\mu_\ell)\Theta(\mu_\ell)\right] \tag{A.15}$$

is also diagonal in m_ℓ and m'_ℓ. Here $N(\epsilon_\mathrm{F}) = M\mathcal{V}k_\mathrm{F}/(2\pi^2)$ is the density of states per spin at the Fermi energy, $\Gamma^2_\ell(x) = (\epsilon_0 x^\ell)/(\epsilon_0 + x)^{\ell+1}$ is the interaction symmetry in terms of energy and $\Theta(x)$ is the Heaviside function.

APPENDIX B

LONG-WAVELENGTH AND LOW-FREQUENCY EXPANSION FOR CHAPTER III

I used the following expansion coefficients in Chapter 3 for analyzing the Gaussian fluctuations at zero and finite temperatures to derive the collective mode spectrum and the time-dependent Ginzburg-Landau equations, respectively.

B.1 Inverse Fluctuation Propagator

In this Appendix, I present explicitly the elements of the inverse fluctuation propagator $\mathbf{F}^{-1}(q)$. The diagonal matrix element of $\mathbf{F}^{-1}(q)$ is given by

$$\begin{aligned}\mathbf{F}^{-1}_{1,1} = \frac{1}{g} \;&+\; \sum_{\mathbf{k}} \big\{ v^2_{\frac{\mathbf{q}}{2}-\mathbf{k}} u^2_{\frac{\mathbf{q}}{2}+\mathbf{k}} \frac{n_f(E_{\frac{\mathbf{q}}{2}-\mathbf{k},1}) - n_f(E_{\frac{\mathbf{q}}{2}+\mathbf{k},1})}{iv_\ell + E_{\frac{\mathbf{q}}{2}-\mathbf{k},1} - E_{\frac{\mathbf{q}}{2}+\mathbf{k},1}} \\ &-\; u^2_{\frac{\mathbf{q}}{2}-\mathbf{k}} v^2_{\frac{\mathbf{q}}{2}+\mathbf{k}} \frac{n_f(E_{\frac{\mathbf{q}}{2}-\mathbf{k},2}) - n_f(E_{\frac{\mathbf{q}}{2}+\mathbf{k},2})}{iv_\ell - E_{\frac{\mathbf{q}}{2}-\mathbf{k},2} + E_{\frac{\mathbf{q}}{2}+\mathbf{k},2}} \\ &+\; u^2_{\frac{\mathbf{q}}{2}+\mathbf{k}} u^2_{\frac{\mathbf{q}}{2}-\mathbf{k}} \frac{1 - n_f(E_{\frac{\mathbf{q}}{2}+\mathbf{k},1}) - n_f(E_{\frac{\mathbf{q}}{2}-\mathbf{k},2})}{iv_\ell - E_{\frac{\mathbf{q}}{2}+\mathbf{k},1} - E_{\frac{\mathbf{q}}{2}-\mathbf{k},2}} \\ &-\; v^2_{\frac{\mathbf{q}}{2}+\mathbf{k}} v^2_{\frac{\mathbf{q}}{2}-\mathbf{k}} \frac{1 - n_f(E_{\frac{\mathbf{q}}{2}-\mathbf{k},1}) - n_f(E_{\frac{\mathbf{q}}{2}+\mathbf{k},2})}{iv_\ell + E_{\frac{\mathbf{q}}{2}-\mathbf{k},1} + E_{\frac{\mathbf{q}}{2}+\mathbf{k},2}} \big\} |\Gamma_{\mathbf{k}}|^2 \end{aligned} \tag{B.1}$$

and the off-diagonal matrix element of $\mathbf{F}^{-1}(q)$ is given by

$$\begin{aligned}\mathbf{F}^{-1}_{1,2} \;&=\; \sum_{\mathbf{k}} u_{\frac{\mathbf{q}}{2}+\mathbf{k}} v_{\frac{\mathbf{q}}{2}+\mathbf{k}} u_{\frac{\mathbf{q}}{2}-\mathbf{k}} v_{\frac{\mathbf{q}}{2}-\mathbf{k}} \big\{ \frac{n_f(E_{\frac{\mathbf{q}}{2}-\mathbf{k},1}) - n_f(E_{\frac{\mathbf{q}}{2}+\mathbf{k},1})}{iv_\ell + E_{\frac{\mathbf{q}}{2}-\mathbf{k},1} - E_{\frac{\mathbf{q}}{2}+\mathbf{k},1}} \\ &-\; \frac{n_f(E_{\frac{\mathbf{q}}{2}-\mathbf{k},2}) - n_f(E_{\frac{\mathbf{q}}{2}+\mathbf{k},2})}{iv_\ell - E_{\frac{\mathbf{q}}{2}-\mathbf{k},2} + E_{\frac{\mathbf{q}}{2}+\mathbf{k},2}} - \frac{1 - n_f(E_{\frac{\mathbf{q}}{2}+\mathbf{k},1}) - n_f(E_{\frac{\mathbf{q}}{2}-\mathbf{k},2})}{iv_\ell - E_{\frac{\mathbf{q}}{2}+\mathbf{k},1} - E_{\frac{\mathbf{q}}{2}-\mathbf{k},2}} \\ &+\; \frac{1 - n_f(E_{\frac{\mathbf{q}}{2}-\mathbf{k},1}) - n_f(E_{\frac{\mathbf{q}}{2}+\mathbf{k},2})}{iv_\ell + E_{\frac{\mathbf{q}}{2}-\mathbf{k},1} + E_{\frac{\mathbf{q}}{2}+\mathbf{k},2}} \big\} |\Gamma_{\mathbf{k}}|^2 \end{aligned} \tag{B.2}$$

where $u^2_{\mathbf{k}} = (1 + \xi_{\mathbf{k},+}/E_{\mathbf{k},+})/2$ and $v^2_{\mathbf{k}} = (1 - \xi_{\mathbf{k},+}/E_{\mathbf{k},+})/2$, and $n_f(x) = 1/[\exp(\beta x) + 1]$ is the Fermi distribution.

For the s-wave case considered in this manuscript, a well defined low frequency and long wavelength expansion is possible in two limits: (I) at zero temperature ($T = 0$) when

population imbalance is zero $P = 0$ such that the Fermi functions in Eqs. (B.1) and (B.2) vanish, and (II) near the critical temperature ($T \approx T_c$) where $|\Delta_0| \to 0$ such that $v_{\frac{\mathbf{q}}{2}\pm\mathbf{k}}$ (when $\xi_{\frac{\mathbf{q}}{2}\pm\mathbf{k},+} > 0$) and $u_{\frac{\mathbf{q}}{2}\pm\mathbf{k}}$ (when $\xi_{\frac{\mathbf{q}}{2}\pm\mathbf{k},+} < 0$) in Eqs. (B.1) and (B.2) vanish. Other than these two limits, there is Landau damping which causes the collective modes to decay into the two quasiparticle continuum.

B.2 Expansion Coefficients at $T = 0$

In this Appendix, I perform a small $\mathbf{q}$ and $iv_\ell \to w + i0^+$ expansion of the effective action at zero temperature ($T = 0$). From the rotated fluctuation matrix $\mathbf{M}^{-1}$ expressed in the amplitude-phase basis, I can obtain the expansion coefficients necessary to calculate the collective modes. I calculate the coefficients only for the case of zero population imbalance $P = 0$, as extra care is needed when $P \neq 0$ due to Landau damping. In the long wavelength ($|\mathbf{q}| \to 0$), and low frequency ($w \to 0$) limits the condition $\{w, q_i q_j (2m_+)\} \ll \min\{2E_{\mathbf{k},+}\}$, is used.

The coefficients necessary to obtain the matrix element $\mathbf{M}^{-1}_{\lambda,\lambda}(q)$ are

$$A = \sum_{\mathbf{k}} \frac{|\Delta_0|^2}{2E^3_{\mathbf{k},+}} \tag{B.3}$$

corresponding to the $(\mathbf{q} = 0, w = 0)$ term,

$$C = \sum_{\mathbf{k}} \left[\xi_{\mathbf{k},+} \frac{E^2_{\mathbf{k},+} - 3|\Delta_0|^2}{8m_+ E^5_{\mathbf{k},+}} - \left(\frac{E^2_{\mathbf{k},+} - 10|\Delta_0|^2}{m_+^2} + \frac{10|\Delta_0|^4}{m_+^2 E^2_{\mathbf{k},+}} + \frac{E^2_{\mathbf{k},+} - |\Delta_0|^2}{m_-^2} \right) \frac{k^2}{24E^5_{\mathbf{k},+}} \right] \tag{B.4}$$

corresponding to the $|\mathbf{q}|^2$ term, and

$$D = \sum_{\mathbf{k}} \frac{E^2_{\mathbf{k},+} - |\Delta_0|^2}{8E^5_{\mathbf{k},+}} \tag{B.5}$$

corresponding to the w^2 term.

The coefficients necessary to obtain the matrix element $\mathbf{M}^{-1}_{\theta,\theta}(q)$ are

$$Q = \sum_{\mathbf{k}} \left[\frac{\xi_{\mathbf{k},+}}{8m_+ E^3_{\mathbf{k},+}} - \left(\frac{E^2_{\mathbf{k},+} - 3|\Delta_0|^2}{m_+^2} + \frac{E^2_{\mathbf{k},+}}{m_-^2} \right) \frac{k^2}{24E^5_{\mathbf{k},+}} \right] \tag{B.6}$$

corresponding to the $|\mathbf{q}|^2$ term, and

$$R = \sum_{\mathbf{k}} \frac{1}{8E_{\mathbf{k},+}^3} \tag{B.7}$$

corresponding to the w^2 term.

The coefficient necessary to obtain the matrix element $\mathbf{M}_{\lambda,\theta}^{-1}(q)$ is

$$B = \sum_{\mathbf{k}} \frac{\xi_{\mathbf{k},+}}{4E_{\mathbf{k},+}^3} \tag{B.8}$$

corresponding to the w term. These coefficients can be evaluated in the BCS and BEC limits, and are given in Section 3.5.2.

B.3 Expansion Coefficients near $T = T_c$

In this Appendix, I derive the coefficients a, b, c_{ij} and d of the time dependent Ginzburg-Landau theory described in Eq. (3.37). I perform a small $\mathbf{q}$ and $iv_\ell \to w + i0^+$ expansion of the effective action near the critical temperature ($T \approx T_c$), where I assume that the fluctuation field $\Lambda(\mathbf{x}, t)$ is a slowly varying function of $\mathbf{x}$ and t.

The zeroth order coefficient $L^{-1}(0,0)$ is given by

$$a = \frac{1}{g} - \sum_{\mathbf{k}} \frac{X_{\mathbf{k},+}}{2\xi_{\mathbf{k},+}} |\Gamma_{\mathbf{k}}|^2 \tag{B.9}$$

where $X_{\mathbf{k},\pm} = (X_{\mathbf{k},\uparrow} \pm X_{\mathbf{k},\downarrow})/2$ and $X_{\mathbf{k},\sigma} = \tanh(\beta\xi_{\mathbf{k},\sigma}/2)$.

The second order coefficient $\partial^2 L^{-1}(\mathbf{q},0)/(\partial q_i \partial q_j)$ evaluated at $\mathbf{q} = 0$ is given by

$$\begin{aligned} c_{i,j} &= \sum_{\mathbf{k}} \left[\left(\frac{X_{\mathbf{k},\uparrow} Y_{\mathbf{k},\uparrow}}{m_\uparrow^2} + \frac{X_{\mathbf{k},\downarrow} Y_{\mathbf{k},\downarrow}}{m_\downarrow^2} \right) \frac{\beta^2 k_i k_j}{32\xi_{\mathbf{k},+}} \right. \\ &+ \left(\frac{2k_i k_j C_-}{m_- \xi_{\mathbf{k},+}} - \delta_{i,j} C_+ \right) \frac{\beta}{16\xi_{\mathbf{k},+}} \\ &+ \left. \left(\frac{\delta_{i,j}}{2m_+} - \frac{k_i k_j}{m_-^2 \xi_{\mathbf{k},+}} \right) \frac{X_{\mathbf{k},+}}{4\xi_{\mathbf{k},+}^2} \right] |\Gamma_{\mathbf{k}}|^2, \end{aligned} \tag{B.10}$$

where $C_\pm = (Y_{\mathbf{k},\uparrow}/m_\uparrow \pm Y_{\mathbf{k},\downarrow}/m_\downarrow)/2$, and $Y_{\mathbf{k},\sigma} = \mathrm{sech}^2(\beta\xi_{\mathbf{k},\sigma}/2)$. Here, $\delta_{i,j}$ is the Kronecker delta.

The coefficient of the fourth order term is approximated by its value at $\mathbf{q} = \mathbf{0}$,

$$\begin{aligned} b &= \frac{1}{\beta} \sum_p \mathbf{G}_{\uparrow,\uparrow}^{\mathrm{sp}}(p) \mathbf{G}_{\downarrow,\downarrow}^{\mathrm{sp}}(p) \mathbf{G}_{\uparrow,\uparrow}^{\mathrm{sp}}(p) \mathbf{G}_{\downarrow,\downarrow}^{\mathrm{sp}}(p) |\Gamma_{\mathbf{k}}|^4 \\ &= \frac{1}{\beta} \sum_{\mathbf{k}, w_\ell} \frac{|\Gamma_{\mathbf{k}}|^4}{(iw_\ell - \xi_{\mathbf{k},\uparrow})^2 (iw_\ell + \xi_{\mathbf{k},\downarrow})^2} \end{aligned} \tag{B.11}$$

and evaluation of the fermionic Matsubara frequency sum leads to

$$b = \sum_{\mathbf{k}} \left(\frac{X_{\mathbf{k},+}}{4\xi_{\mathbf{k},+}^3} - \frac{\beta Y_{\mathbf{k},+}}{8\xi_{\mathbf{k},+}^2} \right) |\Gamma_{\mathbf{k}}|^4. \tag{B.12}$$

The time-dependent coefficient has real and imaginary parts, and for the s-wave case is given by

$$d = \lim_{w \to 0} \sum_{\mathbf{k}} X_{\mathbf{k},+} \left[\frac{1}{4\xi_{\mathbf{k},+}^2} + i\pi \frac{\delta(2\xi_{\mathbf{k},+} - w)}{w} \right] |\Gamma_{\mathbf{k}}|^2 \tag{B.13}$$

where $\delta(x)$ is the Delta function.

B.4 Renormalized Interaction Strength and Molecular Boson Propagator

In this Appendix, I derive first the relation between the fermion-fermion interaction strength and the fermion-fermion scattering length, and later the renormalized molecular boson propagator corrected by the fermion loops in the BEC limit.

B.4.1 Renormalized Interaction Strength

The scattering t-matrix of two fermions, $T_{\mathbf{q}}^{FF}$, can be calculated by summing up the diagrams shown in Fig. B.1. In the diagrammatic representation for the fermion-fermion scattering t-matrix $T_{\mathbf{q}}^{FF}$, single lines represent σ-type fermion propagators. The scattering length is proportional to the t-matrix at zero momentum, and given by

$$T_{\mathbf{0}}^{FF} = \frac{4\pi a_F}{m_{\uparrow\downarrow}}, \tag{B.14}$$

where a_F is the fermion-fermion scattering length, and $m_{\uparrow\downarrow}$ is twice the reduced mass of $\uparrow$- and $\downarrow$-type fermions.

The bubble diagrams shown in Fig. B.1 form a geometric series, which can be summed to give

$$\begin{aligned} -g - g^2\Pi(\mathbf{0},0) - g^3\Pi^2(\mathbf{0},0) - ... &= -g\sum_{n=0}^{\infty}[g\Pi(\mathbf{0},0)]^n \\ &= -\frac{g}{1-g\Pi(\mathbf{0},0)} \\ &= T_{\mathbf{q}}^{FF}. \end{aligned} \tag{B.15}$$

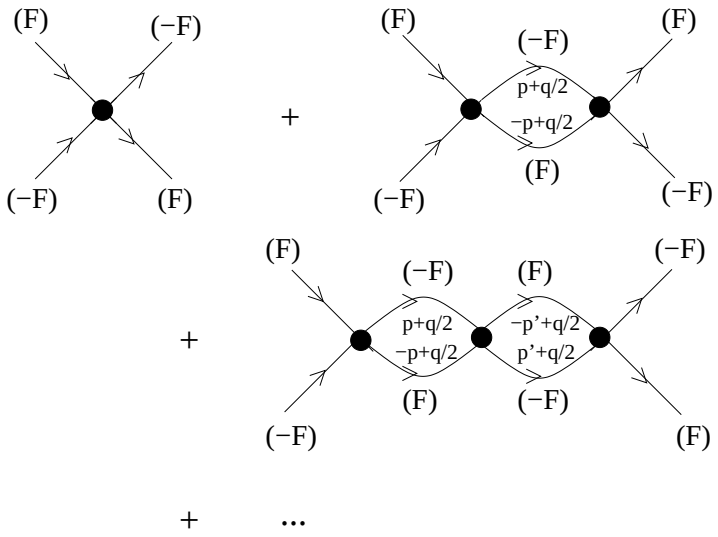

Figure B.1: Diagrammatic representation for the fermion-fermion scattering t-matrix $T_{\mathbf{q}}^{FF}$, where single lines represent σ-type fermion propagators.

Here, $\Pi(\mathbf{0}, 0)$ corresponds to the bubble diagram when $q = 0$, and given by

$$\Pi(\mathbf{0}, 0) = \sum_{p} G_{0,\uparrow}(p) G_{0,\downarrow}(-p), \tag{B.16}$$

where $G_{0,\sigma}(\mathbf{k}, iw_j) = 1/[iw_j - \epsilon_{\mathbf{k},\sigma} + i0^+]$ is the σ-type fermion propagator in vacuum ($\mu_\sigma = 0$). After performing the fermionic Matsubara frequency summation, Eq. (B.15) leads to

$$\frac{1}{g} = -\frac{m_{\uparrow\downarrow} V}{4\pi a_F} + \sum_{\mathbf{k}} \frac{1}{\epsilon_{\mathbf{k},\uparrow} + \epsilon_{\mathbf{k},\downarrow}}, \tag{B.17}$$

which provides the relation between the fermion-fermion interaction strength g and the fermion-fermion scattering length a_F for short-range s-wave interactions.

B.4.2 Renormalized Molecular Boson Propagator

The calculation of renormalized molecular boson propagator corrected by the fermionic loops is very similar to the calculation of renormalized fermion-fermion interactions, and can be calculated by summing up the diagrams shown in Fig. B.2. In the diagrammatic representation of the renormalized molecular boson propagator $D_0(\mathbf{q}, iv_j)$ corrected by the fermionic loops, single lines represent σ-type fermion propagators, double thin lines represent unrenormalized molecular boson propagators, and the double thick line represents the renormalized molecular boson propagator.

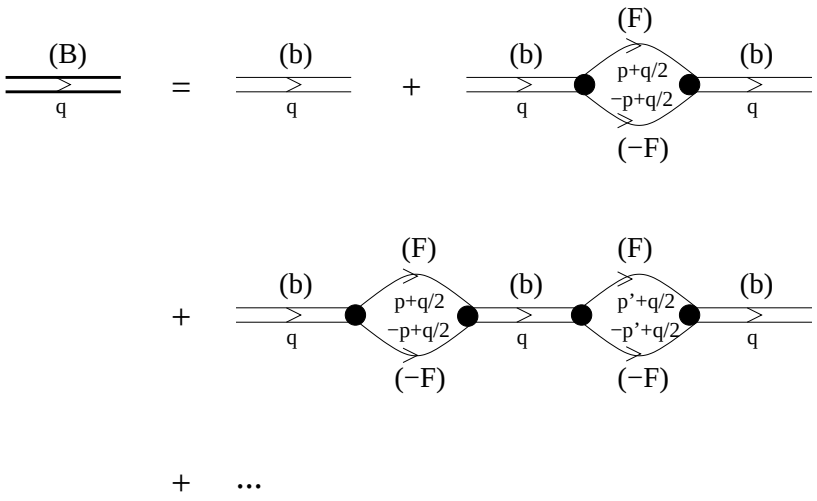

Figure B.2: Diagrammatic representation of the renormalized molecular boson propagator $D_0(\mathbf{q}, iv_j)$ corrected by the fermionic loops, where single lines represent σ-type fermion propagators, double thin lines represent unrenormalized molecular boson propagators, and the double thick line represents the renormalized molecular boson propagator.

The bubble diagrams shown in Fig. B.2 also form a geometric series, which can be summed to give

$$\begin{aligned} -g - g^2\Pi(\mathbf{q}, iv_j) - g^3\Pi^2(\mathbf{q}, iv_j) - ... &= -g\sum_{n=0}^{\infty}[g\Pi(\mathbf{q}, iv_j)]^n \\ &= -\frac{g}{1 - g\Pi(\mathbf{q}, iv_j)} \\ &= D_0(\mathbf{q}, iv_j) \end{aligned} \tag{B.18}$$

Here, $\Pi(\mathbf{q}, iv_j)$ corresponds to the bubble diagram, and given by

$$\Pi(\mathbf{q}, iv_j) = \sum_p G_{0,\uparrow}(p + q/2)G_{0,\downarrow}(-p + q/2), \tag{B.19}$$

where $G_{0,\sigma}(\mathbf{k}, iw_j) = 1/[iw_j - \epsilon_{\mathbf{k},\sigma} + \mu_\sigma + i0^+]$ is the σ-type fermion propagator. After performing the fermionic Matsubara frequency and the momentum summations, and using Eq. (B.17) in Eq. (B.18) leads to

$$D_0(\mathbf{q}, iv_j) = \frac{4\pi}{m_{\uparrow\downarrow}^{3/2}} \frac{1}{|\epsilon_b|^{1/2} - [|\mathbf{q}|^2/(2m_B) - iv_j - \mu_\uparrow - \mu_\downarrow - i0^+]^{1/2}}, \tag{B.20}$$

which provides the renormalized molecular boson propagator. Here, $\epsilon_b = -1/(m_{\uparrow\downarrow}a_F^2)$ is the binding energy, and $m_B = m_\uparrow + m_\downarrow$ is the molecular mass.

B.5 Expansion Coefficients near $T = T_c$ for Optical Lattices

In this Appendix, I derive the coefficients a, b, c_{ij} and d of the time dependent Ginzburg-Landau theory described in Section 3.7.3. I perform a small $\mathbf{q}$ and $iv_\ell \to w + i0^+$ expansion of the effective action near the critical temperature ($T \approx T_c$), where I assume that the fluctuation field $\Lambda(\mathbf{x}, t)$ is a slowly varying function of $\mathbf{x}$ and t.

The zeroth order coefficient $L^{-1}(0,0)$ is given by

$$a = \frac{1}{g} - \frac{1}{M}\sum_{\mathbf{k}} \frac{X_{\mathbf{k},+}}{2\xi_{\mathbf{k},+}} |\Gamma_{\mathbf{k}}|^2 \tag{B.21}$$

where $X_{\mathbf{k},\pm} = (X_{\mathbf{k},\uparrow} \pm X_{\mathbf{k},\downarrow})/2$ and $X_{\mathbf{k},\sigma} = \tanh(\beta\xi_{\mathbf{k},\sigma}/2)$.

The second order coefficient $\partial^2 L^{-1}(\mathbf{q},0)/(\partial q_i \partial q_j)$ evaluated at $\mathbf{q} = 0$ is given by

$$\begin{aligned} c_{i,j} &= \frac{a_c^2}{M}\sum_{\mathbf{k}} \Bigg[\left(X_{\mathbf{k},\uparrow} Y_{\mathbf{k},\uparrow} t_\uparrow^2 + X_{\mathbf{k},\downarrow} Y_{\mathbf{k},\downarrow} t_\downarrow^2\right) \sin(k_i a_c)\sin(k_j a_c) \frac{\beta^2}{8\xi_{\mathbf{k},+}} \\ &+ \left(\frac{4t_- \sin(k_i a_c)\sin(k_j a_c) C_-}{\xi_{\mathbf{k},+}} - 2\delta_{i,j}\cos(k_i a_c) C_+ \right) \frac{\beta}{8\xi_{\mathbf{k},+}} \\ &+ \left(2t_+ \cos(k_i a_c)\delta_{i,j} - \frac{4t_-^2 \sin(k_i a_c)\sin(k_j a_c)}{\xi_{\mathbf{k},+}} \right) \frac{X_{\mathbf{k},+}}{4\xi_{\mathbf{k},+}^2} \Bigg] |\Gamma_{\mathbf{k}}|^2, \end{aligned} \tag{B.22}$$

where $C_\pm = (Y_{\mathbf{k},\uparrow} t_\uparrow \pm Y_{\mathbf{k},\downarrow} t_\downarrow)/2$, and $Y_{\mathbf{k},\sigma} = \mathrm{sech}^2(\beta\xi_{\mathbf{k},\sigma}/2)$. Here, $\delta_{i,j}$ is the Kronecker delta.

The coefficient of the fourth order term is approximated by its value at $\mathbf{q} = \mathbf{0}$, and given by

$$b = \frac{1}{M}\sum_{\mathbf{k}} \left(\frac{X_{\mathbf{k},+}}{4\xi_{\mathbf{k},+}^3} - \frac{\beta Y_{\mathbf{k},+}}{8\xi_{\mathbf{k},+}^2} \right) |\Gamma_{\mathbf{k}}|^4. \tag{B.23}$$

The time-dependent coefficient has real and imaginary parts, and for the s-wave case is given by

$$d = \lim_{w\to 0} \frac{1}{M}\sum_{\mathbf{k}} X_{\mathbf{k},+} \left[\frac{1}{4\xi_{\mathbf{k},+}^2} + i\pi \frac{\delta(2\xi_{\mathbf{k},+} - w)}{w} \right] |\Gamma_{\mathbf{k}}|^2 \tag{B.24}$$

where $\delta(x)$ is the Delta function.

REFERENCES

[1] B. L. van der Waerden, *Sources of Quantum Mechanics*, Dover, (2007).

[2] W. Heisenberg, Z. Phys. **43**, 172 (1927).

[3] F. Reif, *Fundamentals of Statistical and Thermal Physics*, McGraw-Hill, Tokyo (1981).

[4] F. J. Belinfante, Physica **6**, 849 (1939).

[5] W. Pauli and F. J. Belinfante, Physica **7**, 177 (1940).

[6] N. N. Bogoliubov, J. Phys. (U.S.S.R.) **11**, 23 (1947).

[7] A. L. Fetter and J. D. Walecka, *Quantum Theory of Many-Particle Systems*, Dover, New York (1971).

[8] L. Pitaevskii and S. Stringari, *Bose-Einstein Condensation*, Oxford Univ. Press, Oxford (2003).

[9] P. Nozieres and D. Saint-James, J. Phys. **43**, 1133 (1982).

[10] C. C. Bradley, A. Sackett, and R. G. Hulet, Phys. Rev. Lett. **75**, 1687 (1995).

[11] P. A. Ruprecht, M. J. Holland, K. Burnett, and M. Edwards, Phys. Rev. A **51**, 4704 (1995).

[12] J. L. Roberts, N. R. Claussen, S. L. Cornish, E. A. Donnely, E. A. Cornell, and C. E. Wieman, Phys. Rev. Lett. **86**, 4211 (2001).

[13] S. N. Bose, Z. Phys. **26**, 178 (1924).

[14] A. Einstein, Sitz. Ber. Preuss. Akad. Wiss. (Berlin) **1**, 3 (1925).

[15] P. Kapitza, Nature **141**, 74 (1938).

[16] J. F. Allen and A. D. Misener, Nature **141**, 75 (1938).

[17] F. London, Phys. Rev. **154**, 947 (1938).

[18] L. D. Landau, J. Phys. (U.S.S.R.) **11**, 91 (1947).

[19] M. H. Anderson, J. R. Ensher, M. R. Matthews, C. E. Wieman, and E. A. Cornell, Science **269**, 198 (1995).

[20] K. B. Davis, M. -O. Mewes, M. R. Andrews, N. J. van Druten, D. S. Durfee, D. M. Kurn, and W. Ketterle, Phys. Rev. Lett. **75**, 3969 (1995).

[21] F. Dalfovo, S. Giorgini, L. Pitaevskii and S. Stringari, Rev. Mod. Phys. **71**, 463 (1999).

[22] A. J. Leggett, Rev. Mode. Phys. **73**, 307 (2001).

[23] E. A. Cornell and C. E. Wieman, Rev. Mod. Phys. **74**, 875 (2002).

[24] W. Ketterle, Rev. Mod. Phys. **74**, 1131 (2002).

[25] N. W. Ashcroft and N. D. Mermin, *Solid State Physics*, Thomson Learning, (1976).

[26] B. DeMarco and D.S. Jin, Science **285**, 1703 (1999).

[27] Webpage, *Atom traps worlwide*, http://www.uibk.ac.at/exphys/ultracold/atomtraps.html (Accessed 22 May 2007).

[28] C. A. Regal, *Experimental Realization of BCS-BEC Crossover Physics with a Fermi Gas of Atoms*, Ph.D thesis (2006).

[29] M. W. Zwierlein, *High-Temperature Superfuidity in an Ultracold Fermi Gas*, Ph. D. Thesis (2006).

[30] H. K. Onnes, Akad. van Wetenschappen **14(113)**, 818 (1911).

[31] J. Bardeen, L. N. Cooper, and J. R. Schrieffer, Phys. Rev. **108**, 1175 (1957).

[32] L. N. Cooper, Phys. Rev. **104**, 1189 (1956).

[33] M. Tinkham, *Introduction to Superconductivity*, Dover, New York (1996).

[34] J. M. Blatt, S. T. Butler, and M. R. Schafroth, Phys. Rev. **100**, 481 (1955).

[35] J. M. Blatt, *Theory of Superconductivity*, Academic Press, New York (1964).

[36] D. M. Eagles, Phys. Rev. **186**, 456 (1969).

[37] A. J. Leggett, in *Modern Trends in the Theory of Condensed Matter*, edited by A. Peralski and R. Przystawa, Springer-Verlag, Berlin (1980).

[38] A. J. Leggett, J. Phys. (Paris) **C7**, 19 (1980).

[39] H. Heiselberg, Phys. Rev. A **63**, 043606 (2001).

[40] T. -L. Ho, Phys. Rev. Lett. **92**, 090402 (2004).

[41] P. Nozieres and S. Schmitt-Rink, J. Low. Temp. Phys. **59**, 195 (1985).

[42] J. G. Bednorz and K. A. Müller, Z. Physik B **64**, 189 (1986).

[43] M. Drechster and W. Zwerger, Ann. Phys. (Germany) **1**, 15 (1992).

[44] C. A. R. Sá de Melo, M. Randeria, and J. R. Engelbrecht, Phys. Rev. Lett. **71**, 3202 (1993).

[45] R. Haussman, Phys. Rev. B **49**, 12975 (1994).

[46] M. Randeria, in *Bose-Einstein Condensation*, edited by A. Griffin, D. Snoke, and S. Stringari, Cambridge Univ. Press, Cambridge (1995).

[47] Y. Ohashi and A. Griffin, Phys. Rev. A **67**, 033603 (2003).

[48] A. Perali, P. Pieri, L. Pisani, and G. C. Strinati, Phys. Rev. Lett. **92**, 220404 (2004).

[49] J. N. Milstein, S. J. J. M. F. Kokkelmans, and M. J. Holland, Phys. Rev. A **66**, 043604 (2002).

[50] Y. Ohashi and A. Griffin, Phys. Rev. Lett. **89** , 130402 (2002).

[51] S. Chu, Rev. Mod. Phys. **70**, 685 (1998).

[52] C. N. Cohen-Tannoudji, Rev. Mod. Phys. **70**, 707 (1998).

[53] W. D. Phillips, Rev. Mod. Phys. **70**, 721 (1998).

[54] B. DeMarco, *Quantum Behavior of an Atomic Fermi Gas*, Ph.D thesis (2001).

[55] J. L. Roberts, N. R. Claussen, S. L. Cornish, and C. E. Wieman, Phys. Rev. Lett. **85**, 728 (2000).

[56] T. Weber, J. Herbig, M. Mark, H. C. Nagerl, and R. Grimm, Phys. Rev. Lett. **91**, 123201 (2003).

[57] H. T. C. Stoof, M. Houbiers, C. A. Sackett, and R. G. Hulet, Phys. Rev. Lett. **76**, 10 (1996).

[58] K. M. OHara, S. L. Hemmer, M. E. Gehm, S. R. Granade, and J. E. Thomas, Science **298**, 2179 (2002).

[59] C. A. Regal, C. Ticknor, J. L. Bohn, and D. S. Jin, Nature **424**, 47 (2003).

[60] K. E. Strecker, G. B. Partridge, and R. G. Hulet, Phys. Rev. Lett. **91**, 080406 (2003).

[61] J. Cubizolles, T. Bourdel, S. J. J. M. F. Kokkelmans, G. V. Shlyapnikov, and C. Salomon, Phys. Rev. Lett. **91**, 240401 (2003).

[62] S. Jochim, M. Bartenstein, A. Altmeyer, G. Hendl, C. Chin, J. H. Denschlag, and R. Grimm, Phys. Rev. Lett. **91**, 240402 (2003).

[63] D. S. Petrov, C. Salomon, and G. V. Shlyapnikov, Phys. Rev. Lett. **93**, 090404 (2004).

[64] S. Jochim, M. Bartenstein, A. Altmeyer, G. Hendl, S. Riedl, C. Chin, J. H. Denschlag, and R. Grimm, Science **302**, 2101 (2003).

[65] M. W. Zwierlein, C. A. Stan, C. H. Schunck, S. M. F. Raupach, S. Gupta, Z. Hadzibabic, and W. Ketterle, Phys. Rev. Lett. **91**, 250401 (2003).

[66] T. Bourdel, L. Khaykovich, J. Cubizolles, J. Zhang, F. Chevy, M. Teichmann, L. Tarruell, S. J. J. M. F. Kokkelmans, and C. Salomon, Phys. Rev. Lett. **93**, 050401 (2004).

[67] M. Greiner, C. A. Regal, and D. S. Jin, Nature **426**, 537 (2003).

[68] C. A. Regal, M. Greiner, and D. S. Jin, Phys. Rev. Lett. **92**, 040403 (2004).

[69] M. W. Zwierlein, C. A. Stan, C. H. Schunck, S. M. F. Raupach, A. J. Kerman, and W. Ketterle, Phys. Rev. Lett. **92**, 120403 (2004).

[70] M. Bartenstein, A. Altmeyer, S. Riedl, S. Jochim, C. Chin, J. H. Denschlag, and R. Grimm, Phys. Rev. Lett. **92**, 120401 (2004).

[71] C. Chin, M. Bartenstein, A. Altmeyer, S. Riedl, S. Jochim, J. Hecker Denschlag, and R. Grimm, Science **305**, 1128 (2004).

[72] J. Kinast, S. L. Hemmer, M. E. Gehm, A. Turlapov, and J. E. Thomas. Phys. Rev. Lett. **92**, 150402 (2004).

[73] G. B. Partridge, K. E. Strecker, R. I. Kamar, M. W. Jack, and R. G. Hulet, Phys. Rev. Lett. **95**, 020404 (2005).

[74] J. Kinast, A. Turlapov, J. E. Thomas, Q. Chen, J. Stajic, and K. Levin, Science **307**, 1296 (2005).

[75] M. W. Zwierlein, J. R. Abo-Shaeer, A. Schirotzek, C. H. Schunck, and W. Ketterle, Nature **435**, 1047 (2005).

[76] M. W. Zwierlein, A. Schirotzek, C. H. Schunck and W. Ketterle, Science **311**, 492 (2006).

[77] G. B. Partridge, W. Lui, R. I. Kamar, Y. Liao, and R. G. Hulet, Science **311**, 503 (2006).

[78] H. Feshbach, Ann. Phys. (N.Y.) **5**, 357 (1958).

[79] U. Fano, Nuovo Cimento **12** 156, (1935); see also Phys. Rev. A **124**, 1866 (1961).

[80] E. Tiesinga, B. J. Verhaar, and H. T. C. Stoof, Phys. Rev. A **47**, 4114 (1993).

[81] S. Inouye, M. R. Andrews, J. Stenger, H. J. Miesner, D. M. Stamper-Kurn, and W. Ketterle, Nature **392**, 151 (1998).

[82] P. Courteille, R. S. Freeland, D. J. Heinzen, F. A. van Abeelen, and B. J. Verhaar, Phys. Rev. Lett. **81**, 69 (1998).

[83] C. A. Regal and D. S. Jin, Phys. Rev. Lett. **90**, 230404 (2003).

[84] M. Köhl, H. Moritz, T. Stöferle, K. Gnter, and T. Esslinger, Phys. Rev. Lett. **94**, 080403 (2005).

[85] H. Moritz, T. Stöferle, K. Günter, M. Köhl, and T. Esslinger, Phys. Rev. Lett. **94**, 210401 (2005).

[86] T. Stöferle, H. Moritz, K. Gnter, M. Köhl, and T. Esslinger, Phys. Rev. Lett. **96**, 030401 (2006).

[87] J. K. Chin, D. E. Miller, Y. Liu, C. Stan, W. Setiawan, C. Sanner, K. Xu, and W. Ketterle, Nature **443**, 961, (2006).

[88] G. Modugno, F. Ferlaino, R. Heidemann, G. Roati, and M. Inguscio, Phys. Rev. A **68**, 011601(R) (2003).

[89] W. Hofstetter, J. I. Cirac, P. Zoller, E. Demler, and M. D. Lukin, Phys. Rev. Lett. **89**, 220407 (2002).

[90] D. Jaksch, C. Bruder, J. I. Cirac, C. W. Gardiner, and P. Zoller, Phys. Rev. Lett. **81**, 3108 (1998).

[91] M. Greiner, O. Mandel, T. Esslinger, T. W. Hänsch, and I. Bloch, Nature **415**, 39 (2002).

[92] I. Bloch, Nature Physics **1**, 23 (2005).

[93] S. Ospelkaus, C. Ospelkaus, L. Humbert, K. Sengstock, and K. Bongs, Phys. Rev. Lett. **97**, 120403 (2006).

[94] G. Modugno, M. Modugno, F. Riboli, G. Roati, and M. Inguscio, Phys. Rev. Lett. **89**, 190404 (2002).

[95] R. Micnas, J. Ranninger, and S. Robaskiewicz, Rev. Mod. Phys. **62**, 113 (1990).

[96] P. A. M. Dirac, Phys. Zeit. der Sowjetunion **3**, 64 (1933).

[97] R. P. Feynman, Rev. Mod. Phys. **20**, 267 (1948).

[98] H. Kleinert, *Path Integrals in Quantum Mechanics, Statistics, Polymer Physics, and Financial Markets*, World Scientific, Singapore (2004).

[99] V. N. Popov, *Functional integrals and collective excitations*, Cambridge Univ. Press, New York (1987).

[100] J. W. Negele and H. Orland, *Qunatum Many-Particle Systems*, Westview Press, Boulder (1998).

[101] A. Zee, *Quantum Field Theory in a Nutshell*, Princeton Univ. Press, New Jersey (2003).

[102] A. A. Abrikosov, L. P. Gorkov, and I. E. Dzyaloshinski, *Methods of Quantum Field Theory* in Statistical Physics, Dover, New York (1963).

[103] E. Abrahams and T. Tsuneto, Phys. Rev. **152**, 416 (1966).

[104] C. A. Regal, C. Ticknor, J. L. Bohn, and D. S. Jin, Phys. Rev. Lett. **90**, 053201 (2003).

[105] C. Ticknor, C. A. Regal, D. S. Jin, and J. L. Bohn, Phys. Rev. A **69**, 042712 (2004)

[106] J. Zhang, E. G. M. van Kempen, T. Bourdel, L. Khaykovich, J. Cubizolles, F. Chevy, M. Teichmann, L. Tarruell, S. J. J. M. F. Kokkelmans, and C. Salomon, Phys. Rev. A **70**, 030702 (2004).

[107] C. H. Schunck, M. W. Zwierlein, C. A. Stan, S. M. F. Raupach, W. Ketterle, A. Simoni, E. Tiesinga, C. J. Williams, and P. S. Julienne, Phys. Rev. A **71**, 045601 (2005).

[108] K. Günter, T. Stöferle, H. Moritz, M. Köhl, and T. Esslinger, Phys. Rev. Lett. **95**, 230401 (2005).

[109] J. P. Gaebler, J. T. Stewart, J. L. Bohn, and D. S. Jin, cond-mat/0703087.

[110] J. R. Engelbrecht, M. Randeria, and C. A. R. Sá de Melo, Phys. Rev. B **55**, 15153 (1997).

[111] C. H. Pao, S.-T. Wu, and S. K. Yip, Phys. Rev. B **73**, 132506 (2006).

[112] D. E. Sheehy and L. Radzihovsky, Phys. Rev. Lett. **96**, 060401 (2006).

[113] J. L. Bohn, Phys. Rev. A **61**, 053409 (2000).

[114] V. Gurarie, L. Radzihovsky, and A. V. Andreev, Phys. Rev. Lett. **94**, 230403 (2005).

[115] C.-H. Cheng and S.-K. Yip, Phys. Rev. Lett. **95**, 070404 (2005).

[116] L. S. Borkowski and C. A. R. Sá de Melo, cond-mat/9810370.

[117] R. D. Duncan and C. A. R. Sá de Melo, Phys. Rev B **62**, 9675 (2000).

[118] J. Quintanilla, B. L. Gyorffy, J. F. Annett, and J. P. Wallington, Phys. Rev. B **66**, 214526 (2002).

[119] B. C. den Hertog, Phys. Rev. B **60**, 559 (1999).

[120] N. Andrenacci, A. Perali, P. Pieri, and G. C. Strinati, Phys. Rev. B **60**, 12410 (1999).

[121] S. S. Botelho and C. A. R. Sá de Melo, cond-mat/0409368.

[122] M. Iskin and C. A. R. Sá de Melo, Phys. Rev. B **72**, 224513 (2005).

[123] S. S. Botelho and C. A. R. Sá de Melo, J. Low Temp. Phys. **140**, 409 (2005).

[124] G. D. Mahan, *Many-Particle Physics*, Plenum, New York (2000).

[125] R. L. Stratonovich, Dokl. Akad. Nauk (U.S.S.R) **115**, 1097 (1957).

[126] J. Hubbard, Phys. Rev. Lett. **3**, 77 (1959).

[127] T.-L. Ho and R. B. Diener, Phys. Rev. Lett. **94**, 090402 (2005).

[128] Y. Ohashi, Phys. Rev. Lett. **94**, 050403 (2005).

[129] M. Iskin and C.A.R. Sá de Melo, Phys. Rev. Lett. **96**, 040402 (2006).

[130] L. D. Landau and E. M. Lifshitz, *Quantum Mechanics*, Permagon, Oxford (1994).

[131] A. J. Leggett, Rev. Mod. Phys. 47, 331 (1975).

[132] P. Pieri, L. Pisani, and G. C. Strinati, Phys. Rev. B. **70**, 094508 (2004).

[133] M. Greiner, C. A. Regal, J. T. Stewart, and D. S. Jin, Phys. Rev. Lett. **94**, 110401 (2005).

[134] E. Altman, E. Demler, and M. Lukin, Phys. Rev. A **70**, 013603 (2004).

[135] G. E. Volovik, *Exotic Properties of Superfluid* ^{3}He, World Scientific, Singapore (1992).

[136] I. M. Lifshitz, Sov. Phys. JETP **11**, 1130 (1960). [Zh. Eksp. Teor. Fiz. **38**, 1569 (1960)].

[137] A. A. Abrikosov, *Fundamental Theory of Metals*, pages 111-114, North-Holland (1988).

[138] P. Pieri and G. C. Strinati, Phys. Rev. B **61**, 15370 (2000).

[139] I. V. Brodsky, A. V. Klaptsov, M. Yu. Kagan, R. Combescot, and X. Leyronas, Phys. Rev. A **73**, 032724 (2006).

[140] J. Levinsen and V. Gurarie, Phys. Rev. A **73**, 053607 (2006).

[141] J. B. Ketterson and S. N. Song, *Superconductivity*, Cambridge Univ. Press, New York (1999).

[142] G. E. Astrakharchik, J. Boronat, J. Casulleras, and S. Giorgini, Phys. Rev. Lett. **93**, 200404 (2004).

[143] D. T. Son and M. A. Stephanov, Phys. Rev. A **74**, 013614 (2006).

[144] A. Sedrakian, J. Mur-Petit, A. Polls, and H. Müther, Phys. Rev. A **72**, 013613 (2005).

[145] T. Mizushima, K. Machida, and M. Ichioka, Phys. Rev. Lett. **94**, 060404 (2005).

[146] P. Pieri and G. C. Strinati, Phys. Rev. Lett **96**, 150404 (2006).

[147] J. Kinnunen, L. M. Jensen, and P. Torma , Phys. Rev. Lett. **96**, 110403 (2006).

[148] W. Yi and L. M. Duan, Phys. Rev. A **73**, 031604 (2006).

[149] F. Chevy, Phys. Rev. Lett. **96**, 130401 (2006).

[150] T. N. De Silva and E. J. Mueller, Phys. Rev. A **73**, 051602(R) (2006).

[151] M. Haque and H. T. C. Stoof, Phys. Rev. A **74**, 011602 (2006).

[152] W. V. Liu and F. Wilczek, Phys. Rev. Lett. **90**, 047002 (2003).

[153] P. F. Bedaque, H. Caldas, and G. Rupak, Phys. Rev. Lett. **91**, 247002 (2003).

[154] L. Y. He, M. Jin, and P. F. Zhuang, Phys. Rev. B **74**, 024516 (2006).

[155] M. Iskin and C. A. R. Sá de Melo, Phys. Rev. Lett. **97**, 100404 (2006).

[156] M. Iskin and C. A. R. Sá de Melo, cond-mat/0606624 (unpublished).

[157] M. M. Parish, F. M. Marchetti, A. Lamacraft, B. D. Simons, cond-mat/0608651.

[158] C. H. Pao, S.-T. Wu, and S. K. Yip, cond-mat/0604572.

[159] T. Paananen, P. Törmä, and J-P. Martikainen, Phys. Rev. A, **75**, 023622 (2007).

[160] E. Gubankova, A. Schmitt, and F. Wilczek, Phys.Rev. B **74** , 064505 (2006).

[161] L. Y. He, M. Jin, and P. F. Zhuang, cond-mat/0606322.

[162] D. E. Sheehy and L. Radzihovsky, cond-mat/0608172.

[163] C. H. Pao, S.-T. Wu, and S. K. Yip, cond-mat/0608501.

[164] P. Fulde and R. A. Ferrell, Phys. Rev. **135**, A550 (1964).

[165] A. I. Larkin and Y. N. Ovchinnikov, Sov. Phys. JETP **20**, 762 (1965).

[166] W. Yi and L. M. Duan, Phys. Rev. Lett. **97**, 120401 (2006).

[167] M. Iskin and C. A. R. Sá de Melo, cond-mat/0612496.

[168] C. Lobo, A. Recati, S. Giorgini, and S. Stringari, Phys. Rev. Lett. **97**, 200403 (2006).

[169] G. V. Skorniakov and K. A. Ter-Martisosian, Sov. Phys. JETP **4**, 648 (1957).

[170] D. S. Petrov, Phys. Rev. A **67**, 010703(R) (2003).

[171] L. Viverit, C. J. Pethick, and H. Smith, Phys. Rev. A **61**, 053605 (2000).

[172] M. Amoruso, A. Minguzzi, S. Stringari, M. P. Tosi, and L. Vichi, Eur. Phys. J. D **4**, 261 (1998).

[173] W. V. Liu, F. Wilczek, and P. Zoller, Phys. Rev. A **70**, 033603 (2004).

[174] T. Koponen, J. Kinnunen, J. -P. Martikainen, L. M. Jensen, and P Törmä, New J. Phys. **8**, 179 (2006).

[175] A. Koetsier, D. B. M. Dickerscheid, and H. T. C. Stoof, Phys. Rev. A **74**, 033621 (2006).

[176] D. van Oosten, P. van der Straten, and H. T. C. Stoof, Phys. Rev. A **63**, 053601 (2001).

[177] G. B. Arfken and H. J. Weber, *Mathematical methods for physicists*, Harcourt Acad. Press, New York (2001).

VITA

Menderes Iskin was born in Merkez, Tokat, a small city located in the northern part of Turkey, on February 5, 1979. He grew up in Tokat, and attended Namik Kemal and Melik Ahmet Gazi Elementary Schools, and moved to Maltepe, Istanbul in August 1989 with his family where he graduated from Kadikoy Anatolian High School with honors in June 1997. Upon graduation from high school, he moved to Ankara, the capital city of Turkey, and entered Bilkent University in September 1997, where he received the Bachelor of Science degree in Physics with high honors in May 2002. The following August, he moved to Atlanta, Georgia and entered Georgia Institute of Technology, where he received a Master of Science degree in theoretical Physics in August 2004, and is a candidate for the Doctor of Philosophy degree in theoretical Physics as of August 2007.